SELECTIVE CONTROL OF ELECTRICAL NEURAL ACTIVATION USING INFRARED LIGHT

By

Austin Robert Duke

Dissertation

Submitted to the Faculty of the

Graduate School of Vanderbilt University

in partial fulfillment of the requirements

for the degree of

DOCTOR OF PHILOSOPHY

in

Biomedical Engineering

December 2012

Nashville, Tennessee

Approved:

Dr. E. Duco Jansen

Dr. Anita Mahadevan-Jansen

Dr. Peter Konrad

Dr. Robert Galloway

Dr. Hillel Chiel

Dr. Claus-Peter Richter

ABSTRACT

The neurostimulation market is one of the fastest growing sectors of the medical device industry. This is primarily due to both an increasing patient population and recent advances in clinical neural interfaces. However, the need for restored neural function remains largely unmet and will require refinements to current technology and development of novel solutions. To fully control neural function and analyze the dynamics of neural circuitry, it is necessary to have tools capable of selectively exciting and inhibiting sub-populations of neurons. Advances in electrical neural interfaces have greatly improved selective stimulation. In addition, electrical methods of blocking nerve conduction have been demonstrated. Recently, a novel optical stimulation technique was developed whereby pulsed infrared light achieves neural activation with spatiotemporal precision. This dissertation investigates the hypothesis that electrical and optical techniques are complimentary and can be cooperatively applied to control neural function. The synergistic combination of pulsed electric current and infrared light is evaluated in a myelinated mammalian nerve, and the methodology is refined through systematic investigation in both unmyelinated and myelinated nerve preparations. This hybrid approach to neurostimulation exhibits spatial specificity of activation while reducing stimulation currents and optical radiant exposures. Infrared light is not only shown to selectively enhance electrical neural excitation, but also to inhibit electrically initiated axonal activation and block propagating action potentials. The utility of this technique is demonstrated through the modulation of neuromuscular function, with the underlying mechanism likely mediated by local infrared-induced changes in baseline

nerve temperature. Application of infrared light is shown to selectively enhance and inhibit electrically stimulated muscle activity and contraction force in both unmyelinated and myelinated nerves. The results of this work indicate there is a rich set of interactions between light and excitable tissues, and infrared light can be applied as a multi-faceted tool for selectively controlling neural function for both research and clinical applications.

I dedicate this dissertation to my family.

This work would not have been possible without your love, encouragement and support.

ACKNOWLEDGEMENTS

I first want to thank my advisor, Dr. Duco Jansen. He gave me freedom to take chances and pursue my interests, but also provided wise guidance when needed. He made me feel more like a colleague than a student, which did wonders for my confidence. I cannot thank Dr. Hillel Chiel enough for all of the time he devoted to helping me bring this research together. Whether it was providing me dedicated space in his lab for a week at a time, or taking a few minutes to answer a question – his availability and advice were invaluable to me accomplishing this goal. I want to thank Dr. Anita Mahadevan-Jansen for giving perspective to both my project and career as an independent researcher, as well as for challenging me to go above and beyond what is required. I want to thank Dr. Claus-Peter Richter for always asking the tough questions. He always challenged my results and made me take the necessary steps to prove what I found was real. I want to thank Dr. Peter Konrad for his enthusiasm about my research and for taking the time to show me the impact this someday may have. I also want to thank Dr. Bob Galloway for showing me how to make graduate school enjoyable and to see the bigger picture of why it is I do what I do. In addition to the faculty and advisors who helped to guide my research, I want to thank all of my friends at Vanderbilt University and Case Western Reserve University. They provided help with work when I needed a hand, a sounding board to vent to when I was frustrated, a home away from home when I traveled, and just made coming to work every day an enjoyable experience.

I also want to thank my family for all of their love and support. My parents, Bob and Marsha, and my sister, Casey, have loved, encouraged and supported me in

everything that I have ever done. They let me try everything that interested me and never told me that I could not achieve a goal. If times were tough they were there to encourage me and when things went well they were the first to celebrate. I also want to thank my father- and mother-in-law, Ron and Beth Day, and the rest of the Day family for welcoming me from day one. They have treated me just like a son, brother and grandson, and have provided all the love, encouragement and support I could ever want.

Most of all, I want to thank my wife, Amanda. She has stood by me through all the ups and downs of this entire journey. She celebrated with me through the good times, encouraged me when things were not going well, let me spend weeks away so that I could do experiments, listened to all of my practice presentations, was far more patient than I could ever have asked, and was completely loving and selfless as she allowed me to pursue my dream. I could not have done this without her.

TABLE OF CONTENTS

LIST OF FIGURES

Figure

CHAPTER II

INTRODUCTION

Austin R. Duke

Vanderbilt University, Department of Biomedical Engineering

Nashville, TN

2.1 Motivation

Neural control, the selective excitation or inhibition of nervous system function, is a vital tool for both research and clinical applications. Over the past two centuries much about the nervous system, including the communication dynamics between the brain and the rest of the body, has been learned through purposeful perturbations of neural activity. Over the last half century, neurostimulation has also been applied to restore function to muscles and sensory organs lacking nervous control due to either a neurological disorder or trauma. The ability to restore functionality combined with the sizeable patient population has made the neurostimulation market one of the fastest growing sectors of the medical device industry.

Electrical techniques have long served as the method of choice for evoking and controlling biological potentials. Numerous electrically based neuroprosthetics are on the market today. Current clinical neurostimulation applications include, but are not limited to, motor stimulation for the treatment of foot drop (Kottink et al., 2007), deep brain stimulation (DBS) for disorders such as Parkinson's disease (Kern and Kumar, 2007), auditory implants for the profoundly deaf (Shannon, 2012), and vagus nerve stimulation for epilepsy and depression (Groves and Brown, 2005). Advances in electrode and implant technology have greatly improved performance; however, challenges for this technique remain. Methods of selective control with mitigated invasiveness or otherwise detrimental effects must be further refined and electrical block of neural activity needs to be accomplished without generating intense bursts of activity at initial onset.

Recently, pulsed infrared light was demonstrated as an alternative means for stimulating neural activity (Wells et al., 2005). This optical technique, known as infrared

nerve stimulation (INS), offers several attractive qualities for research and clinical neurostimulation applications including fine spatial resolution, absence of stimulation artifact and no required contact between the light source and the target tissue (Wells et al., 2007). However, the ultimate application of INS is potentially limited by laser design constraints and concerns regarding possible laser-induced thermal tissue damage. These limitations must be addressed to ensure the effective and safe clinical application of this innovative technique.

A novel application of the known neural response to infrared light is the synergistic combination of INS with electrical stimulation. Combining both neurostimulation techniques will highlight the strengths of each while mitigating their respective weaknesses. Additionally, infrared light may also provide a means of achieving spatiotemporally precise inhibition through localized changes in nerve temperature (Mou et al., 2012). This selective inhibition could be used to dictate what elements of the target neural tissue are excited electrically, as well as to block unwanted signals from reaching their functional endpoint. Thus, infrared light is an intriguing option for the selectively controlling electrical neural activation. Although optical and electrical techniques of neural control are fundamentally different modalities, which work by different mechanisms, their combination may lead to better, more precise control of nervous system function and a new class of robust and versatile neuroprosthetic devices.

2.2 Specific Aims

The objective of this research is to develop and characterize the use of infrared light for modulating electrically initiated neural excitation. The driving hypotheses for

this work are that (1) infrared light applied in conjunction with electrical stimulation will achieve selective activation with optical radiant exposures that are less than required for INS alone (hybrid electro-optical stimulation); and (2) infrared light will selectively block both the initiation and propagation of neural signals and can be used to regulate neuromuscular function (infrared inhibition). Prior to this work, both hybrid electro-optical stimulation and infrared inhibition existed as untested hypotheses. The specific aims of this thesis were designed to test these hypotheses by demonstrating the feasibility of combined optical and electrical stimulation, establishing a methodology for reliable and repeatable hybrid stimulation, investigating the utility of hybrid electro-optical stimulation for eliciting a motor response and demonstrating and characterizing the block of neural signals and their corresponding functional output with infrared light. Experiments were conducted using *ex vivo* and *in vivo* preparations in both vertebrate and invertebrate neural systems. To accomplish the objectives of this research, the specific aims were outlined as follows:

Specific Aim (1): Determine feasibility of combined optical and electrical neural stimulation of peripheral nerves. In a vertebrate peripheral nerve model (rat sciatic nerve), sub-threshold for stimulation pulses of electrical current were simultaneously applied with sub-threshold for stimulation pulses of infrared light to achieve neural excitation. Evoked potentials from muscles innervated by the sciatic nerve were monitored for the presence of stimulation and to assess the spatial resolution of hybrid stimulation. Sub-threshold currents were varied to determine the associated amount of optical energy required to achieve stimulation. Optical pulses were delayed relative to

electrical pulses to assess potential effects of stimuli concurrency on stimulation thresholds.

Specific Aim (2): Establish a methodology for reliable and repeatable hybrid electro-optical stimulation. Several experiments were designed to spatially and temporally characterize the neural response to hybrid stimulation. Experiments were performed in the tractable buccal nerves of the *Aplysia californica* and validated in the more clinically relevant rat sciatic nerve. The results of the experiments comprising this aim provided information regarding the spatial arrangement of the optical and electrical stimuli, temporal fluctuations in stimulation thresholds and probability of stimulation as a function of stimulus magnitude. The information ascertained here is critical for the successful application of this stimulation paradigm.

Specific Aim (3): Demonstrate hybrid stimulation of a physiologically relevant motor response. In the rat sciatic nerve, hybrid electro-optical stimulation was applied at 15-20 Hz and the force generated by the contraction of the innervated plantarflexor muscles was measured. Experiments in this aim were designed to characterize the physiological response in regards to stimulus parameters, overall force generated and muscle recruitment. Results were then related to the thermal profile stemming from optical stimulation. Acute safety studies were conducted and the nerve analyzed histologically to detect potential morphological changes resulting from hybrid stimulation.

Specific Aim (4): Determine feasibility of blocking action potential initiation and propagation using infrared light. In buccal nerve 2 (BN2) of Aplysia, pulses of infrared light were applied at either the site of electrical activation or at a distal location along the nerve trunk. Electrical recordings from the three branches distal to the nerve trifurcation allowed for detection and characterization of electrically evoked responses with and without infrared exposure to the nerve. In a separate experiment, the muscular innervation of BN2 was left intact and electrically evoked force responses were characterized when infrared inhibition was applied. Results obtained in *Aplysia* were validated in the rat sciatic nerve to demonstrate translation of this technique between species and unmyelinated/myelinated nervous systems.

2.3 Dissertation Outline

The material comprising this dissertation is organized in the following manner:

Chapter I gives an introduction to the problem motivating this work and provides introductory justification for the proposed technological development. The specific aims used to guide this research are also summarized here.

Chapter II provides the relevant background material for the research performed in this work. Topics addressed in this chapter include a brief overview of the peripheral nervous system, descriptions of the mechanism, applications and limitations for electrical stimulation and infrared nerve stimulation, technologies for neural inhibition and the current landscape of the neurostimulation market. The overall significance of this work is also discussed.

In Chapter III, initial feasibility of combining optical and electrical methods of neural stimulation to achieve activation of a mammalian peripheral nerve is demonstrated. This work was published in the November-December 2009 issue of *Journal of Biomedical Optics* (Duke et al., 2009).

Chapter IV details the methodology for achieving reliable and repeatable hybrid electro-optical stimulation. This work describes and shows how to mitigate the spatial and temporal sources of variability identified with hybrid stimulation in both an invertebrate and vertebrate nervous system. This work was published in the June 2012 issue of *Journal of Neural Engineering* (Duke et al., 2012).

The work comprising Chapter V demonstrates the ability to induce a physiological motor response using hybrid electro-optical stimulation. This chapter characterizes the evoked force response and relates it to underlying thermal changes. Morphological changes in the tissue in response to hybrid stimulation are also discussed. This work is in press at *Journal of Neural Engineering*.

Chapter VI demonstrates and characterizes the use of infrared light to selectively block action potential initiation and propagation through a thermally mediated mechanism. This work was submitted to *Nature Communications* in November 2012.

Chapter VII summarizes the results presented in Chapter III through VI and draws conclusions pertaining to the objectives of this research. Future studies for this project and the broad societal impact are also discussed.

Appendix A contains data from a parametric investigation of hybrid-electro optical stimulation. This data is unpublished, but extends the characterization of this stimulation paradigm.

Appendix B describes a study investigating the application of infrared techniques for controlling the beating frequency of the embryonic heart. This work was published in the August 2010 issue of *Nature Photonics* (Jenkins et al., 2010).

2.4 References

Duke AR, Cayce JM, Malphrus JD, Konrad P, Mahadevan-Jansen A, Jansen ED (2009) Combined optical and electrical stimulation of neural tissue in vivo. Journal of Biomedical Optics 14:060501-060503.

Duke AR, Lu H, Jenkins MW, Chiel HJ, Jansen ED (2012) Spatial and temporal variability in response to hybrid electro-optical stimulation. Journal of Neural Engineering 9:036003.

Groves DA, Brown VJ (2005) Vagal nerve stimulation: a review of its applications and potential mechanisms that mediate its clinical effects. Neurosci Biobehav Rev 29:493-500.

Jenkins MW, Duke AR, Gu S, Chiel HJ, Fujioka H, Watanabe M, Jansen ED, Rollins AM (2010) Optical pacing of the embryonic heart. Nature Photonics 4:623-626.

Kern DS, Kumar R (2007) Deep brain stimulation. Neurologist 13:237-252.

Kottink AI, Hermens HJ, Nene AV, Tenniglo MJ, van der Aa HE, Buschman HP, Ijzerman MJ (2007) A randomized controlled trial of an implantable 2-channel peroneal nerve stimulator on walking speed and activity in poststroke hemiplegia. Arch Phys Med Rehabil 88:971-978.

Mou Z, Triantis IF, Woods VM, Toumazou C, Nikolic K (2012) A simulation study of the combined thermoelectric extracellular stimulation of the sciatic nerve of the Xenopus laevis: the localized transient heat block. IEEE Trans Biomed Eng 59:1758-1769.

Shannon RV (2012) Advances in auditory prostheses. Curr Opin Neurol 25:61-66.

Wells J, Kao C, Jansen ED, Konrad P, Mahadevan-Jansen A (2005) Application of infrared light for in vivo neural stimulation. Journal of Biomedical Optics 10:-.

Wells J, Konrad P, Kao C, Jansen ED, Mahadevan-Jansen A (2007) Pulsed laser versus electrical energy for peripheral nerve stimulation. J Neurosci Methods 163:326-337.

CHAPTER III

BACKGROUND

Austin R. Duke

Vanderbilt University, Department of Biomedical Engineering

Nashville, TN

3.1 Peripheral Neural Interfaces

The nervous system coordinates the actions of the body by relaying signals that encode information and provide instruction. Neural interfaces are designed to interact with the nervous system to impart or extract information. As defined by Navarro et al., a neural interface is a "transducer that establishes a neuro-technical contact between a technical device and a neural structure within the body" (Navarro et al., 2005). There are two goals of these neural interfaces: 1) to provide a missing or desired level of control over the nervous system's function; and 2) to acquire information for the purpose of monitoring the health of a particular system or to serve as command and/or feedback signals for driving prostheses (Grill et al., 2009). Neural prostheses interface with the nervous system at two different levels. The central nervous system (CNS), comprised of the brain and spinal cord, is a type of central processing unit for the nervous system, where inputs and outputs to/from other parts of the body are interpreted and controlled. The peripheral nervous system (PNS) links the brain and spinal cord to effector organs, relaying both motor and sensory information. The autonomic nervous system (ANS) is a subset of the PNS that controls bodily functions in an involuntary and reflexive manner. Interfacing at the level of the PNS allows for direct control of motor output as well as imparting and extracting sensory information from neural fibers returning information to the spinal cord and brain; however, effects of PNS stimulation must be interpreted in light of potential contribution by the ANS.

This overview and thesis will focus on current and novel PNS interfaces with primary attention given to controlling neuromuscular function. Full control of the PNS is attained through the selective stimulation or inhibition of a target neuronal population.

The need for restored or enhanced control of peripheral nervous function may arise from numerous causes including nerve trauma, tumor resection, diabetic neuropathy, profound deafness, etc. PNS interfaces are also useful when the connection between the PNS and CNS is severed, as in spine injuries, but the peripheral nerves are left intact. In these cases, neural interfaces bridge the broken gap to restore lost function. Current clinical applications for neural prostheses interfacing with the PNS include upper and lower limb prostheses (Kottink et al., 2007, Polasek et al., 2009), bladder prostheses (Chartier-Kastler et al., 2000), pain management (Slavin, 2008), cochlear and brain-stem auditory prostheses (Shannon, 2012) and vagus nerve stimulation for treatment of epilepsy and depression among other applications (Groves and Brown, 2005).

3.1.1 The Peripheral Nervous System

At its most basic level, the peripheral nervous system is composed of nerve cells, or neurons. Each neuron is comprised of a cell body, dendritic processes for receiving input signals, and an axon (or nerve fiber) for sending output signals to the effector organ or back to neurons in the CNS. Neurons communicate with other cells by passing electrical or chemical signals through synapses. Surrounding the axons is a layer of connective tissue, consisting of type III collagen fibrils and occasional fibroblasts between individual fibers known as the endoneurium (Figure III-1). The endoneurium is home to capillaries that provide nutrients to the axons and functions similar to the blood-brain barrier in that it prevents certain molecules from crossing into the endoneurial fluid. A group of axons forms a fascicle, which is wrapped and held together by a second layer of connective tissue known as the perineurium. The perineurium is composed of

concentric layers of flattened fibroblasts with perineurial cells connected by tight junctions. Groups of fascicles forming the nerve trunk are then held together with the nerve's blood supply by fatty connective tissue known as the epineurium.

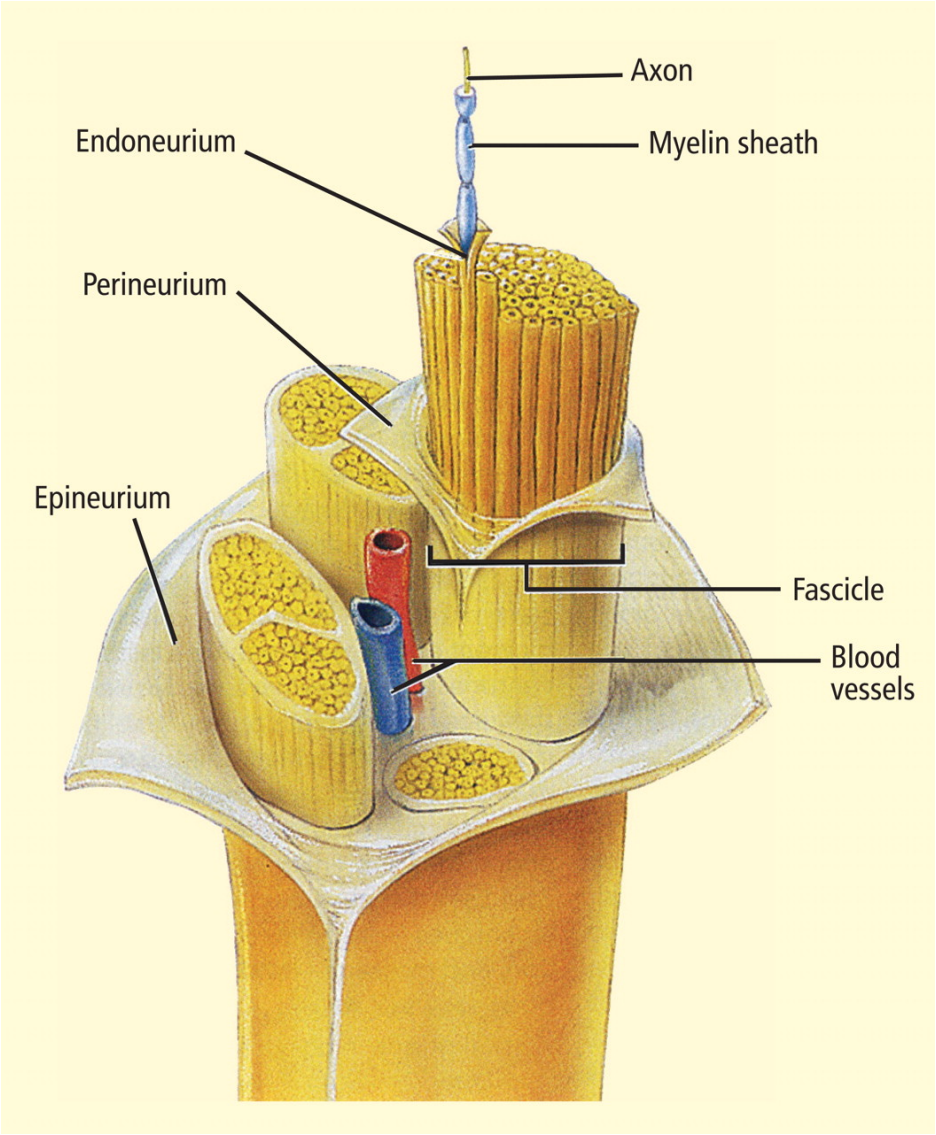

Figure III-1. Vertebrate peripheral nerve structure (Katona, 2010).

Both myelinated and unmyelinated fibers exist within the peripheral nerve trunks of vertebrates. Myelin, produced by Schwann cells in vertebrate peripheral nerves, serves as an insulating layer with the purpose of increasing the speed at which signals travel along the axons. Small intermodal gaps, known as nodes of Ranvier, are locations along myelinated axons where ionic flow occurs. Signals traveling along axons effectively "jump" from one node to the next to increase the conduction velocity. Myelin is approximately 40% water, with the dry mass composed of lipids (70-85%) and proteins (15-30%). This lipid/protein ratio is in contrast to most biological membranes which have a higher protein content (Quarles et al., 2006).

Within a nerve bundle, fascicles exhibit a somatotopic arrangement. Early studies of nerve fiber arrangement led to the discovery that within the distal portion of nerve trunks, most axons are arranged in fascicles innervating only a single muscle, while proximally in the nerve trunk there is a more homogenous arrangement of axons (Sunderland, 1968). However, the subject of topographical arrangement is somewhat controversial. There are two main viewpoints surrounding the arrangement and intermingling of axons between nerve fibers. One view is that fascicles behave like cables, remaining discrete throughout the length of the nerve. A second view is that fascicles split, rejoin and combine throughout the nerve. In a thorough review of efforts to elucidate the topography of peripheral nerve arrangement, Stewart concludes that there is a high degree of somatotopic organization throughout the length of the nerve (Stewart, 2003). Distally, the fascicles align with the cable view of arrangement and, although proximal nerve trunks are plexiform, topographical arrangement is largely maintained. The topographic arrangement of fascicles within peripheral nerves is significant for

peripheral neural prostheses as it implies that stimulation targeted at a single fascicle will yield selective activation of a single muscle (Sweeney et al., 1990).

The invertebrate nervous system shares many features with the vertebrate nervous system; however, there are some notable distinctions. The nervous system of invertebrates covers a wide range of complexity, ranging from a group of neurons with no central processing to advanced species that are able to gather, process and respond to information and stimuli in many different ways. The giant sea slug, *Aplysia californica*, is an example of a higher invertebrate with a simple nervous system compared to most vertebrates, but relatively advanced for invertebrates. Studies of the *Aplysia californica* have aided in the understanding of neural function and were integral to Kandel's work in discovering the physiological basis of memory (Kandel, 2001). The structure of *Aplysia* nerves is slightly different than that of vertebrates (Musio and Bedini, 1990). The core of each nerve is composed of axons and glial cells, with the cytoplasmic projections of the glial cells surrounding one or more axons. A fibrous sheath composed of connective cells and fibrous bundles surrounds the axons with a thin perineurial lamina lining the inside of the outer sheath. Depending on the nerve, axons may be arranged within the nerve according to size or may follow a homogenous distribution. While myelination is a defining characteristic of the vertebrate nervous system, most invertebrates do not have any form of myelination. To enhance the conduction velocity of signals along the *Aplysia* nerve, sodium channels are clustered to effectively produce salutatory conduction as is seen in vertebrate neurons (Johnston et al., 1996).

3.1.2 Signal transmission within the nervous system

Information within the nervous system is transferred by action potentials, brief electrical transients relayed between neurons and the cells with which they communicate. The frequency and spacing of these action potentials encodes information. Control of a neuron and its ultimate target (i.e. muscle) may be accomplished by "artificially" inducing these action potentials.

At rest, a neuron exists at a steady state, with osmotic forces across the cell membrane balanced and the concentration gradients of ions to which the membrane is permeable offset by a resting potential. The resting potential of a neuron may be determined using the Goldman-Hodgkin-Katz (GHK) equation, which calculates the weighted average of the sodium (Na^+), potassium (K^+) and chloride (Cl^-) Nernst potentials. The GHK equation for the resting transmembrane potential of a typical neuron is

$$V_m = \frac{RT}{F} ln \left[\frac{P_K[K]_e + P_{Na}[Na]_e + P_{Cl}[Cl]_i}{P_K[K]_i + P_{Na}[Na]_i + P_{Cl}[Cl]_e} \right] \quad \text{(III-1)}$$

where P_x is the membrane permeability of ion x, R is the universal gas constant, T is the absolute temperature and F is the Faraday constant. This equation assumes the membrane is homogenous and both the electric field and pressure are constant. Calcium (Ca^{2+}) typically plays a limited role in resting membrane potential due to its relatively low concentration and permeability. If divalent ions such as Ca^{2+} are to be considered, the GHK equation takes on a more complicated form (Hille, 2001). The membrane is more permeable to K^+ than Na^+. K^+ tends to diffuse out of the cell while Na^+ stays in the cell,

creating a net loss of ions out of the cell. Na^+/K^+-ATPase (or Na^+/K^+ pump) helps to balance osmotic forces and stabilize membrane voltage by actively pumping 3 Na^+ ions out of the cell and 2 K^+ ions into the cell. This maintains the cell's resting potential by keeping a high concentration of K^+ and a low concentration of Na^+ inside the cell. When the membrane is at rest, the relatively high membrane permeability of K^+ dominates the GHK equation, resulting in a transmembrane potential ranging from -60 to -90 mV.

When the transmembrane potential is depolarized beyond a given threshold (Figure III-2A), the voltage-gated Na^+ channels in the plasma membrane will open. Following its electro-chemical gradient, Na^+ rushes into the cell. After a delay, voltage-gated K^+ channels will also open resulting in K^+ flow out of the cell. At first, the Na^+ influx is greater than the K^+ efflux, which results in a positive-feedback mechanism where the Na^+ current opens more Na^+ channels. The newly opened Na^+ channels do not stay open indefinitely and undergo inactivation where they cannot be opened again for a finite duration of time (several milliseconds) (Figure III-2B). The time that the Na^+ channels are inactive, while the K^+ channels remain open, is known as the refractory period and serves the purpose of promoting unidirectional propagation of the depolarizing/repolarizing wave. The membrane K^+ and Cl^- conductances peak after the Na^+ conductance and will result in a dampening and limited hyperpolarization of the transmembrane potential. Action potentials are “all-or-none”, meaning that the magnitude of depolarization is independent of the stimulus by which it is produced.

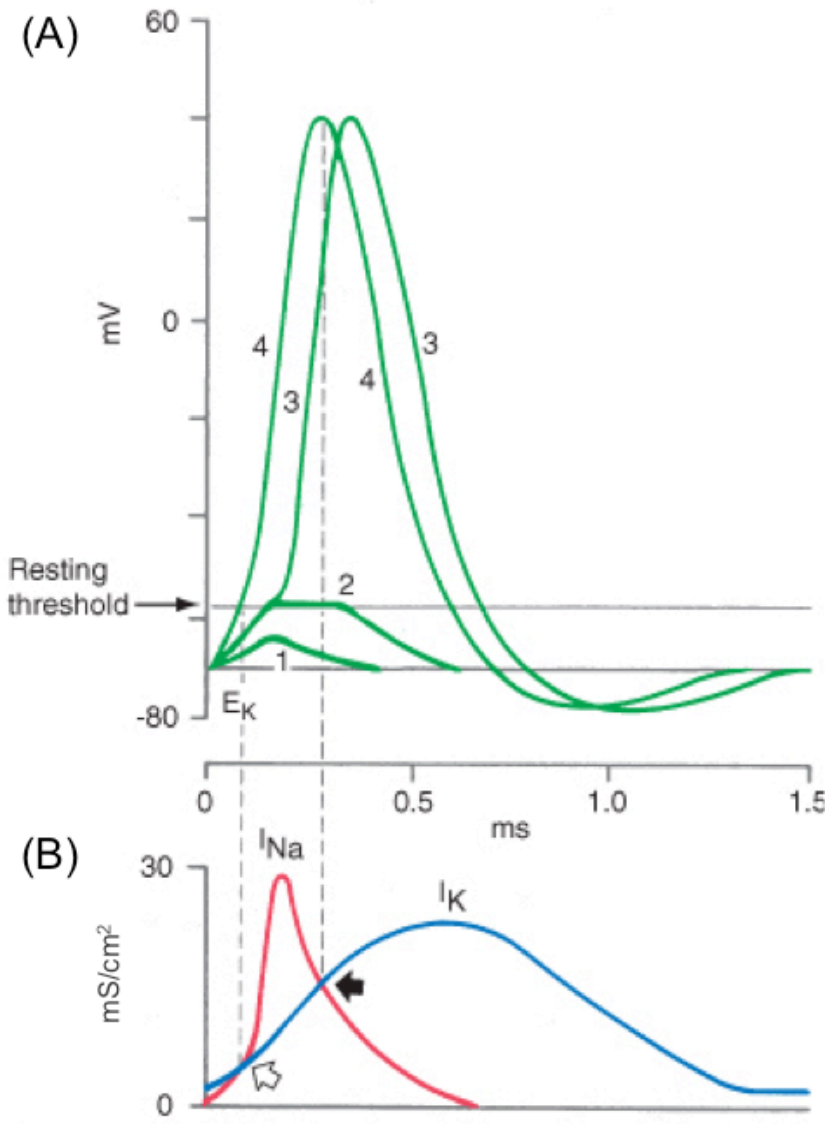

Figure III-2**.** Diagram of the neuronal response to stimuli of different magnitudes. (A) Responses due to (1) sub-threshold, (2) just below threshold, (3) above threshold and (4) supra-threshold stimuli; (B) Timing of sodium and potassium currents. From (Haines and Ard, 2002).

3.2 Neural Stimulation

3.2.1 Electrical Nerve Stimulation

While depolarization of a neuron is naturally accomplished via synaptic currents, a propagating action potential may also be generated following depolarization of the transmembrane potential via stimulation by an electrode (either intracellular or extracellular). Since Luigi Galvani's famous frog experiments in the late 1780's, electrical methods have served as the gold standard for stimulating and monitoring excitable biological tissues. During electrical stimulation, depolarization is achieved by the flow of ionic current between two or more electrodes, where at least one is near the target tissue. The rate of change in transmembrane potential for both myelinated and unmyelinated fibers is determined by the second order difference of the extracellular field potentials (or the second spatial derivative of the voltage along the axis of the nerve) (Rattay, 1986). This function is known as the activating function and is responsible for the changes in transmembrane potential.

Current clinical neural interfaces employ electrical methods of stimulation due to proven efficacy and safety *in vivo*. Compared to alternative methods such as chemical, mechanical or magnetic stimulation, electrical techniques are generally more accurate, reliable, reproducible, and precise. Electrical techniques are well suited for evoking neural activity, as stimulus strength and timing are easily controlled through a wide range of tunable parameters that may be tailored to suit a given application.

3.2.1.1 Mechanism of extracellular electrical stimulation

A myelinated nerve fiber is modeled by the equivalent electrical circuit shown in Figure III-3. Included in this model are the intra-axonal conductivities G_a between each node of Ranvier, the variable nodal membrane conductivities G_m and the nodal membrane capacitances C_m. The model also incorporates intra-axonal (V_i), extracellular (V_e) and resting membrane (V_r) potentials.

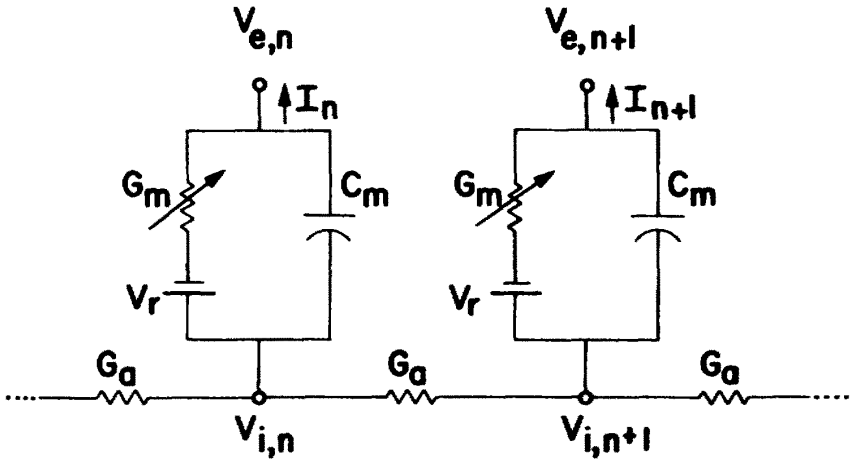

Figure III-3. Myelinated nerve fiber modeled as an equivalent electrical cable network (McNeal, 1976). See text for explanation of symbols.

When a stimulus current is applied, part of the current loads the membrane capacitance, while the other part passes through the ion channels. Analyzing the currents leading into node *n* and subsequently rearranging leads to the following equation for the transmembrane potential at node *n*, V_n, with respect to time:

$$\frac{dV_n}{dt} = \left(G_a \cdot \left(V_{n-1} - 2V_n + V_{n+1} + V_{e,n-1} - 2V_{e,n} + V_{e,n+1}\right) - I_{i,n}\right)/C_m \tag{III-2}$$

where V_n is given by $V_{i,n} - V_{e,n} + V_r$. With $G_a = 1/r_s\Delta x$, where $r_s = 4p_i/\pi d^2$ (p_i = axoplasm resistivity and d – axon diameter) and c_m is the capacitance/cm^2 such that $C_m = \pi dLc_m$, equation (III-2) becomes:

$$\frac{dV_n}{dt} = \frac{1}{c_m}\left\{\frac{1}{r_s\pi dL\Delta x}\left(V_{n-1} - 2V_n + V_{n+1} + V_{e,n-1} - 2V_{e,n} + V_{e,n+1}\right) - (i_{Na} + i_k + i_L + i_P)_n\right\} \tag{III-3}$$

where L is the corrected length of one active axonal segment and the generic ionic current $I_{i,n}$ is replaced by the Hodgkin-Huxley and Frankenhaeuser-Huxley equations for the ionic currents of each species (McNeal, 1976, Rattay, 1986). Rattay identified the second difference quotient of the extracellular potential from Equation (III-3) as being responsible for activation inside of the axon (Rattay, 1986). He named this the *activating function* (AF_n), where

$$AF_n = \left(V_{e,n-1} - 2V_{e,n} + V_{e,n+1}\right) \tag{III-4}$$

Membrane depolarization at node *n* is the result of a positive value for AF_n (McNeal, 1976), which according to equation (III-4) happens when $V_{e,n}$ is more negative than the average value of $V_{e,n-1}$ and $V_{e,n+1}$. This scenario occurs when node *n* is near the cathode. Cathodic stimulation is the more efficient means of electrical stimulation, with threshold currents for excitation 3-7 times lower than for anodic stimulation (Holsheimer, 2003). At the nodes nearest the cathode (negative electrode), transmembrane current flows out of the axon inducing depolarization. At distant nodes, transmembrane current flows into the axon yielding hyperpolarization, creating an effect known as virtual anodes. Generally, depolarization occurs at a few nodes and is relatively strong, whereas hyperpolarization is weakly distributed over a greater number of nodes.

For unmyelinated fibers, introducing $C_m = \pi d \Delta x c_m$ to equation (III-2) yields:

$$\frac{dV_n}{dt} = \frac{1}{c_m}\left\{\frac{1}{r_s d\pi}\left(\frac{V_{n-1} - 2V_n + V_{n+1}}{\Delta x^2} + \frac{V_{e,n-1} - 2V_{e,n} + V_{e,n+1}}{\Delta x^2}\right) - (i_{Na} + i_k + i_L)_n\right\} \tag{III-5}$$

and the corresponding activating function is

$$AF_n = \frac{\left(V_{e,n-1} - 2V_{e,n} + V_{e,n+1}\right)}{\Delta x^2} \tag{III-6}$$

Differences between the myelinated and unmyelinated case only become apparent when the distance between the stimulating electrode and the axon is smaller than the intermodal length (Rattay, 1986).

3.2.1.2 Sub-threshold electrical stimulation

In 1938, Hodgkin took the first look at the response of nerve fibers to a sub-threshold electrical stimulus (Hodgkin, 1938). What he found was that the assumption of an all-or-nothing law referred to a "propagated disturbance" (i.e. action potential) and did not exclude the possibility of graded, non-propagated reactions in the stimulated region.

From his work, Hodgkin noted several key observations related to sub-threshold electrical stimulation. When the electrical stimulus is weak and either cathodic or anodic, Hodgkin found it produces an associated change in potential that behaves as a passive accumulation of charge at the nerve membrane (Figure III-4). However, when the stimulus approached threshold, an additional response, indicative of contribution from a nonlinear active component of the membrane, became present (Figure III-5). The change in membrane potential was directly proportional to the strength of the stimulus, while the active response increased at an accelerating rate as the stimulus approached threshold. The relationship between the stimulus and the responses of the passive and active components were also shown to be different. The potential associated with the passive component rose during the stimulation period followed by an exponential decay, whereas the active response started with an initial inflexion, which continued to grow after the end of the stimulus. Similarly, Hodgkin concluded that the duration of the active response increased and its maximum was delayed further as the stimulus approached threshold.

Interestingly, causing the nerve to go into a refractory period negated the active component of the response, while the passive depolarization was only slightly reduced. In relation to the spatial spread of the passive and active components, Hodgkin demonstrated that the passive component fell off by 67% within 0.5 mm, whereas the active component only diminished by 33% (and may extend for greater distances under certain circumstances). The principles of sub-threshold electrical stimulation as identified by Hodgkin have since been utilized in the development of neural interfaces to achieve selective recruitment of axons through the generation of sub-threshold electrical field-steering currents (Sweeney et al., 1995, Grill and Mortimer, 1997).

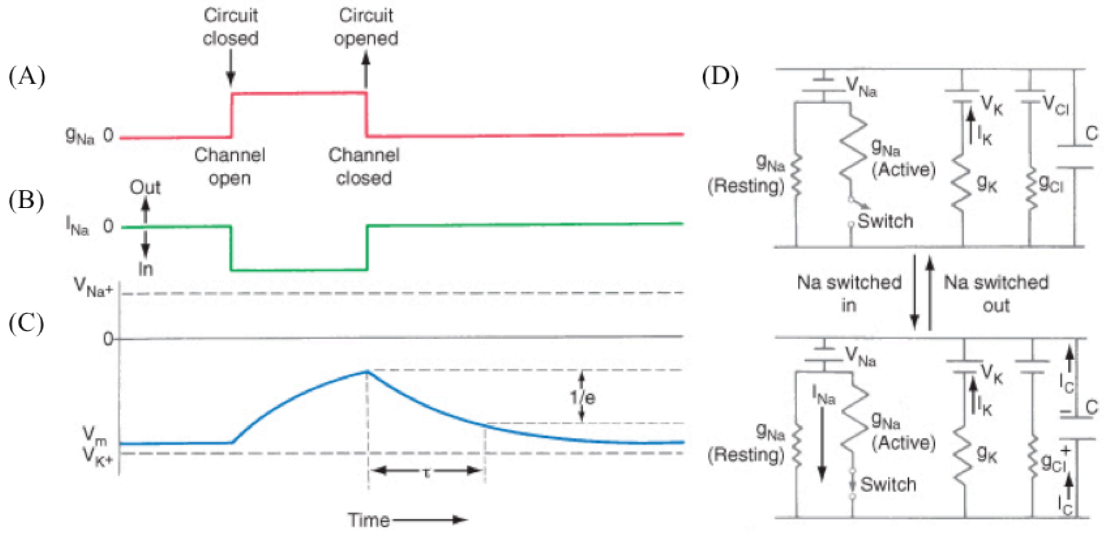

Figure III-4. A sub-threshold electrical stimulus results in a passive change in membrane potential. When the Na^+ channels are first opened the conductance increases (A) and an inward current begins to flow (B). With a sub-threshold electrical stimulus, the membrane is modeled by the equivalent circuit in (D), which yields a voltage response mimicking the passive charging and discharging of a capacitor (C). From (Haines and Ard, 2002).

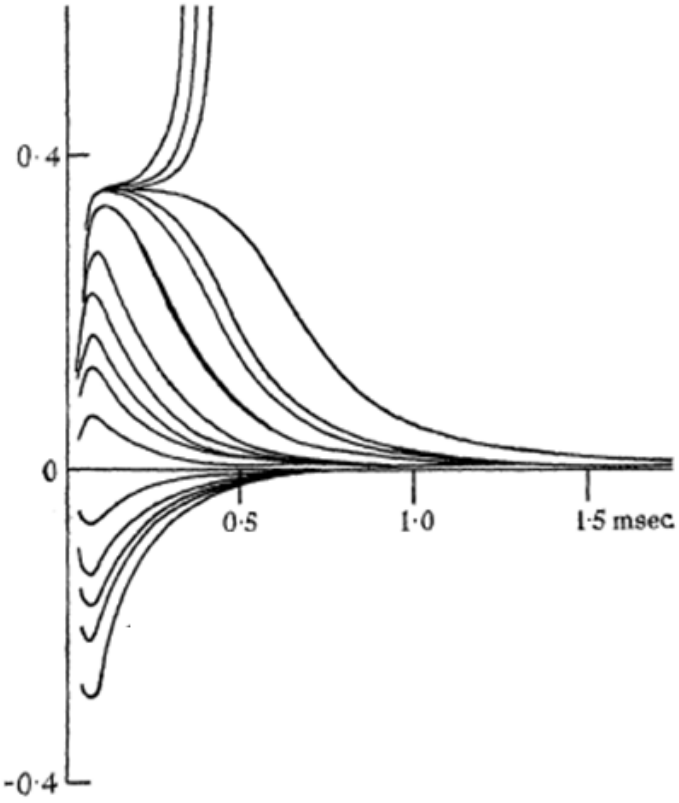

Figure III-5. Sub-threshold responses of the crustacean nerve fiber to electrical stimuli 50 μs in duration with varying intensity. Note how an active membrane component becomes present as the stimulus approaches threshold (50-100% of threshold). The y-axis represents the response measured as a fraction of a propagated action potential. From (Hodgkin, 1938).

3.2.1.3 Selectivity of Electrical Stimulation

The selectivity of neural interfaces is critical not only to their performance, but also their ultimate clinical utility and acceptance. It is selectivity that allows for stimulation of a desired target without unwanted activation of surrounding neural structures. Non-selective stimulation may lead to lack of coordinated movement when fascicles innervating multiple muscles are not synergistically activated, or unwanted motor function when a muscle is activated at an inappropriate time or pain if sensory neurons are improperly recruited.

The goal of a selective neural interface is to activate a specific axon or subset of axons without activating a greater population. There are two types of selectivity that are generally considered: *fiber diameter selectivity* and *spatial selectivity* (Grill and Mortimer, 1995). With fiber diameter selectivity, a sub-population of axons having similar diameter are recruited without the simultaneous activation of axons having different diameters. Spatial selectivity refers to the activation of a group of axons in a given location without activating neighboring axons.

Achieving fiber diameter selectivity may be accomplished through choice of pulse duration. As a general rule, nerve fibers with a large spacing between nodes of Ranvier (typically larger diameter fibers) will have lower stimulation threshold currents for electrical stimulation than nerve fibers with smaller internodal distances (Rattay, 1989, Grill and Mortimer, 1995). Using short, rectangular stimulus pulses increases the difference in threshold currents for stimulation as a function of fiber diameter for fibers located the same distance from the stimulating electrode. For larger diameter fibers (i.e. motor neurons), this effect is most noticeable with the extracellular stimulating electrode

located directly above the node of Ranvier. If the stimulating electrode is displaced between two nodes, then smaller diameter fibers closest to the stimulating electrode will be activated at lower currents. This is due to the location of stimulation occurring closer to the node of Ranvier of the smaller fiber. Thus, to maximize the efficacy of neural interfaces for achieving fiber diameter selectivity of large motor neurons, it is advisable to use electrode contacts that are comparable in size to the internode spacing of the larger diameter fibers (Grill and Mortimer, 1995).

Spatial selectivity occurs as a function of proximity of the target axon to the electrode location. As a rule, stimulation threshold currents are lower for fibers closest to the stimulating electrode. In addition, the use of short duration stimuli will increase the threshold difference between nerve fibers having the same diameter located at different distances from the stimulating electrode. The relative location of the target axon and the stimulating electrode also play a role in fiber diameter selectivity. Overall, the largest diameter fibers (i.e. greatest internode spacing) in close proximity to the stimulating electrode will experience the greatest membrane depolarization. Thus, these fibers will require lower currents for stimulation than distant, small diameter nerve fibers (Rattay, 1989, Grill and Mortimer, 1995, Holsheimer, 2003).

While some degree of selectivity is attained through choice of stimulus waveform, a large focus for the development of peripheral neural interfaces is on the spatial component of selectivity and bringing the electrical stimulation contacts into closer proximity with the target neurons. There are many engineering challenges to accomplish spatial selectivity, which are accompanied by numerous potential solutions. Navarro et al. provide an excellent review of current peripheral neural interfaces (Navarro et al., 2005).

When designing a neural interface to interact with the peripheral nervous system, a consideration that cannot be overlooked is the direct relationship between selectivity and invasiveness (Figure III-6). A clinically applicable interface must solve the optimization problem of achieving selectivity without compromising long-term viability.

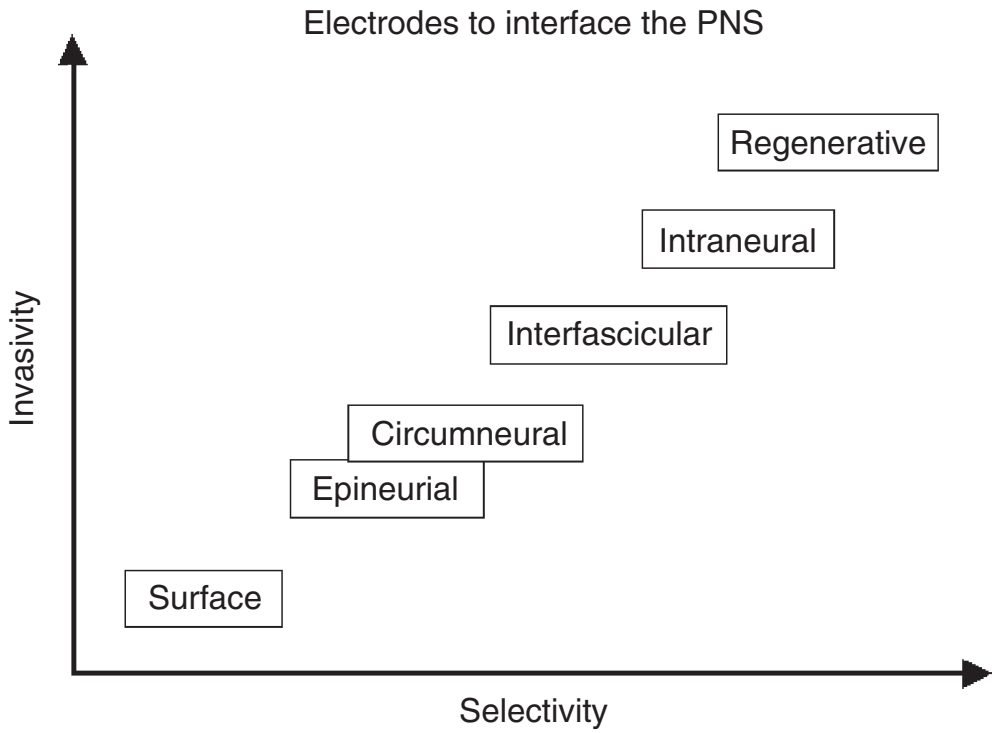

Figure III-6. A general classification of peripheral neural interfaces with respect to the selectivity and invasiveness of each interface (Navarro et al., 2005).

An example of a recent innovation in electrical stimulation interface design that increases selectivity without increasing invasiveness is the Flat Interface Nerve Electrode (FINE). The FINE is a modification of circumneural cuff electrodes that gently reshapes the nerve to bring central fascicles into closer proximity with the electrode contacts and to increase the surface area of the nerve so that more electrical contacts may be added. FINE cuffs are able to achieve fascicular selectivity in stimulation and recording (Tyler and Durand, 2002). The small noncircumferential forces are able to reshape the nerve with none or negligible changes in the nerve's physiology, histology or blood-nerve barrier permeability (Tyler and Durand, 2003). However, the perineurium surrounding the individual fascicles has high impedance, resulting in a uniform voltage distribution and preventing sub-fascicular selectivity.

Intraneural electrode arrays such as the Utah Slanted Electrode Array (USEA) and polymer longitudinal intrafascicular electrode (polyLIFE) penetrate the perineurium to allow direct electrical contact within individual fascicles and improve selectivity beyond what is attainable by extraneural electrodes (Malmstrom et al., 1998, Branner and Normann, 2000). While these intraneural arrays achieve remarkable selectivity, invasiveness is greater than for extraneural electrodes (Figure III-6). In the cat sciatic nerve, USEAs having up 70-100 contacts were monitored for up to 7 months to evaluate safety after extended periods of chronic implantation (Branner et al., 2004). Histology indicated normal morphology and fiber density around the electrodes; however the number of electrical contacts that remained functional for stimulation decreased with time. Proof-of-concept for the USEA has been demonstrated, but evaluation of the long-term safety and function is still needed.

Along with interface design, electrode configuration contributes to the selectivity of electrical stimulation. Electrical fields become more restricted when moving from monopolar stimulation to bipolar and tripolar stimulation (Holsheimer, 2003). With monopolar stimulation, the cathode is placed near the stimulation target and the anode is placed at a distance (generally several times larger than the distance between the cathode and the target). Because of this large separation, the current injected during stimulation is distributed in a relatively even profile (with the relative impedances of the tissue disrupting the uniformity). As the anode is brought nearer to the cathode (i.e. bipolar configuration), current flow begins to preferentially flow along the cathode-anode axis. In this configuration, the activating function of the fibers located parallel to the cathode-anode axis is increased. Thus, selectivity is increased while stimulation thresholds of the fibers nearest to the cathode-anode axis are decreased. These effects are amplified when the cathode is flanked (or "guarded") by anodes on both sides; a configuration known as tripolar stimulation. While thresholds are lower for neural fibers parallel to the cathode-anode axis in bipolar and tripolar stimulation, these configurations have higher stimulation thresholds for producing functional responses (Tarler and Mortimer, 2003). An added limitation is the requirement for additional leads and electrical contacts, which increase the risk of failure and crowd the implant environment. Nerve cuffs such as the FINE demonstrate comparable selectivity with monopolar and tripolar stimulation due to the cuff boundaries acting as virtual anodes (Tarler and Mortimer, 2003).

3.2.1.4 Safety of Electrical Stimulation

A primary strength of electrical methods of neural excitations is the ability to provide safe, chronic stimulation. Merrill composed a review of efficacious and safe protocols for electrical stimulation (Merrill et al., 2005), which is summarized here.

While stimulation-induced tissue damage is not well understood, there are two primary classes of mechanisms that are proposed: 1) overstimulation leading to a change in the local environment, and 2) the creation of toxic electrochemical reaction products. As suggested by Merrill, the fundamental design criterion for a safe stimulation protocol is that "the electrode potential must be kept within a potential window where irreversible Faradaic reactions do not occur at levels that are intolerable to the physiological system or the electrode." Faradaic reactions are one of the two primary mechanisms of charge transfer at the electrode/electrolyte interface, along with non-Faradaic, capacitive mechanisms. Unlike non-Faradaic mechanisms, which yield reversible charge redistribution along the cell membrane, Faradaic charge injections result in electron transfer between the electrode and electrolyte, and an accompanying change in the chemical composition of the electrolyte due to these reduction or oxidation reactions. Faradaic reactions may be reversible or irreversible, with the degree of reversibility depending on the rate of electron transfer at the electrode/electrolyte interface and the rate of mass transport. Faradaic reactions with fast kinetics and slow mass transport allow for reaction products to be reversed before they diffuse away from the electrode by reversing the electrode polarity. If irreversible reaction products do occur and diffuse away from the electrode, they will change the chemical environment and potentially yield

species that are damaging to the tissue and/or electrode. Thus, the general rule is to design a stimulating protocol that will avoid irreversible Faradaic reactions.

The desired stimulation protocol must be selected to optimize stimulation efficacy and safety. Pertinent factors associated with the stimulation protocol include the charge per pulse, waveform type and electrode material. The charge per pulse must be balanced such that it is sufficiently high for action potential initiation, but sufficiently low so as not to induce deleterious Faradaic reactions. Shorter pulses, on the order of tens of microseconds, are best for efficacious stimulation that will avoid Faradaic reactions occurring at longer pulse durations. However, these short pulse durations are not always physiologically appropriate and, given the higher stimulation threshold currents relative to longer pulse durations, may not be possible with battery powered current stimulators.

Several potential stimulating waveforms are shown and rated for their relative efficacy and safety in Figure III-7. While a monophasic stimulus waveform (Figure III-7a) is the most efficacious, it is not well suited for long-term or chronic stimulation due to a propensity for tissue damage. Monophasic pulses achieve greater overpotentials (difference between the electrode's potential and its equilibrium potential), thus causing the Faradaic current to make up a greater fraction of the total injected current. Also, because there is no reversal phase, the electrode capacitance slowly discharges through Faradaic reactions during the inter-pulse interval, allowing unwanted reaction species to diffuse through the tissue throughout the total stimulation duration. Biphasic stimulus waveforms mitigate the harmful effects of monophasic stimulation by providing an initial depolarizing phase that elicits the desired action potential, which is subsequently followed by a hyperpolarizing phase to reverse the direction of electrochemical processes

that occurred during the stimulating phase. With a charge-balanced biphasic waveform (Figure III-7b), changes resulting from Faradaic reactions will be negated if these processes are reversible. However, irreversible reactions during the anodic phase causing electrode corrosion may still occur. A second concern with charge-balanced biphasic waveforms is that the reversal phase will not only reverse Faradaic reactions, but will also suppress action potential initiation; thus increasing stimulation threshold (i.e. charge per pulse) relative to monophasic stimulation. By adding an interphase delay (Figure III-7d) the stimulation threshold becomes much closer to that for a monophasic waveform. Reducing the charge of the second (anodic) phase seeks to reverse reactions resulting from the Faradaic portion of the injected current, while not causing irreversible reactions in the anodic phase (Figure III-7c). Figure III-7e and Figure III-7f show additional biphasic waveforms that can be used to address concerns of tissue damage and corrosion by varying the rate at which the injected current is reversed.

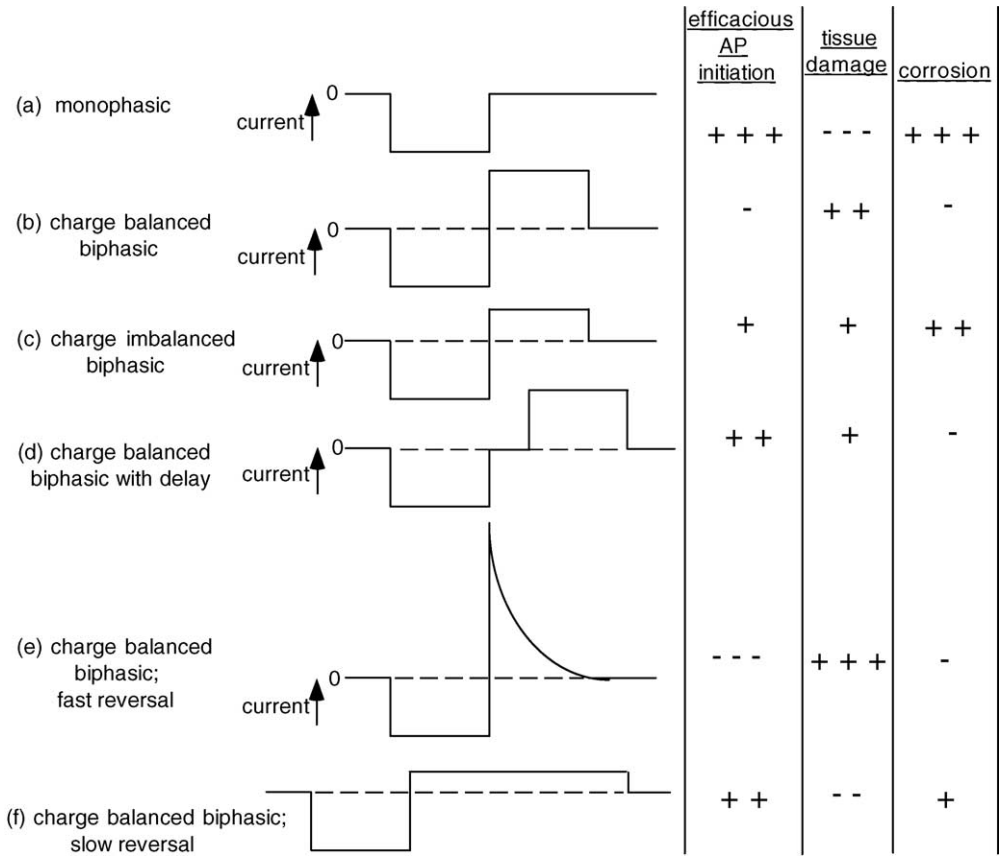

Figure III-7. Comparison of prototypical stimulation waveforms in regards to their relative efficacy and safety, where "+++" is the best (most efficacious / least damaging) and "---" is the worst (Merrill et al., 2005).

The selection of a suitable electrode material is also critical to the safety of electrical stimulation. According to Merrill, the ideal material for a stimulating electrode will meet six requirements: the material must be 1) biocompatible in the absence of stimulation; 2) mechanically suited for the intended application; 3) efficacious for stimulation; 4) lacking Faradaic reactions that are beyond what is tolerable for the surrounding tissue; 5) lacking Faradaic corrosion reactions that will cause premature failure of the electrode; and 6) acceptably stable (in regards to material characteristics (e.g. impedance)) for the implant lifetime. An example of a material meeting these criteria (or can be modified to meet these criteria) is platinum (Pt), which is shown to be non-toxic and non-reactive (Chouard and Pialoux, 1995, Majji et al., 1999). There are potentially harmful reactions that result from using Pt including electrolysis of water, oxidation of saline, oxidation of metal, oxidation of organics and reduction of hydrogen ions (Brummer and Turner, 1977). These reactions should be avoided and can be mitigated using charge-balanced biphasic waveforms. Double layer charging, surface oxidation and hydrogen atom plating are three electrochemical processes by which Pt may safely inject charge into the nervous system (Brummer and Turner, 1977). In regards to mechanical suitability, adding iridium increases the mechanical strength of platinum, which is a relatively soft material.

By choosing an appropriate stimulus waveform and electrode material, chronic safe electrical stimulation is possible. Clinically safe electrical neurostimulation is currently being applied to neural targets including the vagus nerve (Schachter, 2002), auditory nerve (Xu et al., 1997), and sacral nerve (Hassouna et al., 2000) among others.

3.2.1.5 Electrical neuromuscular stimulation

A primary goal of peripheral neural interfaces is to restore or regain control of motor function. Functional electrical stimulation (FES) is a technique where electrical currents are used to stimulate nerves that are affected by some physical trauma or disorder that inhibits or limits the intrinsic activation of these nerves by the body. With FES the targeted nerves innervate muscles, allowing for regained motor function through electrical control.

Skeletal muscle is one of the three primary muscle types found in the body (cardiac and smooth muscle are the other two) and is responsible for maintaining posture as well as voluntary movements. In the absence of neural trauma or neurological disorder, skeletal muscle is controlled by the nervous system. Electrical signals are passed from the CNS to the motor neuron innervating the target muscle. The motor neuron and innervated muscle form what is known as the motor unit. Muscles responsible for gross motor movements are comprised of relatively few motor units that control many muscle fibers. Muscles responsible for dexterous or fine movement contain many motor units, with each controlling only a few muscle fibers. The body activates each muscle in a graded fashion to accomplish a desired task.

A single action potential from a motor neuron results in a quick contraction of a single motor unit. To achieve a sustained contraction, adjacent motor units are asynchronously recruited at 6-8 Hz so that a contraction is shared by multiple motor units and can be maintained with a slow onset of fatigue (Lynch and Popovic, 2008). When the connection between the CNS and the innervated muscle is interrupted, FES is used to artificially activate the motor units. Electrodes provide trains of short electrical pulses

and tension force is determined by the stimulus frequency and intensity. Unlike the asynchronous recruitment of motor units that occurs naturally, FES recruits the motor units synchronously (with each pulse), thus requiring higher stimulus repetition rates to achieve tetanic contractions. An increased rate of muscle fatigue results from the use of higher stimulation frequencies. Thus, it is desirable to use the minimum stimulus repetition rate possible. Typically, stimulus repetition rates of 12 – 15 Hz are the minimum that may be used for muscles that are conditioned to have long twitch durations (Peckham and Knutson, 2005); however, 20 – 40 Hz is common (Lynch and Popovic, 2008). Combining a chosen interface design with an appropriate waveform allows for efficacious, selective and safe control of motor units acutely and long-term so that muscle control may ultimately be restored.

3.2.1.6 Limitations of electrical nerve stimulation

While electrical stimulation has served as the gold standard of neural stimulation both in research and in clinical use, there are several inherent limitations to its effectiveness. One such limitation is the necessity of contact between the electrode and the neurons. While the notion that intracellular electrodes impaling the neuron will cause damage is intuitive, extracellular electrodes also pose risks of tissue damage. Damage due to electrical stimulation is of two primary types: mechanical damage due to the mere presence of the electrode and damage due to electrical stimulation (Agnew and McCreery, 1990). Mechanical damage includes abrasion due to tension on the nerve or relative movement between the nerve and electrode. Damage due to electrical stimulation includes interstitial edema and early axonal degeneration and may result from

electrochemical reactions at the electrode-tissue interface. In chronic stimulation scenarios, interstitial edema may occur at two days and early axonal degeneration after one week if parameters are not properly optimized.

The presence of a stimulation artifact also limits the utility of electrical stimulation. With traditional electrophysiological studies, both stimulation and recording occur in the electrical domain; therefore, an electrical stimulus will directly appear on the neural recording. In some applications, recording the evoked potentials becomes more difficult and recording from a site in the vicinity of the stimulus location is prohibited (Crum and Strommen, 2007). While there are many strategies for eliminating or mitigating a stimulus artifact, its presence remains a fundamental limitation.

Perhaps the most restrictive aspect of electrical stimulation is its relatively limited spatial selectivity due to current spread, yielding an electric field many times larger than the physical size of the electrode (Townshend et al., 1987, Liang et al., 1999). Although the threshold for stimulation increases as the square of the distance from the tip of the electrode, there are many adverse effects stemming from unwanted current spread (Bagshaw and Evans, 1976, Nowak and Bullier, 1996, Tehovnik, 1996). One such example is the small but significant number of cochlear implant patients who experience stimulation of their facial nerve by current originating from their cochlear implant (Bigelow et al., 1998). From a functional perspective, even state-of-the-art cochlear implants experience limitations in the number of independent frequency bands that can be encoded (Berenstein et al., 2008). Although it has long served as the method of choice for neural activation and monitoring, limited spatial selectivity, necessity of contact and the presence of a stimulation artifact are all limitations of electrical stimulation. The fact that

electrical stimulation remains fundamentally unchanged since its discovery is motivating the pursuit of alternative neural stimulation modalities.

3.2.2 Optical Technologies for Neural Stimulation

Although electrical stimulation has long served as the gold standard for neural stimulation, there are other well-known methods of action potential initiation including mechanical, chemical, thermal, magnetic and optical. Of these alternative techniques, optical methods offer an intriguing combination of spatial and temporal precision that has motivated substantial investigation of their capabilities in recent years. The ability to modulate and even evoke action potentials in neurons using light has been known for decades, with Arvanitaki and Chalazonitis (Arvanitaki and Chalazonitis, 1961), as well as Fork (Fork, 1971), showing that light could be used to both excite and inhibit neural activity. However, it was not until recently that optical techniques of neural control began to flourish with the discovery of high spatial and temporal resolution stimulation via caged compounds (Adams and Tsien, 1993), optogenetics (Boyden et al., 2005, Li et al., 2005) and infrared neural stimulation (INS) (Wells et al., 2005b). These novel optical techniques are generating exciting research pertaining to studies of neural function and are potentially intriguing options for many clinical applications.

3.2.2.1 Optical uncaging

Optical uncaging is one of the oldest methods of photostimulation. The premise behind the technique is that the function of a neurotransmitter is masked by a photoremovable caging group (Adams and Tsien, 1993). When exposed to the

appropriate optical illumination, the covalent bond joining the neurotransmitter and the caging group is cleaved, converting the neurotransmitter from an inactive state to an active state. This technique is advantageous for studying the many biological processes characterized by spatiotemporal dynamics that are beyond the capability of traditional tools. Specifically, (1) caging technology offers a precise starting point (i.e. $t = 0$) for studying downstream cellular events; (2) caged inhibitors may be used to study the role of biomolecules with varying temporal dynamics as they pertain to distinct phenomena, such as synaptic vesicle neurotransmitter release (Kuner et al., 2008); and (3) caged sensors may be used to acquiring visual information at precise time points during biological events (e.g. mitosis).

Unfortunately, optical uncaging is not suitable for many clinical applications. The bond between neurotransmitter and most caging groups requires ultraviolet (UV) (<300 nm) light for photolysis. This is due to the relative simplicity with which these compounds can be synthesized in comparison to molecules that are responsive to visible and/or infrared wavelengths (Adams and Tsien, 1993). Because UV light is both toxic to tissue and limited by scattering, two-photon methods of optical uncaging are being developed that allow precise mapping of neuronal circuits (Callaway and Yuste, 2002, Nikolenko et al., 2007). However, the sophisticated nature of these laser sources will pose significant challenges to the miniaturization of this technique that must be overcome for potential clinical applications (Chernov et al., 2012).

3.2.2.2 Optogenetic stimulation

Optogenetics provides a means of spatially and temporally precise stimulation with optical wavelengths and stimulus intensities that are non-toxic to neural tissue. At its core, optogenetics is "the combination of genetic and optical methods to achieve gain or loss of function of well-defined events in specific cells of living tissue" (Deisseroth, 2011). This is accomplished by introducing alga-derived light-activated ion channels into targeted neuronal populations through viral vectors or transgenic species. Upon absorbing a photon, the channel structure undergoes conformational changes leading to current flow (Fenno et al., 2011). The light activated cation channel channelrhodopsin-2 (ChR2) was first used to produce a depolarizing photocurrent in response to blue light (Boyden et al., 2005, Li et al., 2005). While ChR2 was used to demonstrate the potential of optogenetics for neural excitation there are limitations to this particular tool, including desensitization and a deactivation time constant that limits temporal precision. In recent years there have been several additional optogenetic tools developed for excitation that respond to other wavelengths of light, address various limitations and concerns and/or are tailored for specific applications (Fenno et al., 2011).

Although the components of optogenetics have been available and/or in use for some time, the application of optogenetics as a means for neural control began in 2005 (Boyden et al., 2005, Li et al., 2005). Since then, this technique has flourished to become a widely used tool in the neuroscience community, with *Nature* naming optogenetics its "Method of the Year" for 2010 (Anonymous, 2011). Optogenetic techniques have been applied to applications ranging from the deconstruction of parkinsonian neural circuitry (Gradinaru et al., 2009) to the orderly recruitment of peripheral motor neurons (Llewellyn

et al., 2010). Numerous advanced delivery methods, which take advantage of the capabilities of low power and small form factor light-emitting diodes (LEDs) for optogenetic stimulation, have also been developed to aid the application of optogenetics for animal studies (Aravanis et al., 2007, Iwai et al., 2011, Wentz et al., 2011).

While optogenetics is a useful tool for the study of neural circuitry and may have broad therapeutic applications, the primary limitation of this technology is that it is currently confined to limited species of transgenic animals and nonclinical uses (LaLumiere, 2011). For humans and species lacking transgenic models, opsins may be introduced to neural targets via viral transduction. The adeno-associated virus (AAV) is used to deliver genes to neural tissue for human gene therapy (Kaplitt et al., 2007, Christine et al., 2009), and is a good candidate for the delivery of the necessary elements required for optogenetics (Diester et al., 2011). However, successful gene therapy in humans has yet to exhibit overwhelming success and there are many obstacles that must be overcome before this technique is effective and can be applied to optogenetics (Verma and Somia, 1997, Daya and Berns, 2008).

3.2.3 Infrared Nerve Stimulation

Whereas stimulation of caged compounds and microbial opsins inherently require exogenous additives, toxic UV light and/or engineered or genetically modified neurons, INS is a neural stimulation modality where pulsed, low-intensity infrared light directed on a nerve will generate a propagating action potential within an endogenous neural system. Like optical uncaging and optogenetics, the significance of INS is that it is not subject to the fundamental limitations of electrical stimulation. Specifically, INS provides

a contact-free, artifact-free and spatially precise means of neural stimulation with radiant exposures (J/cm^2) below the threshold for laser-induced tissue damage (Wells et al., 2005a, Wells et al., 2005b, Wells et al., 2007b, Wells et al., 2007c). INS also lacks any electrochemical junction between the source of stimulation and the activated tissue.

Figure III-8 presents a comparison of INS and electrical stimulation. First, electrical stimulation requires contact with the nerve bundle (Figure III-8A), whereas the delivery of light to the nerve from the optical fiber is contact free, as illustrated in the cartoon in Figure III-8B. Second, the compound nerve action potentials (CNAPs) in each of the nerve fascicles stimulated electrically contain a stimulation artifact (Figure III-8A), while INS lacks any stimulation artifact (Figure III-8B). Finally, the overall emphasis of the diagram is the potential for superior spatial resolution of INS compared to electrical stimulation. It can be seen that INS recruits a significantly smaller population of axons when compared to electrical stimulation. This is exhibited not only by the smaller magnitude of the CNAP from the nerve fascicle stimulated by INS, but also by the fact that only the gastrocnemius fascicle is stimulated, whereas both the gastrocnemius and the biceps femoris fascicles are stimulated electrically. With INS, the response is confined to the area just beneath the tip of the optical fiber. However, this demonstration is somewhat biased towards INS and recent developments have greatly improved selectivity of recruitment for electrical techniques (section 3.2.1.3).

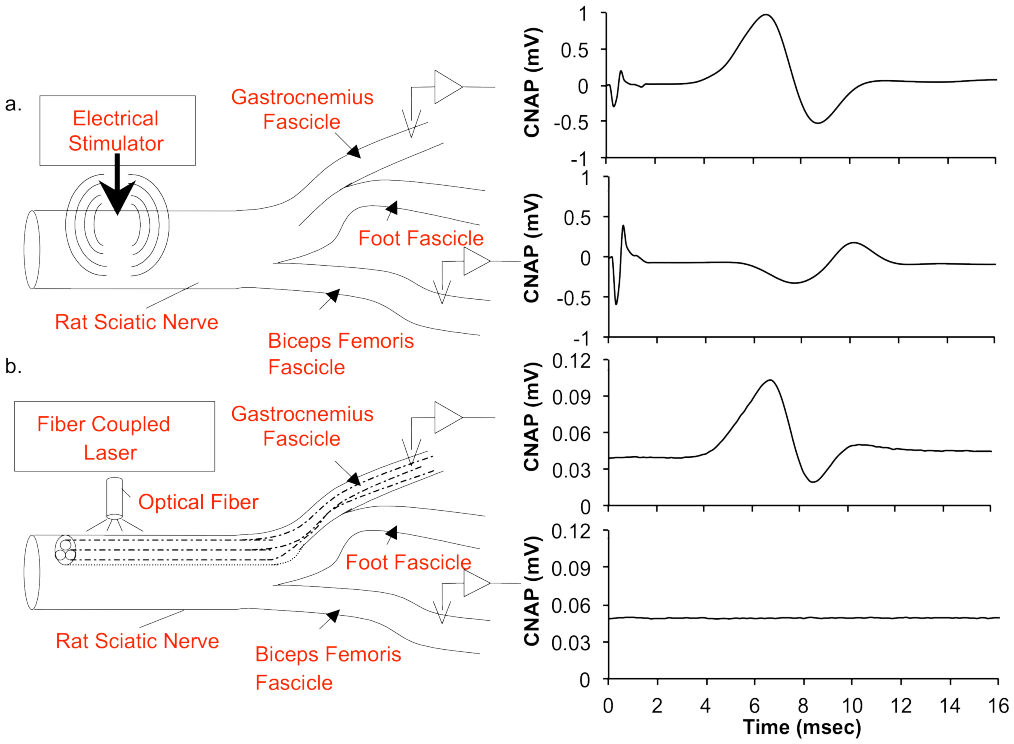

Figure III-8. Illustration of the limitations of electrical stimulation and the benefits of INS. Threshold electrical stimulation (a) necessitates contact, evokes an action potential in both the gastrocnemius and biceps femoris fascicles, and is accompanied by a stimulation artifact. Threshold INS (b) is contact free and spatially precise as only the gastrocnemius fascicle is targeted. Note the lack of stimulation artifact in (b), the contact-free nature of INS and the relative magnitudes of the CNAPs in (a) and (b). Reproduced from (Wells et al., 2007b).

Infrared neural stimulation is so named for the infrared light applied incident to the neural tissue, evoking an action potential. INS has been demonstrated using a variety of laser sources including a free electron laser (λ = 2000–6000 nm; τ_p = 5 μs), a solid-state Ho:YAG laser (λ = 2120 nm; τ_p = 350 μs), a pulsed diode laser (λ = 1850-1890 nm; τ_p = 0.01 - 10 ms) and a continuous wave (CW) single mode diode laser (λ = 1455 nm) (Wells et al., 2005a, Izzo et al., 2007b, Tozburun et al., 2011). At infrared wavelengths, the light-tissue interaction becomes an absorption-dominated event in biological tissue with water being the primary chromophore. All of the aforementioned lasers produce wavelengths with similar absorption coefficients (μ_a) in the rat sciatic nerve (Hale and Querry, 1973, Wells et al., 2005a, Wells et al., 2007b). The absorption is such that the penetration depth in tissue ($1/\mu_a$; the depth at which the initial optical energy is attenuated to 1/e) is approximately 400 μm (Figure III-9). For stimulation of the rat sciatic nerve, using these wavelengths allows the optical energy to be delivered within individual fascicles (50-400 μm in diameter) lying below 150-200 μm of myelin and protective layers. In a systematic study of wavelengths ranging from ~2000-6000 nm, λ = 2120 nm was found to be the optimal wavelength as it has the highest ratio of damaging radiant exposures to stimulation threshold radiant exposures (Wells et al., 2005a) (Figure III-9).

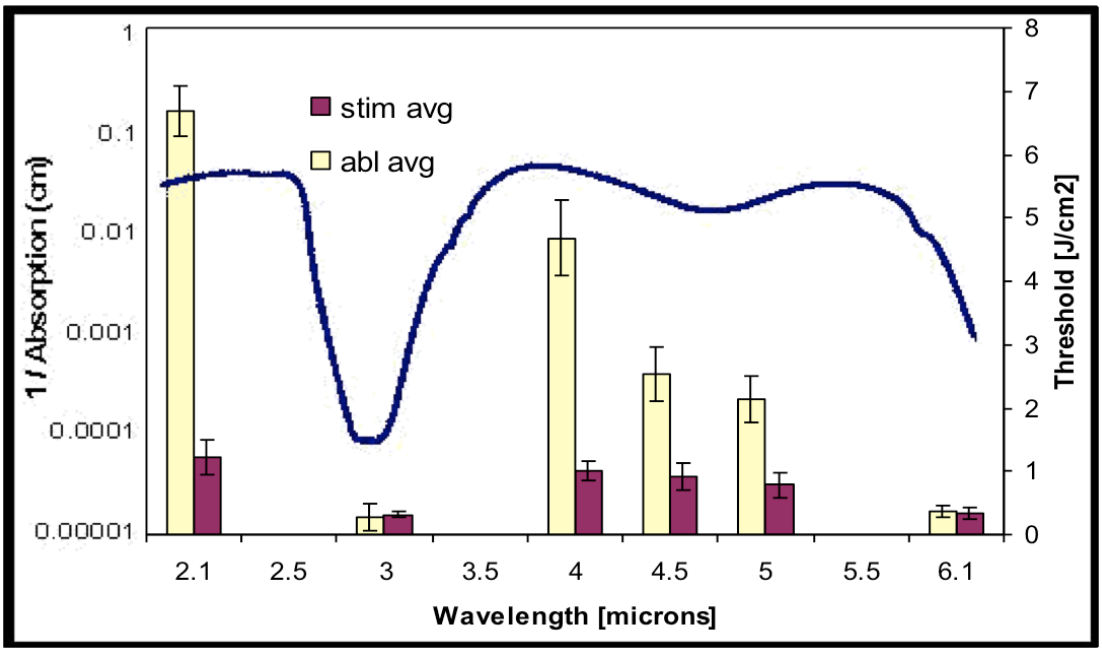

Figure III-9. Wavelength dependence of infrared stimulation. Columns reflect the threshold radiant exposures (J/cm^2) for stimulation and ablation. The blue line provides reference for the absorption of water in tissue as measured with Fourier-Transform Infrared (FTIR) Spectroscopy. The optimal wavelength for stimulation was found to be λ = 2120 nm as it has the highest ratio of damaging radiant exposures to stimulation threshold radiant exposures (Wells et al., 2005a).

3.2.3.1 Mechanism of infrared nerve stimulation

The underlying mechanism of INS is yet to be fully elucidated; however, process of elimination and empirical evidence suggests that it is a thermally mediated process (Wells et al., 2007a). The energy of infrared photons is too low to result in any photochemical reactions and the irradiance is such that multi-photon effects are highly unlikely. Ablative recoil and mechanical effects due to stress confinement are not plausible as stimulation parameters exist below the ablation threshold and outside of the stress confined regime (the pulse durations and penetration depths for INS are within the thermally confined regime). Heating of tissue will always result in volumetric expansion due to larger molecular spacing. Tuedt et al. demonstrated that parameters used for infrared stimulation of the cochlea also produce an optophonic response that is capable of stimulating a hearing cochlea (Teudt et al., 2011). However, the contributions of these effects toward infrared stimulation of peripheral nerves should be minimal as pressure transients associated with optical stimulation were reproduced by a piezoelectric actuator and did not result in the firing of action potentials (Wells et al., 2007a). Thus, thermal effects provide the most plausible mechanism for INS.

Using an Alexandrite laser, stimulation thresholds were found to decrease upon changes in optical and thermal properties as a result of tissue dehydration (Wells et al., 2007a). This led to the hypothesis that an absorption-driven photothermal process is the basis for the mechanism of laser based INS. Wells et al. have shown that for constant radiant exposures at varying pulse durations, an action potential will not fire until all laser energy is deposited (i.e. the end of the optical pulse) (Wells et al., 2007a). This suggests that all laser energy must be deposited and some thermal change must occur prior to

axonal excitation. This finding also implies that longer pulse durations will not only increase the time for action potential initiation, but at some duration stimulation will be less effective as thermal diffusion becomes a factor. Stimulation with equal pulse durations and varying radiant exposures demonstrated that action potential initiation occurs before the end of the laser pulse for supra-threshold stimulation. To assess the effects of tissue baseline temperature, a frog sciatic nerve was stimulated while the nerve's temperature was varied between 0°C and 25°C. No statistically significant change in stimulation threshold radiant exposures were observed over the temperature range, suggesting that there is no baseline temperature threshold that must be met to achieve optical stimulation. These results led to the conclusion that the mechanism of INS is a thermal gradient generated by the laser pulse leading to a temperature rise at the level of the axons (Wells et al., 2007a).

The thermal temperature gradient as a result of INS was characterized in the rat sciatic nerve (Wells et al., 2007a). A thermal camera revealed temperatures increase linearly with increasing radiant exposure. A peak transient temperature rise of 6-8°C was required for optical stimulation, while an average temperature across the Gaussian spot was measured to be approximately 36°C. Based on measured values, the thermal relaxation time (the time required for the tissue temperature to fall to 1/e of the maximum temperature change) was estimated to be approximately 90 ms. As a result, stimulation at 2 Hz for 5 seconds produced a negligible rise in the tissue baseline temperature, while at 5 Hz temperature superposition does occur yielding an increase in baseline tissue temperature (Figure III-10).

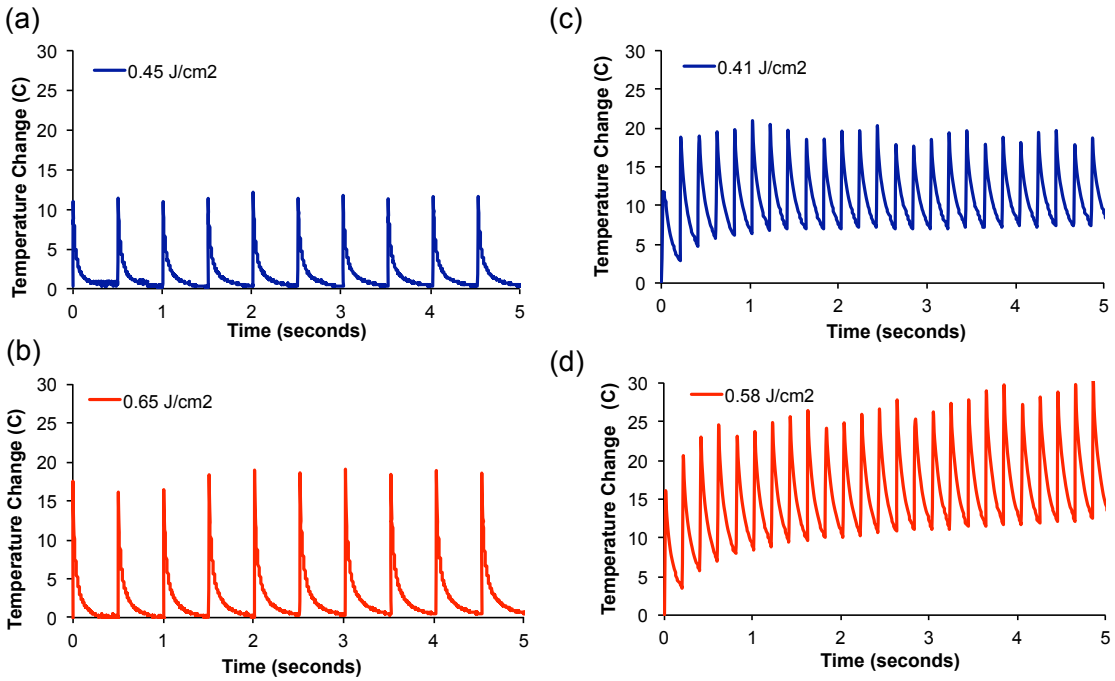

Figure III-10. Baseline temperature increase in response to infrared nerve stimulation. The temperature rise in nerve tissue during 2 Hz stimulation with 0.45 J/cm2 and 0.65 J/cm2 is shown in (a) and (b), respectively. At 2 Hz, the inter-pulse interval is long enough for heat to dissipate away from the stimulation site. In (c) and (d), the temperature rise in response to 5 Hz stimulation at 0.41 J/cm^2 and 0.63 J/cm2 is shown. At 5 Hz, heat does not fully dissipate away from the stimulation site, thus causing temporal superposition of the baseline tissue temperature to occur. From (Wells et al., 2007a).

While data clearly support a photothermal mechanism for INS, the exact translation of thermal energy to activation is yet to be fully explained. Dittami et al showed that intracellular calcium transients are evoked in neonatal cardiomyocytes in response to optical stimulation with 1862 nm light (Dittami et al., 2011). Pharmacological methods revealed that the light primarily affected calcium stores in the mitochondria by acting on the mitochondrial Ca^{2+} uniporter (mCU) and the mitochondrial Na^{+}/Ca^{2+} exchanger (mNCX). However, it may be possible that the mechanism of INS varies between cell types and structures, as well as stimulus parameters (Rajguru et al., 2011).

Recently, an in depth study was conducted by Shapiro et al. to further explicate the mechanism underlying INS (Shapiro et al., 2012). Using a pulsed diode laser (λ = 1889 nm), *Xenopus laevis* oocytes and mammalian HEK cells consistently produced intracellular current transients in response to infrared stimulation, an interesting finding for non-neuronal cell types. Responses were not inhibited by a variety of channel inhibitors, transport inhibitors, or changes to the extracellular solution or physiological recording buffer. By replacing the H_20 in the extracellular recording solution with D_20 the current response to infrared stimulation was significantly reduced, confirming the role of water absorption in the mechanism of infrared excitation. Directly comparing the evoked response to the time course of the temperature change revealed that the currents more closely match the change in solution temperature than the absolute temperature, adding to the aforementioned findings by Wells et al (Wells et al., 2007a). These results led to the hypothesis that "temperature alters the electrical capacitance of the membrane, producing a current proportional to the derivative of capacitance, and thereby to the

derivative of temperature, with respect to time" (Shapiro et al., 2012). Increases in membrane capacitance in response to infrared stimulation were observed in artificial lipid bilayers as well as HEK cells. This increase in membrane capacitance may be explained by the Gouy-Chapman-Stern (GCS) theory of double layer capacitors, where electrical and thermal forces affect the spatial distribution of ions near a charged surface (Grahame, 1947).

3.2.3.2 Applications of INS

Excitement for INS is growing in applications where spatially precise nerve stimulation is necessary, with both therapeutic and diagnostic purposes being targeted. One of the most promising applications of INS is stimulation of the cochlea and auditory nerve for improved cochlear implants (Izzo et al., 2006, Izzo et al., 2007a). Izzo et al. have shown that INS stimulates the auditory neurons directly (as opposed to the inner hair cells) in a spatially precise manner unmatched by electrical stimulation and comparable to low level acoustic tones (Izzo et al., 2007a, Matic et al., 2011). At short pulse widths (35 μs), spiral ganglion cells require very low radiant exposures to achieve stimulation (mJ/cm^2) and may be safely stimulated for hours at high repetition rates (10^1-10^2 Hz) (Izzo et al., 2007b). A novel optical cochlear implant was recently demonstrated in cats, opening the door for further chronic studies (Rajguru et al., 2010).

Along with auditory prosthetics, clinical nerve monitoring is an application well suited for INS. The use of INS for monitoring function of the cavernous nerves and the facial nerve is currently under investigation. The cavernous nerves on the surface of the prostate are responsible for erectile function. Therefore it is imperative that these nerves

be located during prostate resections in order to maintain sexual function. Electrical stimulation is used intra-operatively for mapping the cavernous nerves, but has proven to be inconsistent and unreliable due to the necessity of contact, limited spatial precision and stimulation artifact. Recently, Fried et al. demonstrated that INS provides a contact-free and spatially precise viable alternative for mapping the locations of these nerves (Fried et al., 2007, Fried et al., 2008b). A significant increase in intracavernosal pressure accompanied INS of the cavernous nerve and returned to baseline following cessation of stimulation. The optimal INS parameters for non-damaging cavernous nerve mapping were reported at wavelengths of 1860-1870 nm, radiant exposures greater than 0.35 J/cm^2 and at a pulse rate of 10 Hz (Fried et al., 2008a).

Recently, continuous wave stimulation of the cavernous nerves was demonstrated using diode lasers at 1455 nm, 1550 nm and 1870 nm (Tozburun et al., 2010, Tozburun et al., 2011, 2012). Threshold for effective continuous wave stimulation was reported as a rise in tissue temperature to 41°C. The 1455 nm laser used in these studies was a relatively compact and inexpensive single mode diode coupled to a single-mode-fiber. The use of this laser shows how far INS has come from the physical size of the FEL to small, portable diode lasers. Fried et al. are also currently developing a laparoscopic probe for clinical use (Tozburun and Fried, 2009) and have demonstrated stimulation of the cavernous nerve beneath a layer of fascia (Tozburun et al., 2012). The successful intraoperative mapping of the cavernous nerve suggests the potential widespread application of INS for detecting and monitoring neural networks.

INS of the facial nerve was also demonstrated as a potential method of intraoperative neural monitoring (Teudt et al., 2007). Using a Ho:YAG laser (λ = 2120

nm; τ_p = 250 μs) coupled to a 600 μm diameter fiber optic, spatially selective activation of m. orbicularis oculi, m. levator nasolabialis and m. orbicularis oris was achieved through INS of the facial nerve trunk at 2 Hz. Stimulation radiant exposures ranged from 0.71 to 1.77 J/cm^2, with threshold radiant exposures for damage at greater than 2.0 J/cm^2. While it was possible to stimulate through the fascia surrounding the facial nerve using the Ho:YAG, wavelengths with deeper penetration depths will likely be required for stimulating through additional overlying tissue intraoperatively.

In addition to peripheral neural anatomy, INS has also been successfully demonstrated in the CNS both *in vitro* (Cayce et al., 2010) and *in vivo* (Cayce et al., 2011). In the somatosensory cortex of anesthetized rats, Cayce et al. showed intrinsic fluorescence signals in response to INS of similar magnitude to those evoked by tactile stimulation (Cayce et al., 2011). Using a pulsed diode laser (λ = 1875 nm; τ_p = 250 μs) coupled to a 400 μm diameter fiber, radiant exposures ranging from 0.1 to 0.55 J/cm^2 delivered at 50-200 Hz induced peak changes in intrinsic fluorescence of up to 0.4%. An increase in intrinsic signal magnitude was found to correlate with increasing stimulus repetition rate and radiant exposure. Electrophysiological recordings revealed statistically significant inhibition of neuronal firing as a result of INS. Tactile stimulation following prolonged INS revealed no harmful effects as a result of optical stimulation.

3.2.3.3 Limitations of INS

While INS demonstrates desirable qualities, there are potential limitations that must be addressed before this technology realizes its full potential. One such possible limitation is the reliance on current laser technology, which could potentially hinder

future development of implantable INS devices. The optical laser output required for nerve stimulation currently requires bench-top laser sources. The size of the laser source is dictated by the electrical power required, inherent inefficiency of the conversion from electrical energy to optical laser output, and often large and cumbersome cooling systems needed to remove excess heat from the system.

Peak powers required for INS are often >1 W for peripheral nerve stimulation. With maximum duty factors of typical laser sources for INS ranging from 5-10%, required average powers are approximately tens to hundreds of mW. Implantable INS-based neuroprosthetics will require power sources capable of supplying at least as much electrical power as desired optical output power; however typical power requirements for current medical implants usually only range from tens of μW to a few mW (Schmidt and Skarstad, 2001, Wei and Liu, 2008). Supplying sufficient electrical power to drive an implanted laser source while minimizing implant and/or battery size will be a challenge that must be addressed by advances in either battery or laser technology. Batteries typically comprise 25-60% of the volume of an implanted device (Schmidt and Skarstad, 2001); however, applications like INS that require higher peak powers than average powers result in increased power source size due to the need for an accumulator such as a capacitor or rechargeable battery (Schmidt and Scott, 2011).

The development of implantable or portable electrical power sources capable of meeting the size and power requirements is exacerbated by the inherent electrical-to-optical power conversion inefficiencies of lasers. Typical solid-state lasers, like the Ho:YAG used for much of the work to date investigating INS, convert up to about 10% of their electrical input into useful laser output (Koechner and Bass, 2003). These low

electrical-to-optical conversion efficiencies can be attributed to two primary causes: (1) the poor absorption efficiency by the lasing material, accounting for around 5-10% energy loss; and (2) the sub-optimal energy conversion in the lasing medium, which accounts for 20-30% of the energy loss (Koechner, 2006). Using diode lasers as pump sources can aid in increasing overall solid-state laser system efficiencies up to 20-30% (Koechner and Bass, 2003). The narrow emission wavelength spectrum of these diodes (as compared to flashlamps) results in more efficient utilization of the diode pump output for producing population inversion in the laser material.

Diode lasers are also able to stimulate neural tissue with infrared light and provide system efficiencies up to around 50% (Koechner, 2006). While diode lasers are ubiquitous in the lasing industry, a cost-effective means of achieving wavelengths appropriate for INS is not trivial. The challenge is to find semiconductor materials with the proper active-region band gap that are compatible with high index-contrast mirrors (Dummer et al., 2011). The Capella, manufactured by Lockheed-Martin-Aculight, is an example of a diode laser with tunable wavelength near $\lambda = 1875$ nm that is designed for INS. In general, the small size of the diode bars and the increased overall efficiency allow diode lasers to operate using small power supplies (e.g. a battery), whereas inefficient solid-state lasers must be mains powered. This affords the option of miniaturizing the diode while maintaining appreciable laser output. However, for implantation considerations, whether these diode sources can be miniaturized while maintaining laser output suitable for INS is yet to be determined.

In addition to size constraints, thermal considerations are also of concern for implantable devices. Not only must the diode be temperature-controlled to maintain a

constant wavelength, but substantial heat generation due to battery operation and system inefficiencies must also be managed to avoid appreciable temperature rise in the tissue surrounding the implanted laser source. While bench-top solid-state lasers may rely on elaborate cooling systems to remove energy that has been converted to heat, diode lasers are often air cooled and have duty factors that limit the laser "on" time to mitigate thermal effects such as thermal lensing and damage due to overheating.

The concerns of inefficiency, size and thermal management pose significant engineering challenges to the development of implantable INS-based devices. In an effort to address the issues confronting the miniaturization and translation of INS therapeutics, vertical cavity surface emitting lasers (VCSELs) are being investigated for nerve stimulation applications (Hibbs-Brenner et al., 2009, Dummer et al., 2011). VCSELs, a type of diode laser where the optical beam is emitted orthogonal to the wafer surface, as opposed to conventional edge-emitting diodes, are attractive due to their small size, lower power consumption, high efficiency, and simple packaging. Recently, a 2x2 VCSEL array operating at λ = 1860 nm and measuring 350x350x250 μm^3 was developed for INS (Dummer et al., 2011). The array produced maximum CW power output of nearly 3 mW and system efficiency of 6% (10% for pulsed operation). While thresholds for neural activation are not met with this device, no fundamental concerns have been identified that should hinder the ability of achieving the requisite output. However, the development of this array is targeted towards stimulation in the cochlea, which requires 2-3 orders of magnitude lower radiant exposure than most peripheral nerves. While advanced laser sources such as VCSELs are promising, laser size, inefficiency and heat generation will pose engineering challenges to the development of implantable INS-based devices.

Although the need for miniaturized laser sources is currently hindering implantation, the primary challenge for INS is the limited safety ratio of stimulation. The safety ratio is a metric for the safety of INS, and is defined as the ratio of threshold radiant exposure (J/cm^2) for damage to threshold radiant exposures for stimulation (Wells et al., 2005a). A thorough investigation of the safety of INS was conducted in myelinated peripheral nerves (Wells et al., 2007c). Histopathologic examination was used to assess whether a range of temperature transients required for reliable stimulation existed where no thermal damage to the neural tissue occurred. In this study, laser pulses (λ = 2120 nm; PW = 350 μs) were delivered at repetition rates of 2-8 Hz with radiant exposures varying between 0.2-1.5 J/cm^2 for stimulation and up to 2.5 J/cm^2 for positive control lesions. A total of 162 excised rat sciatic nerves were evaluated in the study, with nerves being extracted acutely, as well as up to 2 weeks following stimulation for survival studies. An expert pathologist specializing in laser tissue interactions evaluated each of the nerves and reported any sign of epineurial or axonal damage. The results indicated that there exists a safe range of radiant exposures between the maximum laser radiant exposure required to stimulate and the minimum laser radiant exposure necessary for damage. However, in survival studies radiant exposures with <1% probability of damage (0.66-0.70 J/cm^2) are limited to approximately twice the radiant exposures required for stimulation (0.34-0.48 J/cm^2) (Figure III-11). In additional experiments, the upper limit for safe laser stimulation repetition rate occurred near 5 Hz and the maximum duration for constant, low repetition rate stimulation (2 Hz) was approximately 4 minutes with adequate tissue hydration.

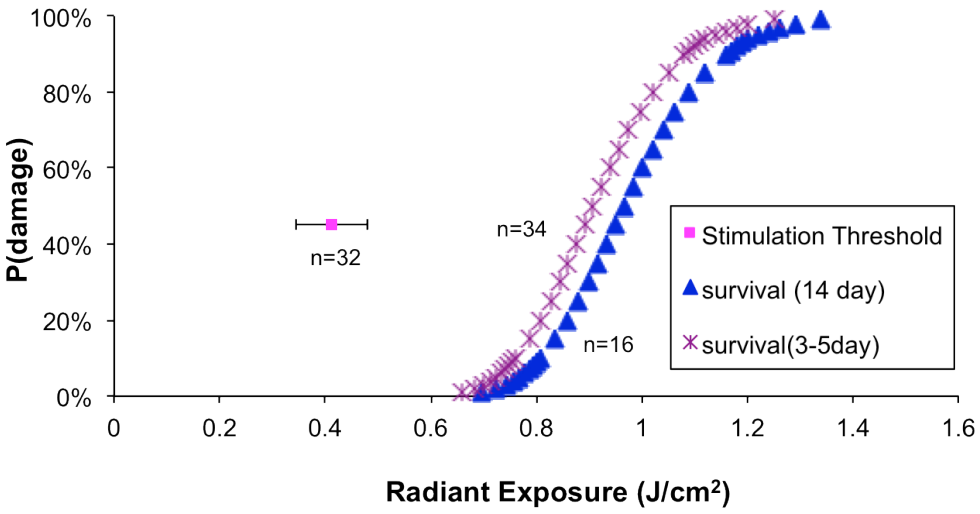

Figure III-11. Probability of damage of rat sciatic nerve as a function of laser radiant exposure compared to the stimulation threshold. Statistical analysis of survival studies was performed for nerves collected 3-5 days and 14 days after laser irradiation. A margin exists between threshold radiant exposures for safe stimulation and nerve damage; however, a >1% probability of nerve damage occurs at radiant exposures that are roughly two-times stimulation threshold (Wells et al., 2007c).

The risk of thermal damage as a result of INS varies by anatomy. While the aforementioned safety study was conducted in the rat sciatic nerve with a visible motor twitch serving as stimulation threshold, INS of the spiral ganglion cells exhibits a reduction in stimulation thresholds by nearly three orders of magnitude due to differences in neural anatomy and measurement of threshold (i.e. neural response vs. visible muscle twitch). In studies of optical cochlear stimulation, continuous stimulation at 13 Hz for up to 6 hours (~10 mJ/cm^2) showed no reduction in compound nerve action potential (CNAP) signals, indicating negligible damage (Izzo et al., 2007b). In the same study, INS at 400 Hz for several hours also showed a steady CNAP response.

In addition to laser size constraints and potential risk of thermal damage, there are other challenges for the ultimate application of INS. For some applications, there will be tissue between the light source and the neuronal target that will absorb a percentage of the infrared light (Tozburun et al., 2012). Not only will this lead to greater overall optical energies, but will also require consideration of possible damage to the intermediary tissue. Because infrared techniques are spatially specific, achieving supra-threshold stimulation for a sufficient target volume may be challenging. For a functional peripheral neuromuscular implant, many discrete INS locations will likely be required to achieve full activation of even a single muscle. In some preparations, such as the cochlea, the presence of a fluid layer will act as an absorber that will limit the infrared light reaching the target tissue (Izzo et al., 2008).

From both tissue damage and laser development perspectives it is desirable to lower stimulation thresholds for INS. Clinical applications requiring long-term

stimulation and/or high repetition rate protocols will benefit from reduced risk of thermal damage as well as relaxed laser design constraints for implantable INS-based stimulators.

3.3 Neural Inhibition

Full control over nervous function requires the ability to not only activate but also silence neural activity. There are many neurological disorders characterized by unwanted nerve activity that would benefit from the ability to inhibit the generation or propagation of action potentials. In research settings, full control of nervous function is attainable through the use of penetrating microelectrodes and micropipettes, which are capable of providing both depolarizing and hyperpolarizing currents. However, these technologies are not practical for large-scale control of hundreds/thousands of neurons simultaneously, especially in intact, behaving subjects, whose movements will dislodge them, damaging both the electrodes and the neurons. Current clinical techniques for conduction block include surgical and pharmacological methods, as well as methods of inducing irreversible lesions, which are limited by lack of specificity, negative side-effects, low success rates and nerve damage (Gallichio, 2004, Ravid et al., 2011). Alternative approaches to the block of action potential propagation, including electrical, thermal and optical techniques, are being investigated to determine their potential merit.

3.3.1 High-frequency electrical conduction block

The ability to block neuromuscular transmission using high-frequency alternating current (AC) has been known since the early 1900s (Wedensky, 1903). Since that time there have been many studies investigating conduction block using high-frequency

alternating current (HFAC) with inconsistent results and no understanding of the mechanism of action. The first methodical demonstration of effective, repeatable and reversible nerve conduction block utilizing HFAC in adult bullfrogs was shown by Kilgore and Bhadra in 2004 (Kilgore and Bhadra, 2004). The same authors followed this shortly thereafter with a demonstration in the rat sciatic nerve (Bhadra and Kilgore, 2005). Complete and robust block of motor action potentials and motor function was possible with frequencies of 2 kHz and greater in the bullfrog and 10-30 kHz in the rat. By modulating the current amplitude of the AC blocking waveform, block of gastrocnemius force in gradations of ± 10% of the total force output was achieved (Kilgore and Bhadra, 2004). The mechanism for high-frequency block (HFB) was conclusively shown to be neural in nature, rather than due to muscle fatigue, and is believed to be the result of tonic depolarization-induced inactivation of sodium channels (Kilgore and Bhadra, 2004, Bhadra et al., 2007).

Recent investigations have taken significant steps towards clinical application of HFB. Much effort has been directed towards reversible electrical block for the restoration of bladder function (Bhadra et al., 2006, Boger et al., 2008, Gaunt and Prochazka, 2009, Mounaim et al., 2010). In small animal models, reversible block of the external urethral sphincter (Bhadra et al., 2006), increase in voiding volume and decrease in bladder pressure (Boger et al., 2008) have been observed with HFB of the pudendal nerves alone and when combined with sacral root stimulation. Recently HFB was demonstrated in the large diameter primate medial nerve (Ackermann et al., 2011b) and in the vagus nerve of humans (Camilleri et al., 2008).

Although HFB is a promising tool for nerve conduction block, there are challenges that must be overcome prior to its clinical application. Like electrical methods of neurostimulation, HFB will require a means of limiting undesirable current spread and targeting selected axons based on location and/or size. Enhanced selectivity of HFB using intrafascicular electrodes is being investigated (Ackermann et al., 2010c, Dowden et al., 2010), though these approaches will face challenges as described previously (see 3.2.1.3). The primary limitation unique to HFB is a brief but intense burst of activity known as the "onset response" that invariably occurs when the high-frequency block is first applied (Bhadra and Kilgore, 2005). This can result in unwanted muscle contractions or pain and must be addressed for the clinical application of HFB (Kilgore et al., 2009, Ackermann et al., 2011b). An area of focus is the elimination or mitigation of the onset response through adjustments to the blocking waveform (Miles et al., 2007) and electrode geometry (Ackermann et al., 2010b), or by combining HFAC with direct current (Ackermann et al., 2011a) or rapid nerve cooling (Ackermann et al., 2010a)

3.3.2 Rapid nerve cooling

That cooling a nerve will decrease its excitability has been known for well over a century (Gotch and Macdonald, 1896). Methods of local and rapid (tens of seconds) cooling have been developed over the last 60 years and used as a means of understanding and manipulating neural conduction (Douglas and Malcolm, 1955, Patberg et al., 1984). Recently this technique was used in combination with HFAC to reversibly block nerve conduction without an onset response (Ackermann et al., 2010a).

As a stand-alone method for nerve conduction block, nerve cooling is effective, fast acting and reversible, but there are significant challenges that must be overcome for this to be a viable clinical technique (Patberg et al., 1984, Ackermann et al., 2010a). Long-term exposure to nerve cooling is known to cause ischemia and reperfusion injury (Jia and Pollock, 1998, 1999). Therefore, exposures lasting longer than several minutes may reduce nerve viability. For chronic applications where intermittent nerve cooling is desired, implantable devices will face challenges in regards to managing heat produced by the cooling system. Borgdorff et al. implanted a liquid-cooling cooling system on the cervical vagus nerve of dogs; however, the heat-producing elements were located outside of the body, limiting portability (Borgdorff and Versteeg, 1984). Ackermann described a nerve cuff combining a thermally insulating material with a thermally conductive nerve interface that would allow for a Peltier device to cool a small regions of a nerve, though this device has yet to be demonstrated (Ackermann et al., 2010a).

3.3.3 Optogenetic inhibition

By genetically introducing light-activated ion channels, such as blue-responsive ChR2, light can be used to depolarize genetically targeted neurons (see 3.2.2.2). To achieve full optogenetic control with temporal and spatial precision, excitatory proteins are combined with light-driven pumps and channels producing hyperpolarizing currents. G protein inward rectifying potassium channels (GIRKs) co-expressed with vertebrate rat rhodopsin 4 (RO4) will hyperpolarize neurons in response to light (Li et al., 2005). The light-driven halorhodopsin chloride pump (NpHR) responds to yellow light with evoked hyperpolarization that will block single action potentials or sustained trains (Zhang et al.,

2007). An exciting advantage of this technique is that Chr2 and NpHR can be co-expressed and are spectrally separated such that a cell's excitation or inhibition is dictated by the wavelength of light. Thus, optogenetics provides a complete, temporally and spatially precise method of reversible neural control.

Since the initial demonstration of inhibition using light-activated GIRK channels and the introduction of NpHR for optogenetic silencing of neurons, modifications and newer technologies are providing improved control over light-driven inhibition. Increased expression of NpHR, especially for *in vivo* studies in mammals, is desirable for inducing large inhibitory photocurrents; however, overexpression results in aggregates forming at the exit of the endoplasmic reticulum (ER) and can lead to cellular toxicity (Gradinaru et al., 2007). By adding ER export signals to NpHR, forming enhanced NpHR (eNpHR), expression and peak photocurrent are greatly increased without cellular toxicity (Gradinaru et al., 2008). Light-driven proton pumps, such as archaerhodopsin-3 (Arch) and *Leptosphaeria maculans* opsin (Mac/LR/Ops), are capable of photocurrent densities that are significantly greater than those produced by NpHR and are spectrally separated allowing discrete subsets of neural populations to be silenced (Chow et al., 2010). As with optogenetic stimulation, the clinical application of this technology is reliant upon the success of gene therapy in humans (see 3.2.2.2).

3.3.4 Heat block

As with nerve cooling, the effects of increased temperature on nerve excitability have long been known. Hodgkin and Katz presented the first evidence of a phenomenon they called "heat block," where action potentials in the squid giant axon decreased in

amplitude and ultimately failed to conduct as the axon's temperature was increased up to 40 °C (Hodgkin and Katz, 1949). Huxley later calculated changes in action potential amplitude and conduction velocity that matched the experimental work of Hodgkin and Katz (Huxley, 1959). In his calculations, Huxley assumed that only the αs and βs (i.e. constants affecting the dynamics of voltage-gated ion channels) of the Hodgkin-Huxley model changed with temperature (Hodgkin and Huxley, 1952). Huxley, as well as Hodgkin and Katz, concluded that the change in temperature enhanced the activity of the falling phase of the action potential more than the rising phase. Since the conductances in Huxley's calculations did not change with temperature, the rising phase (sodium activation) was determined to be overtaken by the permeability changes (inactivation of sodium permeability and activation of potassium permeability) that makeup the recovery phase (Huxley, 1959).

The heat block phenomenon has been further studied and evaluated since the work of Hodgkin, Katz and Huxley. Schauf and Davis modeled nerves to investigate how the extent of demyelination affects the nerve's response to temperature changes (Schauf and Davis, 1974). Their results indicate a steep drop in blocking temperature as the amount of demyelination is increased. Block occurred at 42 °C for normal nerves and at less than 20 °C for nerves with 90% reduction in myelination. In a similar experimental study, Davis et al. increased the temperature of Ringers solution surrounding the electrically stimulated sciatic nerve of normal guinea pigs and those with experimental allergic neuritis (EAN) leading to demyelination (Davis et al., 1976). The results of that study showed action potential block at 44 – 48 °C in normal animals and 34 – 37 °C in EAN animals. Rattay and Aberham further modeled this phenomenon and demonstrated its

importance for accurate simulations in the context of functional electrical stimulation (Rattay and Aberham, 1993). Xu and Pollock demonstrated reversible changes in nerve conduction for normal rats when the sciatic nerve was quickly warmed to 47 °C and then cooled back to 37 °C (Xu and Pollock, 1994).

While all of the aforementioned studies utilized global changes in nerve temperature, Mou et al. recently proposed that local increases in nerve temperature could block both electrical initiation of axonal activation and action potential propagation (Mou et al., 2012). In this study, electrical stimulation of a frog sciatic nerve was modeled while the temperatures of select nodes were increased. Two interesting outcomes were predicted by this study: (1) The model suggests that the temperature required for block of action potential initiation depends on stimulus current and axon diameter. Interestingly, block of action potential initiation was predicted to decrease with increasing stimulus current. (2) Block of action potential propagation was predicted to require greater increase in local temperature and/or spread of temperature across several nodes. If temperatures were insufficient to create thermal block, the action potential decreased in amplitude at the location of temperature increase, but resumed propagation distal to the blocking site. Mou et al. presented limited experimental validation of their model, showing that increased laser output resulted in increased threshold current for action potential initiation.

3.4 Significance

3.4.1 Need for improved neural interfaces

According to the World Health Organization, as many as 1 billion people are affected by neurological disorders worldwide (World Health Organization, 2006). Of the many types of neurological disorders, neurological injuries lead to the greatest reduction in healthy life years. According to a study initiated by the Christopher & Dana Reeve Foundation, approximately 1.9% of the U.S. population (5.6 million) suffers from some form of paralysis, with the leading causes being stroke, spinal cord injury and multiple sclerosis (Christopher & Dana Reeve Foundation, 2009). Spinal cord stimulators currently make up approximately 67% of the neurostimulation applications market; however deep brain stimulators, vagus nerve stimulators, sacral nerve stimulators and gastric stimulators are also successful applications. In the United States alone, the estimated treatable population for these applications will reach 112 million people by 2013, but the market penetration will only average about 7.2% per application (Frost & Sullivan, 2008). These figures do not include the growing number of candidates for functional stimulators designed to restore motor control to the upper and lower extremities; nor do they include candidates for cochlear implants – the most successful neurostimulation device received by approximately 219,000 people worldwide (NIDCD, 2011).

The neurostimulation market is one of the fastest growing sectors of the medical device industry and is expected to accelerate growth over the coming years. The global neurostimulation market is expected to reach $7.6B by 2014 with a compound annual

growth rate of 25.2% from 2009 to 2014 (MarketsandMarkets, 2009). This growth is driven primarily by technological advancements, increased consumer awareness, rising prevalence of age-related neurological disorders, better clinical outcomes, cost-effectiveness, approval of clinical trials and advanced implantable devices.

The need for restored function to people suffering from neural deficits vastly exceeds the current tools and treatments available. Although technological advancements are a driving force behind the growth of this market, the successful treatment of the unreached patient population and the sustained growth of this industry will be driven largely by refinements to current technology and development of novel solutions.

3.4.2 Infrared light as a novel means for controlling neural excitability

This dissertation describes the novel application of infrared light for selective control of electrical neural activity. The primary rationale for the development of this neural control method is to take advantage of the attractive aspects of INS while mitigating the potential limitations. There are two underlying hypotheses for this work: (1) Infrared light applied in conjunction with electrical stimulation will achieve selective activation with optical radiant exposures that are less than required for INS alone; and (2) Infrared light will selectively block both electrically initiated axonal activation and propagation of action potentials, and can be used to regulate neuromuscular function.

Several studies have considered the effects of optical irradiation when delivered concurrently with electrical stimulation (Richter et al., 2011). In a previous study, continuous UV light applied to the Node of Ranvier was shown to raise the electrical stimulation threshold of myelinated nerve fibers, while applying the UV light to the

intermodal region lowered the threshold for electrical stimulation (Booth et al., 1950). As this effect was only observed for ultraviolet wavelengths, it was determined to be the result of a photochemical effect. In a study of cerebellar neurons, a ruby laser and dye laser were shown to reduce the excitability of neurons at high energies. Electron micrographs revealed damage to the mitochondria, which led the authors of the study to conclude that the observed decrease in excitability was due to a local heating of the mitochondria leading to thermal damage (Olson et al., 1981a, Olson et al., 1981b). Uzdensky and Savransky reported an increase in the frequency of electrically evoked action potentials in neurons followed by a subsequent decrease using visible wavelengths (Uzdensky and Savransky, 1997). They concluded their effect was the result of light absorption by flavins yielding calcium release from mitochondria. Interestingly, they also suggest that the increase in activity may be due to a two-photon effect, while the inhibition is likely due to a single-photon effect. Matsuda et al. used an argon laser (457, 488 nm; 50 mW) to investigate the effects of optical irradiation on cathode-make and anode-break excitations, which are characterized by action potential initiation occurring at the cathode when a stimulus is applied and at the anode after a long duration stimulus (>3 ms) is removed (Matsuda et al., 2006). The results of this study showed that continuous optical stimulation has the potential to selectively suppress anode-break excitation.

The aforementioned studies reported modulation of the neural response to electrical stimulation in the presence of optical stimuli; however, full control of the nerve, including inhibition with light in an endogenous neural system, has yet to be demonstrated. The work in this dissertation describes a novel paradigm, whereby infrared

light can be used as a means of either selectively adding to the effects produced by electrical stimulation (hybrid electro-optical stimulation) or block selective electrically evoked responses (infrared inhibition). With hybrid electro-optical stimulation, pulses of each modality are purposefully combined, both spatially and temporally, to achieve a response that is greater than the sum of each individual response. The hypothesis is that a weak electrical stimulus will depolarize the tissue to just below threshold for excitation, and then a pulse of optical energy will bring a spatially confined region to threshold at a radiant exposure that is lower than what is required for INS alone. Thus, electrical stimulation effectively "primes" the excitable tissue for infrared stimulation. Infrared inhibition uses both pulses and pulse trains of infrared light to block the electrically initiated activation of selected axons or selected propagating responses. The transient local temperature increase sufficient to alter ion channel gating permeabilities is the proposed mechanism of action for infrared inhibition.

This investigation develops the use of infrared light for control of electrical neural activity through four main studies: 1) feasibility demonstration of combined optical and electrical stimulation of neural tissue; 2) methodological refinement to achieve reliable and repeatable activation with hybrid stimulation; 3) force generation assessment in response to hybrid stimulation; and 4) demonstration and characterization of infrared block of both electrical neural activation and propagating responses. Through this project, hybrid electro-optical stimulation and infrared inhibition are shown for the first time, unique properties of each technique are discovered and the first demonstrations of infrared neuromuscular control are presented.

3.5 References

Ackermann DM, Foldes EL, Bhadra N, Kilgore KL (2010a) Nerve conduction block using combined thermoelectric cooling and high frequency electrical stimulation. J Neurosci Methods 193:72-76.

Ackermann DM, Jr., Bhadra N, Foldes EL, Wang XF, Kilgore KL (2010b) Effect of nerve cuff electrode geometry on onset response firing in high-frequency nerve conduction block. IEEE Trans Neural Syst Rehabil Eng 18:658-665.

Ackermann DM, Jr., Foldes EL, Bhadra N, Kilgore KL (2010c) Conduction block of peripheral nerve using high-frequency alternating currents delivered through an intrafascicular electrode. Muscle Nerve 41:117-119.

Ackermann DM, Jr., Bhadra N, Foldes EL, Kilgore KL (2011a) Conduction block of whole nerve without onset firing using combined high frequency and direct current. Med Biol Eng Comput 49:241-251.

Ackermann DM, Jr., Ethier C, Foldes EL, Oby ER, Tyler D, Bauman M, Bhadra N, Miller L, Kilgore KL (2011b) Electrical conduction block in large nerves: high-frequency current delivery in the nonhuman primate. Muscle Nerve 43:897-899.

Adams SR, Tsien RY (1993) Controlling cell chemistry with caged compounds. Annu Rev Physiol 55:755-784.

Agnew WF, McCreery DB (1990) Considerations for safety with chronically implanted nerve electrodes. Epilepsia 31 Suppl 2:S27-32.

Anonymous (2011) Method of the Year 2010. Nat Meth 8:1-1.

Aravanis AM, Wang LP, Zhang F, Meltzer LA, Mogri MZ, Schneider MB, Deisseroth K (2007) An optical neural interface: in vivo control of rodent motor cortex with integrated fiberoptic and optogenetic technology. J Neural Eng 4:S143-156.

Arvanitaki A, Chalazonitis N (1961) Excitatory and Inhibitory Processes Initiated by Light and Infra-Red Radiations in Single, Identifiable Nerve Celss. In: Nervous Inhibtion(E., F., ed): Pergamon Press.

Bagshaw EV, Evans MH (1976) Measurement of current spread from microelectrodes when stimulating within the nervous system. Exp Brain Res 25:391-400.

Berenstein CK, Mens LH, Mulder JJ, Vanpoucke FJ (2008) Current steering and current focusing in cochlear implants: comparison of monopolar, tripolar, and virtual channel electrode configurations. Ear Hear 29:250-260.

Bhadra N, Kilgore KL (2005) High-frequency electrical conduction block of mammalian peripheral motor nerve. Muscle Nerve 32:782-790.

Bhadra N, Kilgore K, Gustafson KJ (2006) High frequency electrical conduction block of the pudendal nerve. J Neural Eng 3:180-187.

Bhadra N, Lahowetz EA, Foldes ST, Kilgore KL (2007) Simulation of high-frequency sinusoidal electrical block of mammalian myelinated axons. J Comput Neurosci 22:313-326.

Bigelow DC, Kay DJ, Rafter KO, Montes M, Knox GW, Yousem DM (1998) Facial nerve stimulation from cochlear implants. Am J Otol 19:163-169.

Boger A, Bhadra N, Gustafson KJ (2008) Bladder voiding by combined high frequency electrical pudendal nerve block and sacral root stimulation. Neurourol Urodyn 27:435-439.

Booth J, von MA, Stampfli R (1950) The photochemical action of ultra-violet light on isolated single nerve fibres. Helv Physiol Pharmacol Acta 8:110-127.

Borgdorff P, Versteeg PG (1984) An implantable nerve cooler for the exercising dog. Eur J Appl Physiol Occup Physiol 53:175-179.

Boyden ES, Zhang F, Bamberg E, Nagel G, Deisseroth K (2005) Millisecond-timescale, genetically targeted optical control of neural activity. Nat Neurosci 8:1263-1268.

Branner A, Normann RA (2000) A multielectrode array for intrafascicular recording and stimulation in sciatic nerve of cats. Brain Res Bull 51:293-306.

Branner A, Stein RB, Fernandez E, Aoyagi Y, Normann RA (2004) Long-term stimulation and recording with a penetrating microelectrode array in cat sciatic nerve. IEEE Trans Biomed Eng 51:146-157.

Brummer SB, Turner MJ (1977) Electrochemical considerations for safe electrical stimulation of the nervous system with platinum electrodes. IEEE Trans Biomed Eng 24:59-63.

Callaway EM, Yuste R (2002) Stimulating neurons with light. Curr Opin Neurobiol 12:587-592.

Camilleri M, Toouli J, Herrera MF, Kulseng B, Kow L, Pantoja JP, Marvik R, Johnsen G, Billington CJ, Moody FG, Knudson MB, Tweden KS, Vollmer M, Wilson RR, Anvari M (2008) Intra-abdominal vagal blocking (VBLOC therapy): clinical results with a new implantable medical device. Surgery 143:723-731.

Cayce JM, Kao C, Malphrus JD, Konrad PE, Mahadevan-Jansen A, Jansen ED (2010) Infrared Neural Stimulation of Thalamocortical Brain Slices. IEEE Journal of Selected Topics in Quantum Electronics.

Cayce JM, Friedman RM, Jansen ED, Mahavaden-Jansen A, Roe AW (2011) Pulsed infrared light alters neural activity in rat somatosensory cortex in vivo. Neuroimage 57:155-166.

Chartier-Kastler EJ, Ruud Bosch JL, Perrigot M, Chancellor MB, Richard F, Denys P (2000) Long-term results of sacral nerve stimulation (S3) for the treatment of neurogenic refractory urge incontinence related to detrusor hyperreflexia. J Urol 164:1476-1480.

Chernov MM, Duke AR, Cayce JM, Crowder SW, Sung HJ, Jansen ED (2012) Material considerations for optical interfacing to the nervous system. MRS Bulletin 37:599-605.

Chouard CH, Pialoux P (1995) [Biocompatibility of cochlear implants]. Bull Acad Natl Med 179:549-555.

Chow BY, Han X, Dobry AS, Qian X, Chuong AS, Li M, Henninger MA, Belfort GM, Lin Y, Monahan PE, Boyden ES (2010) High-performance genetically targetable optical neural silencing by light-driven proton pumps. Nature 463:98-102.

Christine CW, Starr PA, Larson PS, Eberling JL, Jagust WJ, Hawkins RA, VanBrocklin HF, Wright JF, Bankiewicz KS, Aminoff MJ (2009) Safety and tolerability of putaminal AADC gene therapy for Parkinson disease. Neurology 73:1662-1669.

Christopher & Dana Reeve Foundation (2009) One Degree of Separation: Paralysis and Spinal Cord Injury in the United States.

Crum BA, Strommen JA (2007) Peripheral nerve stimulation and monitoring during operative procedures. Muscle Nerve 35:159-170.

Davis FA, Schauf CL, Reed BJ, Kesler RL (1976) Experimental studies of the effects of extrinsic factors on conduction in normal and demyelinated nerve. 1. Temperature. J Neurol Neurosurg Psychiatry 39:442-448.

Daya S, Berns KI (2008) Gene therapy using adeno-associated virus vectors. Clin Microbiol Rev 21:583-593.

Deisseroth K (2011) Optogenetics. Nat Methods 8:26-29.

Diester I, Kaufman MT, Mogri M, Pashaie R, Goo W, Yizhar O, Ramakrishnan C, Deisseroth K, Shenoy KV (2011) An optogenetic toolbox designed for primates. Nat Neurosci 14:387-397.

Dittami GM, Rajguru SM, Lasher RA, Hitchcock RW, Rabbitt RD (2011) Intracellular calcium transients evoked by pulsed infrared radiation in neonatal cardiomyocytes. J Physiol 589:1295-1306.

Douglas WW, Malcolm JL (1955) The effect of localized cooling on conduction in cat nerves. J Physiol 130:53-71.

Dowden BR, Wark HA, Normann RA (2010) Muscle-selective block using intrafascicular high-frequency alternating current. Muscle Nerve 42:339-347.

Dummer M, Johnson K, Hibbs-Brenner M, Keller M, Gong T, Wells J, Bendett M (2011) Development of VCSELs for optical nerve stimulation. vol. 7883, p 85.

Fenno L, Yizhar O, Deisseroth K (2011) The development and application of optogenetics. Annu Rev Neurosci 34:389-412.

Fork RL (1971) Laser stimulation of nerve cells in Aplysia. Science 171:907-908.

Fried NM, Rais-Bahrami S, Lagoda GA, Ai-Ying C, Li-Ming S, Burnett AL (2007) Identification and Imaging of the Nerves Responsible for Erectile Function in Rat Prostate, *In Vivo*, Using Optical Nerve Stimulation and Optical Coherence Tomography. Selected Topics in Quantum Electronics, IEEE Journal of 13:1641-1645.

Fried NM, Lagoda GA, Scott NJ, Su LM, Burnett AL (2008a) Laser stimulation of the cavernous nerves in the rat prostate, in vivo: Optimization of wavelength, pulse energy, and pulse repetition rate. Conf Proc IEEE Eng Med Biol Soc 2008:2777-2780.

Fried NM, Lagoda GA, Scott NJ, Su LM, Burnett AL (2008b) Noncontact stimulation of the cavernous nerves in the rat prostate using a tunable-wavelength thulium fiber laser. J Endourol 22:409-413.

Frost & Sullivan (2008) U.S. Neurostimulation Devices Market.

Gallichio JE (2004) Pharmacologic management of spasticity following stroke. Phys Ther 84:973-981.

Gaunt RA, Prochazka A (2009) Transcutaneously coupled, high-frequency electrical stimulation of the pudendal nerve blocks external urethral sphincter contractions. Neurorehabil Neural Repair 23:615-626.

Gotch F, Macdonald JS (1896) Temperature and Excitability. J Physiol 20:247-297.

Gradinaru V, Thompson KR, Zhang F, Mogri M, Kay K, Schneider MB, Deisseroth K (2007) Targeting and readout strategies for fast optical neural control in vitro and in vivo. J Neurosci 27:14231-14238.

Gradinaru V, Thompson KR, Deisseroth K (2008) eNpHR: a Natronomonas halorhodopsin enhanced for optogenetic applications. Brain Cell Biol 36:129-139.

Gradinaru V, Mogri M, Thompson KR, Henderson JM, Deisseroth K (2009) Optical deconstruction of parkinsonian neural circuitry. Science 324:354-359.

Grahame DC (1947) The electrical double layer and the theory of electrocapillarity. Chem Rev 41:441-501.

Grill WM, Mortimer JT (1995) Stimulus Wave-Forms for Selective Neural Stimulation. Ieee Eng Med Biol 14:375-385.

Grill WM, Mortimer JT (1997) Inversion of the current-distance relationship by transient depolarization. IEEE Trans Biomed Eng 44:1-9.

Grill WM, Norman SE, Bellamkonda RV (2009) Implanted neural interfaces: biochallenges and engineered solutions. Annu Rev Biomed Eng 11:1-24.

Groves DA, Brown VJ (2005) Vagal nerve stimulation: a review of its applications and potential mechanisms that mediate its clinical effects. Neurosci Biobehav Rev 29:493-500.

Haines DE, Ard MD (2002) Fundamental neuroscience. New York: Churchill Livingstone.

Hale GM, Querry MR (1973) Optical Constants of Water in the 200-nm to 200-microm Wavelength Region. Appl Opt 12:555-563.

Hassouna MM, Siegel SW, Nyeholt AA, Elhilali MM, van Kerrebroeck PE, Das AK, Gajewski JB, Janknegt RA, Rivas DA, Dijkema H, Milam DF, Oleson KA, Schmidt RA (2000) Sacral neuromodulation in the treatment of urgency-frequency symptoms: a multicenter study on efficacy and safety. J Urol 163:1849-1854.

Hibbs-Brenner M, Johnson K, Bendett M (2009) VCSEL technology for medical diagnostics and therapeutics. vol. 7180, pp 71800-71810.

Hille B (2001) Ion channels of excitable membranes. Sunderland, Mass.: Sinauer.

Hodgkin AL (1938) The Subthreshold Potentials in a Crustacean Nerve Fibre. Proceedings of the Royal Society of London Series B, Biological Sciences 126:87-121.

Hodgkin AL, Katz B (1949) The effect of temperature on the electrical activity of the giant axon of the squid. J Physiol 109:240-249.

Hodgkin AL, Huxley AF (1952) A quantitative description of membrane current and its application to conduction and excitation in nerve. J Physiol 117:500-544.

Holsheimer J (2003) Principles of neurostimulation. Pain Research and Clinical Management 15:17-36.

Huxley AF (1959) Ion movements during nerve activity. Ann N Y Acad Sci 81:221-246.

Iwai Y, Honda S, Ozeki H, Hashimoto M, Hirase H (2011) A simple head-mountable LED device for chronic stimulation of optogenetic molecules in freely moving mice. Neurosci Res 70:124-127.

Izzo AD, Richter CP, Jansen ED, Walsh JT (2006) Laser stimulation of the auditory nerve. Lasers in Surgery and Medicine 38:745-753.

Izzo AD, Suh E, Pathria J, Walsh JT, Whitlon DS, Richter CP (2007a) Selectivity of neural stimulation in the auditory system: a comparison of optic and electric stimuli. Journal of Biomedical Optics 12:-.

Izzo AD, Walsh JT, Jr., Jansen ED, Bendett M, Webb J, Ralph H, Richter CP (2007b) Optical parameter variability in laser nerve stimulation: a study of pulse duration, repetition rate, and wavelength. IEEE Trans Biomed Eng 54:1108-1114.

Izzo AD, Walsh JT, Ralph H, Webb J, Bendett M, Wells J, Richter CP (2008) Laser stimulation of auditory neurons: Effect of shorter pulse duration and penetration depth. Biophysical Journal 94:3159-3166.

Jia J, Pollock M (1998) Cold injury to nerves is not due to ischaemia alone. Brain 121 (Pt 5):989-1001.

Jia J, Pollock M (1999) Cold nerve injury is enhanced by intermittent cooling. Muscle Nerve 22:1644-1652.

Johnston WL, Dyer JR, Castellucci VF, Dunn RJ (1996) Clustered voltage-gated Na+ channels in Aplysia axons. J Neurosci 16:1730-1739.

Kandel ER (2001) The molecular biology of memory storage: a dialogue between genes and synapses. Science 294:1030-1038.

Kaplitt MG, Feigin A, Tang C, Fitzsimons HL, Mattis P, Lawlor PA, Bland RJ, Young D, Strybing K, Eidelberg D, During MJ (2007) Safety and tolerability of gene therapy with an adeno-associated virus (AAV) borne GAD gene for Parkinson's disease: an open label, phase I trial. Lancet 369:2097-2105.

Katona PG (2010) Biomedical engineering in heart-brain medicine: a review. Cleve Clin J Med 77 Suppl 3:S46-50.

Kilgore KL, Bhadra N (2004) Nerve conduction block utilising high-frequency alternating current. Med Biol Eng Comput 42:394-406.

Kilgore KL, Foldes EA, Ackermann DM, Bhadra N (2009) Combined direct current and high frequency nerve block for elimination of the onset response. Conf Proc IEEE Eng Med Biol Soc 2009:197-199.

Koechner W, Bass M (2003) Solid-state lasers: a graduate text: Springer Verlag.

Koechner W (2006) Solid-state laser engineering: Springer Verlag.

Kottink AI, Hermens HJ, Nene AV, Tenniglo MJ, van der Aa HE, Buschman HP, Ijzerman MJ (2007) A randomized controlled trial of an implantable 2-channel peroneal nerve stimulator on walking speed and activity in poststroke hemiplegia. Arch Phys Med Rehabil 88:971-978.

Kuner T, Li Y, Gee KR, Bonewald LF, Augustine GJ (2008) Photolysis of a caged peptide reveals rapid action of N-ethylmaleimide sensitive factor before neurotransmitter release. Proc Natl Acad Sci U S A 105:347-352.

LaLumiere RT (2011) A new technique for controlling the brain: optogenetics and its potential for use in research and the clinic. Brain Stimul 4:1-6.

Li X, Gutierrez DV, Hanson MG, Han J, Mark MD, Chiel H, Hegemann P, Landmesser LT, Herlitze S (2005) Fast noninvasive activation and inhibition of neural and network activity by vertebrate rhodopsin and green algae channelrhodopsin. Proc Natl Acad Sci U S A 102:17816-17821.

Liang DH, Lusted HS, White RL (1999) The nerve-electrode interface of the cochlear implant: current spread. IEEE Trans Biomed Eng 46:35-43.

Llewellyn ME, Thompson KR, Deisseroth K, Delp SL (2010) Orderly recruitment of motor units under optical control in vivo. Nat Med 16:1161-1165.

Lynch CL, Popovic MR (2008) Functional electrical stimulation. Ieee Contr Syst Mag 28:40-50.

Majji AB, Humayun MS, Weiland JD, Suzuki S, D'Anna SA, de Juan E, Jr. (1999) Long-term histological and electrophysiological results of an inactive epiretinal electrode array implantation in dogs. Invest Ophthalmol Vis Sci 40:2073-2081.

Malmstrom JA, McNaughton TG, Horch KW (1998) Recording properties and biocompatibility of chronically implanted polymer-based intrafascicular electrodes. Ann Biomed Eng 26:1055-1064.

MarketsandMarkets (2009) Medical Devices Market Research Report. June 13, 2012.

Matic AI, Walsh JT, Jr., Richter CP (2011) Spatial extent of cochlear infrared neural stimulation determined by tone-on-light masking. J Biomed Opt 16:118002.

Matsuda Y, Niwa M, Iwai H, Kogure S, Honjoe N, Komatsu M, Ishii Y, Watanabe K (2006) Effects of argon laser irradiation on polar excitations in frog sciatic nerve. Lasers Surg Med 38:608-614.

McNeal DR (1976) Analysis of a model for excitation of myelinated nerve. IEEE Trans Biomed Eng 23:329-337.

Merrill DR, Bikson M, Jefferys JG (2005) Electrical stimulation of excitable tissue: design of efficacious and safe protocols. J Neurosci Methods 141:171-198.

Miles JD, Kilgore KL, Bhadra N, Lahowetz EA (2007) Effects of ramped amplitude waveforms on the onset response of high-frequency mammalian nerve block. J Neural Eng 4:390-398.

Mou Z, Triantis IF, Woods VM, Toumazou C, Nikolic K (2012) A simulation study of the combined thermoelectric extracellular stimulation of the sciatic nerve of the Xenopus laevis: the localized transient heat block. IEEE Trans Biomed Eng 59:1758-1769.

Mounaim F, Elzayat E, Sawan M, Corcos J, Elhilali M (2010) New Neurostimulation and Blockade Strategy to Enhance Bladder Voiding in Paraplegics. in Contemporary Engineering Sciences, Hikari Ltd 1313-6569.

Musio C, Bedini C (1990) Fine structure and axonal organization in the buccal ganglia nerves ofAplysia (Mollusca, Gastropoda). Zoomorphology 110:17-26.

Navarro X, Krueger TB, Lago N, Micera S, Stieglitz T, Dario P (2005) A critical review of interfaces with the peripheral nervous system for the control of neuroprostheses and hybrid bionic systems. J Peripher Nerv Syst 10:229-258.

NIDCD (2011) NIDCD Fact Sheet: Cochlear Implants. NIH Publication No. 11-4798. http://www.nidcd.nih.gov/staticresources/health/hearing/FactSheetCochlearImplant.pdf. June 14, 2012.

Nikolenko V, Poskanzer KE, Yuste R (2007) Two-photon photostimulation and imaging of neural circuits. Nat Methods 4:943-950.

Nowak LG, Bullier J (1996) Spread of stimulating current in the cortical grey matter of rat visual cortex studied on a new in vitro slice preparation. J Neurosci Methods 67:237-248.

Olson JE, Schimmerling W, Gundy GC, Tobias CA (1981a) Laser microirradiation of cerebellar neurons in culture. Electrophysiological and morphological effects. Cell Biophys 3:349-371.

Olson JE, Schimmerling W, Tobias CA (1981b) Laser action spectrum of reduced excitability in nerve cells. Brain Res 204:436-440.

Patberg WR, Melchior HJ, Mast JG (1984) Blocking of impulse conduction in peripheral nerves by local cooling as a routine in animal experimentation. J Neurosci Methods 10:267-275.

Peckham PH, Knutson JS (2005) Functional electrical stimulation for neuromuscular applications. Annu Rev Biomed Eng 7:327-360.

Polasek KH, Hoyen HA, Keith MW, Kirsch RF, Tyler DJ (2009) Stimulation stability and selectivity of chronically implanted multicontact nerve cuff electrodes in the human upper extremity. IEEE Trans Neural Syst Rehabil Eng 17:428-437.

Quarles RH, Macklin WB, Morell P (2006) Myelin formation, structure and biochemistry. Basic neurochemistry 1:51-72.

Rajguru SM, Matic AI, Robinson AM, Fishman AJ, Moreno LE, Bradley A, Vujanovic I, Breen J, Wells JD, Bendett M, Richter CP (2010) Optical cochlear implants: evaluation of surgical approach and laser parameters in cats. Hear Res 269:102-111.

Rajguru SM, Richter CP, Matic AI, Holstein GR, Highstein SM, Dittami GM, Rabbitt RD (2011) Infrared photostimulation of the crista ampullaris. J Physiol 589:1283-1294.

Rattay F (1986) Analysis of models for external stimulation of axons. IEEE Trans Biomed Eng 33:974-977.

Rattay F (1989) Analysis of models for extracellular fiber stimulation. IEEE Trans Biomed Eng 36:676-682.

Rattay F, Aberham M (1993) Modeling axon membranes for functional electrical stimulation. IEEE Trans Biomed Eng 40:1201-1209.

Ravid EN, Gan LS, Todd K, Prochazka A (2011) Nerve lesioning with direct current. J Neural Eng 8:016005.

Richter CP, Matic AI, Wells JD, Jansen ED, Walsh JT (2011) Neural stimulation with optical radiation. Laser Photonics Rev 5:68-80.

Schachter SC (2002) Vagus nerve stimulation therapy summary: five years after FDA approval. Neurology 59:S15-20.

Schauf CL, Davis FA (1974) Impulse conduction in multiple sclerosis: a theoretical basis for modification by temperature and pharmacological agents. J Neurol Neurosurg Psychiatry 37:152-161.

Schmidt CL, Skarstad PM (2001) The future of lithium and lithium-ion batteries in implantable medical devices. J Power Sources 97-8:742-746.

Schmidt CL, Scott ER (2011) Energy harvesting and implantable medical devices-first order selection criteria. In: 2011 IEEE International Electron Devices Meeting (IEDM), pp 10.15. 11-10.15. 14: IEEE.

Shannon RV (2012) Advances in auditory prostheses. Curr Opin Neurol 25:61-66.

Shapiro MG, Homma K, Villarreal S, Richter CP, Bezanilla F (2012) Infrared light excites cells by changing their electrical capacitance. Nat Commun 3:736.

Slavin KV (2008) Peripheral nerve stimulation for neuropathic pain. Neurotherapeutics 5:100-106.

Stewart JD (2003) Peripheral nerve fascicles: anatomy and clinical relevance. Muscle Nerve 28:525-541.

Sunderland S (1968) Nerves and nerve injuries. Baltimore,: Williams and Wilkins Co.

Sweeney JD, Ksienski DA, Mortimer JT (1990) A nerve cuff technique for selective excitation of peripheral nerve trunk regions. IEEE Trans Biomed Eng 37:706-715.

Sweeney JD, Crawford NR, Brandon TA (1995) Neuromuscular stimulation selectivity of multiple-contact nerve cuff electrode arrays. Med Biol Eng Comput 33:418-425.

Tarler MD, Mortimer JT (2003) Comparison of joint torque evoked with monopolar and tripolar-cuff electrodes. IEEE Trans Neural Syst Rehabil Eng 11:227-235.

Tehovnik EJ (1996) Electrical stimulation of neural tissue to evoke behavioral responses. J Neurosci Methods 65:1-17.

Teudt IU, Nevel AE, Izzo AD, Walsh JT, Jr., Richter CP (2007) Optical stimulation of the facial nerve: a new monitoring technique? Laryngoscope 117:1641-1647.

Teudt IU, Maier H, Richter CP, Kral A (2011) Acoustic events and "optophonic" cochlear responses induced by pulsed near-infrared laser. IEEE Trans Biomed Eng 58:1648-1655.

Townshend B, Cotter N, Van Compernolle D, White RL (1987) Pitch perception by cochlear implant subjects. J Acoust Soc Am 82:106-115.

Tozburun S, Fried NM (2009) Design of a compact laparoscopic probe for optical stimulation of the cavernous nerves. vol. 7161 (Nikiforos, K. et al., eds), p 716113: SPIE.

Tozburun S, Cilip CM, Lagoda GA, Burnett AL, Fried NM (2010) Continuous-wave infrared optical nerve stimulation for potential diagnostic applications. J Biomed Opt 15:055012.

Tozburun S, Lagoda GA, Burnett AL, Fried NM (2011) Continuous-wave laser stimulation of the rat prostate cavernous nerves using a compact and inexpensive all single mode optical fiber system. J Endourol 25:1727-1731.

Tozburun S, Lagoda GA, Burnett AL, Fried NM (2012) Subsurface near-infrared laser stimulation of the periprostatic cavernous nerves. J Biophotonics.

Tyler DJ, Durand DM (2002) Functionally selective peripheral nerve stimulation with a flat interface nerve electrode. IEEE Trans Neural Syst Rehabil Eng 10:294-303.

Tyler DJ, Durand DM (2003) Chronic response of the rat sciatic nerve to the flat interface nerve electrode. Ann Biomed Eng 31:633-642.

Uzdensky AB, Savransky VV (1997) Single neuron response to pulse-periodic laser microirradiation. Action spectra and two-photon effect. Journal of Photochemistry and Photobiology B: Biology 39:224-228.

Verma IM, Somia N (1997) Gene therapy -- promises, problems and prospects. Nature 389:239-242.

Wedensky N (1903) Die erregung, hemmung und narkose. Pfl√ºgers Archiv European Journal of Physiology 100:1-144.

Wei X, Liu J (2008) Power sources and electrical recharging strategies for implantable medical devices. Frontiers of Energy and Power Engineering in China 2:1-13.

Wells J, Kao C, Jansen ED, Konrad P, Mahadevan-Jansen A (2005a) Application of infrared light for in vivo neural stimulation. Journal of Biomedical Optics 10:-.

Wells J, Kao C, Mariappan K, Albea J, Jansen ED, Konrad P, Mahadevan-Jansen A (2005b) Optical stimulation of neural tissue in vivo. Optics Letters 30:504-506.

Wells J, Kao C, Konrad P, Milner T, Kim J, Mahadevan-Jansen A, Jansen ED (2007a) Biophysical mechanisms of transient optical stimulation of peripheral nerve. Biophysical Journal 93:2567-2580.

Wells J, Konrad P, Kao C, Jansen ED, Mahadevan-Jansen A (2007b) Pulsed laser versus electrical energy for peripheral nerve stimulation. J Neurosci Methods 163:326-337.

Wells JD, Thomsen S, Whitaker P, Jansen ED, Kao CC, Konrad PE, Mahadevan-Jansen A (2007c) Optically mediated nerve stimulation: Identification of injury thresholds. Lasers Surg Med 39:513-526.

Wentz CT, Bernstein JG, Monahan P, Guerra A, Rodriguez A, Boyden ES (2011) A wirelessly powered and controlled device for optical neural control of freely-behaving animals. J Neural Eng 8:046021.

World Health Organization (2006) Neurological disorders: public health challenges: World Health Organization.

Xu D, Pollock M (1994) Experimental nerve thermal injury. Brain 117 (Pt 2):375-384.

Xu J, Shepherd RK, Millard RE, Clark GM (1997) Chronic electrical stimulation of the auditory nerve at high stimulus rates: a physiological and histopathological study. Hear Res 105:1-29.

Zhang F, Wang LP, Brauner M, Liewald JF, Kay K, Watzke N, Wood PG, Bamberg E, Nagel G, Gottschalk A, Deisseroth K (2007) Multimodal fast optical interrogation of neural circuitry. Nature 446:633-639.

CHAPTER IV

COMBINED OPTICAL AND ELECTRICAL STIMULATION OF NEURAL TISSUE IN VIVO

Austin R. Duke[1], Jonathan M. Cayce[1], Jonathan D. Malphrus[1], Peter E. Konrad[1,2], Anita Mahadevan-Jansen[1,2] and E. Duco Jansen[1,2]

[1]Vanderbilt University, Department of Biomedical Engineering

Nashville, TN

[2]Vanderbilt University, Department of Neurological Surgery

Nashville, TN

This chapter was published in:

"Combined optical and electrical stimulation of neural tissue *in vivo*,"

Journal of Biomedical Optics. 14(6), 060501-3 (2009).

4.1 Abstract

Low-intensity, pulsed infrared light provides a novel nerve stimulation modality that avoids the limitations of traditional electrical methods such as necessity of contact, presence of a stimulation artifact and relatively poor spatial precision. Infrared neural stimulation (INS) is, however, limited by a 2:1 ratio of threshold radiant exposures for damage to that for stimulation. In this study, we have shown that this ratio is increased to nearly 6:1 by combining the infrared pulse with a sub-threshold electrical stimulus. Our results indicate a nonlinear relationship between the sub-threshold depolarizing electrical stimulus and additional optical energy required to reach stimulation threshold. The change in optical threshold decreases linearly as the delay between the electrical and optical pulses is increased. We have shown that the high spatial precision of INS is maintained for this combined stimulation modality. Results of this study will facilitate the development of applications for infrared neural stimulation, as well as target the efforts to uncover the mechanism by which infrared light activates neural tissue.

4.2 Introduction

Recent research demonstrating the feasibility and advantages of stimulating neural tissue with infrared light has generated significant interest. Applications of infrared neural stimulation (INS) range from stimulation of the auditory system for improved cochlear implants to cavernous nerve mapping during prostate resections (Wells et al., 2005a, Izzo et al., 2006, Wells et al., 2007a, Fried et al., 2008). While electrical stimulation has long been the method of choice for stimulating neural activity, INS is a capable alternative that provides a contact-free, artifact-free and spatially precise

neural stimulation modality (Wells et al., 2005a, Wells et al., 2005b). However, INS is limited by a narrow window for safe stimulation. Wells et al. have shown that radiant exposures (J/cm^2) generating laser-induced thermal damage are only a factor of 2 greater than those needed for stimulation (Wells et al., 2007b). For INS to be applied at higher repetition rates or radiant exposures much greater than threshold, the range of radiant exposures for safe, yet effective stimulation must be extended. Additionally, implantable INS stimulators may be limited by the laser power necessary for stimulation. Reducing the power requirements of the INS stimulator will facilitate the translation of INS technology into an implantable device.

We hypothesize that the nerve excitability to INS may be enhanced by applying a sub-threshold electrical stimulus concomitantly with the delivery of pulsed infrared light, thus lowering the threshold for optical stimulation while maintaining spatial precision and mitigating the risk of laser-induced tissue damage. To test this hypothesis, we varied the magnitude of the sub-threshold electrical stimulus to determine the relationship between the electrical stimulus magnitude and the requisite amount of optical energy to achieve stimulation. We then investigated the delay of the infrared pulse relative to the electrical pulse to determine the optimal pulse synchronization for minimizing the optical energy required. By reducing the threshold radiant exposure of infrared light needed to achieve stimulation by nearly 3-fold, we have greatly increased the safe and effective range of INS. Finally, it was confirmed that the spatial precision of INS is maintained for this combined optical and electrical stimulation modality.

4.3 Methods

Male Sprague-Dawley rats (300-400g) were anesthetized with 50% urethane (1.5g/kg IP), and the sciatic nerve was exposed from the pelvic cavity to the knee by blunt dissection. An average of 3-4 measurements were taken from 24 nerves, yielding a total of 92 data points for this study. Saline was continuously applied to prevent dehydration of the nerve.

The system diagram used for these experiments is shown in Figure IV-1. An electrical stimulator (Grass S44; Grass Medical Instruments, Quincy, MA) was connected to a bipolar hook electrode placed under the main trunk of the sciatic nerve. A pulsed infrared diode laser (λ=1.875 μm; Lockheed Martin Aculight Capella^{TM}) was coupled to a 400 μm diameter-optical fiber (Ocean Optics). The distal end of the fiber was positioned directly above the nerve and approximately 700 μm from the surface of the nerve, in the same location as the electrode. Using the knife edge technique (Khosrofian and Garetz, 1983), the laser spot size on the nerve was determined to be 0.3584 mm^2. The optical penetration depth in tissue at the selected wavelength was approximately 400 μm, which has been shown to allow selective recruitment of a single 50-200 μm diameter fascicle positioned below the 200 μm-thick perineurium (Wells et al., 2007a). The pulse duration for both electrical and optical stimulation was 2 ms, which was dictated by the minimum pulse duration needed to obtain sufficient pulse energy to optically stimulate the nerve. Pulses were delivered at a repetition rate of 2 Hz for all experiments. Monophasic electrical stimulation was used with stimulation threshold voltages averaging 0.86±0.30 V. The electrical stimulator and the diode laser were synchronized by a digital delay generator (Stanford Research Systems, DGD-535). The Nicolet

Endeavor^{TM} Evoked Potentials System was used for electrophysiological evaluations. Needle electrodes were inserted into the biceps femoris and gastrocnemius in a bipolar configuration.

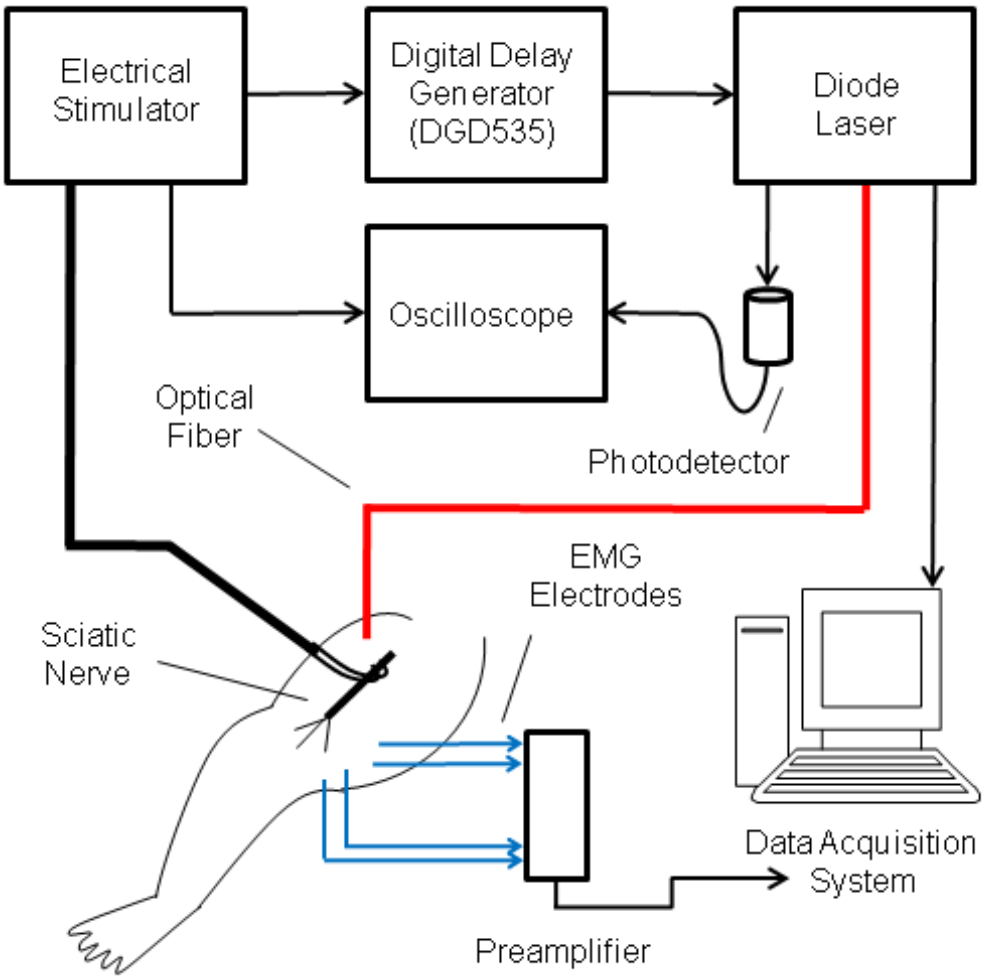

Figure IV-1. Schematic representation of the experimental setup used for all experiments in this study.

Electrical and optical pulses were first delivered simultaneously. For all experiments, stimulation threshold is defined as the minimum induced current (electrical stimulation) and/or radiant exposure (INS) needed to induce a sustained visible compound muscle action potential (CMAP) with each pulse. After finding the electrical stimulation threshold, the electrical stimulus was reduced to a known amount (i.e. 90% of threshold). An optical stimulus was then applied concomitantly with the electrical stimulus, and its magnitude was increased until reaching threshold. The electrical stimulus was removed and stimulation threshold was found using only INS. This process was repeated to establish a relationship describing the relative amounts of electrical and optical energies needed to reach threshold. In a second experiment, electrical stimulation was set to 90% of threshold. Using the digital delay generator, the arrival of the optical stimulus was delayed relative to the electrical stimulus and the amount of additional optical energy needed to achieve stimulation was determined.

4.4 Results

Figure IV-2a demonstrates the effects of combining electrical and optical stimulation. Data points reflect the amount of optical energy (% INS threshold) required to reach the stimulation threshold when applied concurrently with an electrical stimulus (% electrical stimulation threshold). The best-fit line models the data incorporating the known endpoints where 100% of either modality alone is required to reach stimulation threshold. Interestingly, the data does not fit a linear relationship. Rather, the required optical energy can be predicted by a logarithmic relationship:

$$O = 0.22 \ln(1 - E) + 1 \quad \text{(IV-7)}$$

with $R^2 = 0.56$, where O is the optical energy (% INS threshold) and E is the magnitude of the electrical stimulus expressed (% electrical stimulation threshold). The data in Figure IV-2 show significant variance which can be attributed to inter and intra animal variability, limitations of the experimental setup, in particular the spatial localization of the stimulation electrodes and fiber optic and the fact that near the electrical stimulation threshold (the steep part of the curve) minor fluctuations in electrical stimulation may result in significant changes in optical energy required.

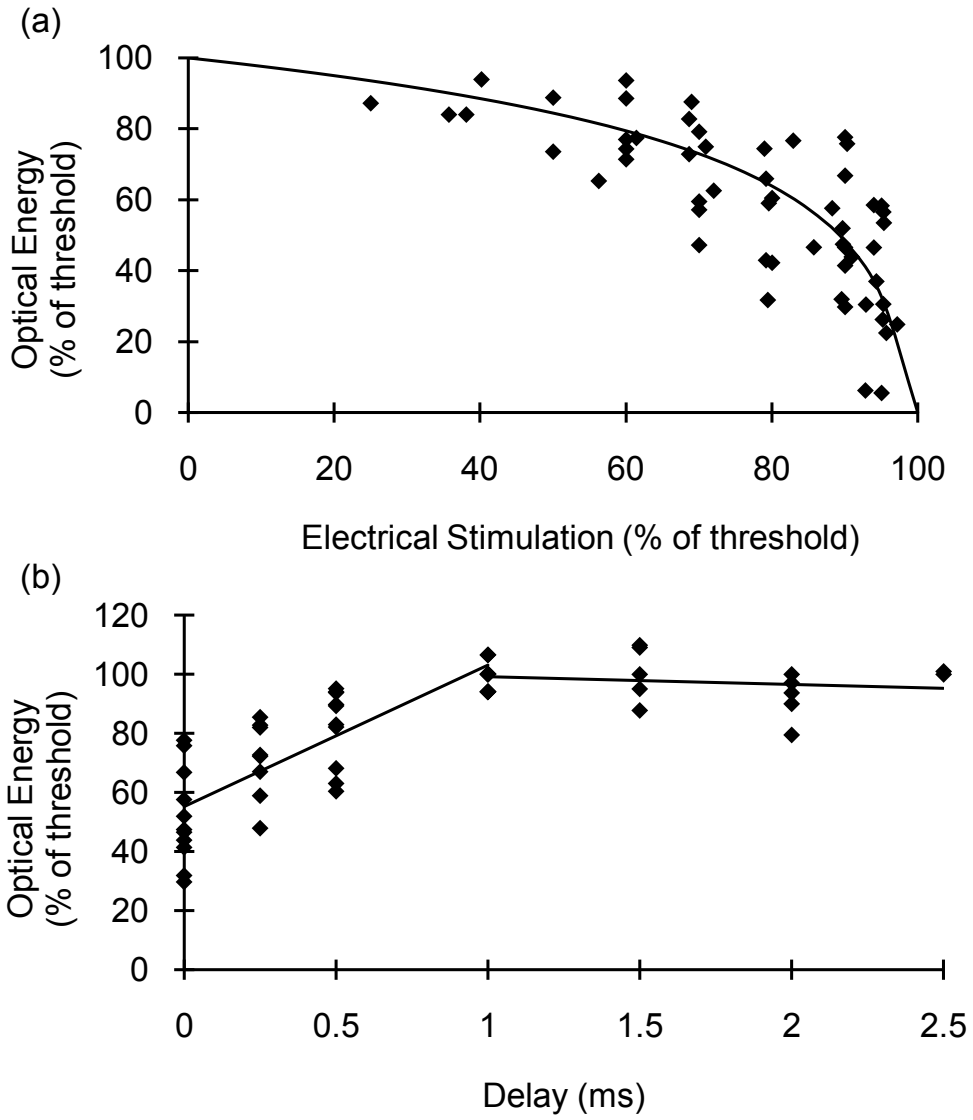

Figure IV-2. Combining optical and electrical stimuli reduces the requisite energy to achieve stimulation threshold. (a) Optical energy (% of threshold) required to reach stimulation threshold as a function of subthreshold electrical stimulus; and (b) optical energy (% of threshold) required to reach stimulation threshold as a function of delay between electrical (90% of threshold) and optical stimuli.

If the electrical stimulus is applied at 95% of the electric threshold, then the optical threshold will be reduced by a factor of nearly 3 according to equation (IV-7). For 80% or 90% of threshold, the optical threshold is reduced by 1.54 fold and 2.03 fold, respectively. This reduction in optical threshold significantly increases the window for safe INS as less energy is required to stimulate, thereby reducing the heat load in the tissue. If the ratio of damage threshold to stimulation threshold for INS alone is assumed to be 2:1, as reported by Wells et al., we can predict that applying an electrical stimulus at 90% of electrical stimulation with INS will increase this ratio to 4.05:1 (Wells et al., 2007b). For electrical stimuli at 80% and 95%, the ratio is predicted to be approximately 3.10:1 and 5.87:1, respectively. Threshold radiant exposures for INS alone averaged 1.69±0.30 J/cm^2. Combined with a sub-threshold electrical stimulus, radiant exposures were reduced to 1.49±0.22 J/cm^2 at 60% of electrical threshold and 0.60±0.29 J/cm^2 at 95% of electrical threshold. While the INS threshold radiant exposures reported here (using a 400 μm fiber) are higher than those previously published for the rat sciatic nerve (and above the published radiant exposures for thermal damage) that were obtained using a 600 μm fiber (Wells et al., 2007b), this can be accounted for by the known fiber diameter dependence of thermal distributions as well as known morphological changes over the length of the nerve. In addition, there are several subtle differences in the laser parameters and endpoint definition between the current and previously reported results. Thus a direct comparison between these absolute values should be made with caution. No visible indication of thermal damage was present at the radiant exposures used in the current study.

Figure IV-2b demonstrates the effects of delaying the optical stimulus relative to the electrical stimulus. The results indicate that the greatest benefit is achieved when the pulses are delivered simultaneously. For delays up to 1 ms, the radiant exposure necessary for stimulation appears to increase linearly. For delay times > 1 ms, there are no benefits of combining the modalities as 100% of the optical threshold is needed to achieve stimulation. Figure IV-3 illustrates that the spatial selectivity of INS is preserved in this combined stimulation modality. Note how the stimulated CMAP is only present in one muscle group.

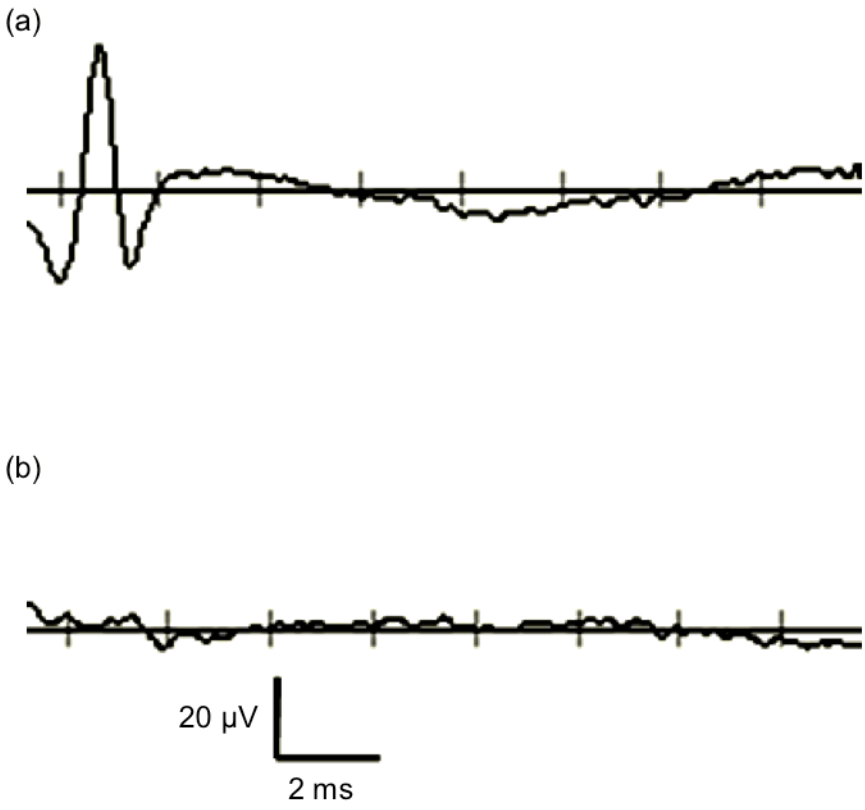

Figure IV-3. Spatial selectivity is maintained with combined optical and electrical stimulation. (a) Average of 20 consecutive recordings of CMAPs from electrodes place in biceps femoris; and (b) the same recordings as (a) for electrodes placed in gastrocnemius. With electrical stimulation alone (not shown), responses were observed on both (a) and (b).

4.5 Discussion and Conclusions

The results of this study confirm the hypothesis that delivery of a sub-threshold electrical stimulus concurrently with INS will lower the required optical energy per pulse to achieve stimulation and thus demonstrate proof of concept for a combined electrical/optical nerve stimulator. This suggests the ratio of safe to damaging radiant exposures of INS may be increased by the simultaneous delivery of a sub-threshold electrical stimulus. These findings are practical for the further developments of INS technology and may also shed light on the underlying mechanism of INS. A significant aspect of these results is that the reduction of INS threshold for a given sub-threshold electrical stimulus does not follow a linear trend (Figure IV-2a). This implies that electrical stimulation and INS do not function by the same mechanism. Otherwise, one would expect that a linear superposition would achieve stimulation as is seen when two simultaneous electrical pulses are combined (Bostock and Rothwell, 1997).

Delivering a sub-threshold electrical stimulus to enhance the excitability of neural tissue to an added electrical stimulus is not a foreign concept (Bostock and Rothwell, 1997, Bostock et al., 2005, Burke et al., 2009). The mechanism by which threshold changes occur as a result of a sub-threshold stimulus has been explained by a mathematical model of induced ionic currents with enhanced excitability primarily following membrane potential. Persistent and transient Na^+ currents initiate "superexcitability;" Na^+ channel inactivation, decay in the leakage current and activation of outward K^+ currents (primarily slow K^+ channels) cause the decline in excitability over time (Bostock et al., 1991, Burke et al., 2009).

While the results of this study are encouraging and highlight the advantages of a combined optical and electrical stimulation modality, a better fundamental understanding of this new stimulation paradigm is necessary for further development. Primarily it must be determined whether a combination of a sub-threshold electrical stimulus with a sub-threshold optical stimulus will result in less tissue damage than INS alone. The effects of laser-induced tissue damage from INS are well characterized, but the damaging effects of electrical stimulation are not as clear – especially in the context of a combined stimulation modality (Wells et al., 2007b). It remains to be determined whether there exists an optimal combination of optical and electrical stimulation parameters that will minimize tissue damage.

Our data emphasize the obvious and practical benefits of combined optical and electrical stimulation. Further evaluation of the available parameters is necessary, but the proof of concept is evident. The sub-threshold electrical stimulus clearly reduces the potential risks of laser-induced damage without interfering with the spatial precision inherent to INS (Figure IV-3). These results will facilitate the development of implantable INS stimulators by reducing required laser power, as well as benefit researchers needing a safe, spatially precise stimulation modality. While the benefits of applying INS concurrently with electrical stimulation suggest that ionic currents contribute to the mechanism of INS, the differences in excitability between delayed optical and electrical stimuli following an initial sub-threshold depolarizing stimulus indicate that the mechanism of INS is more involved.

4.6 References

Bostock H, Baker M, Grafe P, Reid G (1991) Changes in excitability and accommodation of human motor axons following brief periods of ischaemia. J Physiol 441:513-535.

Bostock H, Rothwell JC (1997) Latent addition in motor and sensory fibres of human peripheral nerve. J Physiol 498 (Pt 1):277-294.

Bostock H, Lin CS, Howells J, Trevillion L, Jankelowitz S, Burke D (2005) After-effects of near-threshold stimulation in single human motor axons. J Physiol 564:931-940.

Burke D, Howells J, Trevillion L, McNulty PA, Jankelowitz SK, Kiernan MC (2009) Threshold behaviour of human axons explored using subthreshold perturbations to membrane potential. J Physiol 587:491-504.

Fried NM, Lagoda GA, Scott NJ, Su LM, Burnett AL (2008) Noncontact stimulation of the cavernous nerves in the rat prostate using a tunable-wavelength thulium fiber laser. J Endourol 22:409-413.

Izzo AD, Richter CP, Jansen ED, Walsh JT (2006) Laser stimulation of the auditory nerve. Lasers in Surgery and Medicine 38:745-753.

Khosrofian JM, Garetz BA (1983) Measurement of a Gaussian Laser-Beam Diameter through the Direct Inversion of Knife-Edge Data. Applied Optics 22:3406-3410.

Wells J, Kao C, Jansen ED, Konrad P, Mahadevan-Jansen A (2005a) Application of infrared light for in vivo neural stimulation. Journal of Biomedical Optics 10:-.

Wells J, Kao C, Mariappan K, Albea J, Jansen ED, Konrad P, Mahadevan-Jansen A (2005b) Optical stimulation of neural tissue in vivo. Optics Letters 30:504-506.

Wells J, Konrad P, Kao C, Jansen ED, Mahadevan-Jansen A (2007a) Pulsed laser versus electrical energy for peripheral nerve stimulation. J Neurosci Methods 163:326-337.

Wells JD, Thomsen S, Whitaker P, Jansen ED, Kao CC, Konrad PE, Mahadevan-Jansen A (2007b) Optically mediated nerve stimulation: Identification of injury thresholds. Lasers Surg Med 39:513-526.

CHAPTER V

SPATIAL AND TEMPORAL VARIABILITY IN RESPONSE TO HYBRID ELECTRO-OPTICAL STIMULATION

Austin R. Duke[1], Hui Lu[2], Michael W. Jenkins[3], Hillel J. Chiel[2,3,4] and E. Duco Jansen[1,5]

[1]Vanderbilt University, Department of Biomedical Engineering

Nashville, TN

[2]Case Western Reserve University, Department of Biology

Cleveland, OH

[3]Case Western Reserve University, Department of Biomedical Engineering

Cleveland, OH

[4]Case Western Reserve University, Department of Neurosciences

Cleveland, OH

[5]Vanderbilt University, Department of Neurological Surgery

Nashville, TN

This chapter was published in:

"Spatial and temporal variability in response to hybrid electro-optical stimulation,"

Journal of Neural Engineering. 9(3) 036003 (2012).

5.1 Abstract

Hybrid electro-optical neural stimulation is a novel paradigm combining the advantages of optical and electrical stimulation techniques while reducing their respective limitations. However, in order to fulfill its promise, this technique requires reduced variability and improved reproducibility. Here we used a comparative physiological approach to aid the further development of this technique by identifying spatial and temporal factors characteristic of hybrid stimulation that may contribute to experimental variability and/or a lack of reproducibility. Using transient pulses of infrared light delivered simultaneously with a bipolar electrical stimulus in either the marine mollusk *Aplysia californica* buccal nerve or the rat sciatic nerve, we determined the existence of a finite region of excitability (ROE) with size altered by the strength of the optical stimulus and recruitment dictated by the polarity of the electrical stimulus. Hybrid stimulation radiant exposures yielding 50% probability of firing (RE_{50}) are shown to be negatively correlated to the underlying changes in electrical stimulation threshold over time. In *Aplysia*, but not in the rat sciatic nerve, increasing optical radiant exposures (J/cm^2) beyond the RE_{50} ultimately resulted in inhibition of evoked potentials. Accounting for the sources of variability identified in this study increased the reproducibility of stimulation from 35% to 93% in *Aplysia* and 23% to 76% in the rat with reduced variability.

5.2 Introduction

Traditional electrical techniques have long served as the method of choice for neural activation and monitoring, offering clinical efficacy and safety with well-characterized and modifiable parameters. Despite widespread successful application of

electrical stimulation in both the research and clinical arenas, electrical stimulation is fundamentally limited by the unwanted spread of current away from the stimulation site. Recent innovations in electrical stimulation design have achieved fascicular and sub-fascicular selectivity. The Flat Interface Nerve Electrode (FINE) gently reshapes the nerve to target electric fields, and can achieve fascicular selectivity in stimulation and recording with negligible changes to nerve morphology (Tyler and Durand, 2002, 2003). However, the perineurium surrounding the individual fascicles has high impedance, resulting in a uniform voltage distribution and preventing sub-fascicular selectivity. Intra-fascicular electrode arrays such as the Utah Slanted Electrode Array (USEA) and polymer longitudinal intrafascicular electrode (polyLIFE) penetrate the perineurium to allow direct electrical contact within individual fascicles (Malmstrom et al., 1998, Branner and Normann, 2000). While these intra-fascicular arrays achieve remarkable selectivity, there are concerns regarding the long-term safety of these approaches.

Many researchers are now developing optical methods of neural activation to circumvent the limitations of traditional electrical techniques and/or to complement the benefits of this well-established approach. The ability to modulate and even evoke action potentials in neurons using light has been known for decades (Booth et al., 1950, Arvanitaki and Chalazonitis, 1961, Fork, 1971, Allegre et al., 1994), but recently this method of neural stimulation has become much more promising with the discovery of higher resolution stimulation via caged compounds (Adams and Tsien, 1993), optogenetics (Boyden et al., 2005) and infrared neural stimulation (INS) (Wells et al., 2005b). Whereas stimulation of caged compounds and microbial or plant opsins inherently require exogenous additives and/or engineered neurons, INS is a neural

stimulation modality in which pulsed infrared light will generate a propagating action potential within an endogenous neural system. With INS there is also the lack of current spread, stimulation artifact and necessity of contact with the neural tissue that limits electrical techniques (Wells et al., 2007b). However, there is a restricted range of radiant exposure (J/cm^2), H, that will safely stimulate without the risk of thermally induced tissue damage (Wells et al., 2007c).

Recently, hybrid neural stimulation was developed as a new stimulation modality combining traditional electrical techniques with novel infrared nerve stimulation methods (Duke et al., 2009). The combination of the two techniques utilizes their respective advantages while avoiding their primary limitations. Specifically, hybrid stimulation combines the safety, established characteristics and demonstrated clinical utility of electrical stimulation with the spatial selectivity of INS. While hybrid stimulation does not provide the contact- and artifact-free aspects of INS, the high spatial selectivity of INS remains and will enhance clinical neural interfaces. Additionally, sub-threshold electrical currents should also reduce the problem of electrode corrosion over time. The essence of hybrid stimulation is to combine a sub-threshold electrical stimulus over a broad area, and then bring a spatially selective location to threshold by adding a sub-threshold pulse of infrared light. In doing so, both the electrical current and optical radiant exposures are reduced, effectively achieving spatial selectivity with reduced risk of tissue damage. Previously, hybrid stimulation was shown to reduce optical radiant exposures (J/cm^2) by approximately a factor of 3 when compared to INS alone (Duke et al., 2009). By offering reduced threshold radiant exposures, hybrid nerve stimulation is attractive for biomedical applications requiring spatial selectivity where laser power

constraints and tissue damage are primary concerns. However, further development of this technology will require that the reliability and repeatability of hybrid stimulation be improved.

The experiments demonstrating feasibility of hybrid stimulation in the rat sciatic nerve showed large variations in the reduction of optical radiant exposures (Duke et al., 2009). In these experiments, the electrical threshold was set at a chosen sub-threshold current and the additional optical radiant exposure required to achieve stimulation threshold was determined as a percent of the optical threshold radiant exposure when it was applied alone. The reduction in optical radiant exposures and their variability were both shown to increase as the applied electrical stimulus approached threshold. For an electrical stimulus at 95% of the threshold current, the additional optical energy required for stimulation ranged from 6 - 60% of the optical stimulation threshold. In addition, our unpublished data show a lack of reproducibility with hybrid stimulation from animal to animal. Initial attempts at hybrid stimulation were successful in 23% of rat sciatic nerves and 35% of *Aplysia californica* buccal nerves (unpublished data).

The objective of this study was to identify common factors that play a role in and may be controlled to enhance the reproducibility of hybrid electro-optical stimulation. Using this methodology, we will identify relevant sources of variability in an experimentally tractable and relatively simple neurobiological system. Then we will test these variability sources in a more clinically relevant model, where the complexity of the neural system may obscure their detection. Accordingly, the experimental procedures may differ slightly between the two model neural systems; however, the purpose of this study is to analyze and assess the overarching trends rather than the minor differences in

stimulation protocols. To accomplish these goals, our choices of neural systems are the buccal nerve of the invertebrate marine mollusk *Aplysia californica* and the sciatic nerve of the vertebrate mammal *Rattus norvegicus* (rat). The *Aplysia* buccal ganglion provides a tractable, robust nervous system with large identified neurons and relatively few axons per nerve (Kandel, 1979, Elliott and Susswein, 2002). These advantages facilitate the systematic empirical exploration of potential factors underlying the reproducibility of hybrid stimulation. The myelinated rat sciatic nerve is a more clinically relevant model for hybrid stimulation, but it is less robust than the *Aplysia* nerves, and the fundamental interaction between the optical and electrical stimuli is confounded by the presence of myelin and a less stable nerve preparation. Therefore, we identify and characterize factors contributing to the reproducibility of hybrid stimulation in the *Aplysia* buccal nerve and then evaluate those factors in the rat sciatic nerve to determine whether similar trends are observed. In this study, we will investigate both spatial and temporal factors that may be controlled to reduce variability and enhance reproducibility.

There are two aspects of the spatial component that we address: 1) The relative locations of the optical and electrical stimuli; and 2) the size of the excitable region as a function of the optical stimulus strength. The mechanism of INS was shown to involve a thermal gradient (Wells et al., 2007a). Thus, it is assumed that the thermal gradient and the electrical current path must overlap spatially. However, what is not known is where this overlap may occur, or how the two fields may affect each other. The activating function, which describes the transmembrane potentials leading to the electrical activation of a neuron, results in neurons closest to the cathode being activated first (with larger axons recruited before smaller axons) (Rattay, 1986, Holsheimer, 2003).

Experimentally, stimulation threshold current is shown to increase with increasing distance from the cathode (Ranck, 1975). Given that the electrical stimulus preferentially targets neurons nearest the cathode, we hypothesize that hybrid stimulation will require the lowest optical pulse energies when the optical stimulus is located along the electrical current path and adjacent to the cathode. Like electrical stimulation, increasing INS radiant exposures results in an increase in magnitude of the evoked response, suggesting recruitment of additional axons (Izzo et al., 2008). Therefore, we expect that for a given sub-threshold electrical stimulus, an increase in the sub-threshold optical stimulus will yield an increase in the size of the excitable region for hybrid stimulation.

It has long been known that electrical stimulation thresholds vary over time (Blair and Erlanger, 1935). In examining temporal factors, we seek to evaluate how brief fluctuations (minutes) and long-term trends (minutes to hours) in electrical stimulation thresholds affect optical pulse energies for hybrid stimulation. Correct measures of optical energies for hybrid stimulation require an accurate determination of the electrical "priming" stimulus at the time of the measurement. If one incorrectly assumes that the electrical stimulation threshold is stationary over a fixed period of time, then hybrid stimulation performance will suffer. To address this issue, we measure threshold optical energies for hybrid stimulation while monitoring electrical thresholds over an extended period of time. We hypothesize that if the electrical threshold is known at any point in time, then the additional optical energy required for stimulation can be predicted for a given sub-threshold stimulus. Additionally, we believe that changes in threshold radiant exposures for the optical component of hybrid stimulation will be positively correlated to the changes in the underlying electrical stimulation threshold.

5.3 Materials and Methods

5.3.1 Aplysia californica preparation and electrophysiology

Aplysia californica (n=26) weighing 190-250g (Marinus Scientific, Long Beach, CA) were maintained in an aerated aquarium containing circulating artificial seawater (ASW) (Instant Ocean; Aquarium Systems, Mentor, OH) kept at 16-17 °C. The animals were fed dried seaweed every 1-3 days.

Aplysia were anesthetized with an injection of 333 mM $MgCl_2$ (50% of body weight) prior to dissection. Once anesthetized, animals were dissected and the buccal ganglia were removed and pinned in a recording dish and immersed in *Aplysia* saline (460 mM NaCl, 10 mM KCl, 22 mM $MgCl_2$, 33 mM $MgSO_4$, 10 mM $CaCl_2$, 10 mM glucose, 10 mM HEPES, pH 7.6). Once dissected and pinned, *Aplysia* nerves were left untreated so as not to reduce spontaneous activity. We chose not to discard data from trials where spontaneous activity occurred, as excitability varies with the level of activity. This is an inherent biological factor that we wanted to assess in our study. For each experiment, the nerve of interest (either buccal nerve 2 (BN2), or buccal nerve 3 (BN3)) was anchored in place by pinning the protective sheath around the nerve to the Sylgard® base (Dow Corning, Midland, MI) of the recording dish. Once securely pinned, the nerve to be investigated was suctioned into a nerve-recording electrode to monitor the response to stimulation (Figure V-1a). Nerve suction recording electrodes were made by hand-pulling polyethylene tubing (1.27 mm outer diameter; PE90; Becton Dickinson) over a flame to the desired thickness. Recording electrodes were suction-filled with *Aplysia* saline prior to suctioning of the nerve. Nerve signals were amplified (x1000) and band-

pass filtered (300 – 500 Hz) using an AC-coupled differential amplifier (model 1700; A-M Systems), digitized (Axon Digidata 1440A; Molecular Devices, Sunnyvale, CA) and recorded (Axograph X; Axograph Scientific).

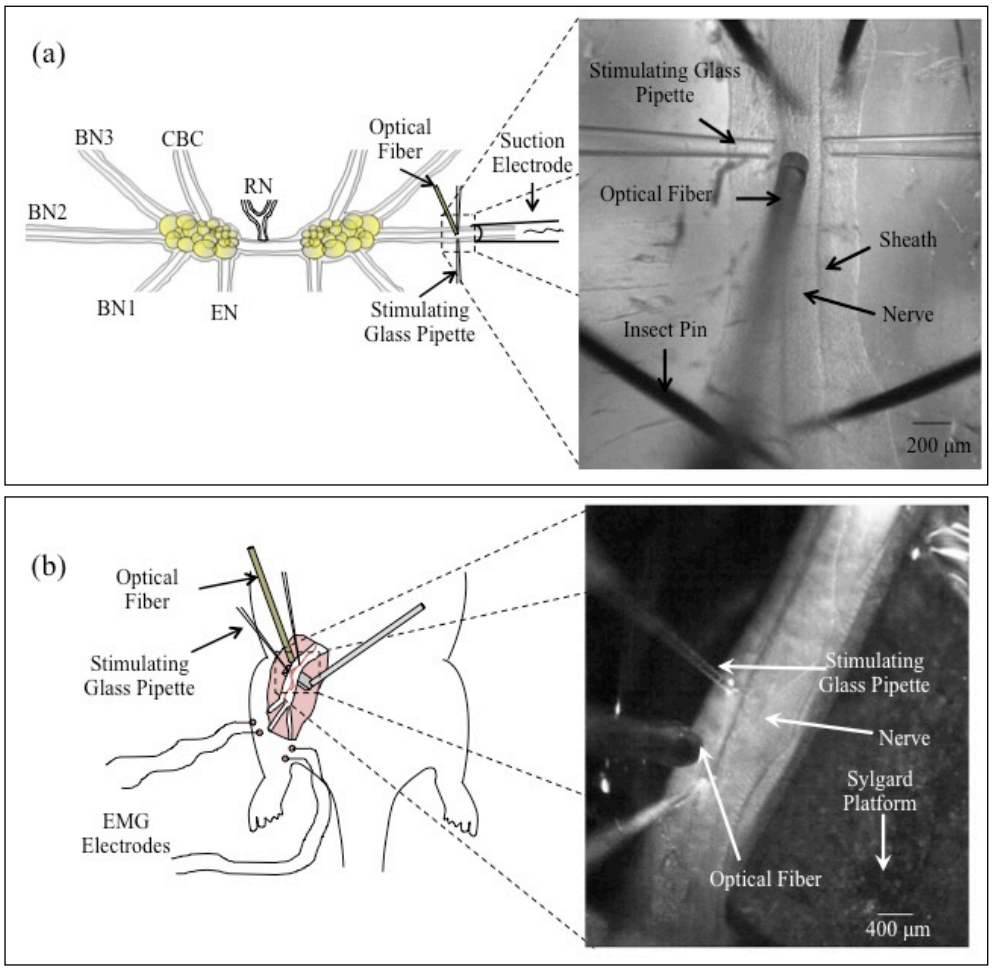

Figure V-1. Experimental setups used to investigate hybrid electro-optical stimulation in the *Aplysia californica* buccal nerve and rat sciatic nerve ((a) and (b), respectively). RN = Radular nerve; CBC = Cerebrobuccal connective; BN3 = Buccal Nerve 3; BN2 = Buccal Nerve 2; BN1 = Buccal Nerve 1; EN = Esophageal Nerve.

5.3.2 Rat preparation and electrophysiology

All rat experiments were performed following protocols approved by the Institutional Animal Care and Use Committee. Female Sprague-Dawley rats (n = 9) weighing 150 – 200g (Charles River) were anesthetized with continuously inhaled isoflurane (induction: 3% isoflurane, 2.0 LPM oxygen; maintenance: 2-2.5% isoflurane, 1.5 LPM oxygen). A rectal probe and heating pad (catalog # 40-90-8, FHC, Bowdoin, ME) were used to maintain the rat at a target body temperature of 35-37 °C throughout the experiment. The lateral sides of the animals' back legs were shaved and the sciatic nerve exposed proximal to the knee via an incision in the overlying muscle. The muscular fascia over the nerve was removed while the nerve's epineurial layer was left intact. Saline was added periodically to keep the nerve from dehydrating throughout the experiment. A custom Sylgard® platform was anchored to a micromanipulator and placed below the sciatic nerve with minimal added tension to minimize motion of the nerve due to the animal's respiration (Figure V-1b)

Evoked muscle action potentials were recorded using paired needle electrodes inserted in the areas of the *biceps femoris* and *gastrocnemius* muscles. EMG signals were amplified (x1000), band-pass filtered (300 – 1000 Hz), digitized and acquired using the same setup as for the *Aplysia*.

5.3.3 Endpoint definition

Analysis of hybrid stimulation requires an appropriately defined endpoint. In the *Aplysia* we defined our endpoint as the visible detection of single and/or compound extracellular nerve spikes in response to stimulation (Figure V-2a). Similarly, the

endpoint for rat experiments was visibly identified single and/or compound muscle action potentials in response to stimulation (Figure V-2b). For both species, we also required that the evoked potentials were frequency locked with the repeating stimulus (i.e. constant delay following a presented stimulus pulse) to distinguish evoked responses from spontaneous activity.

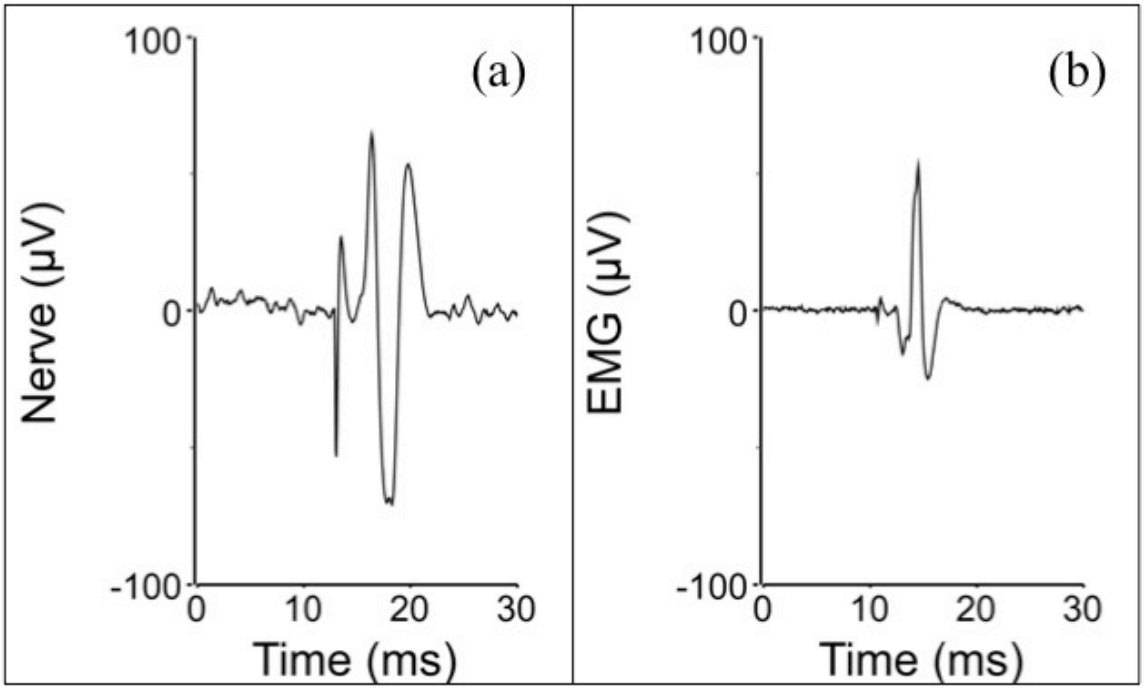

Figure V-2. Evaluation of evoked response in the *Aplysia californica* buccal nerve and the rat sciatic nerve. To evaluate electrical, optical and hybrid stimulation we looked for the presence of single and/or compound extracellular nerve potentials in the *Aplysia* californica buccal nerve and single and/or compound muscle potentials in the innervated muscles of the rat sciatic nerve. A representative recording from (a) the *Aplysia californica* buccal nerve and (b) the innervated muscle (biceps femoris) of the rat sciatic nerve.

5.3.4 Electrical and optical stimulation

Extracellular stimulating electrodes were made from thin-wall borosilicate capillary glass (catalogue #615000; A-M Systems, Everett, WA) pulled to resistances of about 0.2 MΩ (PP-830; Narishige). For each *Aplysia* experiment, two electrodes were capillary filled with *Aplysia* saline and placed on either side of the nerve in contact with the nerve sheath. This created a bipolar stimulus, with the pipettes oriented transverse to the longitudinal axis of the nerve. Pipettes were positioned such that their angle of approach to the nerve was as shallow as was allowed by the edge of the recording dish. For rat experiments, two glass pipettes were filled with normal saline and placed in contact with the nerve along the nerve's longitudinal axis. The stimulating pipette arrangement for each species was chosen based on consistency of stimulation thresholds and ability to achieve reliable supra-threshold stimulation on each nerve tested. Monophasic currents were supplied by a bipolar stimulus isolator (A365R; WPI) and passed between the two pipettes in each preparation. Electrical stimulation was defined as the minimal current that would yield 5 consecutive evoked potentials in response to pulsed stimuli.

For optical stimulation, both a holmium:yttrium-aluminum-garnet (Ho:YAG) solid state laser (SEO Laser 1-2-3, Schwartz Electro-Optics, Orlando, FL) and a tunable pulsed diode laser were used (Capella; Lockheed-Martin-Aculight, Bothwell, WA). We chose two different lasers due to the established performance in peripheral nerves offered by the Ho:YAG and the ease of use and INS-specific design of the Capella. While the Capella was used in our previous demonstration of hybrid nerve stimulation, the Ho:YAG is the laser of choice for much of the INS literature pertaining to peripheral

mammalian nerves (Wells et al., 2005a, Wells et al., 2005b, Teudt et al., 2007, Wells et al., 2007a, Wells et al., 2007b, Wells et al., 2007c). However, the Capella offers vastly improved ease of use and greatly reduced pulse-to-pulse variability when compared with the Ho:YAG. The Capella is also known to work exceptionally well for INS in a wide-array of excitable tissues including the cochlea, somatosensory cortex, embryonic heart, cardiomyocytes and the vestibular system (Izzo et al., 2007a, Harris et al., 2009, Jenkins et al., 2010, Cayce et al., 2011, Dittami et al., 2011). While the Ho:YAG provides pulses of infrared light (λ=2.12 μm) having fixed pulse duration (τ_p=0.25 ms), the Capella has slightly tunable wavelength (λ=1.855-1.875 μm) and a variable pulse duration. The important parameter for INS is penetration depth in tissue (as pulse duration was shown to have negligible effects (Wells et al., 2007a)); therefore we set the Capella to have a wavelength of λ=1.875 μm for all experiments to match the absorption (i.e. penetration depth) of the Ho:YAG laser (Hale and Querry, 1973).

For *Aplysia* experiments, laser output was coupled into either a flat-polished 100 or 200 μm diameter optical fiber (Ocean Optics, Dunedin, FL). For each experiment, the tip of the optical fiber was immersed in the *Aplysia* saline bath and brought into contact with the nerve sheath. The optical fiber was then slowly retracted with a micromanipulator and gently translated back and forth transverse to the nerve until the optical fiber was just out of contact with the nerve sheath. For radiant exposures presented in this study, the laser-irradiated area is assumed to be a circular spot on the incident surface of the nerve sheath having diameter equal to that of the optical fiber (i.e. 0.0314 mm^2 for a 200 μm fiber and 0.00785 mm^2 for a 100 μm fiber). For simplicity, as the optical fiber is just out of contact with the nerve sheath, this assumes no divergence of

the beam from the tip of the optical fiber to incident surface of the nerve sheath. For rat experiments, laser output was coupled into a flat-polished 400 μm diameter optical fiber (Ocean Optics, Dunedin, FL). The fiber diameter for rat experiments was chosen to match the 400-600 μm optical fibers used in mammalian peripheral nerve studies, while smaller fibers were used in *Aplysia* studies to scale with the size of the *Aplysia* buccal nerves (Wells et al., 2005a, Teudt et al., 2007, Duke, 2008). The optical fiber was positioned 500 μm from the incident surface of the nerve at an angle just off of vertical with a layer of saline just covering the surface of the nerve. The laser spot-size was measured using the knife-edge technique where two perpendicular measurements were taken along the axes of the presumed circularly shaped laser spot, yielding an irradiated area of 0.19 mm^2 (Khosrofian and Garetz, 1983). Pyroelectric energy detectors were used to measure pulse energies from the tip of the optical fiber for the Ho:YAG laser (J25, Coherent-Molectron Inc., Santa Clara, CA) and Capella laser (PE50BB-SH-V2, Ophir Optronics Ltd.).

For INS alone, optical stimulation threshold was defined as the minimum radiant exposure that would yield 5 consecutive evoked potentials in response to pulsed stimuli. In the *Aplysia* buccal nerve, using the Capella laser coupled to a 200 mm optical fiber that was retracted just out of contact with the nerve, threshold radiant exposures averaged 8.93 J/cm^2 with a 95% confidence interval of 8.72 – 9.14 J/cm^2 (25 measurements from 7 nerves). In the rat sciatic nerve, using the Ho:YAG laser coupled to a 400 mm optical fiber, threshold radiant exposures averaged 1.12 J/cm^2 with a 95% confidence interval of 0.92 – 1.32 J/cm^2 (12 measurements from 8 nerves).

Previous published studies found threshold radiant exposures in mammalian peripheral nerves ranging from 0.32 to 1.77 J/cm^2 (Wells et al., 2005a, Wells et al., 2005b, Teudt et al., 2007, Wells et al., 2007a, Wells et al., 2007b, Wells et al., 2007c, Duke et al., 2009). However, directly comparing these values with published data is difficult. Ongoing studies in our lab show stimulation thresholds in the rat sciatic nerve from 0.7 – 1.3 J/cm^2 (unpublished). In the cochlea, stimulation thresholds are on the order of mJ/cm^2 (Izzo et al., 2007b). To make direct comparisons it is imperative that certain factors be controlled; in particular, spot-size determination and measures of threshold must be the same. Radiant exposures are highly dependent on the spot-size. Differences in the way spot-sizes are calculated or measured between studies propagate into large differences in reported radiant exposures (due to the squared term in the denominator). In addition to variations in experimental preparations (i.e. neural model system, *in vivo*, *ex vivo*, or *in situ*), thresholds may vary based on the definition of the endpoint for a given study, for example, whether the threshold is defined by the appearance of muscle or nerve action potentials, or by a visibly identified muscle twitch (Izzo et al., 2007b, Wells et al., 2007b, Duke et al., 2009). A noteworthy aspect of this study is that no visible damage or loss of function (as indicated by the response to electrical stimulation) was noticed as a result of stimulation with the radiant exposures used. This is particularly relevant to the *Aplysia*, where optical- and hybrid-evoked potentials remained steady over several hours of stimulation (not shown).

All nerve stimulation was coordinated through computer software (AxoGraph X; AxoGraph Scientific, Sydney, Australia) and applied at a repetition rate of 2 Hz. In both preparations, electrical pulses of 100 μs were used. Optical pulse durations were 250 μs

for the Ho:YAG and 2-3 ms for the Capella lasers, respectively. This is due to the fixed pulse duration of the Ho:YAG and the minimum pulse duration of the Capella required to achieve optical energies for stimulation. Since the underlying mechanism of INS has been shown to be thermally mediated and dependent on a temperature gradient (Wells et al., 2007a), as long as the pulse duration is significantly shorter than the thermal diffusion time (~100 ms), the laser pulse can be considered as an input delta function to the system. For hybrid stimulation, pulses were synchronized such that they ended concurrently. This allowed for the total charge and total thermal deposition to occur simultaneously. Nerve recordings were triggered and acquired for 10 ms prior to stimulation through 140 ms post stimulation.

5.3.5 Experimental methods for spatial factors

To investigate spatial factors contributing to the reproducibility of hybrid stimulation, sub-threshold pulses of electrical current (90% of electrical stimulation threshold) were applied simultaneously with optical pulses of a set magnitude. During hybrid stimulation, the optical fiber was translated across the nerve between the stimulating pipettes using a micromanipulator. A CMOS color USB camera and accompanying software (catalogue #59-367; Edmund Optics, Barrington, NJ) were used to record the position of the optical fiber. A LED was triggered by computer software to flash synchronously with the laser pulse so that we could reconstruct the exact position of the optical fiber at the time of stimulation. The center of the tip of the optical fiber was plotted and correlated to the presence or absence of stimulation as indicated by an evoked potential on the nerve recording.

5.3.6 Experimental methods for temporal factors

Temporal factors were examined by investigating how fluctuations in electrical stimulation threshold over time affect the optical component of hybrid stimulation. Threshold currents were measured every 2-3 min for 1-3 hours to monitor underlying changes in electrical stimulation with time and to assure that hybrid stimulation was not inducing alterations in threshold currents. One hour of each trial was an experimental period where radiant exposures eliciting hybrid stimulation were measured along with electrical stimulation threshold currents. Every 2-3 minutes during this experimental period, electrical stimulation threshold currents were first measured and then the stimulus current was reduced to 90% of electrical stimulation threshold. For the *Aplysia* experiments, five pulses of five different radiant exposures were then systematically applied with the sub-threshold current pulses. For the rat experiments, 8 pulses of 5 five different radiant exposures were applied. The order in which the radiant exposures were applied was determined by a random sequence generator so as to limit any conditioning effects or bias. Each hybrid stimulus pulse was recorded as either a 1 or 0 as determined by the presence (1) or absence (0) of a visibly identified nerve (*Aplysia*) or muscle (rat) action potential. This process was repeated every 2-3 minutes for the duration of the experimental period.

5.3.7 Data analysis

For spatial data, movie files were analyzed with custom software (Matlab r2010b; Mathworks, Natick, MA). Locations of successful stimulation were compared using non-parametric statistical tests. The Two-Sample Kolmogorov-Smirnov test compares two

empirical distributions and responds to both the overall shape and location of the distributions. While this test will indicate if the distributions are statistically different, it will not tell whether it is due to the relative size or location of the distributions. To distinguish whether differences are due to changes in size or location of the region of excitability (ROE), we also performed the Mann-Whitney test, which is a non-parametric test that determines if the median of one data set is greater than another. The interquartile range was used as a measure of the size of the ROE.

Temporal data were aggregated using Matlab with statistical analysis performed in Microsoft Excel (part of Microsoft Office Professional Plus 2010) and Slide Write Plus Version 6 (Advanced Graphics Software, Inc., Encinitas, CA). For each radiant exposure, the number of ones was divided by the sum of ones and zeros to achieve a probability of firing. The cumulative distribution function (CDF) of the standard normal distribution:

$$F(x;\mu,\sigma^2) = \frac{1}{2}\left[1 + \operatorname{erf}\left(\frac{x-\mu}{\sigma\sqrt{2}}\right)\right], x \in R \qquad \text{(V-1)}$$

where x is a random variable with mean m and variance s^2, was then fit to the data to determine the radiant exposure yielding 50% probability of firing (RE_{50}). While the RE_{50} is not practically useful for stimulation, we use this approach as a generally well-accepted model for making comparisons and identifying thresholds (Gibson and Welker, 1983, Hermann et al., 2004, Jenkins et al., 2010, Kirby and Middlebrooks, 2010, Julkunen et

al., 2011). We seek to establish a methodology and identify pertinent considerations for successful hybrid stimulation rather than prescribe optimal conditions for stimulation

5.4 Results

5.4.1 Existence of a bounded excitable region

When translating the optical fiber back and forth across the nerve, it was determined that there exists a finite region between the cathode and anode where hybrid stimulation is possible (Figure V-3). This was observed in all of the nerves tested for both the *Aplysia* (n=42) and the rat (n=13). However, in two rat sciatic nerves, some experimental trials yielded locations of successful hybrid stimulation extending outside of this finite region. During these trials, the electrical stimulation threshold was more variable. Occasionally the electrical component of hybrid stimulation was approaching electrical stimulation threshold, raising the overall excitability of the nerve. For both the *Aplysia* and the rat there were variations in the size and shape of evoked responses between animals, nerves and locations within a single nerve. This suggests that multiple different axons were recruited over the course of the experiments. In each species, there were ROEs consisting of only a single evoked unit and others that exhibited different units depending on the location of the optical fiber and the intensity of the optical stimulus. No apparent differences in ROE were observed when comparing the Capella and Ho:YAG within a single nerve (Figure V-4a-b) or across animals (Figure V-4c-d) for the *Aplysia* or the rat. However, our yield with the Ho:YAG in the rat sciatic nerve was greater due to more reliable optical stimulation. With no obvious differences between the

lasers other than overall yield, we placed greater emphasis on the Capella for the remaining *Aplysia* experiments (due to its ease of use and consistent pulse energies) and the Ho:YAG for the rat (due to the superior results it provided for myelinated nerve fibers).

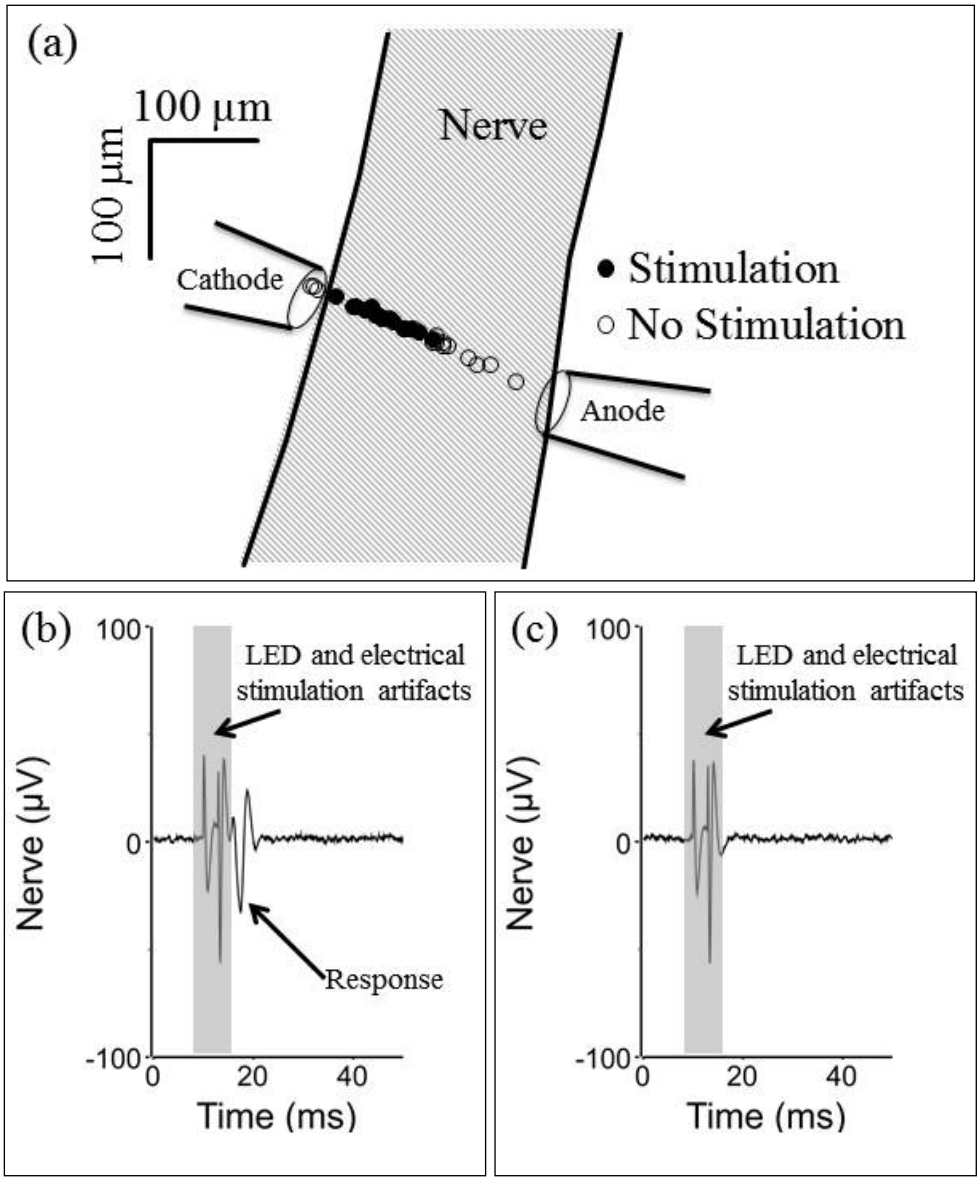

Figure V-3 There exists a finite region of excitability (ROE) for hybrid electro-optical stimulation. (a) The ROE between the cathode and anode where the combination of sub-threshold electrical and optical stimuli will achieve neural activation in an *Aplysia* nerve. Outside of this ROE, stimulation does not occur. (b) Evoked electrical response to hybrid stimulation recorded from the distal nerve. (c) Absence of evoked response outside of ROE. Hybrid stimulus parameters used: 675 mA (100 ms), 4.58 J/cm^2 (3 ms). Electrical stimulation threshold was 750 mA. In (b) and (c) the LED and electrical stimulation artifacts are indicated by the shaded region.

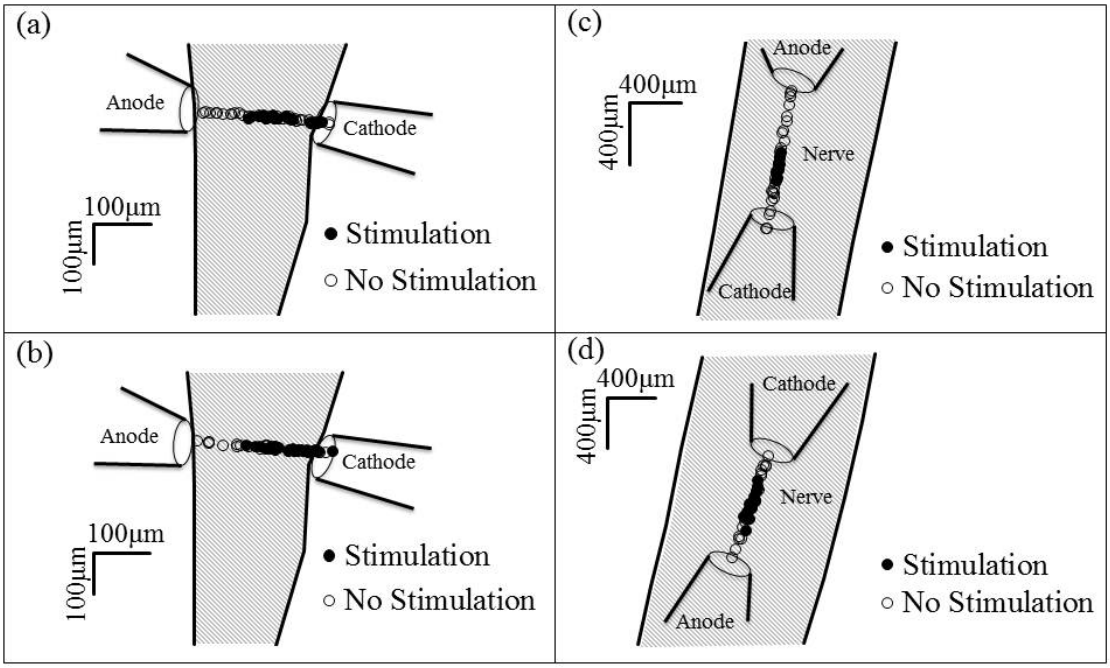

Figure V-4. Both a diode laser (Capella) and solid-state laser (Ho:YAG) exhibit a finite region of excitability (ROE) for hybrid electro-optical stimulation. ROEs for the Capella and Ho:YAG within the same *Aplysia* nerve are shown in (a) and (b), respectively. Typical ROEs observed in the rat sciatic nerve are shown for the Capella (c) and Ho:YAG (d).

5.4.2 Size of the region of excitability

After identifying the existence of a finite region of excitability, we investigated how the strength of the optical stimulus altered its size. With electrical current at 90% of electrical stimulation threshold, we compared ROE size for optical stimuli of 1.78 and 4.71 J/cm^2 using the Capella in the *Aplysia* and 0.29 – 1.18 J/cm^2 with both the Ho:YAG and Capella lasers in the rat. These values were chosen to cover a range of optical radiant exposures that, in the absence of the electrical stimulus, are sub-threshold for stimulation in their respective neural systems. Locations of hybrid stimulation were binned and plotted as a probability histogram by dividing the number of stimuli evoking a response by the total number of attempts for each bin (Figure V-5a-b, d-e). After confirming that the ROE median was the same for each radiant exposure (using the Mann-Whitney test), the Two-Sample Kolmogorov-Smirnov test was applied to determine if the sizes of the distributions were significantly different.

In *Aplysia*, a total of 28 trials were acquired from 3 nerves (3 different animals). In the rat, a total of 26 trials were acquired from 4 nerves (4 different animals). Equal radiant exposures from the same nerve and animal were combined into one data set. In *Aplysia* a statistically significant increase ($p < 0.05$) in ROE size with increasing radiant exposure was observed for all nerve tested (Figure V-5c). For the rat, the results indicated a statistically significant increase in ROE size ($p < 0.05$) for 1 of the 4 animals tested (Figure V-5f) and an insignificant increase ($p > 0.05$) for the remaining nerves. However, combining the results from all 4 rat nerves shows a linear increase in ROE size across the radiant exposures tested. The lack of statistical significance in 3 of the 4 rat nerves tested is likely due to the limited range of radiant exposures tested in each nerve. However the

center of each ROE showed a greater probability of firing at the higher radiant exposure in all nerves (not shown).

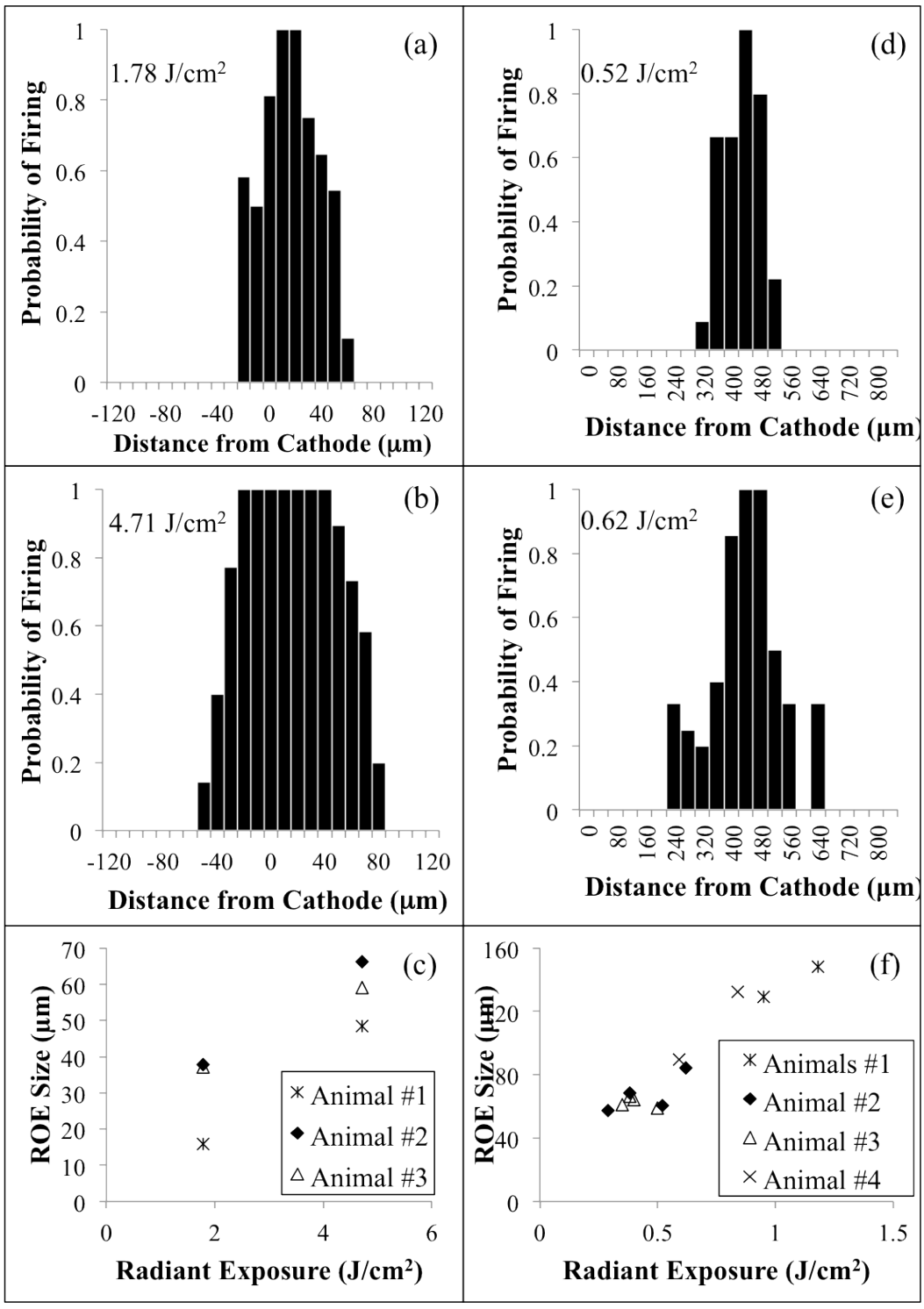

Figure V-5. Region of excitability (ROE) size as a function of radiant exposure in the buccal nerve of *Aplysia californica* (a-c) and the rat sciatic nerve (d-f).

5.4.3 Effects of stimulus polarity

It was hypothesized that the polarity of the electrical stimulus would shift the location of the ROE. To test this, the ROE was identified as before, and then the polarity was reversed (while keeping the electrodes in place) and the new ROE was found. In *Aplysia*, this experiment was repeated using both the Capella and Ho:YAG lasers with a constant optical stimulus (2.42 - 4.71 J/cm^2) across a total of 8 nerves from 7 animals yielding 11 polarity pairs. The Mann-Whitney test was used to evaluate whether a shift in the ROE median occurred with a change in polarity. For all polarity pairs, a reversal in polarity showed a statistically significant shift ($p < 0.05$) in the ROE median such that the ROE was located adjacent to the cathode (Figure V-6). This demonstrates that, for a given electrode arrangement, two unique ROEs may be achieved by simply reversing the direction of the current path. In the rat sciatic nerve, effects of polarity were investigated using both the Ho:YAG and Capella lasers in a total of 6 nerves from 4 animals. A statistically significant shift in the ROE median was observed in 3 of the 6 nerves tested. Of the 3 nerves not showing a statistically significant shift in the ROE median, 2 exhibited successful hybrid stimulation with only one polarity. While statistically significant shifts in the ROE median were observed in half of the nerves tested, changes in location were not as dramatic as in the *Aplysia*.

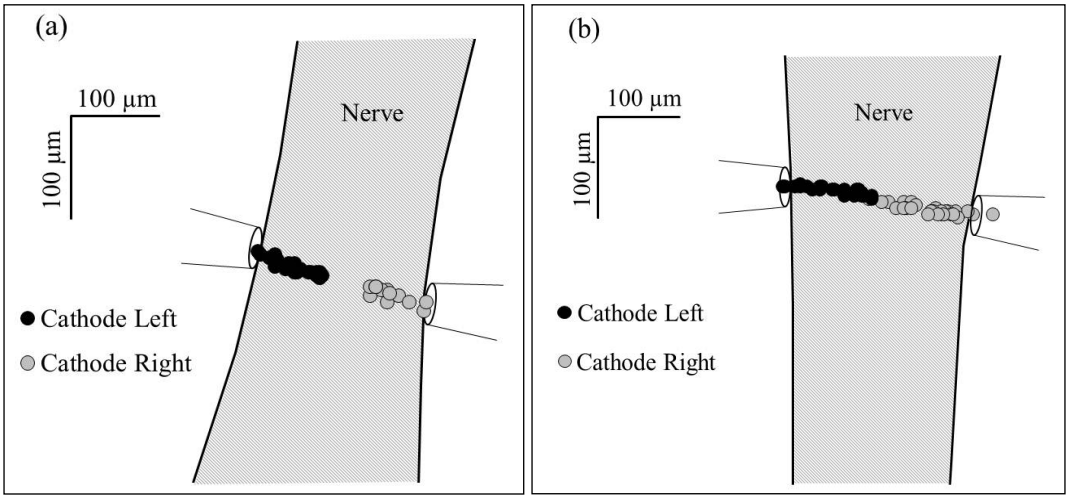

Figure V-6. Changing the polarity of a sub-threshold electrical stimulus in the *Aplysia* buccal nerve yields two distinct regions of excitability (ROEs) with both the (a) Capella (λ=1.875 µm; τ_p=3 ms; H=4.97 J/cm^2) and (b) Ho:YAG laser (λ=2.120 µm; τ_p=0.25 ms; H=2.67 J/cm^2) lasers. The location of the ROE is adjacent to the location of the cathode. Dark colored circles are locations of successful hybrid stimulation when the cathode is located on the left side of the nerve. Light colored circles are locations of successful hybrid stimulation when the polarity is reversed and the cathode is located on the right side of the nerve.

5.4.4 Effects of electrical stimulation threshold on hybrid stimulation

Electrical stimulation threshold currents as well as the RE_{50} for hybrid stimulation were monitored in the same nerve to determine if fluctuations in the former affect the latter. The RE_{50} for hybrid stimulation was determined by first generating probabilities of firing at a given radiant exposure for each time point (by dividing the number of stimulation attempts evoking a response by the number of total attempts) and then fitting those probabilities to a CDF (Eq. (V-1)). The RE_{50} was defined as the radiant exposure providing a 50% probability of firing as indicated by the CDF fit.

For the *Aplysia*, 5 pulses of 5 radiant exposures (using the Capella laser) yielded 25 total data points every 2 min. These data were not sufficient for a reliable CDF fit at each time point, so a sliding window was applied to fit a CDF to 6 min windows of data. Figure V-7a provides an example of the changes in thresholds for electrical stimulation and the optical component of hybrid stimulation over an hour. Each of the 4 *Aplysia* buccal nerves tested had a statistically significant ($p < 0.05$) negative correlation between thresholds for electrical stimulation and the optical component of hybrid stimulation. In the rat, 8 pulses of 5 radiant exposures (using the Ho:YAG laser) yielded 40 total data points every 3 minutes. A sliding window was applied to fit a CDF to 6 min windows of data. Of the two nerves tested, one exhibited a statistically significant ($p < 0.05$) negative correlation between thresholds for electrical stimulation (Figure V-8a) and the optical component of hybrid stimulation and the other showed an insignificant ($p > 0.05$) negative correlation.

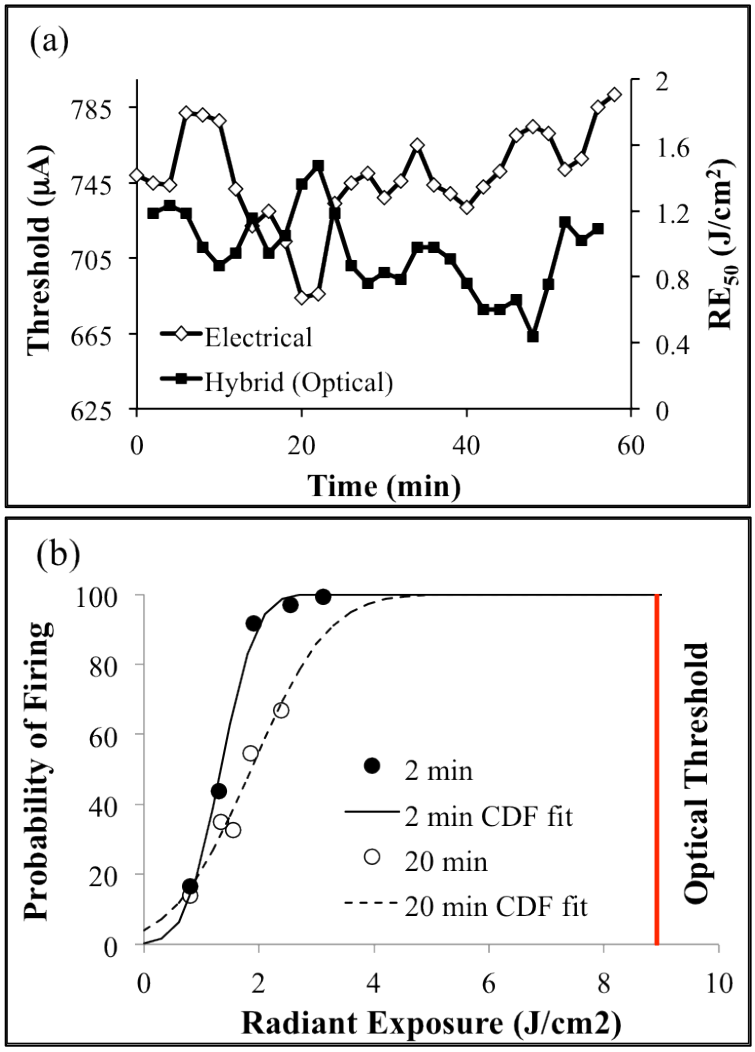

Figure V-7. Electrical stimulation threshold and RE_{50} for hybrid stimulation as a function of time in an *Aplysia californica* buccal nerve. (a) Results from one nerve showing a negative correlation ($r^2 = -0.47$, $p < 0.05$) between thresholds for electrical stimulation and the RE_{50} for hybrid stimulation measured every two minutes. (b) Probability of firing as a function of radiant exposure using data accumulated from all animals. The slope of the cumulative distribution fit (CDF) at 50% probability indicates the amount of variability in hybrid stimulation radiant exposures yielding stimulation over time. Effects of adjusting the electrical priming current every 2 min versus every 20 min is also shown. More frequent adjustments to the priming current increases the slope of the CDF fit, thus reducing variability in threshold radiant exposure for the optical component of hybrid stimulation. Note that the y-intercept for the 20 min adjustment plot is greater than 0, suggesting there is a small probability of firing even with 0 J/cm^2 of optical stimulus. This is due to rare occasions where the electrical stimulation threshold fell below the previously set sub-threshold stimulus before the next adjustment was made.

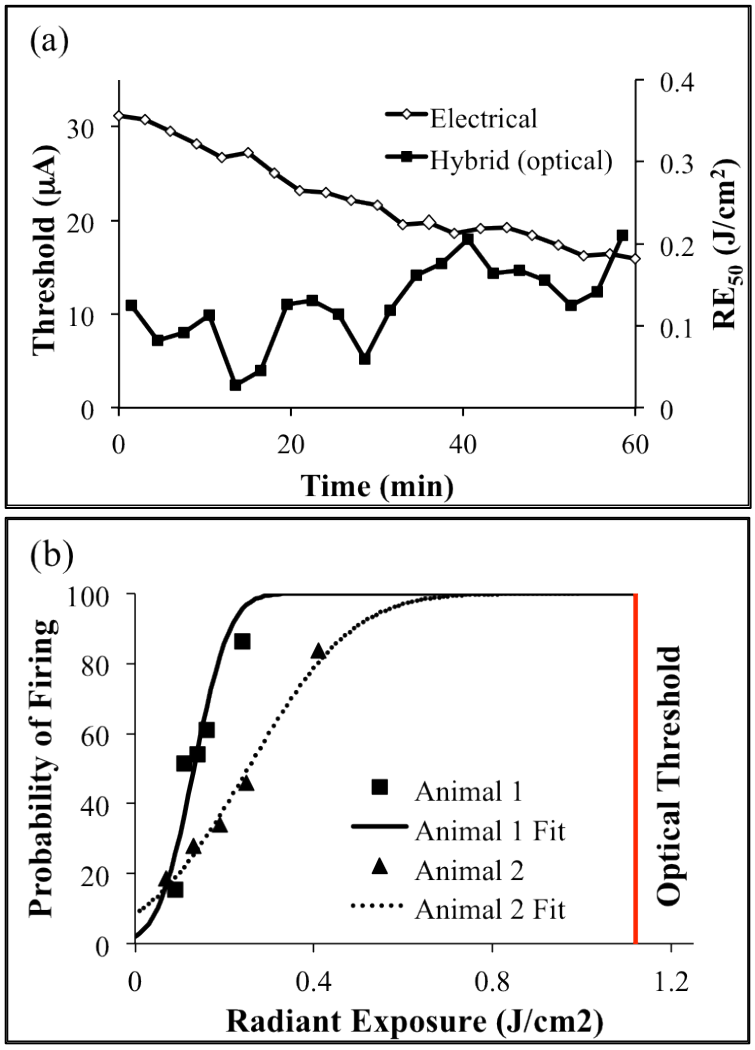

Figure V-8. Electrical stimulation threshold and RE_{50} for hybrid stimulation as a function of time in the rat sciatic nerve. (a) Results from one nerve showing a negative correlation ($r^2 = -0.66$, $p<0.05$) between threshold for electrical stimulation and the RE_{50} for hybrid stimulation measured every two minutes. (b) Probability of firing as a function of radiant exposure in each animal using all data acquired over one hour. The slope of the cumulative distribution fit (CDF) at 50% probability indicates the amount of variability in threshold measurements over time. There is more variability between animals in the rat than in the *Aplysia* (Figure 7b).

To evaluate the consistency over time of the RE_{50} for hybrid stimulation, all of the data acquired from a given nerve were compiled and each radiant exposure was converted to a probability of firing. The probability of firing as a function of radiant exposure was then fit to a CDF. In *Aplysia*, a total of 4 nerves from 4 animals (n = 610 data points at each radiant exposure) yielded a 50% probability of firing at 1.34 J/cm^2 with a 95% confidence interval between 1.13 and 1.55 J/cm^2 (Figure V-7b). Here, the confidence interval is indicative of variability in hybrid stimulation RE_{50} over the hour of measurements, where a narrow confidence interval (and increased slope of the CDF fit) indicates less variability. A subsequent set of experiments was performed in *Aplysia* to determine if increasing the interval between adjustments to the sub-threshold electrical stimulus yielded an increase in the confidence interval (i.e. an increase in variability). For these experiments, the electrical stimulation threshold was measured every 2 min, but the sub-threshold electrical stimulus used for hybrid stimulation was only set to 90% of electrical stimulation threshold at the 0, 20 and 40 min time points. A total of 5 nerves from 3 animals (n = 610 - 900 data points per radiant exposure) yielded a 50% probability of firing of 1.86 J/cm^2 with a 95% confidence interval between 1.40 and 2.33 J/cm^2. When comparing the 2 and 20 min adjustment intervals, the 95% confidence interval for the 20 min adjustment is roughly twice that of the 2 min adjustment. This is also shown in Figure V-7b as a shallower slope in the probability of firing as a function of radiant exposure for the 20 min adjustment. A noteworthy aspect of Figure V-7b is that the y-intercept for the 20 min adjustment plot is greater than 0, suggesting there is a small probability of firing even with 0 J/cm^2 of optical stimulus. This is due to rare occasions

where the electrical stimulation threshold fell below the previously set sub-threshold stimulus before the next adjustment was made.

Figure V-8b shows the results of aggregating data from each rat for the purpose of assessing threshold radiant exposure consistency. Rather than compiling the data from both animals, each animal is plotted separately. The results indicate that threshold variability is more prominent in the rat than in *Aplysia*. Animal #1 has RE_{50} of 0.13 J/cm^2 with a 95% confidence interval of 0.10 – 0.16 J/cm^2, whereas animal #2 has RE_{50} of 0.25 J/cm^2 and a 95% confidence interval of 0.17 – 0.33 J/cm^2.

5.4.5 Hybrid inhibition

In the course of evaluating temporal factors affecting the RE_{50} for hybrid stimulation in the *Aplysia*, it was discovered that at higher radiant exposures, the probability of firing began to decrease rather than asymptotically approach 100% as expected. To further investigate this phenomenon, the electrical stimulus was set to 90% of electrical stimulation threshold every 2 min and 5 pulses of 5 radiant exposures were applied in the manner described above; however, for this experiment the radiant exposures were higher than those used for identifying the RE_{50}. The results from 4 nerves from 2 animals (n = 600 data points per radiant exposure) are shown in Figure V-9. Interestingly, if we define stimulation as >50% probability of firing, then with an electrical priming stimulus of 90% of electrical stimulation threshold, stimulation will occur for radiant exposures from 1.34 to 4.79 J/cm^2 rather than >1.34 J/cm^2 as was initially expected. This raised the question as to whether higher radiant exposures actually inhibit neuronal firing, or whether another mechanism is activated at these

radiant exposures. We applied an electrical stimulus at 110% of electrical stimulation threshold and then added the optical stimulus (3 nerves from 3 animals). In each trial the electrically evoked unit was inhibited by the optical stimulus (Figure V-10). Radiant exposures for inhibition of the electrically evoked unit averaged 7.13 ± 0.51 J/cm^2 over 12 trials. It is important to note that all of these radiant exposures are below optical stimulation threshold radiant exposures and that this process is completely reversible. If radiant exposures are reduced, then the evoked response returns. Hybrid inhibition was investigated in the rat but was not observed.

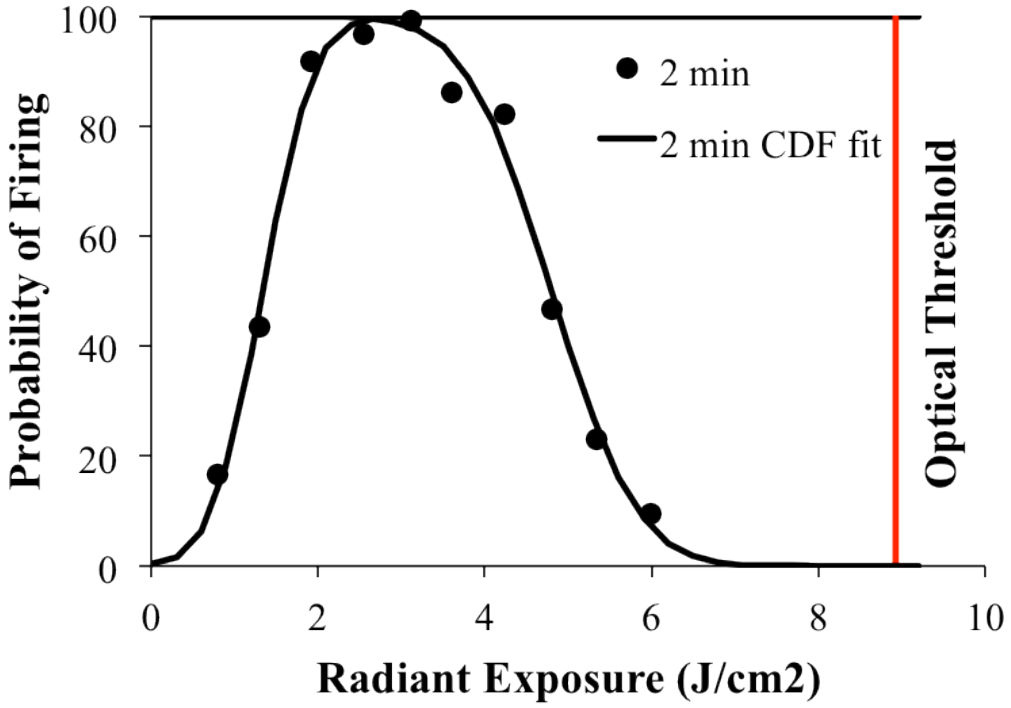

Figure V-9. There is a limited window of radiant exposures for successful hybrid stimulation in the *Aplysia*. A >50% probability of firing with an electrical stimulus at 90% of electrical stimulation threshold requires radiant exposures from 1.34 to 4.79 J/cm^2. Evoked responses to a range of radiant exposures were acquired every two min for one hour. These data were aggregated to achieve a probability of firing for each radiant exposure. The increasing and decreasing phases of the plot were then each fitted to a cumulative distribution function (CDF).

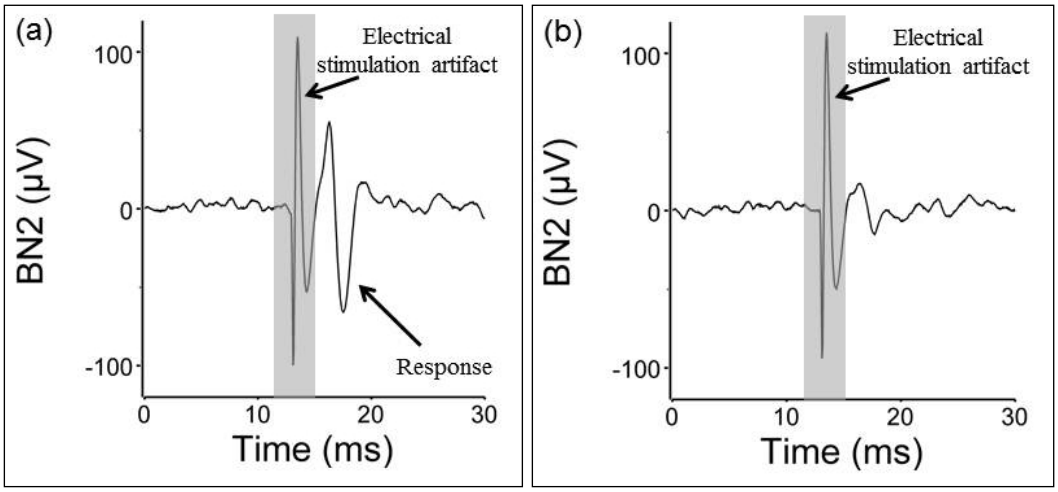

Figure V-10. Optical stimulation of sufficient radiant exposure will inhibit electrically evoked action potentials. In both (a) and (b) a supra-threshold stimulus (110% of threshold) is applied (100 ms, 567 mA). In (a) the optical stimulus (3 ms) is 5.73 J/cm^2, whereas in (b) the optical stimulus is 6.49 J/cm^2. Notice how the electrically evoked action potential is present in (a) but not in (b). The electrical stimulation artifact is indicated by the shaded region.

5.5 Discussion

Reducing the optical energy required to stimulate excitable tissues may facilitate clinical translation of infrared neural interfaces due to the reduced likelihood of thermal tissue damage, and by making the design criteria for laser sources less restrictive. The purpose of this study was to assess potential factors that might contribute to variability in hybrid electro-optical stimulation, as well as to create a methodology for reliable and reproducible hybrid stimulation. We approached this task by comparing trends seen in two different neurobiological systems – the tractable and well-characterized *Aplysia californica* buccal ganglion and the myelinated and more clinically relevant rat sciatic nerve. Given the variability and lack of reproducibility we previously experienced, this approach allowed for identification of factors in the more experimentally tractable system that could subsequently be applied to the more clinically relevant preparation. Some concern may arise as to the translation of hybrid stimulation between an unmyelinated, invertebrate nerve and a myelinated, mammalian nerve. However, this study shows that the information gathered from experiments in the *Aplysia* directly led to improved understanding and performance of hybrid stimulation in the rat sciatic nerve. Although some aspects of the experimental protocol differ between the two preparations (i.e. orientation of stimulating pipettes, source of optical stimulation, endpoint definition), overarching trends were clearly evident across both species. Prior to both adopting the methods used in this study and controlling for the spatial and temporal factors we have assessed, our efficacy for hybrid stimulation in the *Aplysia* buccal nerve and the rat sciatic nerve were 35% and 23%, respectively (unpublished data). In this paper, we are defining *efficacy* as a nerve demonstrating a hybrid stimulation event where a sub-

threshold electrical stimulus and sub-threshold optical stimulus are combined to achieve an evoked response. We are attempting to determine whether or not sub-threshold electrical and optical stimuli were combined to achieve supra-threshold stimulation. At the conclusion of this study, we now have an efficacy of 93% (42/45 nerves) in the *Aplysia* buccal nerve and 76% (13/17 nerves) in the rat sciatic nerve.

Relative mechanical stability between the target neural tissue, optical fiber and electrodes were imperative to achieving reliable and reproducible hybrid stimulation. This allowed for consistent location of the stimuli throughout a given experiment by minimizing nerve movement due to optical fiber movement, fluid flow (*Aplysia*) or animal respiration (rat). Stabilization challenges are likely to be alleviated as hybrid stimulation progresses to multi-modality nerve cuff stimulators where microfabricated cuffs will be able to adapt to changes in nerve shape and movement.

The orientation of the stimulating glass pipettes is also an important part of the physical setup that must be taken into account. In the rat, electrical stimulation was more reliable with the pipettes oriented along the longitudinal axis of the nerve than in a transverse configuration. For electrical stimulation of myelinated nerves, it is necessary to induce longitudinal axonal currents, which may explain the reason that pipettes oriented longitudinally to the nerve were most effective. Recent models of intrafascicular stimulation support these observations. As a function of position relative to nodes of Ranvier, bipolar stimulation with a longitudinal configuration was shown to have less variability in threshold currents as compared to a transverse configuration (Butson et al., 2011). While the *Aplysia* nerves are unmyelinated, and thus do not possess nodes of Ranvier, they do exhibit clustering of voltage-gated sodium channels that may aid in the

conduction of action potentials along the nerves (Johnston et al., 1996). However, it was found in *Aplysia* nerves that electrical stimulation was more reliable with the pipettes oriented transverse to the nerve. Due to the thick outer sheath protecting the nerve, placing the glass pipettes along the longitudinal axis of the nerve may result in electrical current dissipating into the bath rather than penetrating to the axons. When placing the pipettes transverse with respect to the midline of the nerve, the current may take a more direct path through the axonal tissue.

The choice of laser is also a contributor to the reproducibility of hybrid stimulation. The two lasers used in this study differ in many respects, but are expected to perform equally from the point of view of thermal laser-tissue interaction. However, the Ho:YAG laser yielded greater reproducibility in the rat than did the Capella. To understand how this may have occurred, we must examine the two laser sources. The Capella used for this study is a diode laser, which is chopped to produce square pulses having tunable pulse duration at a center wavelength of 1.875 μm. The Ho:YAG laser is a pulsed solid-state laser at 2.12 μm, which produces a 250 μs pulse (full width at half maximum), exhibiting an initial rising phase followed by a decay, with spikes in output energy throughout the pulse duration. The mechanism by which pulsed infrared light produces neural activation is known to be thermally mediated, and directly associated with the absorption of infrared light by water in tissue (Wells et al., 2007a). Which attribute of the laser contributes most significantly to the thermal gradient is the most relevant issue. A comparison of the absorption coefficient as a function of wavelength for pure water reveals that 1.875 μm and 2.12 μm have similar absorption coefficients (μ_a=26.9 cm^{-1} and μ_a=24.01 cm^{-1}, respectively) (Hale and Querry, 1973). Although tissue

is predominantly water, these values may differ slightly in our preparation and are known to be temperature dependent. However, it is unlikely that the differing wavelengths of the lasers is the source of the Ho:YAG laser's superior reproducibility in myelinated peripheral nerves. A second obvious difference is the pulse durations of the two lasers. However, there is conflicting evidence as to whether pulse duration plays a role in optical stimulation thresholds (Izzo et al., 2007b, Wells et al., 2007a). A third possibility is that the broad spectral width of the Capella (15-20 nm, FWHM) causes much of the laser's output to occur at wavelengths that are not optimal for optical stimulation of peripheral, myelinated nerves. In applications with more direct access to the target neural tissue, the effects of spectral width are minimized due to all of the light being absorbed at the site of neuronal activation. However, in peripheral nerves, where the optical energy must penetrate through connective tissue and myelin surrounding the axons, longer wavelengths emitted by the Capella may be absorbed before they ever reach the axons. Thus, stimulation thresholds would be higher and quickly approach damage thresholds. The differing temporal pulse structure has not been investigated, but may also contribute to the relative effectiveness of the lasers. Whereas the Capella is a chopped diode laser exhibiting a square pulse, the Ho:YAG laser has a temporal structure in which the optical energy varies and includes numerous energy spikes throughout the pulse duration (Asshauer et al., 1997). This could result in higher peak power and peak irradiance for the Ho:YAG laser.

There are two broad categories of factors that affect the reproducibility of hybrid stimulation related to the interaction of the optical and electrical stimuli. In the first category are *spatial* factors, where the relative location of the two stimuli determines the

efficacy of stimulation. Our initial working hypothesis was that for a given sub-threshold radiant exposure, hybrid stimulation would be possible for all locations between the cathode and anode of a bipolar stimulus. The results of this study have shown that hypothesis to be false. In Figure V-3, it is clear that there is a finite ROE for the combination of a constant sub-threshold radiant exposure delivered simultaneously with an electrical stimulus that is 90% of electrical stimulation threshold. While Figure 3 is drawn from data in the *Aplysia* buccal nerve, Figure V-4 shows the same results were seen in the rat sciatic nerve as well. Therefore, successful and reproducible hybrid stimulation calls for accurate placement of the optical fiber relative to the site of electrical stimulation.

This raises the question of where the ROE is located. This answer is clearer in *Aplysia*, where the ROE was consistently located adjacent to the cathode. Within a single nerve, the location of the ROE was effectively "steered" by reversing the polarity of the electrical stimulus. In the rat sciatic nerve, half of the nerves showed a statistically significant shift in ROE location upon polarity reversal, though the effect was not as dramatic as in *Aplysia*. In the other trials, the ROE location either did not shift, or hybrid stimulation was ineffective when the polarity was reversed. However, in cases of successful hybrid stimulation, different evoked potentials were recruited for each stimulus polarity. This suggests that hybrid stimulation offers two forms of selectivity, as both the *position* of the optical stimulus and the *polarity* of the electrical stimulus dictate the units recruited. The results also imply that ROE location in the rat sciatic nerve is influenced more by whether or not optical stimulation is possible rather than by the direction of current flow. Anecdotal evidence reveals that there are "sweet spots" on the

sciatic nerve where optical stimulation is most effective; in particular, these spots are found just proximal to the branch point of the fascicles, but also at some additional locations along the nerve trunk. This could potentially be due to thinning of the epineurium, proximity of fascicles to the irradiated surface, or to increased concentration of nodes of Ranvier in these locations.

The existence of a finite ROE with the potential for shifting location in response to polarity reversal must be taken into account for reproducible hybrid stimulation. Much of the previously observed variability is also likely to be due to the relationship between ROE size and applied radiant exposure. The results indicate an approximately linear increase in ROE size over the range of radiant exposures tested (Figure V-4f). Thus, the center of the ROE will have the lowest threshold radiant exposures when combined with a given sub-threshold electrical stimulus. If this is not accounted for (as was the case in (Duke et al., 2009)), then variability in measured thresholds is certainly expected. Furthermore, with the highest probability of firing at the center (Figure V-5), it is likely that an optical stimulus located along the periphery of the ROE will induce a reduced firing rate.

A second category of factors contributing to the reproducibility of hybrid stimulation are *temporal* factors. These factors include how the electrical stimulation threshold and the hybrid stimulation RE_{50} change with time and relative to one another. We initially expected the excitability of a nerve to the combination of electrical and hybrid optical stimuli would follow a similar temporal pattern. However, Figure V-7 and Figure V-8 illustrate a negative correlation between the electrical and hybrid optical stimuli in both the *Aplysia* and rat. If the sub-threshold electrical stimulus is set and the

underlying electrical stimulation threshold subsequently decreases (so that an electrical stimulus is approaching the stimulation threshold), one would expect the threshold for the optical component of hybrid stimulation to be reduced as well. However, the results did not show this to be true. Thus, we may conclude that the underlying mechanisms of optical and electrical stimulation are dissimilar. If the mechanisms were similar, we would expect a positive correlation between thresholds for electrical stimulation and the optical component of hybrid stimulation. Instead, our data show that as the nerve becomes more excitable to electrical stimulation, its excitability in response to optical stimulation decreases. In the rat, an unexpected decay of electrical threshold currents over time was observed (Figure V-8). This decay may be a sign of increased excitability in response to surgery or trauma.

The underlying electrical stimulation threshold must be taken into account to reduce variability and enhance the reproducibility of hybrid stimulation. Whenever short-term fluctuations (minutes) in threshold radiant exposures are present, controlling for these fluctuations yields overall long-term (1 hour) threshold radiant exposures that are consistent (Figure V-7b and Figure V-8b). If electrical stimulation threshold is not controlled over time (as was the case in (Duke et al., 2009)), then the variability of measured thresholds for the optical component of hybrid stimulation will increase. This is evident in Figure V-7b. When the sub-threshold electrical stimulus was only set to the chosen magnitude every 20 min, the threshold for the optical component of hybrid stimulation increased and its 95% confidence interval (indicative of the variability) showed greater than a two-fold increase. It should be noted that while the inter-rat variability represented in Figure V-8b is much greater than in *Aplysia* (Figure V-7b), the

overall variability and reduction in INS threshold are much lower than what was previously reported. Taking the minimum bound of the 95% RE_{50} confidence interval for animal 1 and the maximum bound for animal 2 yields an RE_{50} for hybrid stimulation ranging from 12-29% of the radiant exposures required for optical stimulation alone, as opposed to the roughly 30-80% in the previous study.

In the course of investigating temporal factors affecting hybrid stimulation, it was discovered that elevated radiant exposures (although still below threshold radiant exposures for optical stimulation alone) resulted in a decline in the probability of firing (Figure V-9). Sub-threshold radiant exposures for optical stimulation alone were also shown to inhibit electrically evoked potentials (Figure V-10). These results indicate the potential exists for full hybrid electro-optical control of neural tissue, making it possible to selectively excite or inhibit axons. Preliminary results indicate a spatially confined region of inhibition surrounded by excitation (either hybrid- or electrically evoked), suggesting that this is not an artifact, but is a spatially discrete phenomenon, although it may be due to a different mechanism than the excitatory effect. Without an elucidated mechanism of infrared neural stimulation, it is difficult to conclude how pulsed infrared light inhibits electrically evoked potentials. Recently, it was shown that intracellular calcium increases in response to optical stimulation of cardiomyocytes (Dittami et al., 2011). It is conceivable that for hybrid stimulation, supra-threshold radiant exposures may cause an increase in intracellular calcium that activates calcium-dependent potassium channels, thus hyperpolarizing the cell. Further studies will be required to test this hypothesis.

We previously showed the proof-of-concept potential for combined optical and electrical stimulation of neural tissue (Duke et al., 2009). This study extends that work by outlining some potential sources of variability that may be controlled to provide reproducible hybrid stimulation. The results presented here also demonstrate the potential of combining optical and electrical stimulation techniques by providing further evidence for selectivity as well as the ability to inhibit neuronal firing. Finally, the study demonstrates the translational value of parallel studies in invertebrates and vertebrates. The key aspects of the methodology to capitalize on the potential of hybrid electro-optical stimulation are summarized as follows:

- The optical stimulus, electrical stimulus and target tissue should be mechanically stabilized and controlled relative to one another.
- The laser and target neural anatomy must be taken into account to determine the maximum possible expected reproducibility.
- For constant electrical priming current, the optical stimulus must be located within the region of excitability.
- For constant electrical priming current, the size of the region of excitability depends on the strength of the optical stimulus.
- Variability in the electrical stimulation threshold induces variability in the RE_{50} for hybrid stimulation. This variability can be reduced by frequent adjustments to maintain a constant sub-threshold electrical stimulus relative to the electrical stimulation threshold.

- There is a range of radiant exposures for which hybrid stimulation has >50% probability of firing. Radiant exposures below or above this range have <50% probability of firing.

Having taken these points into account, we have improved our efficacy by threefold in both the *Aplysia californica* buccal nerve and the rat sciatic nerve. There are other potential sources of variability that could be controlled to bring our current efficacy up to 100%. In the *Aplysia*, the three nerves that did not show hybrid stimulation were from animals with questionable health, but were included in the success rate calculations for completeness. In myelinated peripheral nerves, the efficacy of optical stimulation is paramount to the success of hybrid stimulation. Elucidating the mechanism of INS will provide *a priori* knowledge of where on the nerves to stimulate (e.g., near the nodes of Ranvier). Improving the efficacy of optical stimulation will in turn improve the efficacy and reduce variability of hybrid stimulation. Knowing the mechanism of INS will also provide a clearer understanding of the interaction between electrical and optical stimuli that drives hybrid stimulation. In this study we have demonstrated that mechanical stabilization of the nerve, electrodes and optical fiber is of utmost importance. Even with the efforts we have taken to stabilize the system, there is potentially still movement-inducing variability. To address this issue, we envision a hybrid stimulation cuff that moves with the nerve and is thus able to hold the stimuli in place relative to the nerve. However, our results thus far have provided the ability to begin assessing the clinical utility of hybrid neural stimulation. We believe that the concepts and techniques presented in this study will facilitate the application of spatially selective neural

interfaces where thermal tissue damage and/or laser design constraints are currently of concern.

5.6 Acknowledgements

This project was made possible by funds from the Human Frontiers Science Program (HFSP RGP0014/2008-C) and the National Institutes of Health (NS-047073). We would like to thank two anonymous referees whose comments and suggestions helped to improve the final version of this manuscript.

5.7 References

Adams SR, Tsien RY (1993) Controlling cell chemistry with caged compounds. Annu Rev Physiol 55:755-784.

Allegre G, Avrillier S, Albe-Fessard D (1994) Stimulation in the rat of a nerve fiber bundle by a short UV pulse from an excimer laser. Neurosci Lett 180:261-264.

Arvanitaki A, Chalazonitis N (1961) Excitatory and Inhibitory Processes Initiated by Light and Infra-Red Radiations in Single, Identifiable Nerve Celss. In: Nervous Inhibtion(E., F., ed): Pergamon Press.

Asshauer T, Delacretaz G, Jansen E, Welch A, Frenz M (1997) Pulsed holmium laser ablation of tissue phantoms: correlation between bubble formation and acoustic transients. Applied Physics B: Lasers and Optics 65:647-657.

Blair EA, Erlanger J (1935) On the process of excitation by brief shocks in axons. American Journal of Physiology--Legacy Content 114:309.

Booth J, von MA, Stampfli R (1950) The photochemical action of ultra-violet light on isolated single nerve fibres. Helv Physiol Pharmacol Acta 8:110-127.

Boyden ES, Zhang F, Bamberg E, Nagel G, Deisseroth K (2005) Millisecond-timescale, genetically targeted optical control of neural activity. Nat Neurosci 8:1263-1268.

Branner A, Normann RA (2000) A multielectrode array for intrafascicular recording and stimulation in sciatic nerve of cats. Brain Res Bull 51:293-306.

Butson CR, Miller IO, Normann RA, Clark GA (2011) Selective neural activation in a histologically derived model of peripheral nerve. J Neural Eng 8:036009.

Cayce JM, Friedman RM, Jansen ED, Mahavaden-Jansen A, Roe AW (2011) Pulsed infrared light alters neural activity in rat somatosensory cortex in vivo. Neuroimage 57:155-166.

Dittami GM, Rajguru SM, Lasher RA, Hitchcock RW, Rabbitt RD (2011) Intracellular calcium transients evoked by pulsed infrared radiation in neonatal cardiomyocytes. J Physiol 589:1295-1306.

Duke AR, Cayce JM, Malphrus JD, Konrad P, Mahadevan-Jansen A, Jansen ED (2009) Combined optical and electrical stimulation of neural tissue in vivo. Journal of Biomedical Optics 14:060501-060503.

Duke AR, Cayce J.M., van Gessel I., Jansen E.D. (2008) Optical stimulation of the efferent vagus nerve. In: Neural Interfaces Cleveland, OH.

Elliott CJH, Susswein AJ (2002) Comparative neuroethology of feeding control in molluscs. Journal of Experimental Biology 205:877-896.

Fork RL (1971) Laser stimulation of nerve cells in Aplysia. Science 171:907-908.

Gibson JM, Welker WI (1983) Quantitative studies of stimulus coding in first-order vibrissa afferents of rats. 2. Adaptation and coding of stimulus parameters. Somatosens Res 1:95-117.

Hale GM, Querry MR (1973) Optical Constants of Water in the 200-nm to 200-microm Wavelength Region. Appl Opt 12:555-563.

Harris DM, Bierer SM, Wells JD, Phillips JO (2009) Optical nerve stimulation for a vestibular prosthesis. vol. 5, pp 7180-7121.

Hermann M, Hellebart C, Freissmuth M (2004) Neuromonitoring in thyroid surgery: prospective evaluation of intraoperative electrophysiological responses for the prediction of recurrent laryngeal nerve injury. Ann Surg 240:9-17.

Holsheimer J (2003) Principles of neurostimulation. Pain Research and Clinical Management 15:17-36.

Izzo AD, Suh E, Pathria J, Walsh JT, Whitlon DS, Richter CP (2007a) Selectivity of neural stimulation in the auditory system: a comparison of optic and electric stimuli. Journal of Biomedical Optics 12:-.

Izzo AD, Walsh JT, Jr., Jansen ED, Bendett M, Webb J, Ralph H, Richter CP (2007b) Optical parameter variability in laser nerve stimulation: a study of pulse duration, repetition rate, and wavelength. IEEE Trans Biomed Eng 54:1108-1114.

Izzo AD, Walsh JT, Ralph H, Webb J, Bendett M, Wells J, Richter CP (2008) Laser stimulation of auditory neurons: Effect of shorter pulse duration and penetration depth. Biophysical Journal 94:3159-3166.

Jenkins MW, Duke AR, Gu S, Chiel HJ, Fujioka H, Watanabe M, Jansen ED, Rollins AM (2010) Optical pacing of the embryonic heart. Nature Photonics 4:623-626.

Johnston WL, Dyer JR, Castellucci VF, Dunn RJ (1996) Clustered voltage-gated Na+ channels in Aplysia axons. J Neurosci 16:1730-1739.

Julkunen P, Ruohonen J, Saaskilahti S, Saisanen L, Karhu J (2011) Threshold curves for transcranial magnetic stimulation to improve reliability of motor pathway status assessment. Clin Neurophysiol 122:975-983.

Kandel ER (1979) Behavioral biology of Aplysia: a contribution to the comparative study of opisthobranch molluscs: WH Freeman San Francisco.

Khosrofian JM, Garetz BA (1983) Measurement of a Gaussian Laser-Beam Diameter through the Direct Inversion of Knife-Edge Data. Applied Optics 22:3406-3410.

Kirby AE, Middlebrooks JC (2010) Auditory temporal acuity probed with cochlear implant stimulation and cortical recording. J Neurophysiol 103:531-542.

Malmstrom JA, McNaughton TG, Horch KW (1998) Recording properties and biocompatibility of chronically implanted polymer-based intrafascicular electrodes. Ann Biomed Eng 26:1055-1064.

Ranck JB, Jr. (1975) Which elements are excited in electrical stimulation of mammalian central nervous system: a review. Brain Res 98:417-440.

Rattay F (1986) Analysis of models for external stimulation of axons. IEEE Trans Biomed Eng 33:974-977.

Teudt IU, Nevel AE, Izzo AD, Walsh JT, Jr., Richter CP (2007) Optical stimulation of the facial nerve: a new monitoring technique? Laryngoscope 117:1641-1647.

Tyler DJ, Durand DM (2002) Functionally selective peripheral nerve stimulation with a flat interface nerve electrode. IEEE Trans Neural Syst Rehabil Eng 10:294-303.

Tyler DJ, Durand DM (2003) Chronic response of the rat sciatic nerve to the flat interface nerve electrode. Ann Biomed Eng 31:633-642.

Wells J, Kao C, Jansen ED, Konrad P, Mahadevan-Jansen A (2005a) Application of infrared light for in vivo neural stimulation. Journal of Biomedical Optics 10:-.

Wells J, Kao C, Mariappan K, Albea J, Jansen ED, Konrad P, Mahadevan-Jansen A (2005b) Optical stimulation of neural tissue in vivo. Optics Letters 30:504-506.

Wells J, Kao C, Konrad P, Milner T, Kim J, Mahadevan-Jansen A, Jansen ED (2007a) Biophysical mechanisms of transient optical stimulation of peripheral nerve. Biophysical Journal 93:2567-2580.

Wells J, Konrad P, Kao C, Jansen ED, Mahadevan-Jansen A (2007b) Pulsed laser versus electrical energy for peripheral nerve stimulation. J Neurosci Methods 163:326-337.

Wells JD, Thomsen S, Whitaker P, Jansen ED, Kao CC, Konrad PE, Mahadevan-Jansen A (2007c) Optically mediated nerve stimulation: Identification of injury thresholds. Lasers Surg Med 39:513-526.

CHAPTER VI

HYBRID ELECTRO-OPTICAL STIMULATION OF THE RAT SCIATIC NERVE INDUCES FORCE GENERATION IN THE PLANTARFLEXOR MUSCLES

Austin R Duke[1], Erik Peterson[2], Mark A Mackanos[1], James Atkinson[3], Dustin Tyler[2,4] and E Duco Jansen[1,5]

[1]Vanderbilt University, Department of Biomedical Engineering

Nashville, TN

[2]Case Western Reserve University, Department of Biomedical Engineering

Cleveland, OH

[3]Vanderbilt University, Department of Pathology, Microbiology and Immunology

Nashville, TN

[4]Louis Stokes Cleveland Department of Veterans Affairs Medical Center

Cleveland, OH

[5]Vanderbilt University, Department of Neurological Surgery

Nashville, TN

This chapter is in press at *Journal of Neural Engineering*.

6.1 Abstract

Objective: Optical methods of neural activation are becoming important tools for the study and treatment of neurological disorders. Infrared nerve stimulation (INS) is an optical technique exhibiting spatially precise activation in the native neural system. While this technique shows great promise, the risk of thermal damage may limit some applications. Combining INS with traditional electrical stimulation, a method known as hybrid electro-optical stimulation, reduces the laser power requirements and mitigates the risk of thermal damage while maintaining spatial selectivity. Here we investigate the capability of inducing force generation in the rat hindlimb through hybrid stimulation of the sciatic nerve.

Approach: Hybrid stimulation was achieved by combining an optically transparent nerve cuff for electrical stimulation and a diode laser coupled to an optical fiber for infrared stimulation. Force generation in the rat plantarflexor muscles was measured in response to hybrid stimulation with 1-second bursts of pulses at 15 and 20 Hz and with a burst frequency of 0.5 Hz.

Main Results: Forces were found to increase with successive stimulus trains, ultimately reaching a plateau by the 20^{th} train. Hybrid evoked forces decayed at a rate similar to the rate of thermal diffusion in tissue. Preconditioning the nerve with an optical stimulus resulted in an increase in the force response to both electrical and hybrid stimulation. Histological evaluation showed no signs of thermally induced morphological changes

following hybrid stimulation. Our results indicate that an increase in baseline temperature is a likely contributor to hybrid force generation.

Significance: Extraneural INS of peripheral nerves at physiologically relevant repetition rates is possible using hybrid electro-optical stimulation.

6.2 Introduction

The ability to modify and/or control neural activity is essential to the study of neurological function, as well as to the clinical treatment of neural disorders and deficits. While traditional electrical techniques of neural stimulation and monitoring have long been the gold standard, recent innovations are increasing interest in optical methods of neural activation. Optogenetics involves genetic modification of cells with light-sensitive ion channels, enabling control with high temporal and spatial precision (Fenno et al., 2011). This innovative technique has proved to be a valuable tool in the study of neurological function (Gradinaru et al., 2009, Zhang et al., 2010). Recently, optogenetic techniques were used to stimulate sustained muscle contractions in the mouse sciatic nerve. Using this approach, the physiological recruitment order of small diameter nerve fibers before large diameter fibers was maintained and fatigue was reduced when compared to electrical stimulation in the same preparation (Llewellyn et al., 2010). While optogenetic control is a well-suited tool for the study of neural function and behaviors, the clinical application of gene therapies remains a considerable obstacle.

Infrared nerve stimulation (INS) utilizes pulses of infrared light to activate a targeted excitable tissue, without prior genetic modifications of the tissue (Wells et al.,

2005). INS has been successfully demonstrated in various anatomy including peripheral nerves (Wells et al., 2005, Teudt et al., 2007, Fried et al., 2008), somatosensory cortex (Cayce et al., 2011), auditory system (Izzo et al., 2006) and the heart (Jenkins et al., 2010). INS activates excitable cells through a thermal gradient, generated by the absorption of mid-infrared light by water (Wells et al., 2007a). It was recently shown that this thermal gradient results in a reversible increase in the electrical capacitance of the membrane, generating currents that depolarize the cell (Shapiro et al., 2012). While INS provides a non-contact, spatially confined and artifact-free method of neural activation, the thermal deposition resulting from INS yields a limited range of radiant exposures and stimulus repetition rates that are both safe and effective (Izzo et al., 2007, Teudt et al., 2007, Wells et al., 2007c).

INS radiant exposures that are safe and effective vary by anatomy. In the cochlea, radiant exposures on the order of mJ/cm^2 have been shown to consistently stimulate at 400 Hz for several hours without indications of damage or loss of function (Izzo et al., 2007). In the rat sciatic nerve, however, radiant exposures for extraneural stimulation are on the order of J/cm^2. This leads to safe stimulation using radiant exposures up to roughly two-times stimulation threshold and a maximum stimulus repetition rate of approximately 5 Hz (Wells et al., 2007c). Our experiences also suggest that INS is highly specific in regards to locations along the nerve that are susceptible to activation. This potentially yields unreliable activation and/or limited recruitment. While *a priori* knowledge of locations along the axons that are most responsive to infrared stimulation may enhance efficacy and reliability in peripheral nerves, extraneural INS alone is currently not practical for functional stimulation and may have limited potential for studying or

potentially treating neurological disorders/deficits affecting peripheral nerves using meaningful stimulus repetition rates. For example, the generation of a sustained muscle contraction requires at least 12 to 15 Hz stimulus repetition rate (Peckham and Knutson, 2005). If radiant exposures required for INS are applied at these repetition rates, thermal superposition will occur and the likelihood for laser-induced thermal tissue damage will be considerable (Wells et al., 2007c).

Recently, hybrid electro-optical nerve stimulation was developed to address these limitations of INS (Duke et al., 2009, Duke et al., 2012). In principle, hybrid stimulation synergistically combines sub-threshold pulses of electrical current with sub-threshold pulses of infrared light to achieve activation. The electrical current is believed to depolarize the neurons to just below the threshold for action potential initiation, and then the infrared pulse brings a spatially confined region to threshold. This maintains the spatial precision of INS while reducing the required radiant exposures for stimulation, thus mitigating the risk of thermal damage and reducing the laser power specifications. In regards to neuromuscular stimulation, the optical component of hybrid stimulation may provide fine control while the electrical component will add bulk recruitment.

In this study we use hybrid electro-optical stimulation of the sciatic nerve to produce contractions of the plantarflexor muscles in the rat hind limb at stimulus repetition rates of 15 and 20 Hz. While fused tetanic contractions vary by muscle type and may require relatively high stimulus repetition rates, an increased rate of fatigue becomes a concern. Thus, lower stimulus repetition rates for producing functional responses are desirable. A minimum of 12 to 15 Hz is required if the muscles are conditioned to have long-duration twitches (Peckham and Knutson, 2005). While our

desire was to investigate the feasibility of force generation with hybrid electro-optical stimulation rather than the production of fused tetanic responses, we did desire to use stimulus repetition rates that are applicable for functional stimulation. The results of our study suggest that the excitability of the nerve to electrical stimulation increases as a result of an optically induced rise in the baseline tissue temperature.

6.3 Materials and Methods

6.3.1 Rat preparation and electrophysiology

All experiments were performed following protocols approved by the Institutional Animal Care and Use Committee (IACUC). Male Sprague-Dawley rats (n = 20) weighing 250 – 300g (Charles River) were anesthetized with continuously inhaled isoflurane (induction: 3% isoflurane, 3.0 LPM oxygen; maintenance: 1-2.5% isoflurane, 1.5 LPM oxygen). A rectal probe and heating pad (catalog # 40-90-8, FHC, Bowdoin, ME) were used to maintain the rat at a target body temperature of 35-37 °C throughout the experiment. The animals were placed on a polycarbonate platform and their hindlimbs were shaved. The dorsal surface of the foot was then taped to the edge of the platform. An incision was made from the heel to the vertebral column and the skin was separated from the underlying tissue. The biceps femoris was then cut and divided proximal from the Achilles tendon to expose the sciatic nerve. A silk ligature was placed around the Achilles tendon and the calcaneus was then cut. Using blunt dissection, the medial gastrocnemius, lateral gastrocnemius and soleus muscles were separated from the surrounding tissues. The ligature tied to the Achilles tendon was then secured to the hook

of a force transducer (Figure VII-1). The sural and peroneal branches of the sciatic nerve were transected so only innervation of the plantarflexor muscles remained. A clamp was placed on the femur to ensure isometric contractions.

Paired EMG electrodes made from perfluoroalkoxy (PFA)-coated silver wire (0.003" bare, 0.005" coated; A-M Systems, Sequim, WA) were inserted along the length of the medial gastrocnemius, lateral gastrocnemius and soleus muscles (Figure VII-1). EMG signals were amplified (x1000) and band-pass filtered (300 – 1000 Hz) using an AC-coupled differential amplifier (model 1700; A-M Systems), digitized (Axon Digidata 1440A; Molecular Devices, Sunnyvale, CA) and recorded (Axograph X; Axograph Scientific).

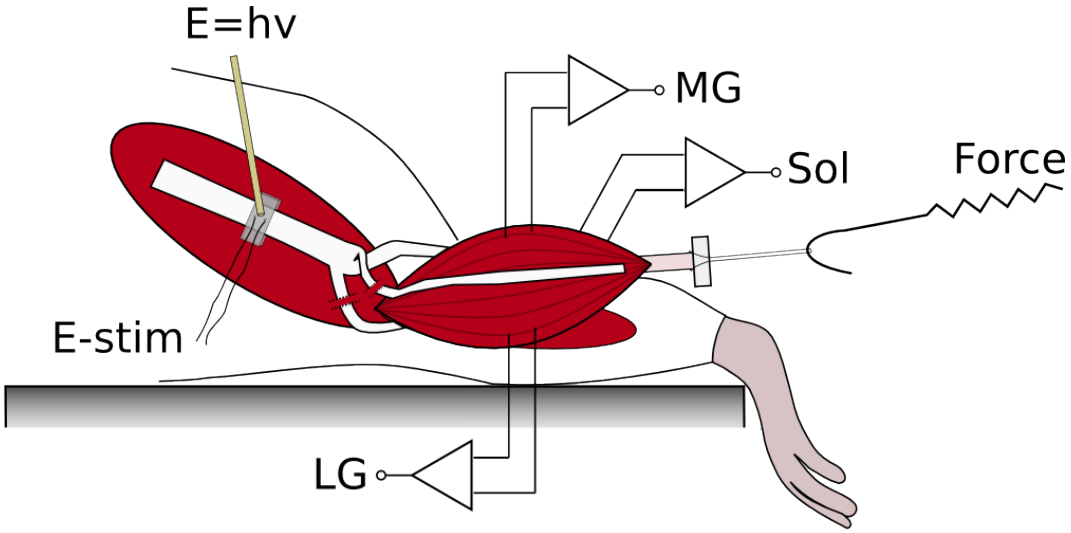

Figure VI-1. Diagram of the surgical area indicating locations of hybrid stimulation and recording. The nerve cuff is placed around the main trunk of the sciatic nerve to provide electrical stimulation. An optical fiber was positioned directly above and just out of contact with the nerve cuff. The medical gastrocnemius (MG), lateral gastrocnemius (LG) and soleus (Sol) muscles were separated from the surrounding tissue. With the Achilles tendon in tact, the calcaneus was cut and attached to a force transducer. Paired EMG electrodes were inserted into MG, LG and Sol to record evoked activity.

6.3.2 Hybrid electro-optical stimulation

Hybrid electro-optical stimulation was applied using an optically transparent nerve cuff in conjunction with a fiber optic. Electrical stimulation was provided by a rectangular nerve cuff modeled after the Flat Interface Nerve Electrode (FINE) (Tyler and Durand, 2003). The FINE is designed to enhance the selectivity of extraneural electrical stimulation by gently reshaping the nerve such that more centrally located axons are brought closer to the periphery (Tyler and Durand, 2002). For these experiments we were not concerned with the selectivity of electrical stimulation. As such, we used the physical structure of the FINE, but our implementation was not targeted towards electrical selectivity.

The nerve cuff was made by molding Sylgard®-184 (Dow-Corning; Midland, MI). The inner height and width of the cuff were 0.4 mm and 4 mm, respectively. Cuff wall thickness was 0.6 mm and the length along the nerve was 4 mm. Sylgard® was chosen due to the low optical absorption of polydimethylsiloxane (PDMS) at near- and mid-IR wavelengths (Cai et al., 2008). To assess the optical transmission of the cuff, we used a spectrophotometer (Lambda 900; Perkin-Elmer) to measure the amount of light transmitted through a 0.6 mm slab of Sylgard®. Transmission measurements were averaged for 200 ms with a 2 nm step size. To validate the measurements, optical power from a 1875 nm diode laser (Capella; Lockheed-Martin-Aculight, Bothell, WA) coupled to a fiber optic was measured using a thermopile sensor (PS19Q, Molectron) with and without a 0.6 mm slab of Sylgard® located between the sensor and fiber tip. Two platinum foil contacts (area = 0.14 mm^2) were embedded within one surface of the cuff and arranged along the length of the nerve. Teflon-coated stainless steel wire (0.002”

bare, 0.0045" coated; A-M Systems, Sequim, WA) was soldered to the contacts and used to connect with the electrical stimulator. Bipolar electrical stimulation was applied between the two Pt contacts using a constant-current stimulus isolator (A365R, WPI). Charge-balanced, 100 μs biphasic pulses with 50 μs phase separation (cathodic first) were used for all experiments.

Optical stimulation was applied with a 0.4 mm diameter fiber optic (NA = 0.22; Ocean Optics, Dunedin, FL) connected to a tunable pulsed diode laser (Capella). The wavelength (λ = 1875 nm) and pulse duration (2 ms) were constant for all experiments. The laser spot size on the nerve was measured using the knife-edge technique (Khosrofian and Garetz, 1983). The optical fiber was positioned perpendicular to and just out of contact with a 0.6 mm thick slab of Sylgard®, and a razor blade was placed against the opposite side of the Sylgard® slab. By translating the fiber optic perpendicular to the blade and measuring the optical power using a thermopile sensor, we were able to determine the size of the laser spot incident on the nerve surface to be 0.24 mm^2.

In all experiments, the cuff was placed around the sciatic nerve near the main branch (Figure VII-1). The optical fiber was then used to irradiate through the top layer of the cuff to find a location along the nerve, between the Pt contacts, yielding an EMG and/or twitch that responded one-to-one with the laser pulses. In some cases, the tibial branch was visually observed to divide from the bottom of the main nerve trunk, away from the site of INS. In those cases, the cuff was repositioned distal to the branch point along the tibial nerve so as to ensure successful stimulation of the plantarflexor muscles. Once a successful location was identified, the Pt contact closest to the fiber optic was set to be the cathodic stimulus, as this was previously shown to provide the optimal overlap

of the electrical current and optical thermal response for hybrid stimulation (Duke et al., 2012). For hybrid stimulation, optical and electrical stimulus pulses were coordinated using computer software (Axograph X). Pulses were timed such that the optical pulse and the first phase (cathodic) of the electrical stimulus ended simultaneously.

6.3.3 Experimental protocol

Unless specified otherwise, all experimental trials were conducted as follows. Experimental trials were comprised of 20 stimulation episodes. Each episode consisted of a 1 sec stimulus train of 15 or 20 Hz preceded and followed by 0.5 sec with no stimulation (Figure VI-2). This yielded total episode duration of 2 sec. Episodes were applied consecutively with negligible delay, effectively delivering pulse bursts at 0.5 Hz over a period of 40 sec. The recorded force for a single episode, or ensemble average of episodes, was determined as the peak force generated during the last 500 ms of the stimulus train. For each nerve, an electrical recruitment curve was generated using the stimulus parameters to be measured while modulating electrical amplitude. Electrical stimulation threshold was defined for each repetition rate as the current generating 10% of the maximum overall force. Recruitment achieving 10% of the maximum force has been used to define threshold currents previously and forces up to 10% of the overall maximum force may be considered negligible (Tyler and Durand, 2002, Tarler and Mortimer, 2003, Schiefer et al., 2008). Periodically throughout the experiment the nerve was stimulated with 2X the current generating the maximum force. Any changes in maximum contraction force resulted in an associated change in the 10% force used to determine stimulation threshold currents.

Experimental trials were comprised of four separate runs (Figure VI-2): 1) electrical stimulation at the threshold current (3 episodes); 2) sub-threshold electrical stimulation where the current was reduced to 90% of threshold (i.e. 90% of the current required to generate 10% of the maximum force) (3 episodes); 3) hybrid stimulation combining sub-threshold pulses of electrical stimulation with pulses of infrared light (20 episodes); and 4) repeated measures of sub-threshold electrical stimulation (3 episodes) or hybrid stimulation (1 episode). Between experimental trials, saline was applied to prevent dehydration and the nerve and muscles were allowed to rest for ~2 min.

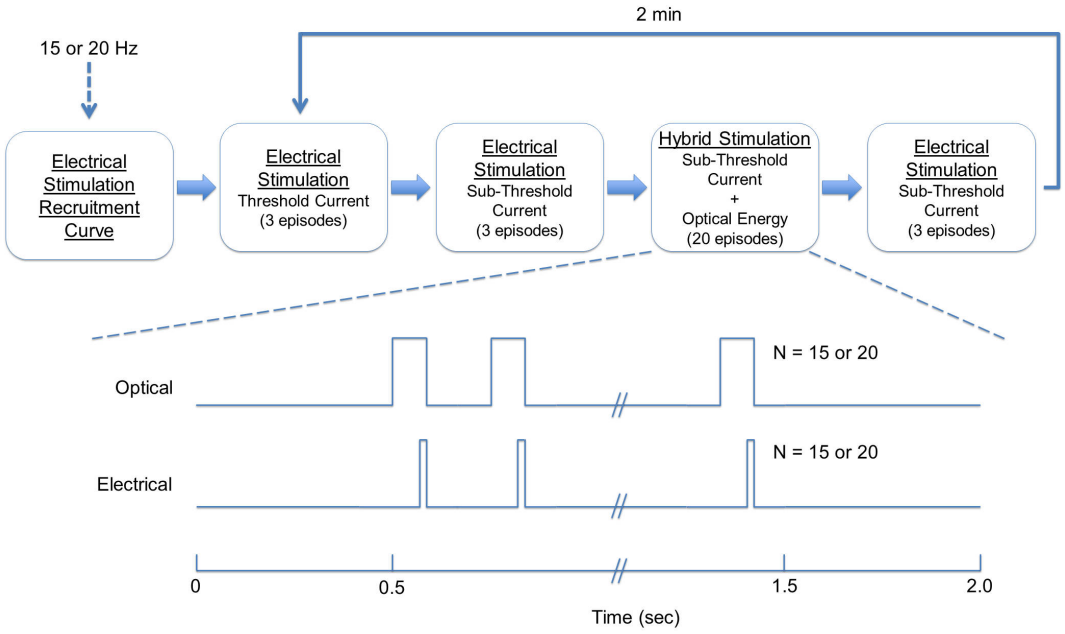

Figure VI-2. Experimental protocol used for investigating force generation with hybrid electro-optical stimulation. Threshold current was defined as the current necessary to generate 10% of the maximum force for a given parameter set (as determined by the electrical stimulation recruitment curve). Sub-threshold current was defined as 90% of the threshold current.

6.3.4 Tissue morphology studies and histology

Histological analysis was performed to assess the acute changes in nerve morphology in response to hybrid stimulation at physiologically relevant (15 and 20 Hz) repetition rates. With the cuff placed along the sciatic nerve, proximal to the branch point, 20 episodes of 1 sec bursts of combined optical and electrical stimulation were applied with burst frequency of 0.5 Hz. After the experimental stimulus, a positive control demonstrating visible damage was added to each nerve using optical stimulation alone (no cuff). The edges of the cuff and the locations of the optical fiber were marked with blue tissue dye (Delasco, Council Bluffs, IA). Nerves were harvested immediately after the animal was sacrificed and placed in formalin. Nerves were processed and embedded in paraffin, cut longitudinally in 5 μm sections and stained with hematoxylin and eosin (H&E) and Masson's trichrome stains.

6.4 Results

6.4.1 Optical transmission of nerve cuff

Using a spectrophotometer we found that a 0.6 mm thick slab of Sylgard® transmitted ~93% of light at wavelengths typically used for INS (1450 nm, 1875 nm, 2120 nm; Figure VI-3). Given the index of refraction mismatch between air and Sylgard®, much of the ~7% light loss can be attributed to Fresnel reflections at the Sylgard®-air interface rather than to absorption within the Sylgard® itself. Transmission fell to 73% at 1746 nm, but was >90% for the majority of the wavelengths tested. Using a thermopile sensor and the diode laser source (λ = 1875 nm), we verified that ~93% of the

optical power was transmitted when a 0.6 mm slab of Sylgard® was placed between the sensor and the fiber optic. Using the optical fiber to stimulate through the cuff, INS threshold was found to be 2.03±0.43 J/cm^2 at 2 Hz. Radiant exposures were determined using the measured radiant energy transmitted through the nerve cuff and the measured spot size as described above (Section 2.2). INS threshold was determined as the minimum radiant exposure required to evoke an EMG response with 5 consecutive laser pulses.

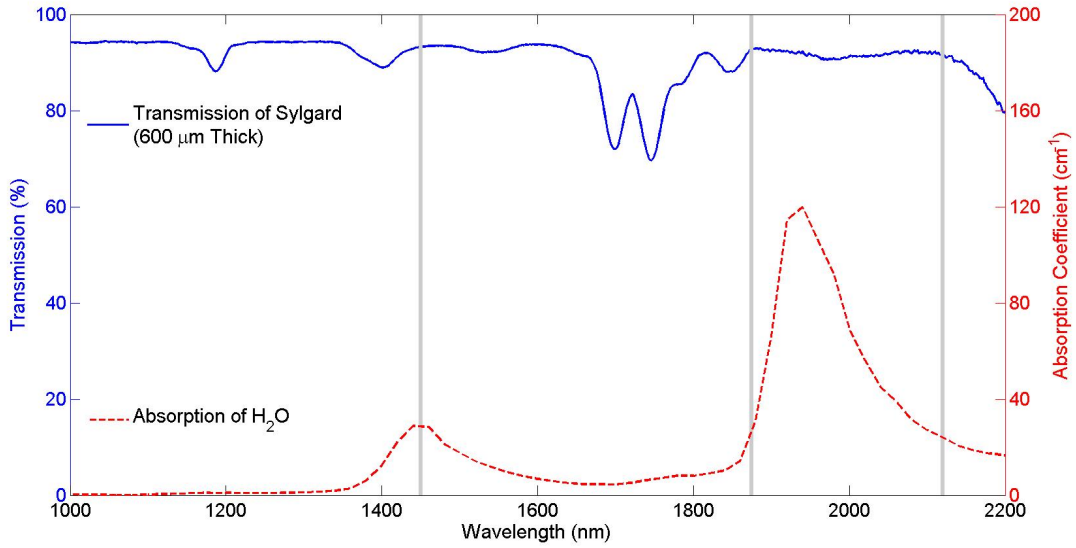

Figure VI-3. Infrared transmission of a Sylgard® nerve cuff. The 0.6 mm thick Sylgard® cuff used in these experiments transmits ~93% of light (blue solid line) at wavelengths typically used for optical stimulation (gray bands). For reference, the water absorption curve is shown (red dash line), which indicates the absorption coefficient of light in tissue as a function of wavelength (Hale and Querry, 1973).

6.4.2 Hybrid force generation

Hybrid electro-optical stimulation was investigated by combining pulses of infrared light with sub-threshold pulses of electrical current. Examples of typical results for 20 Hz stimulation are shown in Figure VI-4. An electrical recruitment curve for the rat plantarflexor muscles is shown in Figure VI-4a. After finding the threshold and sub-threshold currents (Figure VI-4a – inset), pulses of infrared light were combined with pulses of sub-threshold electrical current to produce hybrid stimulation. In Figure VI-4b, the force response to threshold electrical stimulation (blue line), sub-threshold electrical stimulation before (thin black line) and after (thin black dotted line), and hybrid stimulation (thick red line) are shown. In this example there is a clear rise in the generated force for both electrical and hybrid stimulation over the duration of stimulation; however, the responses exhibit a ripple effect rather than a smooth fusion of force that would be expected at higher repetition rates than were tested here. While typical responses are shown in Figure VI-4b, force responses that were either fused or more characteristic of low-rate twitches were also observed. The force response to sub-threshold electrical stimulation recorded after hybrid stimulation varied in magnitude relative to the force generated by the same current prior to hybrid stimulation. In Figure VI-4b there is negligible difference between the before and after measurements; however in some cases the measurement made after hybrid stimulation was noticeably greater.

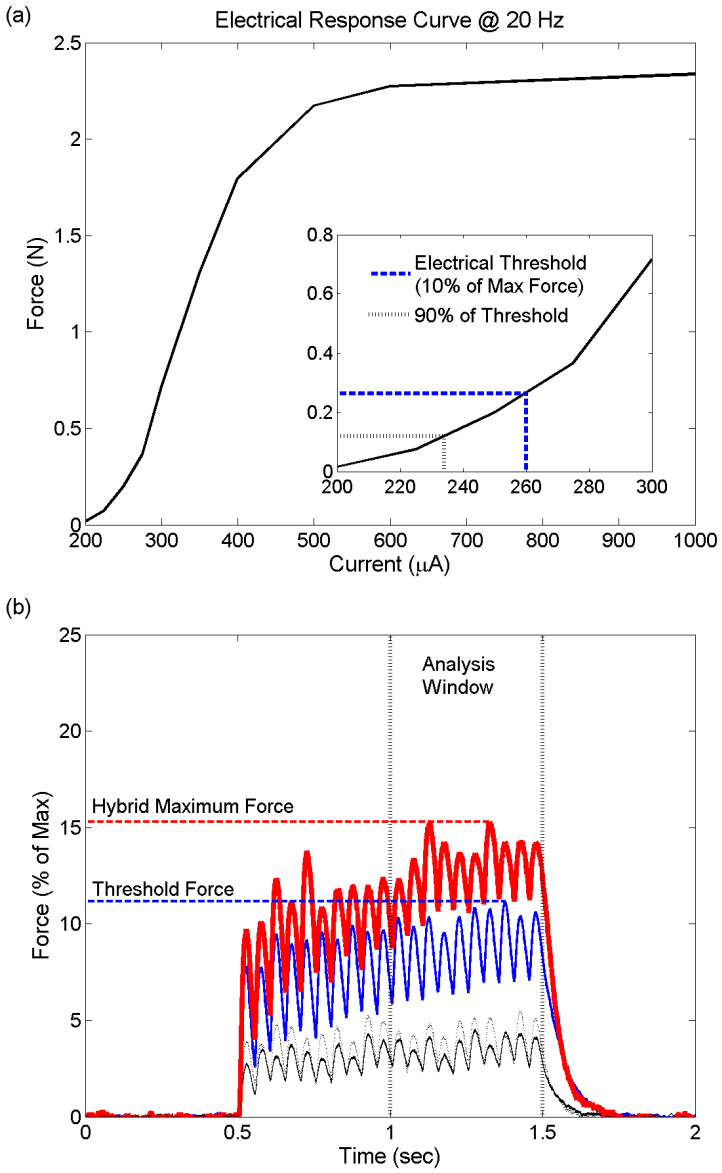

Figure VI-4. Typical force generation for 20 Hz electrical and hybrid stimulation. In (a) an electrical recruitment curve using the Sylgard® cuff is shown. Threshold electrical stimulation was defined as the current generating 10% of the maximum force at a given repetition rate ((a) inset; blue dash). Sub-threshold stimulation ((a) inset; black dash) was then defined as 90% of the threshold current. Forces evoked by the sub-threshold electrical stimulus before (b; thin black line) and after (b; black dotted) hybrid stimulation were similar. Forces generated using hybrid stimulation (b; thick red line) were comparable or exceeded the force generated by threshold electrical stimulation (b; blue line). Maximum forces were defined as the peak force generated during the last 500 ms of the stimulus train.

EMG recordings from the medial gastrocnemius, lateral gastrocnemius and soleus muscles revealed that hybrid electro-optical stimulation produced forces of equal or greater magnitude using relative contributions from each muscle that were different than near-threshold electrical stimulation alone. In Figure VI-5, EMGs and evoked forces are shown for maximal electrical stimulation (Figure VI-5a) sub-threshold electrical stimulation (Figure VI-5b), threshold electrical stimulation (Figure VI-5c) and hybrid stimulation (Figure VI-5d, e). The sub-threshold stimulation produces very little activation of any of the muscles, generating no force. Threshold electrical stimulation generates approximately 10% of the maximum force through a balanced recruitment of all three muscles relative to their respective maxima. In the same nerve, hybrid stimulation evoked a greater force response while preferentially recruiting the medial gastrocnemius muscle. In comparison to threshold electrical stimulation, hybrid stimulation in Figure VI-5d produces a force that is approximately 50% of the maximum force, while the soleus and lateral gastrocnemius muscles experience less activation. The extent of preferential recruitment demonstrated by hybrid stimulation varied across experiments.

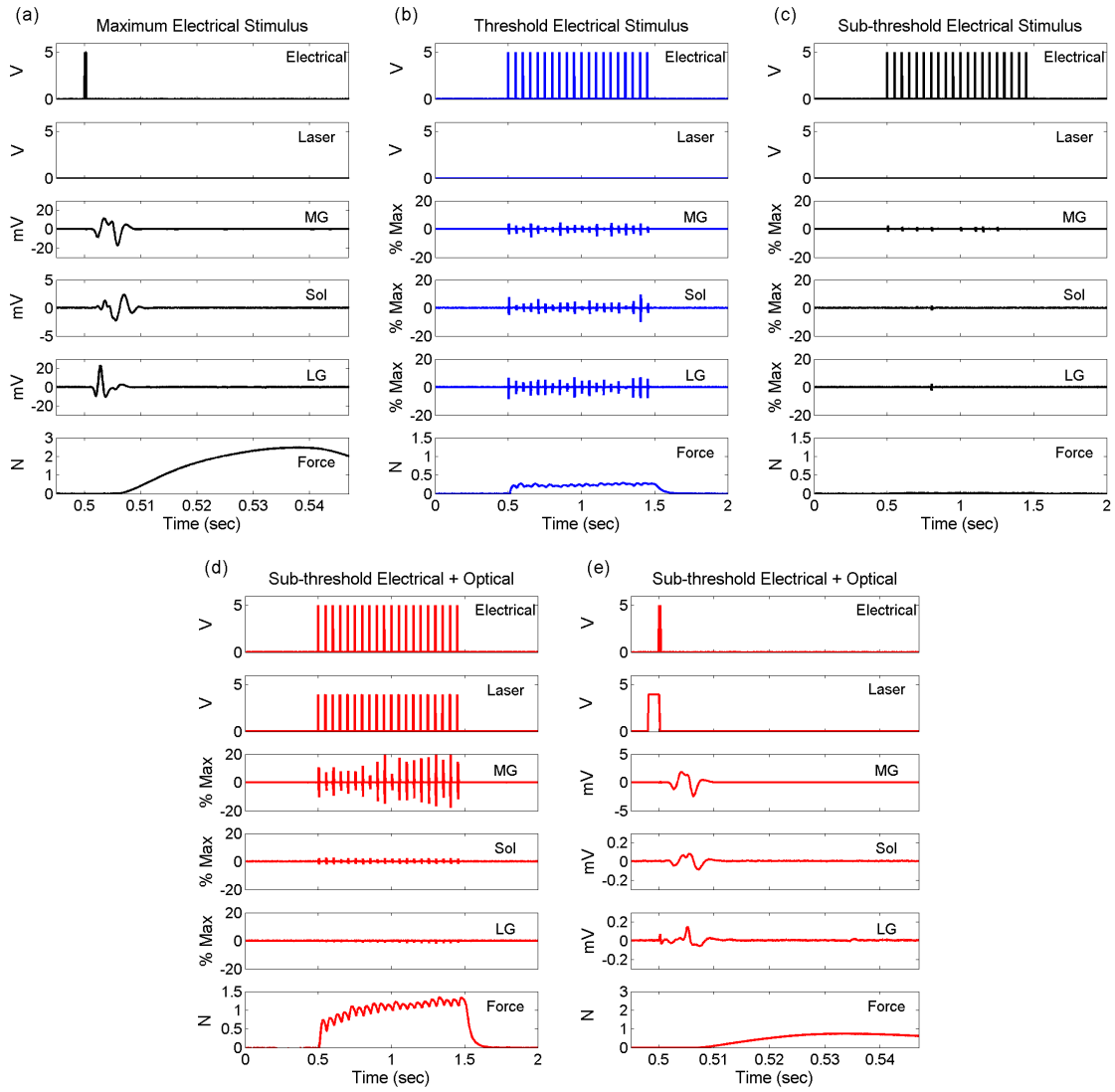

Figure VI-5. Hybrid electro-optical stimulation generates force using a different combination of motor units than electrical stimulation alone. Each panel (a-e) plots the electrical and optical stimulus triggers; the EMG trace from the medial gastrocnemius (MG), soleus (Sol) and lateral gastrocnemius (LG) muscles; and the resulting force generated on the Achilles tendon. Panel (a) shows the response to the first electrical pulse in a 1-second, 20 Hz train generating maximum muscle force. Note the scale difference between Sol and MG/LG. Panel (b) is the response due to electrical stimulation that generates 10% of the maximal force measured. Panel (c) is the response generated using electrical current that is 90% of the amplitude used in (b). Panel (d) is the result of adding 0.65 (J/cm2) of optical stimulus to the electrical stimulus used in (c). Panel (e) shows the first response to the hybrid stimulus depicted in panel (d). Note the scale differences between MG and Sol/LG in (d) and between panels (a) and (d). In this trial, forces evoked by electrical stimulation are generated by activating MG, LG, and Sol, whereas the force evoked by hybrid stimulation is generated primarily through MG activation. In panels (b-c), EMG traces are plotted as a percent of the maximum EMG shown in panel (a).

6.4.3 Characterization of hybrid force response

While electrical stimulation produced force responses that were consistent from episode to episode, hybrid stimulation generated forces that increased with successive episodes towards a plateau (Figure VI-6a). We modified our experimental protocol to further characterize this response and to investigate whether lasting changes in the nerve's excitability were occurring. Rather than following hybrid stimulation with a repeat measurement of the sub-threshold electrical force response, we instead applied a single additional episode of hybrid stimulation, using the same hybrid stimulation parameters, at various delay times relative to the end of the 20^{th} hybrid stimulation episode. It was determined that the magnitude of the force response to the 21^{st} hybrid stimulation episode followed an exponential decay (τ = 3.13 sec) with increasing time after the 20^{th} hybrid stimulation episode (Figure VI-6b). To further validate that no lasting changes in the nerve's excitability occurred, we repeated the experiment demonstrated in Figure VI-6a and observed no obvious changes in the sigmoid shape or absolute force (data not shown).

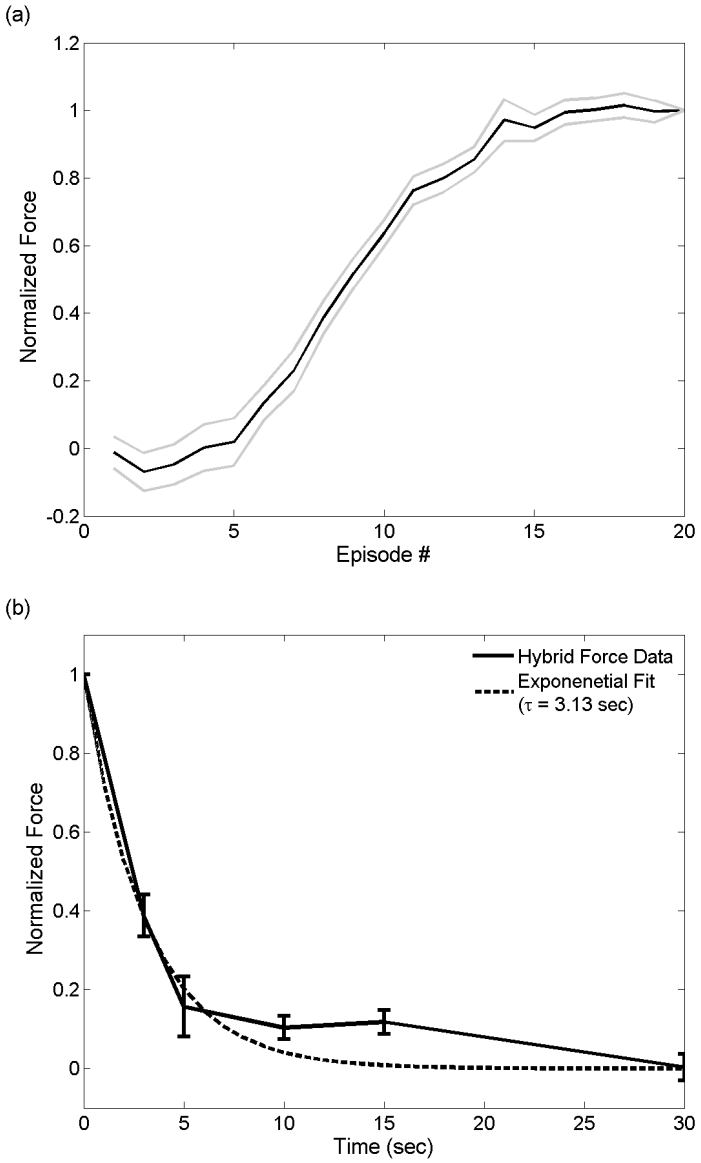

Figure VI-6. The force response to hybrid electro-optical stimulation exhibits a sigmoid recruitment profile with successive stimulus episodes. In (a), the evoked force builds towards a plateau with each additional train (n = 17 rats; mean ± S.E.M.). (b) As time elapses following the final train, the response to a single additional train exhibits exponential decay (n = 10 rats; $\tau = 3.13$ sec; $R^2 = 0.66$; error bars are ± S.E.M.). Electrical stimulus is 90% of the current required to generate 10% of the maximum force. Optical stimulation is 0.59 J/cm^2. Trains are 20 Hz with bursting frequency of 0.5 Hz. Data are normalized to the average force produced by the 20th stimulus episode.

Given the time constant of the exponential decay, we investigated how the rate at which trains were delivered affected the absolute force recruited by hybrid stimulation. As the bursting frequency decreased (i.e. greater time between each train), the maximum force also decreased and the onset of the force plateau occurred at an earlier episode/train (Figure VI-7).

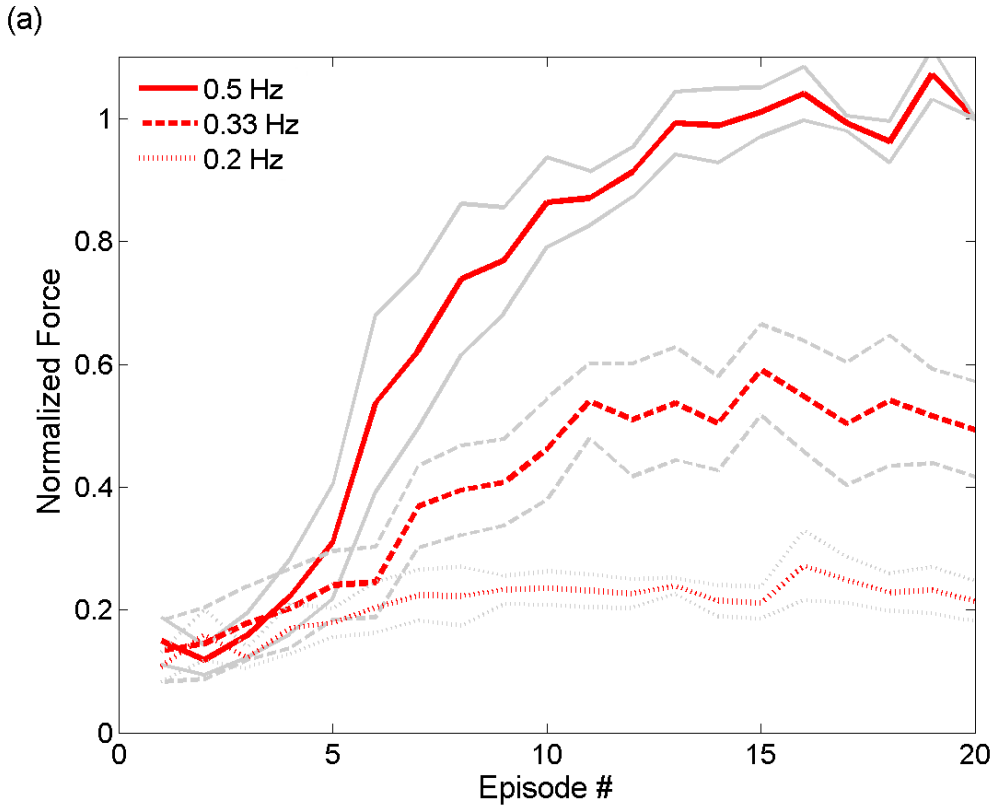

Figure VI-7. The burst frequency for hybrid stimulation determines the magnitude of the force generated. After a total of 20 pulse trains (1 sec, 20 Hz), those with burst frequency of 0.5 Hz produce forces that are roughly 2x and 5x greater than the forces generated by trains with burst frequency of 0.33 Hz and 0.2 Hz, respectively. With a decay time constant of ~3 sec (Figure VI-6b) the results indicate that reduced superposition will occur for trains having burst frequency of 0.33 Hz (2 seconds between trains), and minimal to no superposition will occur for trains with burst frequency of 0.2 Hz (4 seconds between trains).

Over the range of radiant exposures tested, the hybrid-generated force increased steadily with increasing radiant exposure (Figure VI-8). The maximum average recruited force with hybrid stimulation, as a percentage of the maximum force evoked by electrical stimulation, was 32.2% with 0.75 ± 0.01 J/cm^2 at 20 Hz. Hybrid stimulation at 15 Hz generated less force as a percentage of the maximum than at 20 Hz.

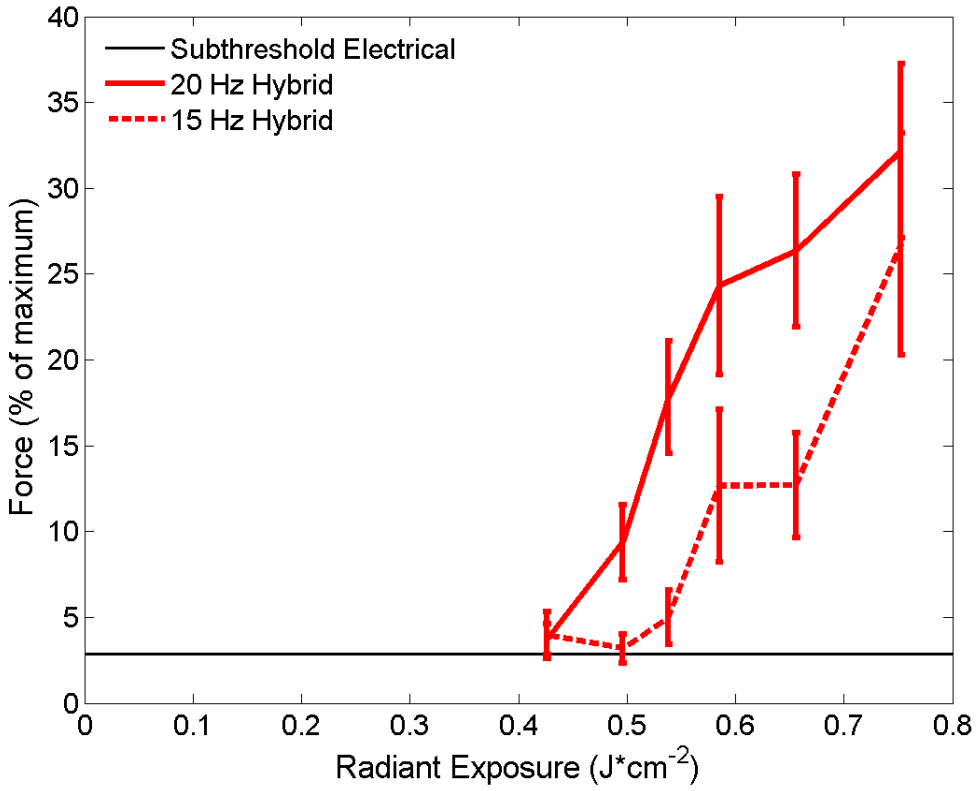

Figure VI-8. Hybrid stimulation combining sub-threshold electrical and optical stimuli yields an evoked force response that increases with optical radiant exposure. Average maximum forces are plotted as a function of radiant exposure and stimulus repetition rate. The black bar indicates the baseline force provided by the sub-threshold electrical stimulus. Combining trains of optical pulses with sub-threshold electrical pulses generates ~30% of the total force produced by maximum electrical stimulation at 20 Hz. When the optical and electrical stimuli are combined at 20 Hz (red solid line), both the magnitude of the force generated and the normalized fraction of the total force are greater than at 15 Hz (red dash). Vertical error bars are +/- S.E.M.

6.4.4 Tissue temperature effects

In the context of INS, infrared light is well-known to cause an increase in tissue temperature at repetition rates greater than ~5 Hz (Wells et al., 2007a). To test whether the observed episode-dependent increase in generated force was related to presumed increasing tissue temperature, the electrical stimulus was omitted from the initial episodes to allow optical heating without nerve activation. Sub-threshold optical stimulation was applied for 17 episodes, followed by hybrid stimulation for an additional 3 episodes (Figure VI-9; dashed line). The addition of the sub-threshold electrical stimulus on the 18^{th} episode generated forces that were initially ~1.5x greater than hybrid stimulation after 18 episodes, though the evoked forces began to converge by the 20^{th} episode. A second experiment tested the effects of tissue temperature on force generation by applying sub-threshold optical stimulation for 19 episodes and then stimulating with a sub-threshold electrical stimulus alone for the 20^{th} episode (Figure VI-9; dotted line). The results of this experiment showed that following preconditioning of the nerve with optical stimulation, the previously sub-threshold electrical stimulus produced a force that matched the 20^{th} episode of hybrid stimulation trials.

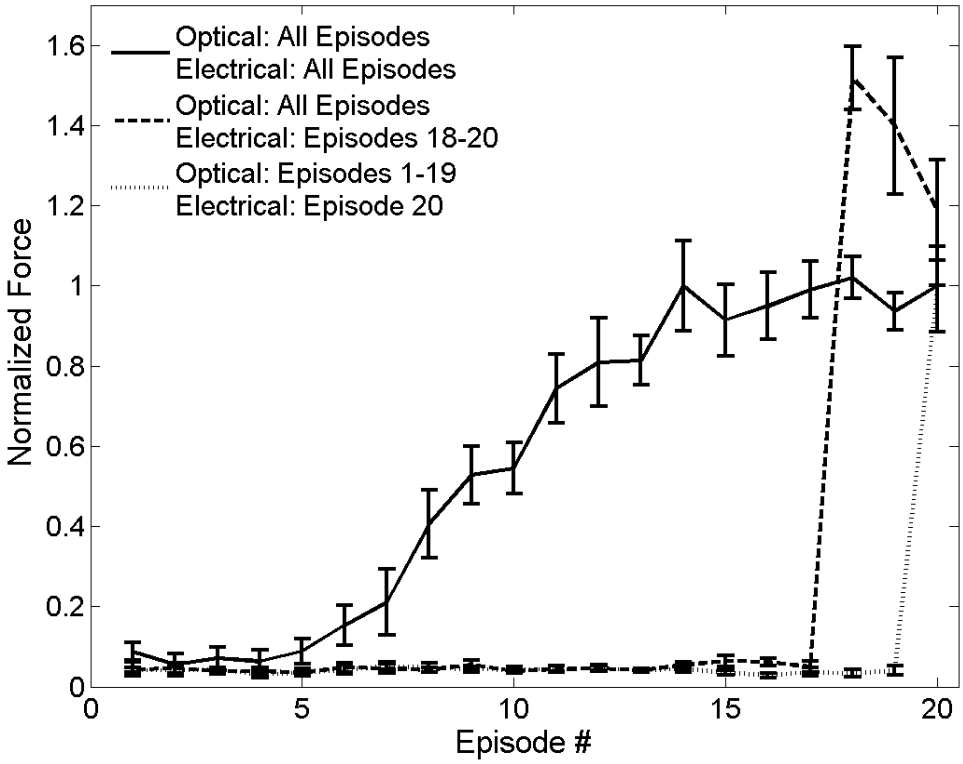

Figure VI-9. Preconditioning the nerve with sub-threshold optical stimulation enhances the force response to electrical stimulation. Hybrid stimulation (solid line) exhibits a sigmoid recruitment curve with increasing episode number. When sub-threshold optical stimulation is applied at 20 Hz prior to hybrid stimulation (dashed line) a greater force is evoked when compared to full hybrid trials (solid line). In trials consisting of an electrical stimulus following optical preconditioning (dotted line), similar force is generated as compared to the full hybrid trials. Forces are normalized to the maximum force of the 20th hybrid stimulus episode. The baseline evoked force in response to sub-threshold electrical stimulation was subtracted from force measurements where electrical stimulation was applied.

6.4.5 Nerve morphology following hybrid stimulation

To detect the presence of possible morphological changes, nerves were stimulated with hybrid electro-optical stimulation at both 15 and 20 Hz using increasing levels of optical radiant energy. Electrical stimulation current was set to sub-threshold levels, while optical stimulation radiant exposures ranged from 0.59 – 1.43 J/cm^2. A positive control was added to each nerve using optical stimulation alone (10 Hz, 10 sec, ~5 J/cm^2). A negative control consisted of placing the cuff on the nerve and electrically stimulating with sub-threshold current, but without the application of infrared pulses. Nerve samples were processed as described in the Methods section. Similar results were seen with both H&E and Masson's trichrome stains. Figure VI-10 shows representative results from nerves stimulated at 20 Hz and stained with Masson's trichrome. Signs of thermally induced morphological changes were not observed at radiant exposures used to characterize the force response to hybrid electro-optical stimulation in this study (maximum radiant exposure in Figure VI-8 is 0.75±0.03 J/cm^2). The first signs of morphological changes were observed at 0.82 J/cm^2 for 20 Hz stimulation, though in some cases radiant exposures as high as 0.92 J/cm^2 (also at 20 Hz) showed no structural changes. The morphological changes observed were hyalinzation of the epineurium and vacuolization of the axon bundle that continued more deeply as radiant exposures increased.

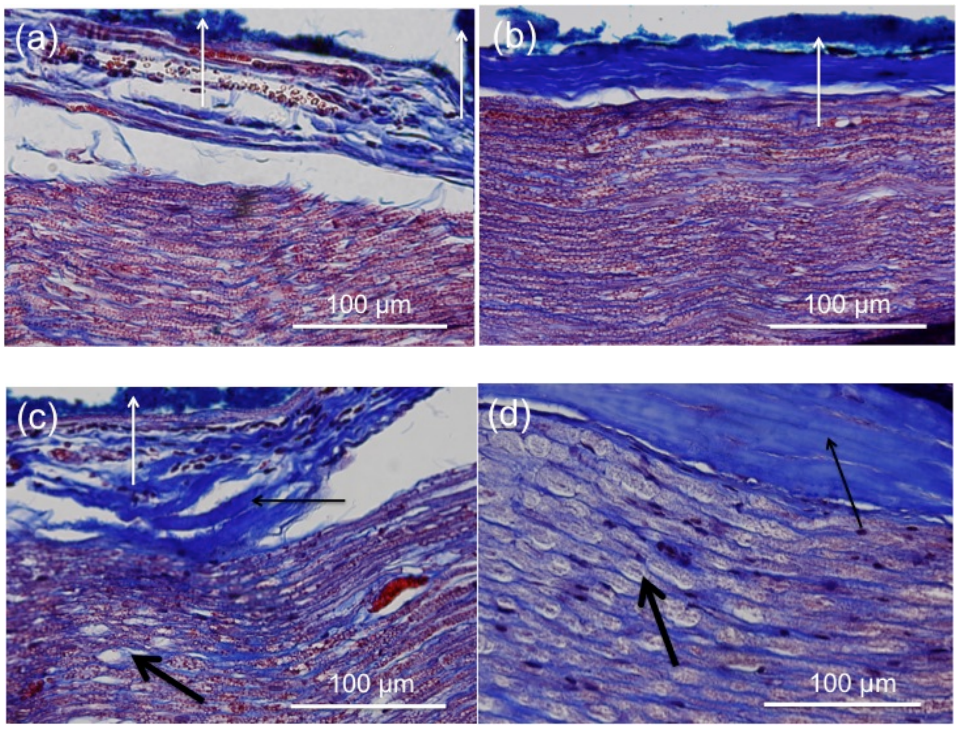

Figure VI-10**.** Histological analysis of rat sciatic nerves following hybrid electro-optical stimulation. Representative images from longitudinal sections of nerves with Masson's trichrome staining are shown. Locations of stimulation were marked with blue tissue dye (a-c; white arrow). The nerve sample exposed to hybrid electro-optical stimulation using 0.67 J/cm^2 showed no signs of thermally induced morphological changes (b). When the radiant exposure was increased (1.28 J/cm^2), collagen hyalinization of the epineurium (c; thin black arrow) and mild vacuolization occurred (c; thick black arrow). Neural tissue exposed to the positive control (4.98 J/cm^2) showed extended regions of collagen hyalinization of the epineurium (d; thin black arrow) and vacuolization of the axon bundle (d; thick black arrow). A negative control (a) followed the same protocols as b-d; however, no infrared pulses were applied.

6.5 Discussion

Hybrid electro-optical stimulation was recently developed as a nerve stimulation paradigm with the selectivity of infrared nerve stimulation, but with mitigated risk of thermal tissue damage (Duke et al., 2009, Duke et al., 2012). While previous efforts concentrated on demonstrating feasibility and improving the reliability of hybrid stimulation, our goal in this work was to investigate the physiological response to hybrid electro-optical stimulation in the mammalian peripheral nerve. Although INS is capable of safely and reliably stimulating mammalian peripheral nerves, laser-induced thermal tissue damage becomes a risk at repetition rates of 5 Hz and above (Wells et al., 2007c). Here we show that hybrid electro-optical stimulation may be used to characterize the response to optical stimulation at repetition rates that will provide meaningful force generation. In this work we have demonstrated sustained contraction of the rat plantarflexor muscles in response to hybrid stimulation of the rat sciatic nerve, verified the capability of spatially discrete stimulation, characterized the unique properties of the hybrid stimulation force response and shown that this method produces no detectable thermally induced changes in nerve morphology for acute stimulation at 15-20 Hz repetition rates.

Although not the primary emphasis of this work, the use of the optical stimulus in conjunction with the nerve cuff does have important implications. In addition to reducing the risk of thermal damage, a second goal of hybrid electro-optical stimulation is to relax laser design constraints for the ultimate goal of implanting INS-based technologies. Based on our transmission measurements (Figure VI-3), biocompatible PDMS-based cuffs could provide a suitable means of securing optical fibers and/or infrared light-

sources to peripheral nerves. The Sylgard® used in our cuff absorbs negligible optical energy, essentially making it a transparent scaffolding material for wavelengths typically used for INS stimulation. We did, however, notice an increase in INS threshold using our cuff when compared to previous studies. It is possible that the increased heat conduction away from the stimulation site by the cuff material, as opposed to air, increases the optical stimulation threshold. This is not likely, however, due to the short duration of the laser stimulus pulse (2 ms) relative to the time constant for thermal diffusion ($\tau \sim 90$ ms (van Gemert and Welch, 1989, Wells et al., 2007a)). The increase in stimulation threshold is most likely due to the method of threshold determination. Areas of enhanced excitability have been observed in peripheral nerves. Rather than seek out these preferred locations where thresholds would likely be lowest, we instead positioned our nerve cuff and then found the INS threshold for that limited portion of the nerve. Our threshold measurements show significant variance, which may indicate that for some nerves the cuff was located at a position that was more susceptible to INS than for others.

A primary appeal of optical stimulation techniques such as INS is potential spatial selectivity. Here we have shown that hybrid stimulation is capable of producing comparable forces as near-threshold electrical stimulation using a different set of motor units. The example illustrated by Figure 4 shows that electrical stimulation alone produced a rather balanced recruitment of both the lateral gastrocnemius/soleus and medial gastrocnemius branches of the sciatic nerve, while hybrid stimulation preferentially recruited the medial gastrocnemius branch. The degree to which a particular muscle was preferentially activated with hybrid stimulation varied considerably across all trials; however different activation patterns between hybrid and electrical

stimulation were frequently observed. In this study we made no systematic effort to determine whether the position of the optical fiber could be used to predict which muscle experienced activation. However, both a functional map of the sciatic nerve produced using INS and the ability to recruit different neural and motor units by adjusting hybrid stimulation parameters were shown previously and suggest the potential this type of prediction (Wells et al., 2007b, Duke et al., 2012). A significant challenge for functional nerve stimulation is limiting fatigue of the stimulated muscles (Levy et al., 1990). By generating the same force using a different set of motor units, hybrid neural interfaces could conceivably tackle this obstacle by alternating between hybrid stimulation and electrical stimulation to prevent fatiguing a single group of motor units.

Forces generated by hybrid electro-optical stimulation were comparable to near-threshold electrically generated forces (Figure VI-4b) and exhibited an increased magnitude with increasing stimulus strength (Figure VI-8). While we did observe fused force responses in some cases, much of our results demonstrated rippling, which is indicative of a muscle contraction that is not completely fused (Figure VI-4b). Consistently fused forces generated at these repetition rates will likely require muscles that are conditioned and/or well-suited for low-rate stimulation (Peckham and Knutson, 2005). Using the nerve cuff in conjunction with an optical fiber, we were able to achieve contraction forces of the rat plantarflexor muscles that increased with increasing stimulus strength. Maximum force produced by hybrid stimulation using our experimental setup was approximately 30% of the maximum force produced electrically. In the future we envision incorporating more locations of hybrid stimulation within a single nerve cuff to achieve further muscle activation. The FINE array, used as the model for the cuff in this

study, is designed to apply gentle pressure that reshapes the nerve. This helps limit the amount of epineurial tissue between a fascicle and the surface of the nerve, without occluding blood supply to the nerve. This helps to mitigate the absorption and scattering of infrared light in superficial tissues, thus more efficiently delivering infrared energy to the axons (Tyler and Durand, 2002). By incorporating more electrical contacts and sources of infrared light within the cuff, full coverage of the nerve is certainly possible. While we expected the absolute force to be less for 15 Hz stimulation than for 20 Hz stimulation, the reduced percentage of the overall force was not expected. At 15 Hz, the greater inter-pulse interval allows for more thermal diffusion to occur, decreasing both the rate of temperature rise and the overall temperature achieved at the site of absorption for a given optical parameter set. Reduced rise in baseline temperature with 15 Hz stimulation, when compared to 20 Hz, may be the reason for the observed difference in normalized force.

While the complete mechanism of INS is yet to be elucidated, experimental evidence indicates the absorption of infrared energy by the tissue water content creates a temporal and spatial thermal gradient that leads to activation (Wells et al., 2007a). Recently, it was further discovered that the thermal gradient causes a reversible increase in membrane capacitance that produces depolarizing currents (Shapiro et al., 2012). While the capacitance increase alone was not shown to bring the membrane to threshold, applying a sub-threshold voltage step with optical stimulation was able to produce an action potential. Our results indicate that for hybrid electro-optical stimulation, a baseline temperature increase also likely plays an important role.

Characterization of the force generated versus episode number for hybrid stimulation led to the hypothesis that thermal accumulation contributes to hybrid-evoked force. Forces generated by supra-threshold electrical stimulation showed a consistent response for 20 consecutive stimulus episodes having inter-pulse frequency of 20 Hz and burst frequency of 0.5 Hz (data not shown). However, hybrid stimulation force consistently increased to a plateau when plotted versus episode number (Figure VI-6a), approximating the accumulation of heat. For optical irradiation where inter-pulse and burst frequency are less than the thermal diffusion time, the baseline tissue temperature will increase and reach thermal equilibrium (Wells et al., 2007a). The spatial extent of the temperature rise will also increase, bringing a larger region of the nerve to threshold. Following hybrid stimulation, forces exhibited an exponential decay with $\tau = 3.13$ sec, which is slower than the rate of thermal diffusion in tissue. This suggests that while a baseline temperature increase likely plays a role, the relationship between temperature and force is complex. We also observed that decreasing the burst frequency (i.e. increasing the duration between each train) reduced the overall force attained by hybrid stimulation (Figure VI-7). With more time between each train, less thermal superposition occurs due to increased diffusion away from the stimulation site. Assuming that baseline temperature contributes to the overall force, one would expect that increased duration between trains would lead to less force generation, which matches our results.

To more directly assess the potential contributions of a baseline temperature rise, we preconditioned the nerve with a 20 Hz sub-threshold for stimulation optical stimulus that should cause an increase in baseline temperature (Figure VI-9). Following optical preconditioning, a sub-threshold electrical stimulus produced forces that matched hybrid

stimulation with no preconditioning. When hybrid stimulation was applied after optical preconditioning, the evoked force was approximately 1.5X greater than with no preconditioning. The enhanced response for hybrid stimulation following optical preconditioning may be due to an increase in the effectiveness of stimulation in the absence of muscle fatigue (Figure VI-9; dashed line). Without preconditioning, the increased effectiveness of continued hybrid stimulation may be counterbalanced by fatigue (Figure VI-9; solid line). These results indicate that a sub-threshold for stimulation optical stimulus will increase the excitability of the nerve to both electrical and hybrid stimulation. Although no direct measures of tissue temperature were obtained, we can safely assume that the stimulated volume experienced a rise in temperature due to the inter-pulse frequency being less than the thermal diffusion time (Wells et al., 2007a). Other sub-threshold responses to optical stimulation may contribute to the enhanced excitability following optical preconditioning; however, we feel that an increase in baseline temperature best fits the data as a whole.

Previous studies have shown that combining sub-threshold pulses of electrical current and infrared light will lead to action potential initiation (Duke et al., 2009, Duke et al., 2012). However, in this study, we have conclusively shown that INS is also capable of enhancing the neurons' response to electrical stimulation. Optically preconditioning the nerve, effectively increasing the tissue's baseline temperature, yielded electrically- and hybrid-evoked force responses that were comparable or greater than for hybrid stimulation with no preconditioning (Figure VI-9). Essentially, we are proposing that optical stimulation increases the nerve's baseline temperature, thus enhancing the nerve's excitability to electrical stimulation in that region. In related experiments, Wells et al.

showed that stimulation thresholds for INS were not affected by changing the baseline tissue temperature (Wells et al., 2007a). While our results neither confirm nor negate the findings of Wells et al., we do show that a presumed increase in baseline tissue temperature likely increases the force generated in response to either electrical or hybrid electro-optical stimulation. We previously observed that increasing the infrared radiant exposure beyond a certain threshold will result in reversible inhibition of neural activity (Duke et al., 2012). Recent modeling studies demonstrated that this is due to non-uniform rate increases in the temperature-dependent Hodgkin-Huxley gating mechanisms (Mou et al., 2012). No inhibition was observed during this current study; however, reduction in evoked force with further increases in radiant exposure may occur.

In addition to characterizing the physiological response to hybrid stimulation, we have also demonstrated that no detectable thermally induced changes in tissue morphology occur for acute experiments as investigated here. Further studies are necessary to assess the chronic and long-term response to this form of stimulation.

6.6 Conclusion

Investigating extraneural infrared nerve stimulation of peripheral nerves at physiologically relevant repetition rates is possible using hybrid electro-optical stimulation. We have shown that hybrid stimulation of peripheral nerves is capable of generating sustained muscle contractions. Evoked forces similar to electrical stimulation are attainable while recruiting alternate sets of motor units. The hybrid force response is believed to result from an increase in the tissue baseline temperature, which will yield enhanced excitability to electrical stimulation. This stimulation paradigm is shown to

avoid detectable thermal tissue damage for acute stimulation. Future studies will be required to assess long-term viability.

6.7 Acknowledgements

This project was made possible by funds from the Department of Defense (HR0011-10-1-0074) and the National Institutes of Health (NS-047073). We would like to thank Evelyn Okediji for her histology expertise. We would also like to thank Dr. Hillel Chiel for his critical review of the manuscript.

6.8 References

Cai DK, Neyer A, Kuckuk R, Heise HM (2008) Optical absorption in transparent PDMS materials applied for multimode waveguides fabrication. Opt Mater 30:1157-1161.

Cayce JM, Friedman RM, Jansen ED, Mahavaden-Jansen A, Roe AW (2011) Pulsed infrared light alters neural activity in rat somatosensory cortex in vivo. Neuroimage 57:155-166.

Duke AR, Cayce JM, Malphrus JD, Konrad P, Mahadevan-Jansen A, Jansen ED (2009) Combined optical and electrical stimulation of neural tissue in vivo. Journal of Biomedical Optics 14:060501-060503.

Duke AR, Lu H, Jenkins MW, Chiel HJ, Jansen ED (2012) Spatial and temporal variability in response to hybrid electro-optical stimulation. J Neural Eng 9:036003.

Fenno L, Yizhar O, Deisseroth K (2011) The development and application of optogenetics. Annu Rev Neurosci 34:389-412.

Fried NM, Lagoda GA, Scott NJ, Su LM, Burnett AL (2008) Noncontact stimulation of the cavernous nerves in the rat prostate using a tunable-wavelength thulium fiber laser. J Endourol 22:409-413.

Gradinaru V, Mogri M, Thompson KR, Henderson JM, Deisseroth K (2009) Optical deconstruction of parkinsonian neural circuitry. Science 324:354-359.

Hale GM, Querry MR (1973) Optical Constants of Water in the 200-nm to 200-microm Wavelength Region. Appl Opt 12:555-563.

Izzo AD, Richter CP, Jansen ED, Walsh JT (2006) Laser stimulation of the auditory nerve. Lasers in Surgery and Medicine 38:745-753.

Izzo AD, Walsh JT, Jr., Jansen ED, Bendett M, Webb J, Ralph H, Richter CP (2007) Optical parameter variability in laser nerve stimulation: a study of pulse duration, repetition rate, and wavelength. IEEE Trans Biomed Eng 54:1108-1114.

Jenkins MW, Duke AR, Gu S, Chiel HJ, Fujioka H, Watanabe M, Jansen ED, Rollins AM (2010) Optical pacing of the embryonic heart. Nat Photonics 4:623-626.

Khosrofian JM, Garetz BA (1983) Measurement of a Gaussian Laser-Beam Diameter through the Direct Inversion of Knife-Edge Data. Applied Optics 22:3406-3410.

Levy M, Mizrahi J, Susak Z (1990) Recruitment, force and fatigue characteristics of quadriceps muscles of paraplegics isometrically activated by surface functional electrical stimulation. J Biomed Eng 12:150-156.

Llewellyn ME, Thompson KR, Deisseroth K, Delp SL (2010) Orderly recruitment of motor units under optical control in vivo. Nat Med 16:1161-1165.

Mou Z, Triantis IF, Woods VM, Toumazou C, Nikolic K (2012) A simulation study of the combined thermoelectric extracellular stimulation of the sciatic nerve of the Xenopus laevis: the localized transient heat block. IEEE Trans Biomed Eng 59:1758-1769.

Peckham PH, Knutson JS (2005) Functional electrical stimulation for neuromuscular applications. Annu Rev Biomed Eng 7:327-360.

Schiefer MA, Triolo RJ, Tyler DJ (2008) A model of selective activation of the femoral nerve with a flat interface nerve electrode for a lower extremity neuroprosthesis. IEEE Trans Neural Syst Rehabil Eng 16:195-204.

Shapiro MG, Homma K, Villarreal S, Richter CP, Bezanilla F (2012) Infrared light excites cells by changing their electrical capacitance. Nat Commun 3:736.

Tarler MD, Mortimer JT (2003) Comparison of joint torque evoked with monopolar and tripolar-cuff electrodes. IEEE Trans Neural Syst Rehabil Eng 11:227-235.

Teudt IU, Nevel AE, Izzo AD, Walsh JT, Jr., Richter CP (2007) Optical stimulation of the facial nerve: a new monitoring technique? Laryngoscope 117:1641-1647.

Tyler DJ, Durand DM (2002) Functionally selective peripheral nerve stimulation with a flat interface nerve electrode. IEEE Trans Neural Syst Rehabil Eng 10:294-303.

Tyler DJ, Durand DM (2003) Chronic response of the rat sciatic nerve to the flat interface nerve electrode. Ann Biomed Eng 31:633-642.

van Gemert MJ, Welch AJ (1989) Time constants in thermal laser medicine. Lasers Surg Med 9:405-421.

Wells J, Kao C, Jansen ED, Konrad P, Mahadevan-Jansen A (2005) Application of infrared light for in vivo neural stimulation. Journal of Biomedical Optics 10:-.

Wells J, Kao C, Konrad P, Milner T, Kim J, Mahadevan-Jansen A, Jansen ED (2007a) Biophysical mechanisms of transient optical stimulation of peripheral nerve. Biophysical Journal 93:2567-2580.

Wells J, Konrad P, Kao C, Jansen ED, Mahadevan-Jansen A (2007b) Pulsed laser versus electrical energy for peripheral nerve stimulation. J Neurosci Methods 163:326-337.

Wells JD, Thomsen S, Whitaker P, Jansen ED, Kao CC, Konrad PE, Mahadevan-Jansen A (2007c) Optically mediated nerve stimulation: Identification of injury thresholds. Lasers Surg Med 39:513-526.

Zhang F, Gradinaru V, Adamantidis AR, Durand R, Airan RD, de Lecea L, Deisseroth K (2010) Optogenetic interrogation of neural circuits: technology for probing mammalian brain structures. Nat Protoc 5:439-456.

CHAPTER VII

REVERSIBLE AND SELECTIVE INHIBITION OF NEURAL ACTIVITY WITH INFRARED LIGHT

Austin R. Duke[1], Michael W. Jenkins[2], Hui Lu[3], Jeffrey M. McManus[3], Hillel J. Chiel[3,2,4], and E. Duco Jansen[1,5]

[1]Vanderbilt University, Department of Biomedical Engineering

Nashville, TN

[2]Case Western Reserve University, Department of Biomedical Engineering

Cleveland, OH

[3]Vanderbilt University, Department of Biology

Cleveland, OH

[4]Case Western Reserve University, Department of Neurosciences

Cleveland, OH

[5]Vanderbilt University, Department of Neurological Surgery

Nashville, TN

Material in this chapter was submitted to *Nature Communications* in November 2012.

7.1 Abstract

Analysis and control of neural circuitry requires the ability to selectively activate or inhibit neurons. Previous work has shown that infrared laser light can selectively excite neural activity in both unmyelinated and myelinated axons. However, inhibition of neuronal firing with infrared light has only been observed in limited cases, is not well understood and has not been precisely controlled. Using an experimentally tractable unmyelinated preparation for detailed investigation and a myelinated preparation for validation, we report that it is possible to selectively inhibit electrical initiation of axonal activation, as well as both block or enhance the propagation of action potentials of specific motor neurons. Thus, we demonstrate a spatially and temporally precise optical method of controlling both inhibition and activation of components of the nervous system. We believe this technique is well suited for non-invasive investigations of diverse excitable tissues and may ultimately be applied for treating neurological disorders.

7.2 Introduction

Along with further elucidation of mechanisms underlying neural function, burgeoning interest in deep brain stimulation (Martens et al., 2011), pain management (Slavin, 2008), functional electrical stimulation (Peckham and Knutson, 2005), and brain-computer interfaces (Konrad and Shanks, 2010) have created a demand for higher levels of neural specificity and control. Advances in electrical neural interface design have overcome many technical and biological challenges required to successfully excite and inhibit neural structures (Kilgore and Bhadra, 2004, Grill et al., 2009). Additionally,

novel optical methods of spatially and temporally precise neural control have become increasingly popular (Fenno et al., 2011, Richter et al., 2011a). Optogenetics, a technique whereby light-responsive ion channels are introduced into targeted cells, has become a promising new technology for exciting and inhibiting small groups of neurons with high spatial and temporal precision (Fenno et al., 2011). In this work we will demonstrate the utility of an alternative optical technique for neural control using pulses of infrared light. The capability of pulsed infrared light to provide precise spatiotemporal activation of diverse excitable tissues through a thermally-mediated process without modifications of native neural structures has been shown (Wells et al., 2005, Izzo et al., 2006, Teudt et al., 2007, Wells et al., 2007, Fried et al., 2008, Jenkins et al., 2010, Cayce et al., 2011, Dittami et al., 2011, Shapiro et al., 2012). Recently, we have also observed instances of inhibited activity in response to infrared light, though the mechanisms of action were unclear (Cayce et al., 2011, Duke et al., 2012b).

Global temperature changes leading to block of nerve conduction, a phenomenon known as “heat block”, have been investigated in both unmyelinated and myelinated nerves (Hodgkin and Katz, 1949, Rattay and Aberham, 1993). Recent modeling studies indicate the potential for block of action potential (AP) initiation and propagation with local increases in nerve temperature (Mou et al., 2012). Thermal neural inhibition is the result of non-uniform rate increases in the temperature-dependent Hodgkin-Huxley gating mechanisms, causing the rate of inactivation of sodium channels and activation of potassium channels to overwhelm activation of sodium channels (Huxley, 1959, Rattay and Aberham, 1993, Mou et al., 2012). This leads to either a faster and weaker response,

or complete but reversible block of AP generation or propagation (Hodgkin and Katz, 1949, Huxley, 1959).

Here we demonstrate the use of infrared pulses to reversibly control electrically initiated AP generation and propagation, as well as neuromuscular function with high spatiotemporal specificity in both the unmyelinated buccal nerve 2 (BN2) of *Aplysia californica* and the myelinated rat sciatic nerve. We believe the mechanism of infrared inhibition, as with infrared stimulation, is thermally mediated.

7.3 Methods

7.3.1 Aplysia preparation and nerve dissection

Aplysia californica (n = 4) weighing 250-350g (Marinus Scientific, Long Beach, CA) were maintained in an aerated aquarium containing circulating artificial seawater (ASW) (Instant Ocean; Aquarium Systems, Mentor, OH) kept at 16-17 °C. The animals were fed dried seaweed every 1-3 days.

Aplysia were anesthetized with an injection of 333 mM $MgCl_2$ (~50% of body weight) prior to dissection. Once anesthetized, animals were dissected and the buccal ganglia were removed and pinned in a recording dish and immersed in *Aplysia* saline (460 mM NaCl, 10 mM KCl, 22 mM $MgCl_2$, 33 mM $MgSO_4$, 10 mM $CaCl_2$, 10 mM glucose, 10 mM HEPES, pH 7.6). *Aplysia* buccal ganglia are symmetric, so each hemi-ganglion has an associated buccal nerve 2 (BN2). Each BN2 was transected just distal to its attachment to its respective hemiganglion and anchored in place by pinning the protective sheath around the nerve to the Sylgard® base (Dow Corning, Midland, MI) of the recording dish.

7.3.2 *Aplysia* electrophysiology

Once securely pinned, the three distal branches of BN2 were suctioned into nerve-recording electrodes to monitor the response to stimulation. Nerve-recording electrodes were made by hand-pulling polyethylene tubing (1.27 mm outer diameter, 0.86 mm inner diameter; PE90; Becton Dickinson) over a flame to the desired inner diameter. Recording electrodes were suction-filled with *Aplysia* saline prior to suctioning of the nerve. Nerve signals were amplified (x1000) and band-pass filtered (300 – 500 Hz) using an AC-coupled differential amplifier (model 1700; A-M Systems), digitized (Axon Digidata 1320A; Molecular Devices, Sunnyvale, CA) and recorded (AxoGraph X; AxoGraph Scientific).

Extracellular stimulating electrodes were made from thin-wall borosilicate capillary glass (catalogue #6150; A-M Systems, Everett, WA) pulled to a diameter of about 40 μm and resistances of about 0.1 MΩ (model P-80/PC; Sutter Instruments, Novato, CA). For each experiment, an electrode was capillary-filled with *Aplysia* saline and positioned on the top surface of the nerve, in contact with the nerve sheath, using a micromanipulator. The return electrode was positioned at a distance in the bath to create monopolar stimulation. Monophasic currents supplied by a stimulus isolator (A360; WPI) were used for all experiments.

7.3.3 Rat sciatic nerve preparation

All experiments were performed following protocols approved by the Institutional Animal Care and Use Committee (IACUC). Male Sprague-Dawley rats (n = 2) weighing

250 – 300g (Charles River) were anesthetized with continuously inhaled isoflurane (induction: 3% isoflurane, 3.0 LPM oxygen; maintenance: 2-2.5% isoflurane, 1.5 LPM oxygen). A rectal probe and heating pad (catalog # 40-90-8, FHC, Bowdoin, ME) were used to maintain the rat at a target body temperature of 35-37 °C throughout the experiment. The animals were placed on a polycarbonate platform and their hindlimbs were shaved. The dorsal surface of the foot was then taped to the edge of the platform. An incision was made from the heel to the vertebral column and the skin was separated from the underlying tissue. The biceps femoris was then cut and divided proximal from the Achilles tendon to expose the sciatic nerve. The sural and peroneal branches of the sciatic nerve were transected so only innervation of the plantarflexor muscles remained.

7.3.4 Rat sciatic nerve electrophysiology

Paired EMG electrodes made from perfluoroalkoxy (PFA)-coated silver wire (0.003” bare, 0.005” coated; A-M Systems, Sequim, WA) were inserted along the length of the medial gastrocnemius and lateral gastrocnemius muscles. EMG signals were amplified (x100) and band-pass filtered (100 – 1000 Hz) using an AC-coupled differential amplifier (model 1700; A-M Systems), digitized (20kHz; Axon Digidata 1440A; Molecular Devices, Sunnyvale, CA) and recorded (AxoGraph X; AxoGraph Scientific).

7.3.5 Delivery of infrared light to nerves

Two tunable diode laser systems were used throughout our investigation. Laser 1 consisted of a prototype tunable diode laser (Capella; Lockheed-Martin-Aculight,

Bothell, WA) with wavelength λ = 1450 nm coupled to a 200 μm diameter fiber optic (Ocean Optics, Dunedin, FL). Laser 2 comprised a similar and commercially available diode laser (λ = 1860 nm) coupled to a 100 μm diameter fiber optic. For rat experiments, Laser 1 was coupled to a 400 μm diameter fiber optic. Fiber optics were secured in place using micromanipulators. The differences in laser wavelengths and fiber optic diameters were not critical for the results reported in this paper (see section 7.4.2).

7.3.6 Infrared inhibition of action potential generation in *Aplysia*

To investigate the inhibition of electrically initiated axonal activation in *Aplysia*, fiber optics from laser systems 1 and 2 were positioned such that they flanked the stimulating electrode transverse to the nerve's longitudinal axis as shown in Figure VII-2A. Laser 1 supplied 0.5 ms pulses at 4.43 ± 0.30 J/cm^2 and Laser 2 supplied 5 ms pulses at 8.34 ± 0.78 J/cm^2. Differences in pulse durations and fiber optic diameters used were due to laser power constraints and nerve working area. The 1450 nm laser used in these experiments produces five times the power of the 1860 nm laser (25W and 5W, respectively), and thus requires shorter pulse durations to achieve appropriate output. The discrepancy in required radiant exposures can be largely attributed to the difference in absorption for the wavelengths used. The absorption of infrared light in tissue can be approximated by the absorption of infrared light by water (Wells et al., 2007). The absorption coefficient of water at 1860 nm (μ_a = 12.8 cm^{-1}) is roughly 2.5 times less than at 1450 nm (μ_a = 32.7 cm^{-1}) (Hale and Querry, 1973). Thus, greater radiant exposures must be provided at 1860 nm to generate the same overall absorption and associated temperature increase as at 1450 nm. Threshold radiant exposures for inhibition at 1450

nm are similar to our prior observations in *Aplysia* using a diode laser operating at 1875 nm (Duke et al., 2012a). Infrared absorption at 1875 nm ($\mu_a \approx 26$ cm^{-1}) is much closer to that of 1450 nm, further confirming that the wavelength is not as critical as absorption and thermal conversion of light in tissue.

Each trial (N = 3 nerves, n = 5) consisted of a series of repeating 500 ms episodes. For each episode, a monophasic electrical stimulus (τ_{pe} = 0.25 ms) providing current sufficient to generate consistent APs on all three recording electrodes (461.4 ± 36.2 μA) was applied at t = 100 ms. Because the laser pulses and the electrical pulse have different durations, they were all synchronized to end at the same time. This allowed total charge and total heat deposition to occur simultaneously. Effects of varying this time are discussed below. Each trial followed an ABACABACA pattern in which nerves were stimulated electrically (A), then either Laser 1 or Laser 2 was added (B), then the laser was removed leaving only electrical stimulation (A), followed by the other laser being added (C), and then the process was repeated. Nerve responses for each condition were analyzed using the integrated compound nerve action potential (iCNAP): the ensemble average for each condition within a given trial was rectified and summed over a finite interval following the electrical stimulation artifact.

To verify that differences in laser sources, pulse durations and fiber diameters did not play a role in our results, we performed a limited set of experiments where the 1450 nm laser was set to a constant pulse duration and alternately coupled to either of two 200 μm diameter fibers that were positioned on either side of the micropipette. With this preparation, both the fiber diameter and laser source were constant; only the position of

the fiber was variable. Results from this limited study (data not shown) demonstrated that the results shown in Figure VII-2 were not an artifact of the use of a two-laser system.

7.3.7 Effect of relative pulse timing on infrared inhibition in *Aplysia*

To characterize how the relative timing of the infrared and electrical pulses affects threshold radiant exposures for inhibition of AP initiation, a single infrared pulse (λ = 1450 nm, τ_{po} = 0.5 ms) was delivered at time points before and after an electrical stimulus (τ_{pe} = 0.25 ms). The timing scheme was such that t = 0 corresponded to the infrared and electrical pulses ending simultaneously. The infrared pulse was delivered over the range of t = -20 ms to t = 0.5ms (N = 3 nerves, n = 4 for each time point). For each trial, the electrical stimulus was 110% of the threshold current, where electrical threshold was defined as the minimum current required to initiate 5 consecutive evoked responses. Infrared pulses (n = 10) at 5 different radiant exposures were applied for each time point. The presence (1) or absence (0) of an evoked response was recorded and aggregated to achieve the probability of a stimulated response for each radiant exposure. At each time point, the probability versus radiant exposure data is fit to the cumulative distribution function (CDF). Threshold for infrared inhibition at each time point was defined as the radiant exposure generating $\leq$ 50% of an evoked response (Duke et al., 2012a).

7.3.8 Infrared inhibition of nerve conduction in *Aplysia*

We also investigated the capability of infrared light to block propagating action potentials. The *Aplysia* BN2 nerve preparation was as described previously, except a single 200 μm fiber optic coupled to the 1450 nm laser source was positioned

approximately 1 cm distal to the site of electrical stimulation, but proximal to the nerve trifurcation (Figure VII-5A). Each trial (N = 3 nerves, n = 11 trials) consisted of one 10 sec episode. Monophasic electrical stimuli (τ_{pe} = 0.25 ms; 659.1 ± 18.9 μA) providing consistent responses on all three branches of BN2 were delivered at 4 Hz for the duration of the trial. At 4 sec, pulses of infrared light (τ_{po} = 0.2 ms) were delivered at 200 Hz for 3 seconds. Nerve responses were analyzed using the iCNAP as described in section 7.3.6.

7.3.9 *Aplysia* preparation for muscle force measurements

To test whether infrared neural inhibition could modulate neuromuscular transmission, an *Aplysia* (422 g) was anesthetized as described above. The animal's buccal mass was removed and placed in a Petri dish within a solution of 50% *Aplysia* saline and 50% isotonic $MgCl_2$. Both buccal nerves 2 were severed at their attachment points to the buccal ganglia. Incisions were made through the dorsal and ventral surfaces of the buccal mass, and further incisions were made to remove the radula-odontophore and pharyngeal tissue, leaving the I1/I3 muscle split into two separate halves with each half innervated by its buccal nerve 2. The rest of the buccal mass and the ganglia were discarded. The muscle halves were moved to a recording dish with a Sylgard® surface in the back half of the dish. Each I1/I3 half was glued (Duro Quick-Gel SuperGlue, Henkel Corp., Avon, OH) by its anterior edge to the glass bottom of the dish just in front of the Sylgard®. After gluing, the dish was filled with *Aplysia* saline. Each buccal nerve 2 was gently stretched and pinned on the Sylgard® surface. Force transducers (Grass Technologies, West Warwick, RI) were attached to the medial portions of the I1/I3 halves using silk sutures. Polyethylene suction electrodes were attached to the ends of

each BN2. A 200 μm diameter fiber optic coupled to the 1450 nm laser source was positioned distal (~1 cm) to the suction electrode and proximal to the nerve trifurcation.

Electrical stimulation was applied using the nerve suction electrodes. Control trials consisted of 5 repetitions of electrical stimulation (τ_{pe} = 1 ms, 0.7 mA) delivered at 10 Hz for 2 sec. Each repetition was followed by an interval of 12 seconds with no stimulation (Figure VII-7B). Experimental trials consisted of the same protocol, but infrared pulses (τ_{po} = 0.2 ms; 0.50 J/cm^2) were applied at 200 Hz for 3 seconds beginning 1 second before the third electrical stimulus. Five control and experimental trials were repeated per parameter set with 3 min between each trial to allow the nerve to rest.

Movies of the muscle contraction were acquired for two of the experimental trials using a USB microscope (DinoLite AD413ZT) positioned above the preparation.

7.3.10 Infrared inhibition of nerve conduction in the rat sciatic nerve

Block of action potential conduction was also investigated in the rat sciatic nerve. A monopolar nerve cuff electrode was placed around the trunk of the sciatic nerve and a 400 μm diameter fiber optic was positioned 500 μm above the tibial branch (Figure VII-10A). Each trial (N = 3 nerves, n = 15 trials) consisted of one 10 sec episode. Monophasic electrical stimuli (τ_{pe} = 0.1 ms; 750 μA) were delivered at 4 - 8 Hz for the duration of the trial. At 4 sec, pulses of infrared light (τ_{po} = 0.2 ms; 75.7 mJ/cm^2) were delivered at 200 Hz for 3 seconds. Nerve responses were analyzed using the iEMG (Llewellyn et al., 2010), which was calculated in the same manner as the iCNAP (see section 7.3.6).

7.3.11 Nerve temperature

Nerve temperature changes in response to infrared inhibition were measured in both an *Aplysia* and rat nerve. BN2 of an *Aplysia* (314 g) was dissected and secured to a recording dish as described in section 7.3.1. The saline level of the Sylgard-covered dish was lowered so that it was just covering the surface of the nerve (Figure VII-1). A 200 μm fiber optic coupled to the 1450 nm laser was positioned above the nerve such that the tip of the fiber was just out of contact with the nerve. Infrared pulses (τ_{po} = 0.2 ms; 0.52 J/cm^2) were delivered at 200 Hz for 3 sec. A thermal imaging camera (FLIR Systems Thermovision A20) with 2.7 mrad spatial resolution (approximately 300 μm per pixel) was positioned 30 cm above the nerve. Images were acquired at 60 Hz for 25 seconds. Rat temperature measurements were made using the same instrumentation and focal distance while applying infrared pulses (τ_{po} = 0.2 ms, 0.12 mJ/cm^2, 200 Hz) to the rat sciatic nerve *in vivo*.

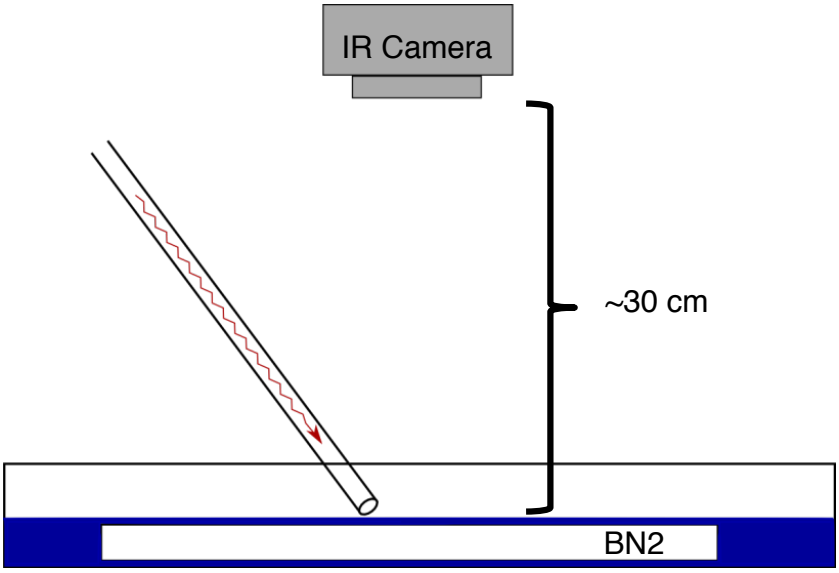

Figure VII-1. Schematic representation of *Aplysia* nerve temperature measurements. Temperature was measured using a thermal imaging camera positioned 30 cm above the nerve preparation. Using parameters previously found to block action potential propagation (τ_{po} = 0.2 ms; 0.52 J/cm^2; 200 Hz; 3 sec), the nerve temperature rises by approximately 8 °C (Figure VII-5E). The thermal camera used has limited spatial resolution (2.7 mrad). Thus the temperature rise is averaged over the area equivalent to a single pixel, which approximately corresponds to the laser spot.

To find the temperature change required for nerve conduction block in *Aplysia*, we averaged all trials (N = 3 nerves, n = 11 trials) and found the minimum duration of laser exposure for which the BN2c iCNAP was significantly reduced. Significance was determined using $p < 0.004$ in *Aplysia* and $p < 0.002$ in the rat after correcting for multiple comparisons using the Bonferroni method. This duration was then compared to the measured temperature (Figure VII-5E) to determine the induced temperature rise. The same procedure was applied to the rat, where minimum infrared exposure duration required to significantly reduce the iEMG for LG was determined and compared to the measured temperature change (Figure VII-10E).

7.3.12 Radiant exposure determination

Radiant exposures normalize applied optical energy per unit area. Radiant energy was measured using an energy meter and pyroelectric energy detector (Nova II, Ophir; PE50BB-VR-ROHS, Ophir). In *Aplysia,* the radiant exposure was determined by dividing the radiant energy by the area of the circular fiber tip (i.e. 0.0314 mm^2 for a 200 μm diameter fiber), since the fiber was assumed to be in contact with the outer surface of the nerve sheath. In order to report radiant exposure at the level of the axons, many assumptions and calculations would be necessary. We chose to report the measured value at the tip of the fiber optic prior to any additional assumptions for simplicity and accuracy.

For the rat experiments where the optical fiber is not in contact with any tissue, the laser spot size incident on the nerve surface was measured using the knife-edge technique (Khosrofian and Garetz, 1983). Thus, we report a measured spot-size (0.0026

cm^2) to provide greater accuracy. These methods of radiant exposure determination are consistent with published literature (Richter et al., 2011b, Duke et al., 2012a).

7.3.13 Data acquisition and analysis

Amplified and filtered nerve responses were acquired at 5 kHz. AxoGraph X software (AxoGraph Scientific) was used to coordinate stimulation and inhibition protocols, and to record acquired data. Post-acquisition data analysis was performed using a combination of AxoGraph X, Matlab (Matlab r2010b) and Microsoft Excel. The Kolmogorov-Smirnov test revealed data were not normally distributed. Therefore, we compared data using the Mann-Whitney test with $\alpha = 0.05$ and applied the Bonferroni method to adjust for multiple comparisons.

7.4 Results

7.4.1 Infrared inhibition of electrically initiated action potentials in *Aplysia*

To investigate the inhibition of electrically initiated axonal activation, we first provided nonspecific supra-threshold electrical stimulation to the main trunk of BN2. BN2 provides a robust and experimentally tractable *ex vivo* preparation with substantial length and a distal trifurcation allowing for simultaneous recording of multiple branches, and a muscular target that is known and tractable to study. Electrically evoked responses were recorded on each of the three distal branches of BN2 - BN2a, BN2b and BN2c (Warman and Chiel, 1995, Nargeot et al., 1997) – allowed the primary compound nerve

action potential (CNAP) to be deconvolved and resolved into some of its spatial components. Synchronizing the electrical stimulus with an infrared pulse from a single laser selectively inhibited initiation of an AP ordinarily appearing on one branch of BN2. Alternating between laser sources demonstrated that each blocked initiation of different electrically evoked responses (Figure VII-2C). When both lasers provided pulses of infrared light simultaneously, responses on two branches were inhibited, while an electrically activated response remained largely unchanged on the third branch (Figure VII-2D). Removing the infrared pulses unblocked electrically evoked responses on all three branches, indicating selective inhibition is completely reversible. The integrated CNAP (iCNAP) was used as a metric for the level of electrical activation for each branch (see section 7.3.6). Each laser induced a reduction in the iCNAP magnitude of a selective axonal projection (Figure VII-2E). As a control, BN2a was not targeted for inhibition; thus, no change in the iCNAP of BN2a was observed.

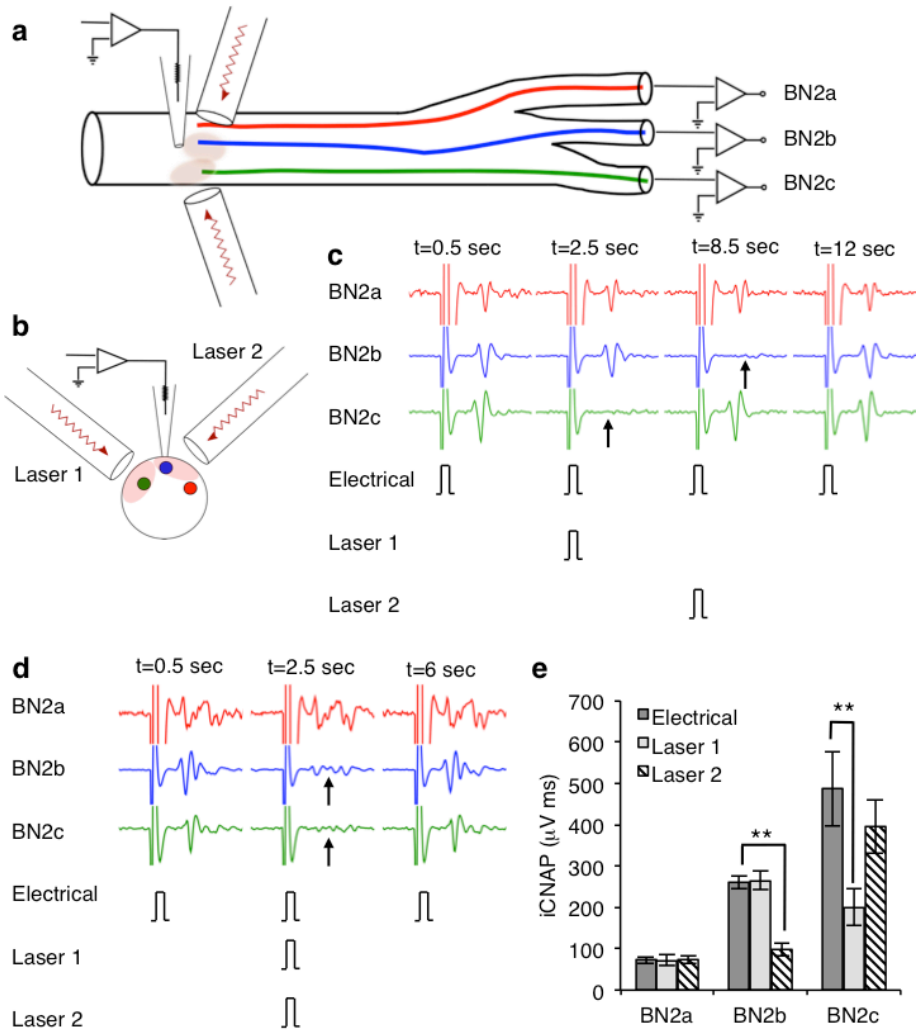

Figure VII-2. Infrared inhibition of AP initiation. (a) A micropipette providing supra-threshold extracellular electrical stimulation to BN2 is flanked by two optical fibers. Extracellular nerve recordings are obtained from the three distal branches. (b) Nerve cross-section schematic at the site of inhibition. Axons are arranged in locations consistent with observed results and nerve backfills (data not shown). (c) Neural recordings from branches of BN2 showing selective inhibition (arrows) of AP generation. Each laser inhibits initiation of an AP projecting to a single nerve branch. Laser 1 (4.43 ± 0.30 J/cm^2) inhibits an AP projecting to BN2c, while Laser 2 (8.34 ± 0.78 J/cm^2) inhibits an AP projecting to BN2b. Upon removal of the infrared pulse, electrically evoked APs return, indicating reversibility. (d) Neural recordings from branches of BN2 showing combined inhibition of two nerve branches. Applying infrared pulses from both lasers simultaneously inhibits APs projecting to BN2b and BN2c (arrows), while electrically evoked APs projecting to BN2a are unaffected. Each trace in (c) and (d) is 30 ms. (e) Average iCNAP recorded from BN2a, BN2b (** $p < 0.01$), and BN2c (** $p < 0.01$) in response to electrical only, electrical plus Laser 1 and electrical plus Laser 2 (N = 3 nerves, n = 5 trials). Data are presented as mean ± SEM.

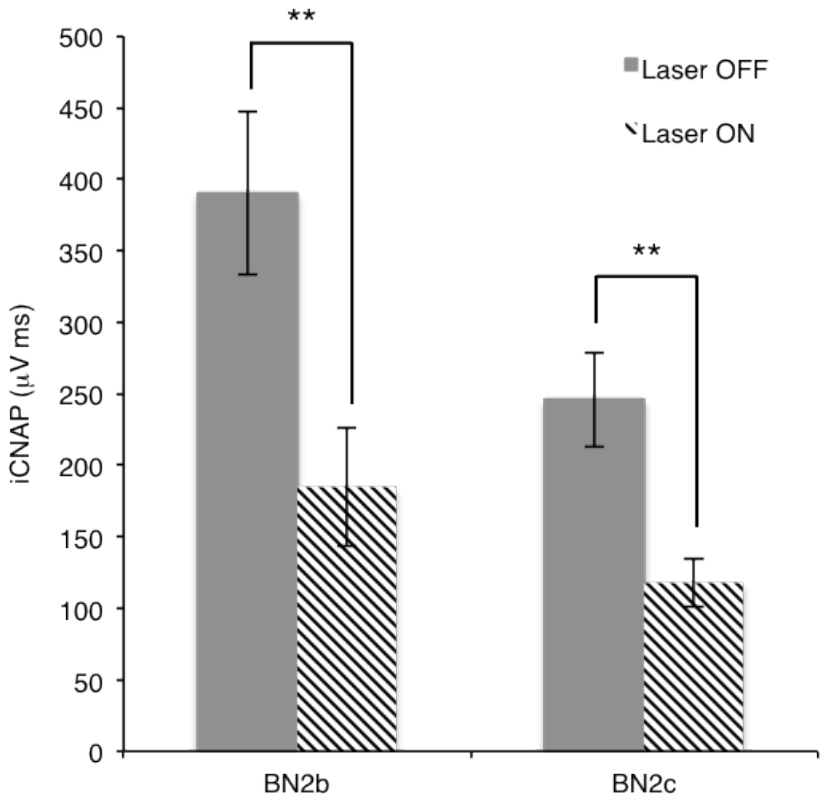

Figure VII-3. Pulsed infrared light inhibits electrical initiation of axonal activations in BN2 of *Aplysia*. Single laser pulses delivered synchronously with electrical stimulation at the site of axonal activation will reduce the amplitude of the evoked iCNAP. Significant reductions are seen in both BN2b ($n = 12$, ** $p < 0.01$) and BN2c ($n = 6$, ** $p < 0.01$) when compared to electrical evoked responses when infrared light is not applied. Selectivity was not investigated as in Figure VII-2.

To further characterize infrared inhibition of action potential initiation, we investigated how the relative timing of electrical and infrared pulses affected threshold radiant exposures for inhibition. We found that there exists a narrow window surrounding the delivery of the electrical pulse in which the infrared pulse can be applied to inhibit electrical initiation. With the infrared pulse (τ_{po} = 0.5 ms) delivered prior to the electrical pulse (τ_{pe} = 0.25 ms), threshold radiant exposures for inhibition slowly increased as the timing between the pulses increased (Figure VII-4). Inhibition reliably occurred with the infrared pulse delivered as much as 10 ms prior to the start of the electrical pulse. However, infrared pulses that were delivered earlier required radiant exposures that generated infrared stimulation in the absence of any electrical stimulus (Wells et al., 2005). Threshold radiant exposures for inhibition rapidly increased when the infrared pulse was delivered after the electrical stimulus, primarily due to the evoked potential propagating away from the site of initiation before the infrared pulse arrived. Inhibition occurred reliably when the infrared pulse was delayed 0.25 ms after the electrical pulse, but was not observed when the infrared pulse was delayed by 0.5 ms. Minimum threshold radiant exposures for inhibition occurred when the infrared pulse was delivered 0.25 ms before the electrical pulse. While some studies and applications will utilize precise timing of infrared and electrical pulses for block of action potential initiation, many applications could benefit from a high frequency train of infrared pulses that are not synchronized with the electrical pulses, as was demonstrated in Figure VII-5.

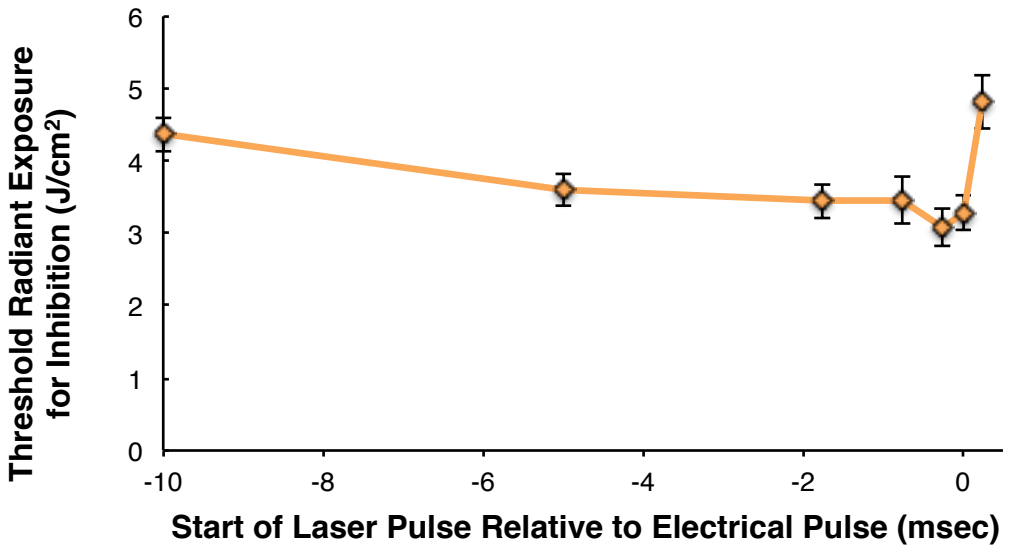

Figure VII-4. Effect of relative pulse timing on threshold radiant exposures for inhibition. Infrared pulses (τ_p = 0.5 ms) delivered up to 10 ms before a supra-threshold electrical stimulus (τ_p = 0.25 ms) will consistently inhibit action potential initiation, though threshold radiant exposures for inhibition are higher than for shorter delay intervals. Inhibiting radiant exposures increase sharply when the infrared pulse is delivered after the electrical stimulus (N = 2 nerves, n = 4 trials). Data are presented as mean ± SEM.

7.4.2 Laser system comparison

Differences in pulse durations and fiber optic diameters used were due to laser power constraints and nerve working area. The 1450 nm laser used in these experiments produces five times the power of the 1860 nm laser (25W and 5W, respectively), and thus requires shorter pulse durations to achieve appropriate output. The discrepancy in required radiant exposures can be largely attributed to the difference in absorption for the wavelengths used. The absorption of infrared light in tissue can be approximated by the absorption of infrared light by water (Wells et al., 2007). The absorption coefficient of water at 1860 nm ($\mu_a = 12.8$ cm^{-1}) is roughly 2.5 times less than at 1450 nm ($\mu_a = 32.7$ cm^{-1}) (Hale and Querry, 1973). Thus, greater radiant exposures must be provided at 1860 nm to generate the same energy density (since the energy density (J/cm^3) is the product of the radiant exposure (J/cm^2) and the absorption coefficient (cm^{-1})) and associated temperature increase as at 1450 nm. Threshold radiant exposures for inhibition at 1450 nm are similar to our prior observations in *Aplysia* using a diode laser operating at 1875 nm (Duke et al., 2012a). Infrared absorption at 1875 nm ($\mu_a \approx 26$ cm^{-1}) is much closer to that of 1450 nm, further confirming that the wavelength is not as critical as absorption and thermal conversion of light in tissue. To verify that differences in laser sources, pulse durations and fiber diameters did not play a role in our results, we performed a limited set of experiments where the 1450 nm laser was set to a constant pulse duration and alternately coupled to either of two 200 μm diameter fibers that were positioned on either side of the micropipette. Results from this limited study (data not shown) demonstrated that the results shown in Figure VII-2 were not an artifact of the use of a two-laser system.

7.4.3 Infrared inhibition of nerve conduction in *Aplysia*

A 200 μm fiber optic was positioned over the nerve trunk distal to the site of supra-threshold electrical stimulation (~1 cm) targeting the proposed location of axons projecting to BN2c (Figure VII-5A). A train of low radiant exposure (0.50 ± 0.02 J/cm^2), high frequency (200 Hz) infrared pulses produced a rise in local tissue temperature and blocked responses projecting to BN2c (Figure VII-5B). During conduction block, BN2c iCNAP magnitude was lower than before and after the infrared train (Figure VII-5D). Blocked conduction began during the second half of the infrared pulse train and became stronger as the infrared block continued. This is likely due to the rate of temperature increase over the duration of the infrared train (Figure VII-5E). As infrared exposure begins, temperature may not be sufficient for block. However, as the temperature increases beyond the threshold for inhibition (~7.0 °C), the effect is strengthened (Figure VII-5F).

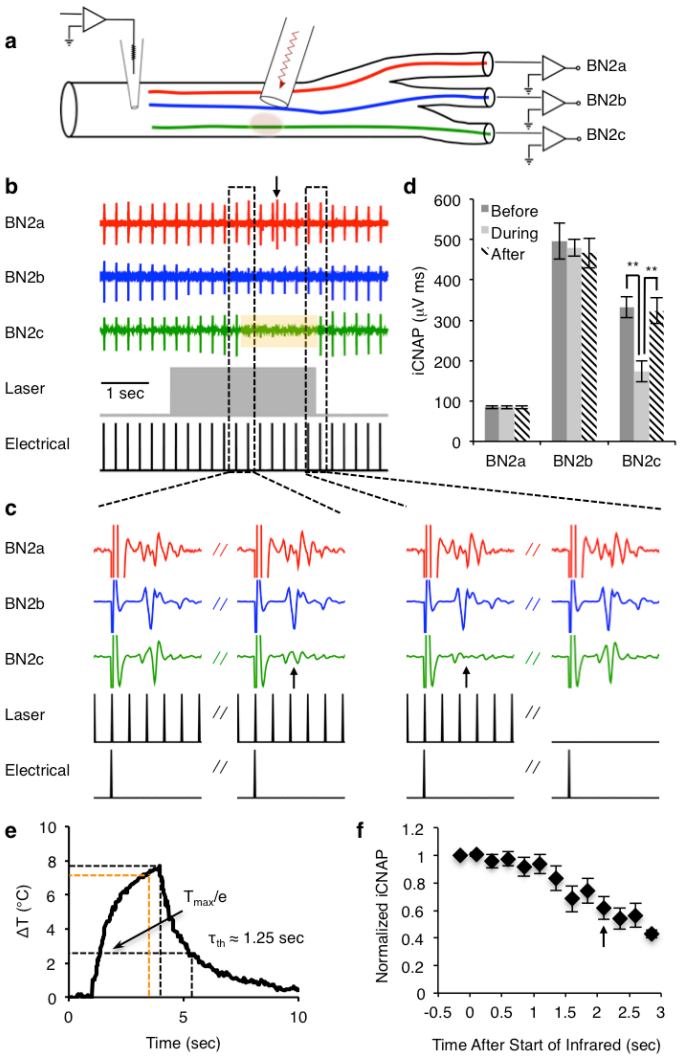

Figure VII-5. Nerve conduction block in BN2 of *Aplysia*. (a) A micropipette electrically stimulated APs propagating to the three branches of BN2. Infrared pulses were delivered to the nerve via a 200 μm diameter optical fiber, distal to the electrical stimulus. (b) Infrared exposure (indicated schematically by a gray bar) inhibits propagation of APs projecting to BN2c (highlighted by a yellow bar). A single spontaneous response is evident on the BN2a recording (arrow). This was occasionally observed before, during and after infrared exposure. APs on BN2b show some inhibition on this recording. Electrical artifacts are blanked for clarity. (c) Evoked and inhibited responses (arrows) are expanded. Each trace is 30 ms. (d) Average (1 sec) iCNAP for responses immediately preceding and following the infrared stimulus train, as well as the final 1 sec of laser exposure (** $p < 0.01$; N = 3 nerves, n = 11 trials). (e) Local temperature increases by approximately 8 °C during the 3 second infrared exposure. The thermal relaxation time is approximately 1.25 sec. (f) As duration of infrared exposure increases, magnitude of the BN2 iCNAP decreases. The location where reduction in BN2 iCNAP becomes significant ($p < 0.004$) is indicated by an arrow in (f) and orange dashed lines in (e). Data are presented as mean ± SEM.

We also observed that BN2b experienced inhibition as well as enhancement in response to infrared exposure, and that this was consistent for a given nerve and fiber optic location (Figure VII-6A-D). Unlike BN2c, which we targeted for infrared inhibition, magnitudes of responses projecting to BN2b were observed to increase or decrease in amplitude during infrared exposure. In the three nerves tested we observed a different response for BN2b in each nerve. In the first nerve, BN2b iCNAP amplitudes were significantly ($p < 0.01$) reduced (Figure VII-6A), whereas in the second nerve they were noticeably enhanced (Figure VII-6B). There was no change in the third nerve (Figure VII-6C). Each response was consistent within a given nerve, though we did not attempt to produce both inhibition and enhancement in the same nerve. Aggregate data showed no significant change in BN2b, while BN2c showed significant ($p < 0.01$) reduction in iCNAP amplitude (Figure VII-5C). Interestingly, in a few trials the peak-to-peak CNAP magnitude of BN2c was found to increase slightly just before inhibition.

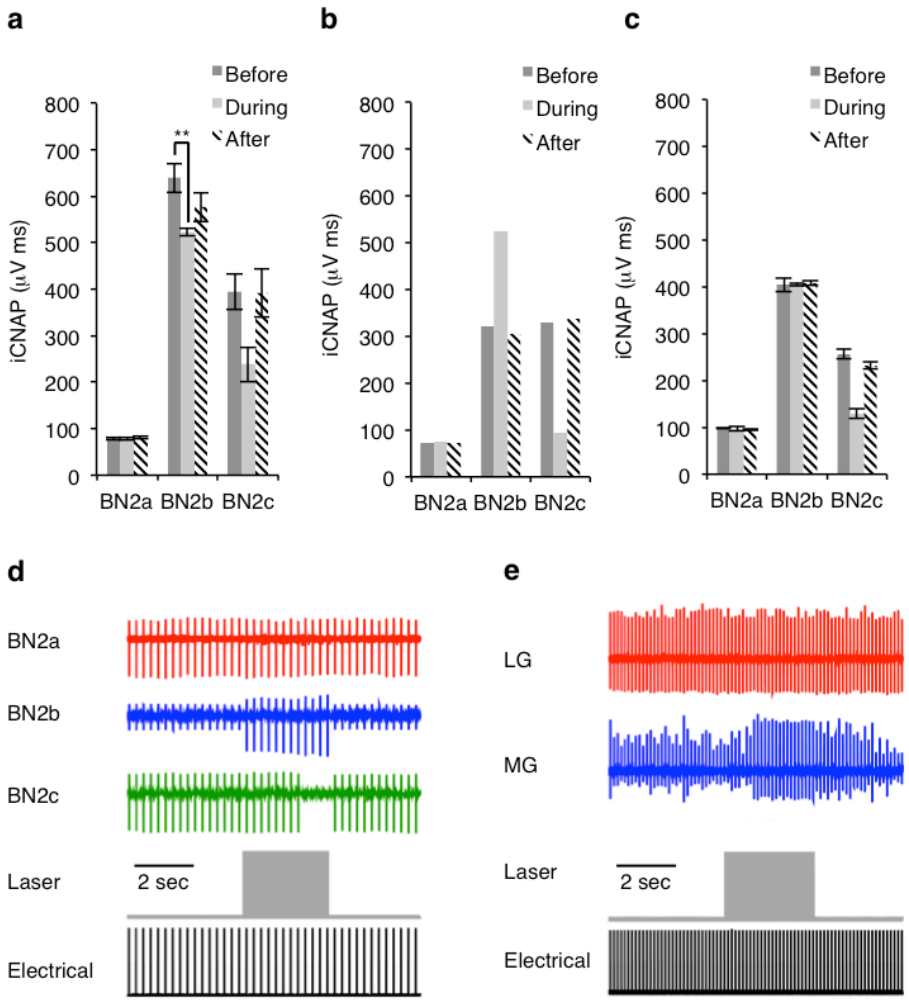

Figure VII-6. Varied responses to infrared exposure in BN2 of *Aplysia* and the rat sciatic nerve. While investigating conduction block of axons projecting to BN2c, those projecting to BN2b were observed to be either blocked (n = 5; ** $p < 0.01$) (a), enhanced (n = 2) (b) or experienced no change (n = 4) (**c**). Each type of response was observed consistently within a given nerve at specific locations. Panel (d) illustrates enhanced propagating potentials in response to an infrared stimulus (τ_{po} = 0.2 ms; 0.52 J/cm^2; 200 Hz) on BN2. Panel (**e**) shows EMG recordings from MG increase in peak-to-peak amplitude during the infrared pulse train (τ_{po} = 0.2 ms; 0.12 J/cm^2; 200 Hz). Following infrared pulses, the EMG responses begin to return to their pre-infrared exposure magnitudes. EMG recordings from LG are unchanged in response to infrared pulses. Electrical stimulation artifacts in (d) and (e) have been blanked for clarity. Data are presented as mean ± SEM.

7.4.4 Inhibition of neuromuscular transmission in *Aplysia*

To demonstrate functional relevance of infrared control, the effects on muscle force were measured. Distal BN2 muscle innervation was left intact and contraction force of the I1/I3 muscles was measured (Figure VII-7A). When infrared pulses were applied beginning 1 second before a propagating electrical stimulus, measured forces were reduced by nearly 80% when compared to control trials using only electrical stimulation (Figure VII-7B-D). Reduction in generated force was titrated by adjusting the radiant exposure of the infrared pulses (Figure VII-8) and by changing the position of the fiber optic (data not shown). Results suggest inhibition of part of the motor pool affects contraction in a specific muscle region (Figure VII-9).

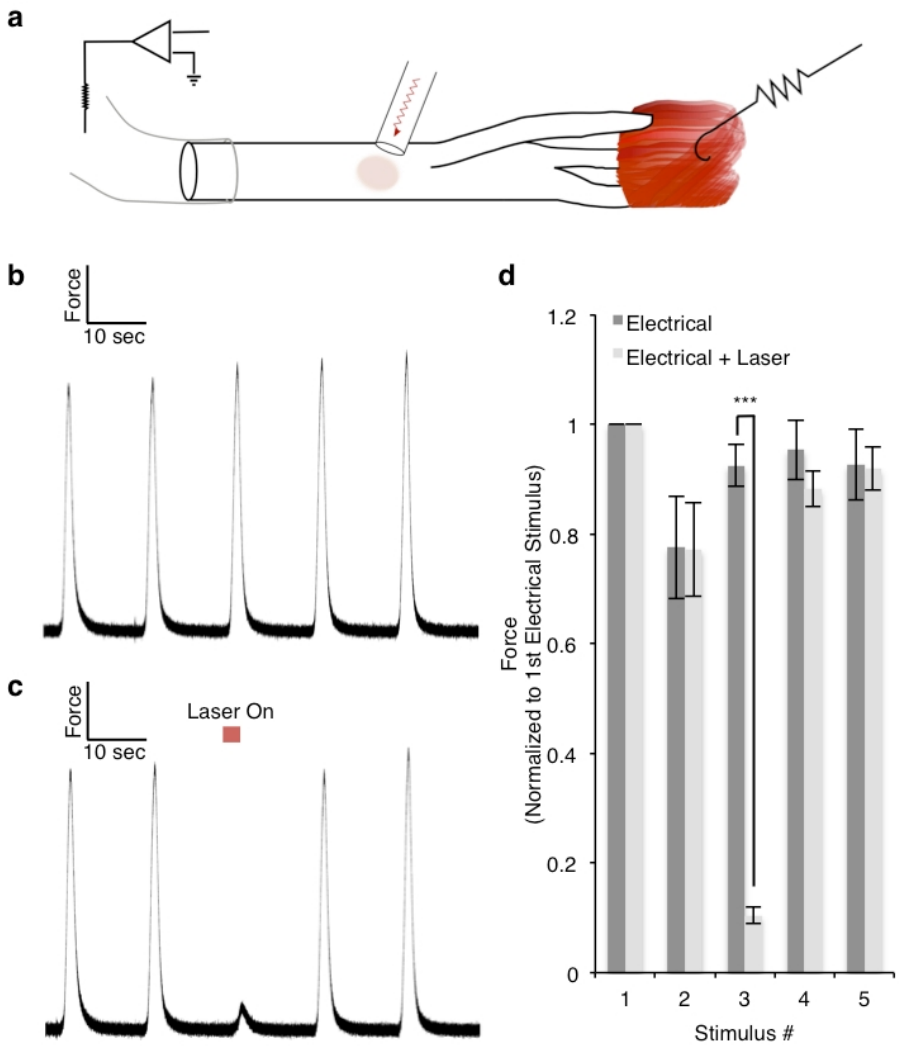

Figure VII-7. Infrared inhibition of electrically evoked muscle contraction. (a) A suction electrode stimulated muscle contractions in the I1/I3 muscles as measured by a force transducer. A 200 mm diameter optical fiber positioned distal (~ 1 cm) to the electrical stimulus inhibited AP propagation of some motor units. (b) Electrically-evoked force in response to 2-sec stimuli (t_{pe} = 1 ms; 0.7 mA; 10 Hz) separated by a 12-second interval. (c) A 3-sec infrared pulse train (l = 1450 nm; t_p = 0.2 ms; 0.54 J/cm^2; indicated by horizontal red bar) at 200 Hz delivered in conjunction with the third electrical stimulus inhibited force generation. (d) Average I1/I3 contraction force in response to electrical stimulation with and without the infrared pulse train (*** $p < 0.001$; without laser, N = 2 nerves, n = 10 trials; with laser, N = 2 nerves, n = 10 trials). Data are presented as mean ± SEM.

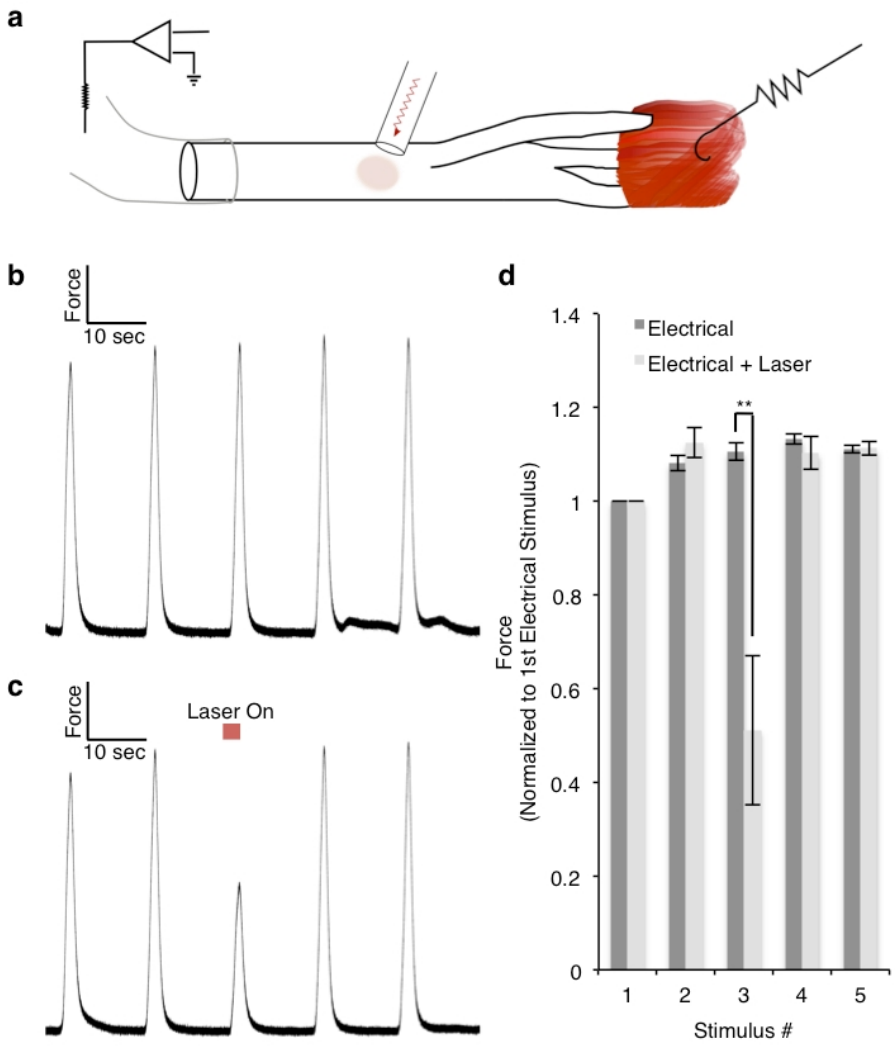

Figure VII-8. Titration of muscle force inhibition. Infrared inhibition is capable of titrating electrically evoked force. By decreasing the radiant exposure, less of the muscle force is inhibited when compared to Figure VII-7. (a) A suction electrode stimulates the nerve to induce muscle contractions in the I1/I3 muscles as measured by a force transducer. A 200 mm diameter optical fiber placed distal to the electrical stimulus inhibits action potential propagation along motor units. (b) Electrically evoked force (t_{pe} = 1 ms; 0.7 mA; 10 Hz) in response to five 2-sec stimuli. (c) In the same preparation, a 3-sec infrared pulse train (l = 1450 nm; t_{po} = 0.2 ms; 0.50 J/cm^2; indicated by a horizontal red bar) at 200 Hz delivered in conjunction with the third electrical stimulus inhibits force generation. (d) Average I1/I3 contraction force in response to electrical stimulation with and without the infrared pulse train; ** $p < 0.01$ (without laser, n = 5 trials; with laser, n = 5 trials). Data are presented as mean ± SEM.

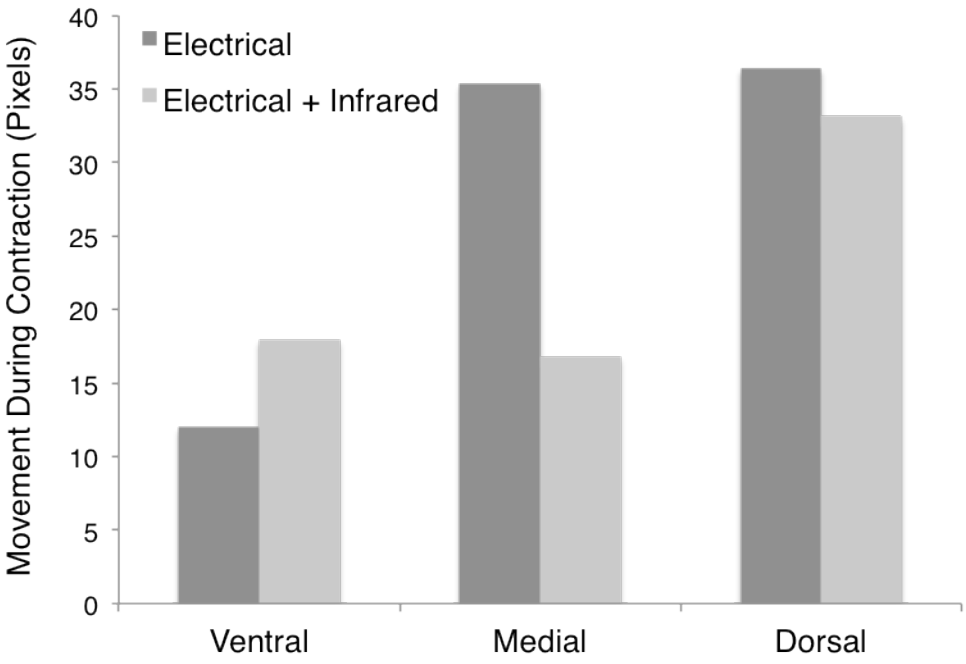

Figure VII-9. Evoked muscle movement in response to infrared inhibition. Using a video of the muscle movement, pixel shift for points located at ventral, medial and dorsal positions on the I1/I3 muscle were determined in response to electrical stimulation with and without infrared inhibition. The medial portion of the muscle consistently experiences less movement in response to infrared inhibition, whereas the ventral portion shows increased movement. Of the trials shown (n = 2), electrical stimulation plus infrared inhibition resulted in increased movement of the dorsal portion of the muscle for one trial and less movement in the other.

7.4.5 Inhibition of neuromuscular transmission in the rat

Inhibiting and exciting effects of infrared exposure on propagating APs were validated in a myelinated mammalian nerve. Applying infrared pulses to the tibial branch of the rat sciatic nerve, approximately 1 cm distal to the site of electrical stimulation, reduced evoked EMG amplitude of the lateral gastrocnemius (LG) and the medial gastrocnemius (MG) (Figure VII-10). Enhanced propagated responses were observed as in *Aplysia* and depended on the location of the fiber optic and current path of the electrical stimulus (Figure VII-6E). Threshold temperature for inhibition of LG integrated EMG (iEMG) (~5.2°C) was determined as for *Aplysia* (see section 7.3.11).

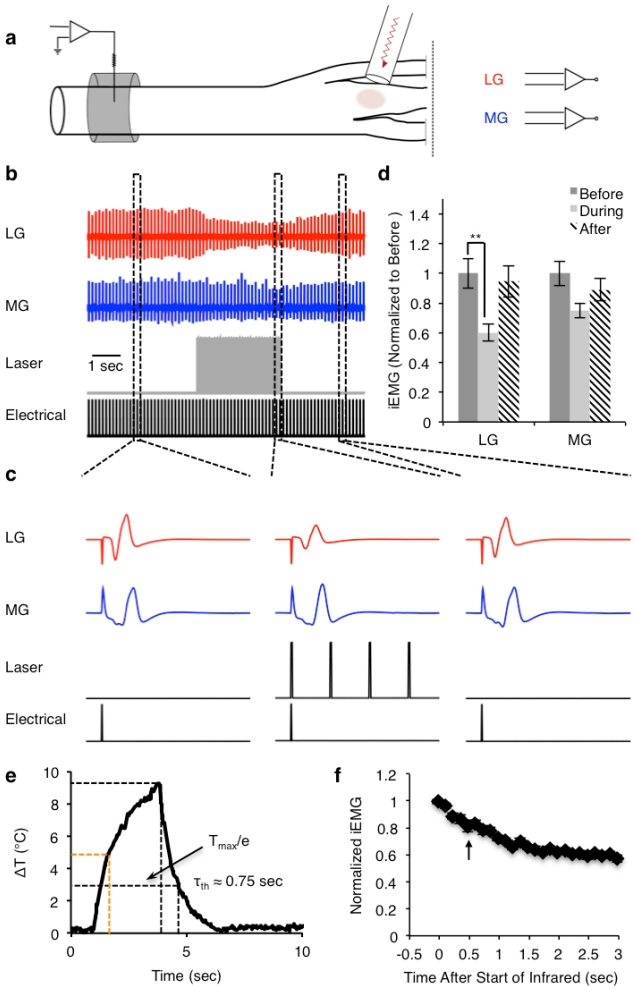

Figure VII-10. Nerve conduction block in the rat sciatic nerve. (a) A monopolar cuff electrode stimulated propagating APs along the nerve trunk. A 400 mm diameter fiber optic coupled to a diode laser was positioned over the tibial branch. (b) A train of infrared pulses (l = 1450 nm; t_{po} = 0.2 ms; indicated schematically by a gray bar) at 200 Hz reduces the amplitude of EMG recordings for MG and LG. Electrical artifacts are blanked for clarity. (c) Single EMG responses are shown before, during and after infrared inhibition. Each trace is 20 ms. (d) Average iEMG for MG and LG before, during and after laser exposure (** $p < 0.01$; N = 2 nerves, n = 12 trials). Because of differences in absolute magnitude between the nerves tested, iEMG were normalized to the average iEMG for 1 sec prior to infrared exposure. (e) Local temperature increases by approximately 9 °C during the 3 second infrared exposure. The thermal relaxation time is approximately 0.75 sec. (f) Increasing duration of radiant exposure yields greater reduction in the iEMG for LG. The location where reduction in iEMG for LG first becomes significant ($p < 0.002$) is indicated by an arrow in (f) and orange dashed lines in (e). Data are presented as mean ± SEM.

7.5 Discussion

Our results demonstrate infrared light can be used as a precise, reversible form of non-contact and artifact-free neural control. Electrically initiated responses were turned off in all *Aplysia* nerves tested (Figure VII-3) and selectivity was demonstrated (Figure VII-2). In BN2 of *Aplysia*, preferential inhibition of APs propagating to BN2c was demonstrated in all trials tested. However, when evaluating each nerve individually, only one showed negligible change in the iCNAP of BN2b (Figure VII-6A-C). Responses recorded at all three branches were consistent for a given nerve and fiber location. Repositioning the fiber optic altered the response of branches BN2b and BN2c. Thus, careful positioning and the use of smaller diameter multi-mode fibers or single mode fiber optics could improve specificity.

Though propagation of specific APs were blocked in both *Aplysia* (Figure VII-5) and rat (Figure VII-10), we were unable to block propagating responses using single laser pulses with similar radiant exposures as were required for initiation block (data not shown). Providing a higher frequency train (200 Hz) of lower radiant exposure pulses achieved reproducible nerve conduction block. Mou et al. proposed propagation block would require a greater local temperature increase distributed over a larger area than is required for initiation block (Mou et al., 2012). This may be due to the AP safety factor allowing propagation to continue when local excitability is reduced (Hodgkin, 1937).

Both infrared stimulation and infrared inhibition are believed to be thermally driven processes (Wells et al., 2007, Mou et al., 2012, Shapiro et al., 2012). Sub-threshold infrared stimuli for stimulation are also known to combine with sub-threshold electrical stimuli to achieve axonal activation (Duke et al., 2009, Duke et al., 2012a). This

may explain the enhancement of the propagated responses (Figure VII-6D-E). A pulse from an infrared laser produces a Gaussian-shaped temperature gradient within the irradiated tissue (Wells et al., 2007). For thermal block, the tissue must achieve a critical temperature where sodium activation is overcome by sodium inactivation and potassium activation (Huxley, 1959, Rattay and Aberham, 1993, Mou et al., 2012). This most likely occurs for axons traversing the center of the laser spot, close to the site of optical absorption (i.e. near the surface in our preparation). Axons located near the periphery will experience a graded temperature change depending on their proximity to the center of the laser spot. While this increase in temperature may not be sufficient to achieve direct infrared-induced stimulation, it is possible that the temperature increase combined with passive spread of sub-threshold depolarization will activate some axons. Greater control over both excitation and inhibition will be achieved by optimizing light delivery to the desired axons, for example by using smaller diameter fiber optics.

The ultimate application of this technique will be contingent on the absence of long-term thermally-induced changes in tissue morphology or function. While infrared radiant exposures required to inhibit AP generation are much lower than stimulation thresholds reported previously (Duke et al., 2012a), the maximum temperature rise induced during propagation block was approximately 8 °C in *Aplysia* and 9 °C in the rat (Figure VII-5E and Figure VII-10E). Several factors must be taken into account when evaluating the reported infrared-induced rise in tissue temperature (Figure VII-5E and Figure VII-10E). The dimensions of the temperature profile are determined by the fiber optic diameter and numerical aperture, tissue optical properties (e.g. absorption and scattering) and tissue thermal properties. The infrared thermal camera we used to

measure the induced temperature rise (see description above) has limited spatial resolution of approximately 300 μm per pixel. The assumed laser spot size during *Aplysia* stimulation was 200 μm in diameter and the measured spot size in the rat was approximately 600 μm in diameter. Thus, in both cases the thermal measurement will be an average temperature across the laser spot, rather than an accurate measure of the peak temperature.

For *Aplysia* measurements, the saline level surrounding the nerve was lowered to just cover the nerve sheath and the fiber optic was positioned just out of contact with the saline/sheath surface (Figure VII-1). This is in contrast to the experimental setup where both the fiber optic and BN2 were immersed in saline. This setup was necessary for temperature measurements to allow the IR wavelengths (blackbody radiation) from radiative heat transfer to be detected by the thermal camera without being shielded by water absorption. By creating this insulating air interface, the measured temperatures will be overestimated. In models of laser-tissue interactions, the air-tissue interface is often assumed to be adiabatic with heat reflecting back into the simulated volume (Pfefer et al., 2000). As these temperatures are recorded at the surface of the nerve sheath, which is the primary site of optical absorption and conversion to thermal energy, they will overestimate the temperature at the axonal level. The increased rate of thermal diffusion in the rat sciatic nerve compared to *Aplysia* BN2 is most likely due to perfusion in the rat removing heat from the infrared exposed spot.

Lack of long-term thermally induced functional and morphological changes will be required for many applications of infrared inhibition. Visually identifiable thermal damage was not observed, though low temperature thermal damage is not always

possible to detect visually or with traditional light microscopic techniques (Thomsen, 1991). Thermal injury is dependent on laser power (i.e. temperature) and the duration for which the temperature is maintained. Thermal changes are for sufficiently short durations, with low temperature damage reversible for exposures ranging from 25 min to several hours (Thomsen, 1991, Anderson and Ross, 1994). Infrared radiant exposures required for neural stimulation are reduced when combining infrared stimuli with sub-threshold electrical stimuli (Duke et al., 2009, Duke et al., 2012a). A similar strategy may be employed to minimize requisite temperatures for potential applications requiring long-term infrared inhibition.

Both unmyelinated and myelinated axons experience inhibition, suggesting the mechanism of action between nerve fiber types is strongly related, and supporting the use of invertebrates for both fundamental and translational studies of the nervous system. Interestingly, non-excitable cells are also known to respond to infrared-induced temperature gradients (Shapiro et al., 2012). The use of lasers to create highly localized thermal changes targeting specific cells or even localized regions of membrane may be a useful technique for probing cell function.

Infrared light is an intriguing tool for studying neural function and is being investigated for clinical applications ranging from cochlear implants (Rajguru et al., 2010) to intraoperative nerve monitoring (Fried et al., 2007). In this study, nerve exposure to infrared radiation is shown to be a multi-faceted phenomenon. This points to a rich set of interactions between the nervous system and optical/thermal energy that may be exploited to further understand and control the nervous system and more general cell functions.

7.6 References

Anderson R, Ross E (1994) Laser-tissue interactions. Cutaneous Laser Surgery Mosby: Philadelphia, PA 9.

Cayce JM, Friedman RM, Jansen ED, Mahavaden-Jansen A, Roe AW (2011) Pulsed infrared light alters neural activity in rat somatosensory cortex in vivo. Neuroimage 57:155-166.

Dittami GM, Rajguru SM, Lasher RA, Hitchcock RW, Rabbitt RD (2011) Intracellular calcium transients evoked by pulsed infrared radiation in neonatal cardiomyocytes. J Physiol 589:1295-1306.

Duke AR, Cayce JM, Malphrus JD, Konrad P, Mahadevan-Jansen A, Jansen ED (2009) Combined optical and electrical stimulation of neural tissue in vivo. Journal of Biomedical Optics 14:060501-060503.

Duke AR, Lu H, Jenkins MW, Chiel HJ, Jansen ED (2012a) Spatial and temporal variability in response to hybrid electro-optical stimulation. Journal of Neural Engineering 9:036003.

Duke AR, Lu H, Jenkins MW, Chiel HJ, Jansen ED (2012b) Spatial and temporal variability in response to hybrid electro-optical stimulation. J Neural Eng 9:036003.

Fenno L, Yizhar O, Deisseroth K (2011) The development and application of optogenetics. Annu Rev Neurosci 34:389-412.

Fried NM, Rais-Bahrami S, Lagoda GA, Ai-Ying C, Li-Ming S, Burnett AL (2007) Identification and Imaging of the Nerves Responsible for Erectile Function in Rat Prostate, *In Vivo*, Using Optical Nerve Stimulation and Optical Coherence Tomography. Selected Topics in Quantum Electronics, IEEE Journal of 13:1641-1645.

Fried NM, Lagoda GA, Scott NJ, Su LM, Burnett AL (2008) Noncontact stimulation of the cavernous nerves in the rat prostate using a tunable-wavelength thulium fiber laser. J Endourol 22:409-413.

Grill WM, Norman SE, Bellamkonda RV (2009) Implanted neural interfaces: biochallenges and engineered solutions. Annu Rev Biomed Eng 11:1-24.

Hale GM, Querry MR (1973) Optical Constants of Water in the 200-nm to 200-microm Wavelength Region. Appl Opt 12:555-563.

Hodgkin AL (1937) Evidence for electrical transmission in nerve: Part I. J Physiol 90:183-210.

Hodgkin AL, Katz B (1949) The effect of temperature on the electrical activity of the giant axon of the squid. J Physiol 109:240-249.

Huxley AF (1959) Ion movements during nerve activity. Ann N Y Acad Sci 81:221-246.

Izzo AD, Richter CP, Jansen ED, Walsh JT (2006) Laser stimulation of the auditory nerve. Lasers in Surgery and Medicine 38:745-753.

Jenkins MW, Duke AR, Gu S, Chiel HJ, Fujioka H, Watanabe M, Jansen ED, Rollins AM (2010) Optical pacing of the embryonic heart. Nat Photonics 4:623-626.

Khosrofian JM, Garetz BA (1983) Measurement of a Gaussian Laser-Beam Diameter through the Direct Inversion of Knife-Edge Data. Applied Optics 22:3406-3410.

Kilgore KL, Bhadra N (2004) Nerve conduction block utilising high-frequency alternating current. Med Biol Eng Comput 42:394-406.

Konrad P, Shanks T (2010) Implantable brain computer interface: challenges to neurotechnology translation. Neurobiol Dis 38:369-375.

Llewellyn ME, Thompson KR, Deisseroth K, Delp SL (2010) Orderly recruitment of motor units under optical control in vivo. Nat Med 16:1161-1165.

Martens HC, Toader E, Decre MM, Anderson DJ, Vetter R, Kipke DR, Baker KB, Johnson MD, Vitek JL (2011) Spatial steering of deep brain stimulation volumes using a novel lead design. Clin Neurophysiol 122:558-566.

Mou Z, Triantis IF, Woods VM, Toumazou C, Nikolic K (2012) A simulation study of the combined thermoelectric extracellular stimulation of the sciatic nerve of the Xenopus laevis: the localized transient heat block. IEEE Trans Biomed Eng 59:1758-1769.

Nargeot R, Baxter DA, Byrne JH (1997) Contingent-dependent enhancement of rhythmic motor patterns: an in vitro analog of operant conditioning. J Neurosci 17:8093-8105.

Peckham PH, Knutson JS (2005) Functional electrical stimulation for neuromuscular applications. Annu Rev Biomed Eng 7:327-360.

Pfefer TJ, Smithies DJ, Milner TE, van Gemert MJ, Nelson JS, Welch AJ (2000) Bioheat transfer analysis of cryogen spray cooling during laser treatment of port wine stains. Lasers Surg Med 26:145-157.

Rajguru SM, Matic AI, Robinson AM, Fishman AJ, Moreno LE, Bradley A, Vujanovic I, Breen J, Wells JD, Bendett M, Richter CP (2010) Optical cochlear implants: evaluation of surgical approach and laser parameters in cats. Hear Res 269:102-111.

Rattay F, Aberham M (1993) Modeling axon membranes for functional electrical stimulation. IEEE Trans Biomed Eng 40:1201-1209.

Richter CP, Matic AI, Wells JD, Jansen ED, Walsh JT (2011a) Neural stimulation with optical radiation. Laser Photonics Rev 5:68-80.

Richter CP, Rajguru SM, Matic AI, Moreno EL, Fishman AJ, Robinson AM, Suh E, Walsh JT (2011b) Spread of cochlear excitation during stimulation with pulsed infrared radiation: inferior colliculus measurements. J Neural Eng 8:056006.

Shapiro MG, Homma K, Villarreal S, Richter CP, Bezanilla F (2012) Infrared light excites cells by changing their electrical capacitance. Nat Commun 3:736.

Slavin KV (2008) Peripheral nerve stimulation for neuropathic pain. Neurotherapeutics 5:100-106.

Teudt IU, Nevel AE, Izzo AD, Walsh JT, Jr., Richter CP (2007) Optical stimulation of the facial nerve: a new monitoring technique? Laryngoscope 117:1641-1647.

Thomsen S (1991) Pathologic analysis of photothermal and photomechanical effects of laser-tissue interactions. Photochem Photobiol 53:825-835.

Warman EN, Chiel HJ (1995) A new technique for chronic single-unit extracellular recording in freely behaving animals using pipette electrodes. J Neurosci Methods 57:161-169.

Wells J, Kao C, Jansen ED, Konrad P, Mahadevan-Jansen A (2005) Application of infrared light for in vivo neural stimulation. Journal of Biomedical Optics 10:-.

Wells J, Kao C, Konrad P, Milner T, Kim J, Mahadevan-Jansen A, Jansen ED (2007) Biophysical mechanisms of transient optical stimulation of peripheral nerve. Biophysical Journal 93:2567-2580.

CHAPTER VIII

CONCLUSIONS AND FUTURE DIRECTIONS

Austin R. Duke

Vanderbilt University, Department of Biomedical Engineering

Nashville, TN

8.1 Summary and Conclusions

8.1.1 Summary

The overall objective of this research project was to develop innovative optical techniques for controlling neural function. Pulsed infrared light was previously shown to induce direct activation of axons *in vivo* (Wells et al., 2005). In this work, spatially precise infrared light was investigated for its potential to modulate electrically initiated axonal activation and to block propagating action potentials. In Chapter II, current and novel electrical and optical methods of neural control were discussed, and motivations for their combination were presented. The work contained in this dissertation describes the (1) proof-of-concept demonstration of combined optical and electrical stimulation (Chapter III); (2) development of a methodology for reliable and repeatable hybrid electro-optical stimulation (Chapter IV); (3) application of hybrid stimulation for force generation (Chapter V); and (4) demonstration and characterization of infrared light for inhibiting electrically initiated activation, blocking nerve conduction and modulating neuromuscular function (Chapter VI).

In Chapter III, the hypothesis that the combination of sub-threshold for stimulation electrical and optical stimuli will achieve neural activation was tested in the rat sciatic nerve. Varying the strength of the sub-threshold electrical stimulus revealed that the additional optical energy required for stimulation followed a logarithmic relationship and decreased by as much as three-fold when compared to thresholds for INS alone. From this it was deduced that optical and electrical stimulation work by differing mechanisms; otherwise a simple linear superposition of optical and electrical energy

would achieve activation. Delaying the timing of the INS pulse relative to the electrical pulse reduced the benefits of combined stimulation when compared to delivering the pulses simultaneously. Delivering the optical stimulus prior to the electrical stimulus was subsequently demonstrated and revealed that hybrid stimulation with greater pulse separation is possible when the optical stimulus is delivered first (Appendix A). From this we can conclude that INS effects relevant to hybrid stimulation last longer than the effects of electrical stimulation. Compound muscle action potentials monitored during hybrid stimulation revealed that selective activation of muscle groups is possible. The primary conclusion drawn from this study is that combined optical and electrical stimulation of neural tissue *in vivo* is feasible and may be beneficial to the neurostimulation community.

Chapter IV details the establishment of a methodology for reliable and repeatable hybrid electro-optical stimulation. While feasibility of this neurostimulation paradigm was shown, the ultimate application of this technique will require low variability and high repeatability. Spatial and temporal sources of variability were identified in the tractable nervous system of the *Aplysia californica* and then validated in the more clinically relevant rat sciatic nerve. A limited region of excitability (ROE) for hybrid stimulation was identified adjacent to the cathode and the location could be shifted within a given nerve by changing the polarity of electrical stimulation. For a constant electrical stimulus, the size of the ROE was determined by the strength of optical stimulation. Electrical stimulation threshold was found to vary with time. Failure to account for this variation was shown to induce greater variability in the optical energy required for stimulation. A surprising finding from these experiments is that there is a limited range of radiant

exposures (all sub-threshold for INS) for which hybrid stimulation will occur. Outside of this window, the probability of firing goes to 0%. An optical stimulus was also found to inhibit electrically evoked responses at the site of action potential initiation. Optical inhibition was observed and systematically investigated in the *Aplysia*, but was not observed during limited investigation in the rat. From this study it was concluded that for successful hybrid stimulation: (1) the target tissue, electrode(s) and optical stimulus must be mechanically stable; (2) the optical stimulus must be located within the ROE adjacent to the cathode; (3) the strength of the stimuli must be taken into account to determine the size of the ROE; (4) variability in electrical stimulation threshold must be accounted for to mitigate variability in hybrid stimulation thresholds; and (5) stimulation radiant exposures must be between thresholds for hybrid stimulation and optical inhibition.

Chapter V describes the application of hybrid electro-optical stimulation to induce contraction forces in muscles of the rat hind limb. These results are significant because it is the first time that INS-based stimulation of a peripheral nerve was used to produce a physiological response. Prior to this demonstration, INS of peripheral nerves was only capable of safely producing muscle action potentials and twitches. In general, physiological applications of INS were confined to the auditory system (Matic et al., 2011) and embryonic hearts (Jenkins et al., 2010). In this study, hybrid stimulation at 15-20Hz generated force responses comparable to electrical stimulation at the same repetition rates. The hybrid force response exhibited unique characteristics that were indicative of an underlying increase in baseline temperature. With successive stimulus trains, the hybrid-evoked force incrementally increased from negligible magnitude to plateau at roughly 30% of the total contraction force. Following the maximal force,

hybrid-evoked forces were found to decay at a rate slower than that for thermal diffusion, suggesting the relationship between force and baseline temperature is complex. Increasing the interval between stimulus trains decreased both the slope at which the force increased as well as the maximum recruited force. Preconditioning the nerve with sub-threshold optical stimulation at 20 Hz enhanced the nerve's response to both electrical and hybrid stimulation. These results led to the conclusion that hybrid electro-optical stimulation is capable of generating physiological force responses in mammalian nerves through a mechanism likely mediated by a baseline temperature increase.

Chapter VI describes the capability of infrared light for selectively and reversibly inhibiting electrically initiated axonal activation and blocking nerve conduction. This work marks the first demonstration of infrared light as a means of neural inhibition. In unmyelinated *Aplysia* buccal nerves, pulsed infrared light synchronized with a supra-threshold electrical stimulus inhibited the initiation of select axons. With the infrared light applied distal to the site of electrical stimulation, propagating action potentials were blocked from conducting beyond the region of infrared exposure. By maintaining the neuromuscular innervation, the use of infrared light to regulate muscle contraction was also demonstrated. Nerve conduction block was validated in the rat sciatic nerve to show that this technique is applicable to myelinated mammalian nerves as well. In both *Aplysia* and the rat, the mechanism of infrared inhibition was proposed to be a thermally mediated phenomenon whereby a local temperature increase alters the gating function of membrane ion channels. The results of this study indicate that the interaction of infrared light and neural tissue is multi-faceted and well suited for controlling neural function.

8.1.2 Plausible Mechanism

In addition to demonstrating the potential for inhibition of neural activity using infrared light, the work described in Chapter VI also leads to a plausible explanation for how infrared light is applied towards both hybrid electro-optical stimulation and infrared inhibition. Hodgkin and Huxley introduced gating variables to express the time and voltage dependence of the ionic conductances (Hodgkin and Huxley, 1952). The equation for the potassium conductance is:

$$g_K = \bar{g}_K n^4 \quad \text{(VIII-1)}$$

where g_k (conductance/cm^2) is a constant and n is the dimensionless gating variable ranging from 0 to 1 that indicates the portion of molecules in a certain position (e.g. inside of the membrane). Similarly, the sodium conductance is given by:

$$g_{Na} = m^3 h \bar{g}_{Na} \quad \text{(VIII-2)}$$

where m is the portion of activating molecules on the inside of the membrane and h is the proportion of activating molecules on the outside. Each gating variable is time, voltage and temperature dependent, and is modeled by:

$$n = [-(\alpha_n + \dot{\beta}_n) \cdot n + \alpha_n] \cdot k \quad \text{(VIII-}$$

3)

where α_n and β_n are the opening and closing rates of the gates and k is a thermal coefficient (Rattay and Aberham, 1993). Equation (VIII-3) is also used to model the other gating variables (i.e. m and h). Frankenhaeuser and Huxley extended the original Hodgkin-Huxley equations to myelinated fibers, which involved slight variations to equations (VIII-1) and (VIII-2), as well as the addition of a delayed non-specific ionic current, $i_{P,}$ and its gating variable p (Frankenhaeuser and Huxley, 1964, Rattay and Aberham, 1993).

The thermal coefficient, k, in equation (VIII-3) determines the acceleration of the opening and closing rates for each gate as the temperature deviates from a predetermined baseline (Rattay and Aberham, 1993). k is determined by

$$k = Q_{10}{}^{(T-T_0)/10} \quad \text{(VIII-4)}$$

where T is the actual temperature and Q_{10} is a constant used to quantify rate acceleration for a 10 °C increase in temperature. Hodgkin et al. found that a Q_{10} of 3 would allow for comparisons across temperature (Hodgkin et al., 1952). However, a Q_{10} of 3 will not simulate an action potential in mammalian axons at 37 °C. Thus, accurate simulations matching empirical results require a distinct temperature coefficient for each α and β (Rattay and Aberham, 1993, Mou et al., 2012). To model empirical results accurately, the temperature coefficients for the n, h and p rate constants are all close to 3, while the m

rate constants are approximately half that. Thus, as the nerve temperature increases, the rates of sodium inactivation (*h*) and potassium activation (*n*) overtake the rate of sodium activation (*m*). This results in an action potential that is either faster and weaker, or completely and reversibly blocked (Hodgkin and Katz, 1949, Huxley, 1959).

Understanding how this increase in temperature both enhances and inhibits the nerve's response to electrical stimulation requires a closer look at the relationship between nerve temperature and the threshold electrical current for stimulation. Figure VIII-1 shows the results of modeling simulations investigating how electrical stimulation threshold changes with temperature for various nerve fiber diameters. NEURON software (version 7.2) was used to model the myelinated *Xenopus laevis* sciatic nerve and simulate the response to an extracellular electrical point stimulus (Hines and Carnevale, 1997, Mou et al., 2012). The temperature of the node of Ranvier directly beneath the electrical stimulus was adjusted independent of all other nodes and internodes to reflect the temperature change resulting from an ideally targeted infrared pulse (Mou et al., 2012). When the temperature of the node was increased to 45 °C (with T_0 = 20 °C), the threshold current for an electrically initiated action potential occurring at that node was reduced by up to ~20%. Hybrid electro-optical stimulation as described in Chapters III – V is likely the result of this temperature increase. In those studies, the electrical stimulation threshold was first found at baseline temperature (T_0) and then subsequently reduced to 90% of threshold. Providing a concurrent increase in nerve temperature via infrared laser exposure reduces the requisite current for stimulation, thus achieving hybrid activation with a previously sub-threshold electrical stimulus. However, if laser exposure is such that the node temperature surpasses a certain threshold (45 °C for these

modeling studies), electrically initiated axonal activation will be blocked. Above 45 °C, axons ≥ 10 μm in diameter were unable to elicit a propagating action potential at currents many times greater than threshold at T_0. Axons ≤ 5 μm in diameter were still able to elicit propagating responses, though they required currents that were often much greater than at T_0. This phenomenon explains the results presented in Chapter VI. Therefore a critical temperature that divide's the nerve's response into two regimes: below the critical temperature the electrical stimulation threshold is reduced to produce hybrid electro-optical stimulation; above the critical temperature the axonal initiation of action potentials is inhibited.

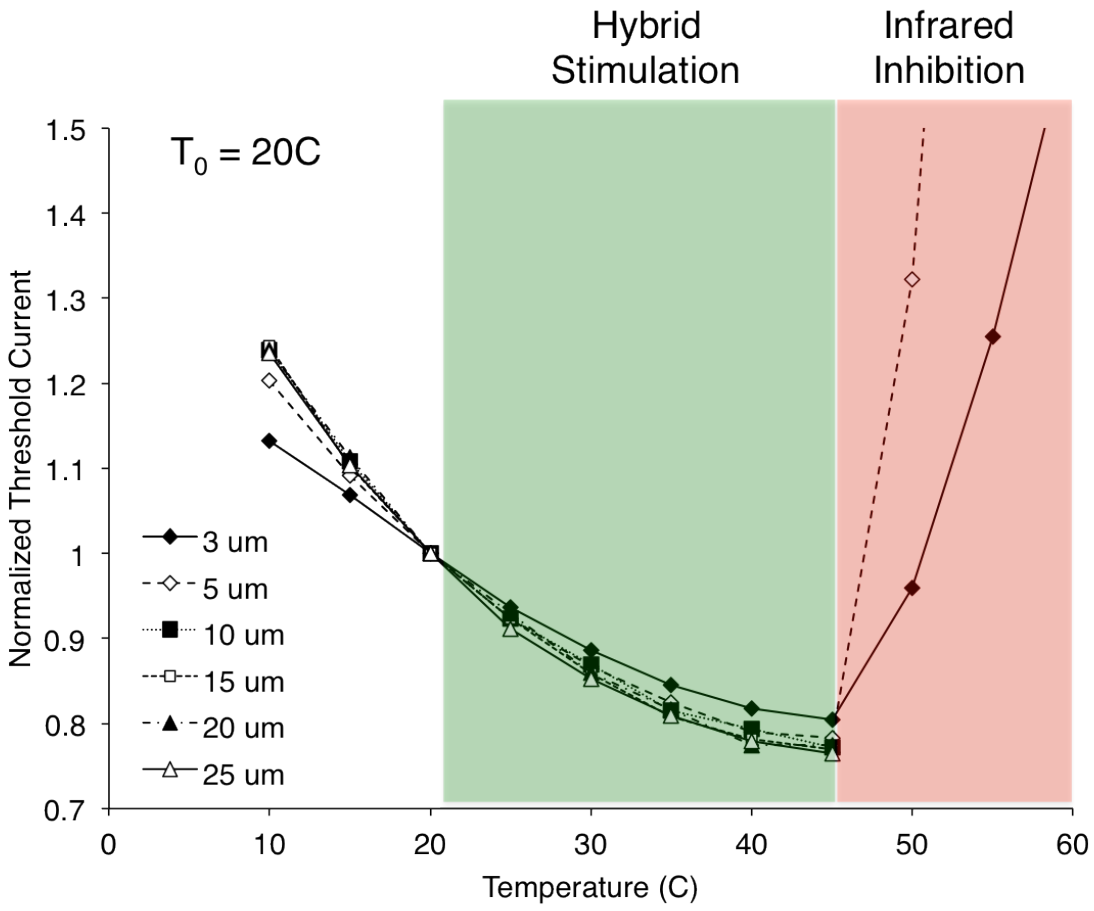

Figure VIII-1. A critical temperature divides an axon's response to electrical stimulation. Simulations reveal that below the critical temperature (green shaded region), electrical stimulation threshold is reduced compared to baseline nerve temperature (T_0 = 20 °C). This provides an explanation for hybrid electro-optical stimulation, whereby pulses of infrared light delivered concurrently with electrical stimulation create transient increases in nerve temperature and achieve neural activation with electrical currents that are less than what is required at baseline nerve temperature. Above the critical temperature (red shaded region), stimulation threshold currents for small diameter fibers are greatly increased, while larger diameter fibers are unable to evoke any response. This reflects infrared inhibition, where electrically initiated axonal activation is reversibly blocked by laser-induced transient increases in nerve temperature.

The effect of temperature on the Hodgkin-Huxley gating variables, and their ultimate effects on ionic conductance, provides a plausible explanation for how a laser-induced temperature rise can lead to both hybrid electro-optical stimulation and infrared inhibition. However, interpretation of the simulation results must take into considerations the limitation of the model. This model of a single, myelinated axon only looks at the effect of constant temperature in a single node and does not consider the spatial and temporal evolution of a laser-induced temperature rise in three dimensions. Any laser-induced capacitive currents are also neglected in this model (Shapiro et al., 2012). It is possible that the hybrid electro-optical stimulation described in Chapters III and IV is different than what is presented in Chapter V. In Chapter V, a presumed increase in baseline temperature of the rat sciatic nerve resulting from infrared pulses was shown to enhance the force of the plantarflexor muscles produced by electrical stimulation. This aligns well with the mechanism described above. However, in Chapters III and IV, responses at low repetition rate (2 Hz), where evoked thermal effects of each laser pulse are independent of prior or subsequent pulses, may align with the initial proposed hypothesis that the sub-threshold electrical stimulus lowers the threshold for optical stimulation. Shapiro et al. demonstrated that oocytes expressing voltage-gated sodium and potassium channels exhibit a transient capacitive current in response to infrared stimulation and will fire an action potential if the infrared pulse is combined with a just sub-threshold depolarizing electrical stimulus (Shapiro et al., 2012). Rather than two distinct mechanisms, it is more likely that transient capacitive currents and local increases in temperature both contribute to hybrid electro-optical stimulation, as well as infrared

inhibition. The next iteration of models and simulations should seek to incorporate both effects.

8.1.3 Conclusion

The work and accompanying discussion comprising this dissertation reveal a new technology for probing and controlling excitable tissues. As fast as the neuromodulation market is growing, limitations of current neurotechnology provide the greatest obstacle for treating patients with neurological deficits. Using infrared light to enhance electrical neural stimulation will leverage the proven track record of electrical techniques to usher in a new wave of INS-based devices with potentially improved spatial selectivity. Infrared light is also presented as a new tool for inhibiting neuronal activation and propagation in native tissues without any need for modifications or genetic engineering. Although the work in this dissertation is directed towards the peripheral nervous system, no fundamental roadblocks are foreseen which will limit the application of this technique in other excitable tissues.

8.2 Future Directions

8.2.1 Parametric Studies

To date, limited information regarding the most effective parameters for hybrid stimulation has been attained. In the initial feasibility study (Chapter III), the optical energy required for stimulation as a function of the sub-threshold electrical stimulus was

determined; however, these results were somewhat inconsistent and clouded by variability in the data. Based on these results and limited studies of pulse timings, nearly all of the experiments in Chapters IV and V were conducted with the electrical stimulus set to 90% of stimulation threshold and the stimulus pulses delivered such that they ended simultaneously. While the choice of these parameters is certainly justifiable, it would be worthwhile to determine the optimal parameter set for minimizing both the optical energy and electrical current required for stimulation. These studies could be performed in the tractable *Aplysia* nervous system and subsequently validated in the rat. Now that sources of variability have been identified, optical stimulation threshold as a function of the electrical stimulus magnitude can be more accurately determined. Similarly, electrical threshold could be determined as a function of a sub-threshold optical stimulus. Limited investigations of the relative timing and pulse durations of the two modalities were investigated in *Aplysia* (Appendix A), but these results have yet to be validated in the rat. These experiments will be an excellent place to start for a researcher becoming familiar with this project.

8.2.2 Modeling studies

While this project provides the first demonstrations of hybrid electro-optical nerve stimulation and infrared inhibition, optimizing efficacy and tailoring these techniques to diverse applications will likely require further mechanistic understanding of how light and current interact with neural tissue to achieve excitation or inhibition. The mechanism of INS has yet to be fully elucidated; however, recent investigations reveal it to be mediated by a thermal gradient that results in a depolarizing capacitive current (Wells et

al., 2007, Shapiro et al., 2012). While a complete mechanistic exploration of INS is beyond the scope of this project, modeling studies will provide a better understanding of how the induced electric field and thermal profile interact in tissue. Infrared inhibition as demonstrated in Chapter VI is believed to be the result of local temperature increases causing the falling phase of the action potential to overtake the rising phase. Modeling studies have demonstrated this mechanism and could be combined with accurate thermal models to greatly enhance the understanding and application of infrared inhibition (Rattay and Aberham, 1993, Mou et al., 2012).

The first step for these studies will be the development of an appropriate model of the laser-induced thermal profile resulting from INS and infrared inhibition. There are three primary components to this model: (1) an adaptable material grid that can be used to represent the nerve, cuff and surrounding tissue/material; (2) a simulation of light propagation through the grid; and (3) a heat transfer model to determine the temperature profile as a function of time. The modular adaptable grid will allow optical and thermal properties to be specified for complex geometry across three dimensions. Using the optical properties, a Monte Carlo simulation will statistically predict photon movement through the grid and indicate the fraction of, and location where light is reflected from the grid, absorbed in the grid or transmitted through the grid. Using the light absorption information from the Monte Carlo simulation as input, the heat transfer model will then solve the bioheat equation to determine how heat within the tissue changes with time. Such a model structure currently exists for skin (Pfefer et al., 1996, Pfefer et al., 2000) and is in the process of being adapted for nerve stimulation. In its current state, the heat transfer model provides an explicit finite difference solution of the Fourier heat

conduction equation (Pfefer et al., 2000). This will need to be extended to include perfusion when simulating stimulation lasting for several seconds. Using this model, the effects of optical properties and stimulation parameters can be used to investigate the spatial and temporal temperature profile in the stimulated tissue.

The electrical potential field induced by electrical stimulation must also be modeled. Methods suitable for this stage of modeling were described previously by Schiefer et al. (Schiefer et al., 2008). Briefly, 2D nerve cross sections are imported into Maxwell 3D (Ansoft, Pittsburgh, PA), a software platform designed for electromagnetic field simulations. Once imported in Maxwell, the nerve cross section is extruded and a nerve cuff can be added. The electrical potentials induced by electrical stimulation from the cuff are then calculated and can be imported into Matlab (Mathworks, Natick, MA) for interpolation.

At this point both a thermal profile and an electric potential field are generated. Simple experiments can then be performed to determine the spatial and temporal overlap created by various sets of parameters used for hybrid electro-optical stimulation. This could provide further evidence for the sources of spatial variability discussed in Chapter IV. While modeling hybrid stimulation in this way will provide insight into some of the spatial and temporal characteristics of this stimulation modality, there is very limited information regarding the interaction of these techniques. For instance, potential effects of temperature on the electric field will not be taken into account. A complete model of hybrid electro-optical stimulation is not possible without a mechanism for INS. However, recent investigations have provided sufficient information regarding this mechanism to begin developing more complex models.

The first step towards a full model of hybrid electro-optical stimulation will be to develop an appropriate computational model in the NEURON simulation environment (Hines and Carnevale, 1997). NEURON facilitates the development of computational models of neurons and neural networks, and possesses a strong developer community. NEURON is routinely used to determine the nerve's response to electrical stimulation. However, the general effects of temperature on the nerve's response to electrical stimulation (e.g. Q10 factor) may also be investigated by incorporating a 3D temperature profile overlaying the nodes of each axon within a nerve. Because NEURON is highly extensible, the model can be modified to incorporate new information regarding the mechanism of INS and infrared inhibition. Shapiro et al. showed that the thermal gradient resulting from infrared absorption by water induces a reversible change in membrane capacitance leading to depolarization (Shapiro et al., 2012). The Gouy-Chapman-Stern (GCS) theory of double layer capacitors (Grahame, 1947) can be used to calculate the capacitance change in response to INS by accounting for the electrical and thermal factors affecting the spatial distribution of ions near the membrane surface. Using this theory and the techniques described by Shapiro et al., the capacitive currents induced by INS can be incorporated into the model. Although a purely capacitive mechanism of INS may not fully explain how transient infrared radiation excites neural tissue, the addition of this mechanism to a computational neural model will greatly increase the number of questions that may be investigated.

8.2.3 Development of hybrid neural interfaces

Further research and the ultimate application of hybrid electro-optical stimulation and infrared inhibition will require the development of appropriate neural interfaces. In this work hybrid neuromuscular stimulation was demonstrated using a rudimentary system (Chapter V). An IR-transparent PDMS-based cuff modeled after the FINE array (Tyler and Durand, 2002) was secured to the nerve. A fiber optic was secured to an external micromanipulator and oriented perpendicular to the cuff surface. While this implementation of hybrid stimulation was useful for demonstrating the feasibility of neuromuscular stimulation, a neural interface integrating both the optical and electrical stimuli will be the next step towards the eventual implantation and clinical application of this technology.

PDMS-based cuffs will be an excellent choice for developing the next generation of hybrid devices due to their mechanical properties and transparency at wavelengths appropriate for stimulation. Using the rectangular FINE as model geometry, electrical contacts and IR sources can be fixed in the cuff wall to provide multiple discrete locations of hybrid stimulation around the circumference of the nerve.

The crux of this design will be the embedding of the light sources within the cuff wall. Ideally discrete laser sources, such as Vertical-Cavity Surface-Emitting Lasers (VCSELs) would be embedded during the molding stage. This would allow for flexible and adaptive movement of the cuff while providing conductive heat transfer away from the VCSELs themselves. However, while VCSELs are currently in development for medical applications, those suitable for INS are not yet ready for *in vivo* testing (Hibbs-Brenner et al., 2009, Dummer et al., 2011). An alternative method of integrating an IR

light source in the cuff is to embed side-firing optical fibers within the cuff wall. Preliminary results showed the stimulation of a rabbit sciatic nerve using a side-firing fiber optic implanted in a PDMS cuff (data not shown). This will be a suitable approach for the next generation of hybrid neural interfaces as all of the components, save for the cuff, can be externalized – this includes the power source and the diode. By utilizing an appropriate tether, which have been driven to commercial availability by the success of optogenetics, this type of cuff could be implanted for chronic laboratory studies. This would also allow more cumbersome laser sources, such as the Ho:YAG, to be coupled to an animal wearing an implantable hybrid cuff. The fiber optics used for the work in this dissertation are rigid and not suitable for regular deformations as a result of implantation in the peripheral nervous system; however, there are strategies for developing fiber optics appropriate for implantable optical nerve stimulation applications (Chernov et al., 2012).

Alternative designs for a hybrid neural interface should also be investigated. In addition to extraneural cuffs, intraneural electrode arrays are becoming increasingly popular for electrical nerve stimulation. This concept could be modified to investigate the potential for intraneural hybrid stimulation. A hybrid intraneural interface was recently developed (Wang et al., 2010). The device entailed a tapered multi-mode optical fiber with the tip covered in a thin gold film, allowing the fiber to both transmit light and record electrical activity. This type of design could be applied to hybrid stimulation by using the metallic film for stimulation. While intraneural arrays have challenges as described in Chapter II, bringing the optical stimulus in close proximity to the neural axons will likely reduce stimulation thresholds and could enhance selectivity.

8.2.4 Coordinated neuromuscular stimulation

To date, hybrid stimulation has been used for force generation in nonspecific muscle groups innervated by the tibial branch of the rat sciatic nerve (Chapter V). While the spatial precision of INS and infrared inhibition are attractive, they also limit the total volume of neural tissue that can be recruited by a single stimulus. Therefore, in order to properly analyze selectivity and achieve meaningful control of neuromuscular function, multiple infrared sources must be combined and discretely positioned around the nerve and fascicles. Following the development of the cuff described above, investigating motor control with hybrid stimulation will be possible. This study could begin by determining the selectivity and degree of overlap for each hybrid stimulus using an overlap matrix as described by Tyler and Durand (Tyler and Durand, 2002). Essentially, the matrix represents the relative force shared by the *i*th and*j*th hybrid stimuli on a scale from 0 to 1. A value of 0 indicates that the *j*th stimulus could not reproduce any of the function produced by the *i*th stimulus and a value of 1 indicates that the *j*th stimulus is capable of producing all of the function generated by the *i*th stimulus. For an appropriate test of function, the hybrid cuff could be placed on the sciatic nerve of cat and the forces corresponding to plantarflexion, dorsiflexion, toe-in rotation and toe-out ration measured (Tyler and Durand, 2002). While extraneural INS may not be suitable for recruiting central fascicles of large nerves, the FINE reshapes the nerve to bring central axons closer to the periphery. If the use of a FINE style cuff for hybrid stimulation does not allow for full coverage of the nerve using hybrid stimulation, there may be interesting spatial and temporal combinations of electrical stimulation, INS and hybrid used to reproduce physiological force generation. After determining the selectivity of hybrid

stimulation, acute experiments can be conducted to attempt functional stimulation. By securing a hybrid cuff to the sciatic nerve of a cat, hybrid stimulation can be used for the coordinated recruitment of the muscles required for standing. Even limited demonstration of this sort of functional control would rapidly propel hybrid electro-optical stimulation forward.

8.2.5 Applications of infrared control

The demonstration of infrared light for controlling neural activity is an exciting finding as it provides a new tool for reversibly turning off parts of the nervous system. While there are many potential applications, it will be important to choose easily attainable outcomes as this approach is not yet fully characterized and will need to be shown useful for garnering further support. One application that could be of great significance is enhanced selectivity of neuroprosthetics for FES. This could be tested along with the selectivity experiments described previously. While stimulating the nerve electrically to generate full muscle recruitment, infrared inhibition could be added at discrete locations to determine the percent reduction in force for each muscle. Demonstrating this in combination with hybrid electro-optical stimulation will show the utility of infrared light for enhancing current neural interfaces. Other worthwhile applications to investigate are the selective inhibition of cerebal-buccal interneurons and their effect on feeding patterns in *Aplysia* and the use of infrared inhibition in combination with optical pacing to control the beating frequency of embryonic hearts.

8.3 Research Considerations

The protection of research subjects and the societal impact of this research were considered throughout the course of these studies and are discussed below.

8.4 Protection of Research Subjects

No human subjects were used in this research. The focus of this project was technology development and testing through preclinical studies. As this technology interfaces with the nervous system, animal experimentation was necessary. The proper ethical use and treatment of animal subjects was ensured for all experiments comprising this project. All experiments were conducted in accordance with protocols approved by the Institutional Animal Care and Use Committee (IACUC). Lab personnel identified on IACUC protocols and involved with these experiments completed required training provided by the American Association for Laboratory Animal Science (AALAS) Learning Library.

Appropriate training on general lab safety and standard chemical, biological and radiation safety was required for personnel involved in this study in compliance with institutional guidelines.

8.5 Significance and Societal Implications

The need for restored function to those affected by neurological disorders and trauma greatly outweighs the number of treatments available. Successful neuroprosthetic devices have been developed, but treating the increasing unreached patient population will require the development of additional novel neurotechnologies. Recently developed

optical methods of neural stimulation hope to fill some of this void. While infrared nerve stimulation demonstrates great promise as a therapy for lost neural function, chronic implantation of this technology is challenged by laser design constraints. Additionally, some applications may be limited by a risk of thermal tissue damage. Hybrid electro-optical neural stimulation is an innovative technology that addresses both of these issues by reducing the required optical energy for spatially selective stimulation. Future embodiments of this technology may restore lost function of arms and legs to wounded veterans, hearing to children with profound deafness or bladder control to those with spinal cord injuries among other potential applications.

While functional restoration with hybrid stimulation remains a future target, the work described in this dissertation represents incremental steps towards this goal. The proof-of-concept demonstration of hybrid stimulation represents a new paradigm of neural stimulation. This work showed that although the modalities likely function by different mechanisms, they can work synergistically to activate neural tissue. This project utilized hybrid stimulation for peripheral nerve applications; however, this technique could be applied to applications such as the auditory prostheses or stimulation of the central nervous system. While hybrid stimulation does not maintain the contact- and artifact-free nature of INS, these characteristics are not nearly as important as spatial selectivity for implantable devices. Thus, for any application of INS it will be desirable to reduce the requisite optical energy for stimulation for the purpose of alleviating laser design constraints and mitigating thermal tissue damage. Essentially, hybrid stimulation could be the driving force behind many INS-based neuroprosthetics.

This work demonstrates the first functional motor response with an INS-based technique. While auditory responses from cochlear stimulation are possible, prior to this work INS was only used to elicit muscle twitches from peripheral nerve stimulation. The results described in Chapter V of this dissertation demonstrate, for the first time, that pulsed infrared light can be used to generate physiological muscle contractions. This is momentous for the field of INS because it demonstrates this method is more than just an interesting observation – it can be used to create physiologically relevant responses.

In addition to neurostimulation, a means of spatiotemporally precise inhibition is crucial for full control of nervous system function. The use of infrared light for artifact-free, contact-free and selective block of action potential initiation and propagation is shown for the first time. The use of this technique to modulate neuromuscular function is also demonstrated. This study reveals that interaction of infrared light with neural tissue is a dynamic and multi-faceted phenomenon capable of full control of neural activity. The development of this novel tool will facilitate numerous and diverse studies of neural circuitry and dynamics and offers an intriguing option for enhancing current neural interfaces.

From a methodological perspective, Chapters IV and VI provide justification for the use of invertebrates in this type of research. While the vertebrate and invertebrate nervous systems have notable differences (e.g. vertebrate nerves are myelinated whereas invertebrate nerves are not), they remain largely similar. Much of what is known today about neurophysiology was ascertained through experimentation with the invertebrate nervous system. Yet, at the present there is a general feeling that invertebrate studies are not as valuable towards the design of neural interfaces. In this work, the utility of

invertebrate experimentation for the development of neural interfaces was demonstrated. While a direct jump from invertebrate studies to clinical trials is neither practical nor feasible, establishing fundamental trends using these tractable systems prior to validation in a more clinically relevant model is demonstrated to be a valuable pathway.

While the vision of infrared neural control as a neural therapy is still waiting to be realized, the promise of this technique is demonstrated by this work. Combining optical and electric methods of neural stimulation was shown to be possible and efforts were made to develop a methodology to make hybrid stimulation practical. Generating muscle contractions revealed the potential for this stimulation modality. Infrared light was shown to block neural activity and modulate neuromuscular output. The aforementioned future considerations lay out a framework of experiments to further refine and investigate the application of infrared light for neural control. Accomplishing these proposed objectives will bring hybrid electro-optical stimulation and infrared inhibition much closer to their ultimate clinical application.

8.6 References

Chernov MM, Duke AR, Cayce JM, Crowder SW, Sung HJ, Jansen ED (2012) Material considerations for optical interfacing to the nervous system. MRS Bulletin 37:599-605.

Dummer M, Johnson K, Hibbs-Brenner M, Keller M, Gong T, Wells J, Bendett M (2011) Development of VCSELs for optical nerve stimulation. vol. 7883, p 85.

Frankenhaeuser B, Huxley AF (1964) The Action Potential in the Myelinated Nerve Fiber of Xenopus Laevis as Computed on the Basis of Voltage Clamp Data. J Physiol 171:302-315.

Grahame DC (1947) The electrical double layer and the theory of electrocapillarity. Chem Rev 41:441-501.

Hibbs-Brenner MK, Johnson KL, Bendett M (2009) VCSEL technology for medical diagnostics and therapeutics. vol. 7180 (Anita, M.-J. and Jansen, E. D., eds), p 71800T: SPIE.

Hines ML, Carnevale NT (1997) The NEURON simulation environment. Neural Comput 9:1179-1209.

Hodgkin AL, Katz B (1949) The effect of temperature on the electrical activity of the giant axon of the squid. J Physiol 109:240-249.

Hodgkin AL, Huxley AF (1952) A quantitative description of membrane current and its application to conduction and excitation in nerve. J Physiol 117:500-544.

Hodgkin AL, Huxley AF, Katz B (1952) Measurement of current-voltage relations in the membrane of the giant axon of Loligo. J Physiol 116:424-448.

Huxley AF (1959) Ion movements during nerve activity. Ann N Y Acad Sci 81:221-246.

Jenkins MW, Duke AR, Gu S, Chiel HJ, Fujioka H, Watanabe M, Jansen ED, Rollins AM (2010) Optical pacing of the embryonic heart. Nature Photonics 4:623-626.

Matic AI, Walsh JT, Jr., Richter CP (2011) Spatial extent of cochlear infrared neural stimulation determined by tone-on-light masking. J Biomed Opt 16:118002.

Mou Z, Triantis IF, Woods VM, Toumazou C, Nikolic K (2012) A simulation study of the combined thermoelectric extracellular stimulation of the sciatic nerve of the Xenopus laevis: the localized transient heat block. IEEE Trans Biomed Eng 59:1758-1769.

Pfefer TJ, Kehlet Barton J, Chan EK, Ducros MG, Sorg BS, Milner TE, Nelson JS, Welch AJ (1996) A three-dimensional modular adaptable grid numerical model

for light propagation during laser irradiation of skin tissue. Selected Topics in Quantum Electronics, IEEE Journal of 2:934-942.

Pfefer TJ, Smithies DJ, Milner TE, van Gemert MJ, Nelson JS, Welch AJ (2000) Bioheat transfer analysis of cryogen spray cooling during laser treatment of port wine stains. Lasers Surg Med 26:145-157.

Rattay F, Aberham M (1993) Modeling axon membranes for functional electrical stimulation. IEEE Trans Biomed Eng 40:1201-1209.

Schiefer MA, Triolo RJ, Tyler DJ (2008) A model of selective activation of the femoral nerve with a flat interface nerve electrode for a lower extremity neuroprosthesis. IEEE Trans Neural Syst Rehabil Eng 16:195-204.

Shapiro MG, Homma K, Villarreal S, Richter CP, Bezanilla F (2012) Infrared light excites cells by changing their electrical capacitance. Nat Commun 3:736.

Tyler DJ, Durand DM (2002) Functionally selective peripheral nerve stimulation with a flat interface nerve electrode. IEEE Trans Neural Syst Rehabil Eng 10:294-303.

Wang J, Borton DA, Zhang J, Burwell RD, Nurmikko AV (2010) A neurophotonic device for stimulation and recording of neural microcircuits. Conf Proc IEEE Eng Med Biol Soc 2010:2935-2938.

Wells J, Kao C, Mariappan K, Albea J, Jansen ED, Konrad P, Mahadevan-Jansen A (2005) Optical stimulation of neural tissue in vivo. Optics Letters 30:504-506.

Wells J, Kao C, Konrad P, Milner T, Kim J, Mahadevan-Jansen A, Jansen ED (2007) Biophysical mechanisms of transient optical stimulation of peripheral nerve. Biophysical Journal 93:2567-2580.

APPENDIX A

PARAMETRIC EXPLORATION: UNPUBLISHED RESULTS

Austin R. Duke

Vanderbilt University, Department of Biomedical Engineering

Nashville, TN

A.1 Abstract

The following work consists of unpublished results related to the exploration of available parameters for hybrid electro-optical stimulation. Specifically, these experiments were designed to investigate the relationship between the relative timing and duration of the optical and electrical stimuli.

A.2 Background and motivation

The relative timing and pulse durations of the optical and electrical stimuli are pertinent to both the parametric optimization of hybrid electro-optical stimulation and the elucidation of its mechanism. In feasibility experiments, threshold radiant exposures for hybrid stimulation were determined for optical stimuli delivered 0-2.5 ms after the electrical stimulus, while both pulse durations were kept constant at 2 ms (Duke et al., 2009). The results showed that threshold radiant exposures increased linearly for optical stimuli delayed up to 1 ms after the start of the electrical stimulus; however beyond a 1 ms delay, threshold radiant exposures were no different than those for INS alone. In this initial study, threshold radiant exposures for optical stimuli delivered prior to the electrical stimulus were not investigated, nor were the effects of varying pulse durations.

It is reasonable to assume that threshold radiant exposures for hybrid stimulation will trend differently when the optical stimulus is delivered before, rather than after the electrical stimulus. The membrane's response to a sub-threshold electrical stimulus lasts for only a few milliseconds, implying that the optical and electrical stimuli will act independently if the optical stimulus is delayed more than approximately 1 ms after the electrical stimulus. However, INS is a thermally mediated process with a thermal

relaxation time constant that is relatively long when compared to the pulse durations of the stimuli ($\tau \sim 90$ ms) (Wells et al., 2007). Thus, a sub-threshold optical pulse could potentially be delivered several milliseconds before the sub-threshold electrical stimulus and still achieve hybrid excitation.

The effects of pulse duration for optical and electrical stimuli have been investigated for each modality independently, but not in the context of hybrid stimulation. There is conflicting evidence as to whether optical pulse duration affects stimulation thresholds for INS. In the rat sciatic nerve, INS threshold radiant exposures were not significantly different for pulse durations ranging from 5 μs to 5 ms (Wells et al., 2007). However, in the gerbil cochlea, threshold radiant exposures were found to increase when pulse durations were increased from 35 μs to 1 ms (Izzo et al., 2007). For electrical stimulation, increasing the duration of sub-threshold depolarizing pre-pulses was found to decrease the excitability of the neuron due to inactivation of the sodium channels (Grill and Mortimer, 1997).

This study was designed to test the effects of optical and electrical pulse timing and duration related to hybrid nerve stimulation in the experimentally tractable *Aplysia californica* buccal nerve.

A.3 Materials and Methods

Aplysia californica (n = 8) weighing 210 - 370g (Marinus Scientific, Long Beach, CA) were maintained in an aerated aquarium containing circulating artificial seawater (ASW) (Instant Ocean; Aquarium Systems, Mentor, OH) kept at 16-17 °C. The animals were fed dried seaweed every 1 - 3 days.

Aplysia preparation followed methods described previously (Duke et al., 2012). Briefly, *Aplysia* were anesthetized with an injection of 333 mM $MgCl_2$ (50% of body weight) and the buccal ganglia were removed, pinned in a recording dish and immersed in *Aplysia* saline. For each experiment, the nerve of interest (either buccal nerve 2 (BN2), or buccal nerve 3 (BN3)) was anchored in place by pinning the protective sheath around the nerve to the Sylgard® base (Dow Corning, Midland, MI) of the recording dish. Once securely pinned, the nerve to be investigated was suctioned into a polyethylene nerve-recording electrode (1.27 mm outer diameter flame-pulled to desired thickness; PE90; Becton Dickinson) to monitor the response to stimulation Recording electrodes were suction-filled with *Aplysia* saline prior to suctioning of the nerve. Nerve signals were amplified (x1000) and band-pass filtered (300 – 500 Hz) using an AC-coupled differential amplifier (model 1700; A-M Systems), digitized (Axon Digidata 1440A; Molecular Devices, Sunnyvale, CA) and recorded (Axograph X; Axograph Scientific).

A.3.1 Hybrid stimulation

Extracellular stimulating electrodes were made from thin-wall borosilicate capillary glass (catalogue #615000; A-M Systems, Everett, WA) pulled to resistances of about 0.2 MΩ (PP-830; Narishige). For each *Aplysia* experiment, two electrodes were capillary filled with *Aplysia* saline and placed on either side of the nerve in contact with the nerve sheath. This created a bipolar stimulus, with the pipettes oriented transverse to the longitudinal axis of the nerve. Pipettes were positioned such that their angle of approach to the nerve was as shallow as was allowed by the edge of the recording dish. Biphasic currents (cathodic first; 50 μs phase separation) were supplied by a bipolar

stimulus isolator (A365R; WPI) and passed between the two pipettes. For all experiments, electrical stimulation current was set to 90% of threshold where electrical stimulation threshold was defined as the minimum current that would yield 5 consecutive evoked potentials in response to pulsed stimuli.

A diode laser was used for optical stimulation (Capella; Lockheed-Martin-Aculight, Bothwell, WA). The wavelength was set to λ = 1450 nm, which provides similar absorption in water when compared to other wavelengths used for INS (Hale and Querry, 1973). The advantage of this laser for these experiments is that it provides 5X the optical power of Capella lasers operating at other wavelengths. This allows for sufficient optical pulse energies with much shorter durations than would be possible with less powerful lasers. The output of the laser was coupled into a flat-polished 200 μm diameter optical fiber (NA = 0.22; Ocean Optics, Dunedin, FL). For each experiment, the tip of the optical fiber was immersed in the *Aplysia* saline bath and brought into contact with the nerve sheath. The optical fiber was then slowly retracted with a micromanipulator and gently translated back and forth transverse to the nerve until the optical fiber was just out of contact with the nerve sheath. For radiant exposures presented in this study, the laser-irradiated area is assumed to be a circular spot on the incident surface of the nerve sheath having diameter equal to that of the optical fiber (i.e. 0.0314 mm^2 for a 200 μm). For simplicity, as the optical fiber is just out of contact with the nerve sheath, this assumes no divergence of the beam from the tip of the optical fiber to incident surface of the nerve sheath. A pyroelectric energy detector (PE50BB-SH-V2, Ophir Optronics Ltd.) was used to measure pulse energies from the tip of the optical fiber.

All nerve stimulation was coordinated through computer software (AxoGraph X; AxoGraph Scientific, Sydney, Australia) and applied at a repetition rate of 2 Hz. For each experiment, electrical pulse durations were set using Axograph while optical pulse durations were set with the laser hardware. The timing of the pulses was established using the Axograph stimulus protocol. Nerve recordings were triggered and acquired for 10 ms prior to stimulation through 140 ms post stimulation.

A.3.2 Relative pulse timing

Pulse durations for the optical stimuli and each phase of the electrical stimuli were set to 250 μs. Optical stimuli were delivered at various time points before and after the start of the electrical stimuli, where the start of each electrical stimulus was designated as time t = 0. The timing of the optical stimuli covered a range extending from t = -20 ms to t = 0.5 ms. For each trial, the optical pulse was randomly set to a time within this range and hybrid stimulation consisting of 5 radiant exposures with 10 pulses each was applied. At least 3 trials for each timing scheme were repeated in each nerve (n = 6 nerves). The response to each hybrid stimulus was then evaluated and scored for the presence (1) or absence (0) of an evoked response. For each radiant exposure within a given timing scheme, the number of ones was divided by the sum of ones and zeros to achieve a probability of firing. The cumulative distribution function (CDF) of the standard normal distribution:

$$F(x;\mu,\sigma^2) = \frac{1}{2}\left[1 + \operatorname{erf}\left(\frac{x-\mu}{\sigma\sqrt{2}}\right)\right], x \in R \tag{A-1}$$

where x is a random variable with mean m and variance s^2, was then fit to the data to determine the radiant exposure yielding 50% probability of firing (RE_{50}).

A.3.3 Relative pulse duration

To test the effects of pulse duration, either the optical or electrical pulse duration was fixed while the other was varied. Stimuli were timed such that the optical pulse ended at the same time as the first phase of the electrical stimulus, allowing for the total charge and total thermal deposition to occur simultaneously. For varying optical pulse durations, each phase of the electrical stimulus was set to 100 μs while the optical pulse duration was varied between 100 and 3000 μs (n = 4 nerves). For varying electrical pulse durations, the optical stimulus was set to 250 μs, while the electrical pulse duration was varied from 50 - 250 μs (n = 5 nerves). RE_{50} values were determined as described above.

A.4 Results

A.4.1 Relative pulse timing

Optical stimuli were delivered over a range extending from 20 ms before to 0.5 ms after the start of a biphasic electrical stimulus. Radiant exposures up to 3.34 J/cm^2 were used to determine the RE_{50} value for a given timing scheme. Figure A-1 shows the RE_{50} value for each optical pulse timing. RE_{50} values are plotted as the percent change in radiant exposure from the RE_{50} at t=0 (i.e. stimuli delivered simultaneously).

Limited success with hybrid stimulation was observed for optical pulses delivered after the electrical stimulus. None of the six nerves tested exhibited successful hybrid

stimulation when the optical stimulus was delayed by only 0.5 ms relative to the start of the electrical stimulus. Here, successful hybrid stimulation is defined as a CDF fit of the data with $R^2 \geq 0.85$. Five nerves showed successful hybrid stimulation when optical pulses were delayed up to 0.125 ms relative to the electrical stimulus and three were successful for delays up to 0.25 ms. The two nerves that showed no hybrid stimulation beyond 0.125 ms also exhibited a steep increase in radiant exposure (>100% increase). In contrast, with the optical stimulus delivered 3 ms before the electrical stimulus, all six nerves showed successful hybrid stimulation. Five of the six showed successful stimulation for optical stimuli delivered 10 ms prior to the electrical stimuli and two were successful when delivered as much as 20 ms before their corresponding electrical stimulus.

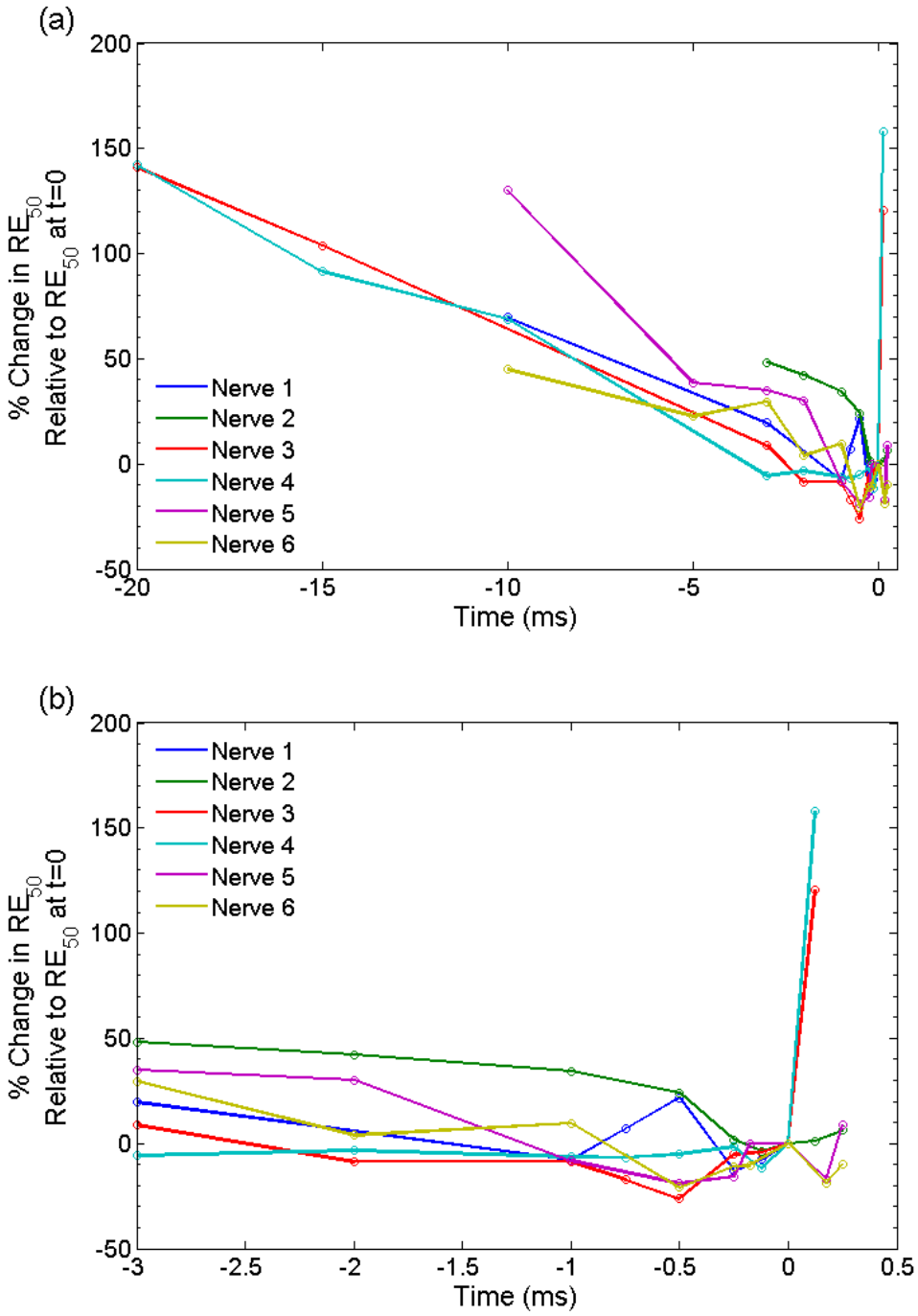

Figure A-1. Effect of pulse timing on RE_{50} for hybrid electro-optical stimulation. The RE_{50} was determined for optical stimuli delivered at various times relative to the start of their corresponding electrical stimulus. (a) shows the percent change in RE_{50} for various timing schemes relative to the RE_{50} when the stimuli were delivered simultaneously (i.e. t = 0 ms). (b) is the same as (a) with focus on times between -3 ms and 0.5 ms.

A general trend reflected in the data is that the RE_{50} rises when the optical stimulus is delivered before or after the electrical stimulus. However, this trend does not hold for all timing schemes. When the optical stimulus was delivered 0.25 ms before the electrical stimulus, all of the nerves showed ≤2% increase and 5/6 nerves showed a reduction in RE_{50} when compared to the RE_{50} at t=0. With the optical stimulus delivered 1 ms prior to the electrical stimulus, four nerves still showed a reduction in RE_{50}. Not until the optical stimulus was delivered >3ms before the electrical stimulus did all six nerves exhibited a consistent rise in RE_{50}. The minimum RE_{50} for half of the nerves actually occurred when the optical stimulus was delivered 0.5 ms before the electrical stimulus, rather than when the stimuli were delivered simultaneously. Three nerves also showed no change or reduced RE_{50} values for optical stimuli delivered up to 0.25 ms after the electrical stimulus.

A.4.2 Relative pulse duration

The effects of pulse duration on RE_{50} are shown in Figure A-2. Figure A-2a depicts the effects of varying the optical pulse duration while keeping the electrical pulse duration constant at 100 μs. The results indicate no statistically significant change ($p>0.05$) in RE_{50} between optical pulse durations over the range of 100 μs to 3000 μs. Figure A-2b shows how the RE_{50} changes as the electrical pulse duration is varied between 50 μs and 250 μs while the optical pulse duration is kept constant at 250 μs. Pulse durations longer than 100 μs resulted in an increase in RE_{50}. A statistically significant increase ($p<0.05$) in RE_{50} was observed for electrical pulse duration of 250 μs when compared to 50 - 100 μs pulse durations.

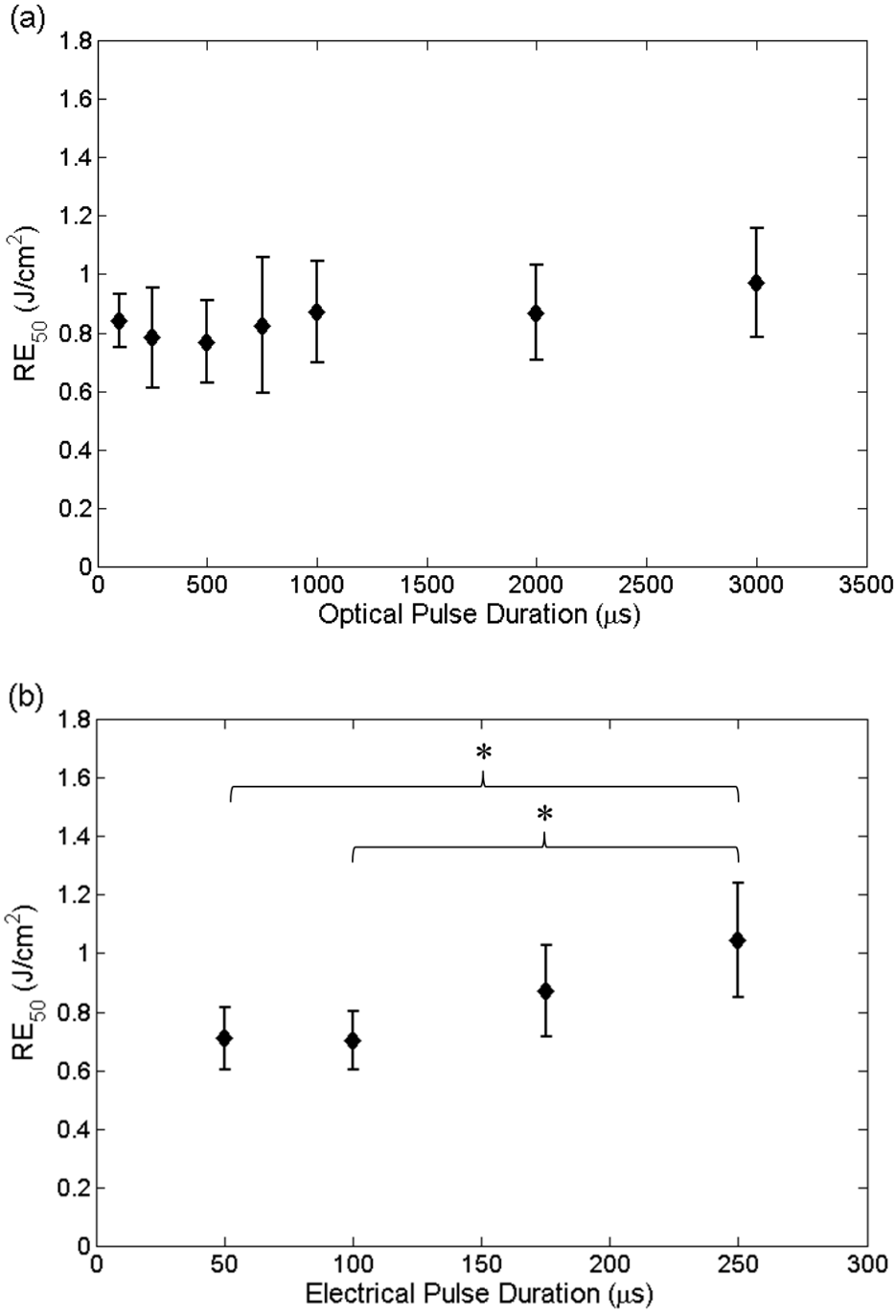

Figure A-2. Effect of pulse duration on RE_{50} for hybrid electro-optical stimulation. (a) While maintaining the electrical pulse duration at 100 μs, increasing the optical pulse duration from 100 μs to 3000 μs showed no change in RE_{50}. (b) With optical pulse duration maintained at 250 μs, increasing the electrical pulse duration from 50 μs to 250 μs yielded an increase in RE_{50} for 100 μs and 250 μs pulse durations. *: $p<0.05$.

A.5 Discussion

The intent of this study was to identify, in the experimentally tractable *Aplysia* buccal nerve, a relationship between radiant exposures for hybrid stimulation and the relative timing and pulse durations of the optical and electrical stimuli. These experiments build upon previous results (Duke et al., 2009) and will contribute to both the parametric optimization and mechanism elucidation for hybrid electro-optical stimulation.

The results of this study indicate a stark difference between hybrid stimulation RE_{50} for optical stimuli delivered before and after their corresponding electrical stimulus (Figure A-1). For optical pulses delivered after the electrical pulse, hybrid stimulation was successful as long as there was some overlap between the 250 μs optical pulse and the 250 μs cathodic phase of the electrical pulse. However, when the optical pulse was delivered more than 250 μs after the start of the electrical pulse, hybrid stimulation was completely ineffective and an RE_{50} was not possible to identify. There are two potential explanations for why this was observed: (1) the membrane's response to sub-threshold electrical stimulation lasts for only a few milliseconds and is back to its resting potential before the optical stimulus is delivered; and (2) the anodic phase of the electrical stimulus negates the effects produced by the cathodic phase, counteracting the contributions of the optical stimulus. Repeating this study with a monophasic electrical stimulus will test this second explanation and may increase the time by which the optical stimulus can be delayed. In contrast, the optical stimulus may be delivered many milliseconds prior to the electrical stimulus and still be effective. This result aligns with the thermal/capacitive mechanism of INS. Infrared absorption leads to membrane capacitance changes

associated with increased temperatures. Depolarizing membrane potentials resulting from these infrared-evoked membrane capacitance changes were shown to last for tens to hundreds of milliseconds (Shapiro et al., 2012). Previously it was suggested that the sub-threshold electrical stimulus depolarizes the membrane, effectively lowering the threshold for optical stimulation (Duke et al., 2009). The results presented here, however, suggest an alternative explanation whereby the optical stimulus creates a transient temperature increase that reduces the threshold for electrical stimulation.

This study is the first time that optical and electrical pulse durations for hybrid stimulation were systematically evaluated. For constant electrical pulse duration, increasing the optical pulse duration from 100 μs to 3000 μs was shown to have no significant effect on the RE_{50} (Figure A-2a). This is a similar result to what was published by Wells et al. for INS alone (Wells et al., 2007). These results suggest that it is indeed a rise in temperature that is most important for hybrid stimulation. Because all the pulse durations tested in this study were much shorter than the thermal diffusion time (van Gemert and Welch, 1989, Wells et al., 2007), it is expected that they each produced the same rise in temperature for the corresponding RE_{50} identified in Figure A-2a. What remains to be seen is whether it is the baseline temperature rise or the temperature gradient that matters most. Increasing the pulse duration may provide insight into this matter; however, pulse durations will eventually reach a point where thermal diffusion, rather than the thermal gradient, will cause an increase in RE_{50}.

For constant optical pulse duration, increasing the electrical pulse duration was found to increase the RE_{50}. Grill and Mortimer demonstrated that an electrical pre-pulse having magnitude equal to 95% of threshold reduces stimulation currents for a

subsequent pulse; however, increasing the duration of the electrical pre-pulse decreased its effect (Grill and Mortimer, 1997). Their results were explained by the time constants of the Hodgkin-Huxley sodium activation (**m**) and inactivation (**h**) gating parameters. The time constant for the activation parameter is much shorter than that for the inactivation parameter, allowing **m** to increase before **h** has time to decrease. For longer duration pre-pulses, the inactivation parameter is able to counterbalance the activation parameter, preventing or reducing the enhanced excitability observed with shorter duration pulses. This phenomenon is known as accommodation, where sodium channel inactivation results in a reduction in the number of axons available to be recruited, thus increasing stimulation threshold (Merrill et al., 2005). This effect may also explain the results observed in this study.

The results of this study indicate that the minimum hybrid stimulation RE_{50} will likely occur for an optical pulse duration of 250-500 μs and electrical pulse duration of 50-100 μs. A full parametric optimization is required to confirm these results; however, the data presented here provide a reference point from which to start.

A.6 References

Duke AR, Cayce JM, Malphrus JD, Konrad P, Mahadevan-Jansen A, Jansen ED (2009) Combined optical and electrical stimulation of neural tissue in vivo. Journal of Biomedical Optics 14:060501-060503.

Duke AR, Lu H, Jenkins MW, Chiel HJ, Jansen ED (2012) Spatial and temporal variability in response to hybrid electro-optical stimulation. Journal of Neural Engineering 9:036003.

Grill WM, Mortimer JT (1997) Inversion of the current-distance relationship by transient depolarization. IEEE Trans Biomed Eng 44:1-9.

Hale GM, Querry MR (1973) Optical Constants of Water in the 200-nm to 200-microm Wavelength Region. Appl Opt 12:555-563.

Izzo AD, Walsh JT, Jr., Jansen ED, Bendett M, Webb J, Ralph H, Richter CP (2007) Optical parameter variability in laser nerve stimulation: a study of pulse duration, repetition rate, and wavelength. IEEE Trans Biomed Eng 54:1108-1114.

Merrill DR, Bikson M, Jefferys JG (2005) Electrical stimulation of excitable tissue: design of efficacious and safe protocols. J Neurosci Methods 141:171-198.

Shapiro MG, Homma K, Villarreal S, Richter CP, Bezanilla F (2012) Infrared light excites cells by changing their electrical capacitance. Nat Commun 3:736.

van Gemert MJ, Welch AJ (1989) Time constants in thermal laser medicine. Lasers Surg Med 9:405-421.

Wells J, Kao C, Konrad P, Milner T, Kim J, Mahadevan-Jansen A, Jansen ED (2007) Biophysical mechanisms of transient optical stimulation of peripheral nerve. Biophysical Journal 93:2567-2580.

APPENDIX B

OPTICAL PACING OF THE EMBRYONIC HEART

Michael W. Jenkins[1], Austin R. Duke[2], Shi Gu[1], Hillel J. Chiel[3], Hisashi Fujioka[4], Michiko Watanabe[5], E. Duco Jansen[2] and Andrew M. Rollins[1]

[1]Department of Biomedical Engineering, Case Western Reserve University

Cleveland, OH

[2]Department of Biomedical Engineering, Vanderbilt University

Nashville, TN

[3]Department of Biology, Case Western Reserve University

Cleveland, OH

[4]Department of Pharmacology, Case Western Reserve University

Cleveland, OH

[5]Department of Pediatrics, Case Western Reserve University

Cleveland, OH

B.1 Abstract

Light has been used to noninvasively alter the excitability of both neural and cardiac tissue (Gimeno et al., 1967, Fork, 1971, Nathan et al., 1976, Balaban et al., 1992, Allegre et al., 1994, Hirase et al., 2002, Wells et al., 2005a, Wells et al., 2005b, Wells et al., 2007a, Smith et al., 2008). Recently, pulsed laser light has been shown to be capable of eliciting action potentials in peripheral nerves and in cultured cardiomyocytes (Wells et al., 2005a, Wells et al., 2005b, Wells et al., 2007a, Smith et al., 2008). Here, we demonstrate for the first time optical pacing (OP) of an intact heart *in vivo*. Pulsed 1.875 μm infrared laser light was employed to lock the heart rate to the pulse frequency of the laser. A laser Doppler velocimetry (LDV) signal was used to verify the pacing. At low radiant exposures, embryonic quail hearts were reliably paced *in vivo* without detectable damage to the tissue, indicating that OP has great potential as a tool to study embryonic cardiac dynamics and development. In particular, OP can be utilized to control the heart rate, and thereby alter stresses and mechanically transduced signaling.

B.2 Scientific Letter

The avian embryo is an important model for studying the mechanisms driving normal development and the abnormalities leading to congenital defects. The embryonic heart is one of the first organs to develop and in avian models begins beating at around 40 hours of incubation. The progression of a single heart tube into a four-chambered heart (cardiac looping) is shaped by mechanical stimuli from the flowing blood and pumping heart which influence molecular and cellular responses that regulate development (Bartman and Hove, 2005, Poelmann et al., 2008, North et al., 2009, Pardanaud and

Eichmann, 2009). Much remains unknown about the mechanisms of cardiac looping, in part because of a lack of suitable non-destructive tools with which to study the minute (< 2 mm) organ. In the adult heart, the exquisite control achievable using electrical pacing has been critical to advancing our understanding of cardiac electrophysiology. Unfortunately, electrical pacing of the embryonic heart is invasive and difficult to achieve consistently and without tissue damage. A simple noninvasive technique to control heart rate would allow one to manipulate forces applied to cells in early developing embryos, enabling a new class of experiments exploring the roles of mechanotransduction and electrical activation.

It has been previously shown that ultraviolet and visible light can noninvasively increase the excitability of neuronal and myocardial cells (Gimeno et al., 1967, Fork, 1971, Nathan et al., 1976). In particular, Gimeno *et al* demonstrated that exposure to visible light accelerated the heart rate in the early chick embryo (Gimeno et al., 1967). More recently, Smith *et al* employed focused femtosecond pulses (780 nm) from a Ti:Sapphire laser to induce paced contractions in individual and small groups of cardiomyocytes with success rates up to 60% (Smith et al., 2008). Unfortunately, the high-powered pulses produce reactive oxygen species that can damage the cell, and optically pacing an entire heart is not currently possible with this method. In 2005, Wells *et al* demonstrated that pulsed infrared light could reliably elicit compound action potentials in mammalian peripheral nerves in a one-to-one fashion at radiant exposures well below the damage threshold (Wells et al., 2005a, Wells et al., 2005b, Wells et al., 2007b). The stimulation threshold paralleled the inverse water absorption curve with ~2 μm light producing the highest damage-to-stimulation threshold ratio. Although the

mechanism is not well understood, it has been suggested that temperature gradients caused by infrared light absorption open ion channels (Wells et al., 2007a). To date, comparable pulsed infrared laser stimulation of cardiomyocytes or cardiac tissue has not been demonstrated. Here, we describe the use of pulsed infrared light to pace hearts of intact quail embryos, suggesting a promising new tool for studying embryonic cardiac dynamics and development.

Figure B-1 shows the experimental setup. A pulsed infrared diode laser (λ=1.875 μm; Capella^{TM}, Lockheed Martin Aculight) centered at 1875 nm coupled light into a 400 μm core multimode fiber. A micromanipulator positioned the fiber in close proximity to (500 μm), but not in contact with the embryo (see Figure B-1A), illuminating an area of approximately 0.3 mm^2 on the inflow region of the heart tube. The stimulation laser employed a red HeNe laser coupled into the same fiber for aiming, which allowed precise positioning of the stimulation pulses. The optical power of the HeNe laser light illuminating the sample was low (0.9 mW) and the sample was illuminated only briefly (< 10 s) in order to position the fiber. The stimulation laser trigger signal was recorded to document the timing and duration of the stimulation pulses. A laser Doppler velocimeter (LDV, Moor Instruments Ltd.) was used to monitor the heartbeat of the embryos. The LDV probe was positioned approximately 1 mm from the heart with a micromanipulator (see Figure B-1A). The LDV signal was only intended for heartbeat detection; therefore, the LDV probe was not oriented identically with every heart, so no significance should be drawn from the shape of the LDV signals. The trigger from the laser was also directed to a white light emitting diode (LED), which flashed on and off with the pulsing of the laser

and was visible under a video microscope. The output of the video microscope was recorded by a laptop computer for real-time guidance and documentation.

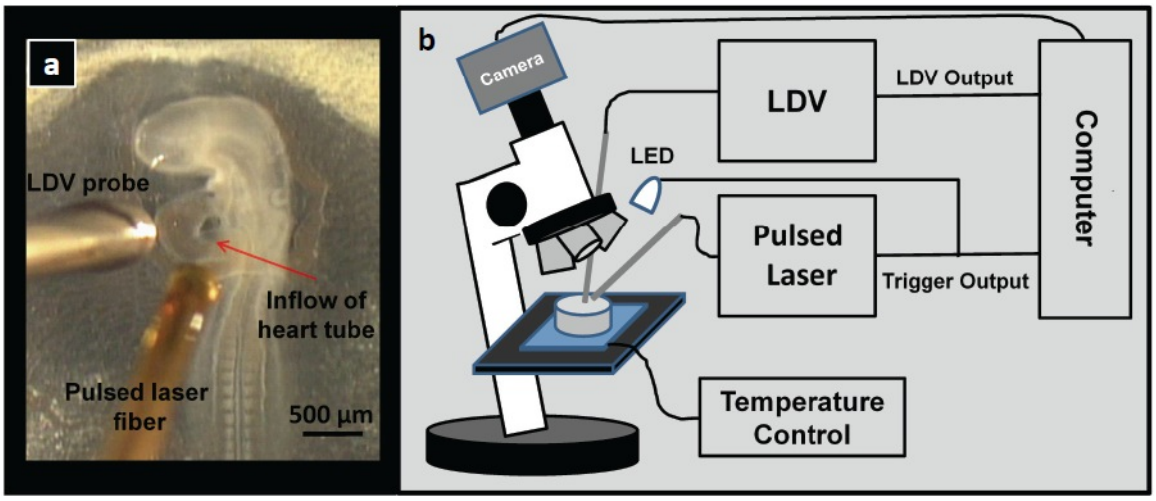

Figure B-1. Optical pacing setup. a, Photograph of a 53 hour quail embryo in the New culture. b, Block diagram of the setup of the optical pacing experiment. Embryos in the Petri dish under the microscope were stimulated by a pulsed infrared laser, while a laser Doppler velocimeter probe measured blood flow. The LDV output and trigger pulse from the laser were recorded to verify pacing. Also, the trigger pulse from the laser activated a white light LED which was observable in the video. The video output from the microscope camera was recorded at video rate (29.97 fps) by a laptop computer.

Figure B-2 demonstrates optical pacing of an embryonic heart using a pulsed laser. The spikes in the blue traces represent when the laser was emitting light, while the red traces show the heart rate of the embryo. Figure B-2a presents a recording from a stage 17 quail embryo in a New culture paced at 2 Hz. The dashed box in Figure B-2a is expanded for a close up view in Figure B-2b. Clearly the laser pulse and heart rate are synchronized with each laser pulse eliciting a heartbeat. In Figure B-2a, the time interval between successive heartbeats before laser stimulation was 1.58±0.038 s (0.634 Hz) and the interval decreased to 0.4996±0.017 s (2.004 Hz) during pacing. After the stimulation pulses ceased and the heart rate stabilized the time interval between heartbeats increased to 1.44±0.042 s (0.693 Hz). At this point it is not known why the heart rate was slightly higher after pacing than before, but a similar increase occurred in most of the embryos tested. Although we cannot rule out damage, a physiological explanation for the post-pacing rate increase could be enhanced calcium ion influx during pacing. Figure B-2c exhibits the heart beating in synchrony with the laser pulses as the frequency of the pulses is changed between 2 and 3 Hz.

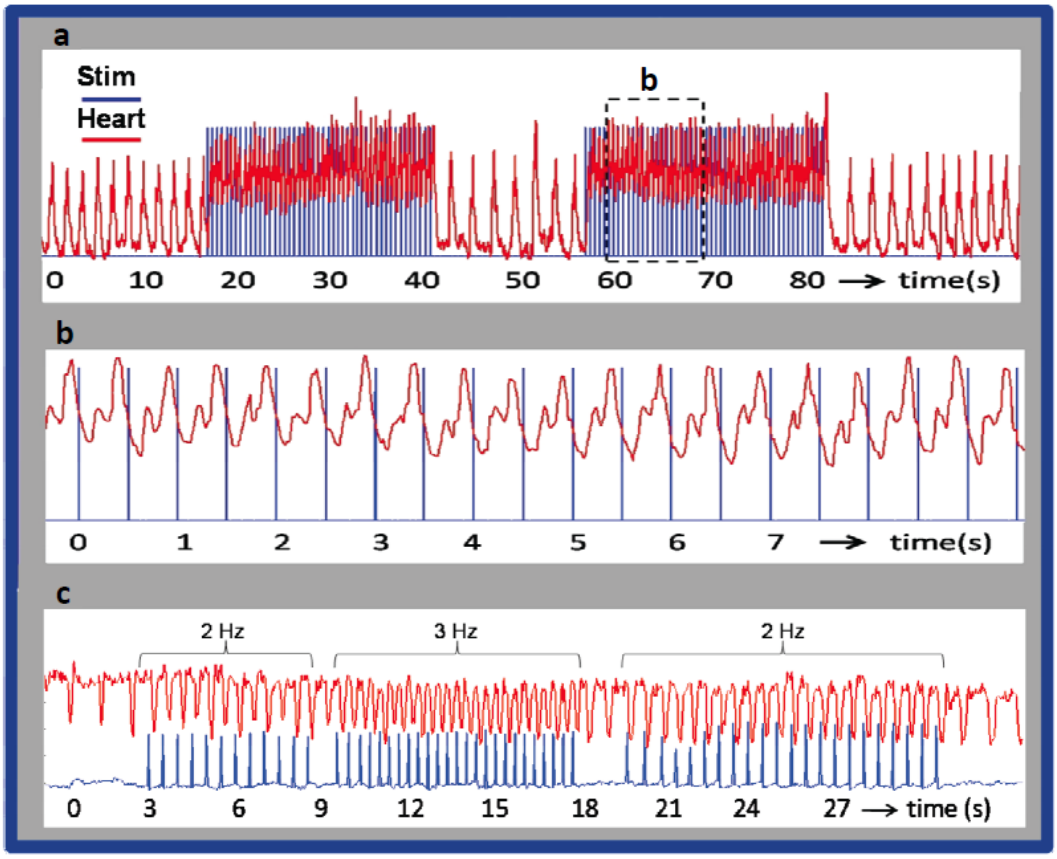

Figure B-2. Optical pacing of the embryonic quail heart. The trigger pulse (blue) from the pulsed laser is superimposed on the LDV recordings (red) of heart rate. (a) presents a recording from a stage 17 (59 hour) quail embryo in a New culture paced at 2 Hz. The laser pulse duration was 1 ms and the radiant exposure was 0.92 J/cm^2 per pulse. The laser pulses were directed toward the inflow region of the heart tube. The laser pulses were turned on and off several times to demonstrate the robustness of optical pacing. The heart rate increased from 0.634 to 2 Hz when the stimulation laser pulses were started and decreased to 0.693 Hz by the end of the trace in 2a. (b) The dashed box in 2a is expanded for a close up view in 2b. Clearly the trigger pulse and LDV signal were synchronized with each laser pulse eliciting a heartbeat. (c) presents a recording from a stage 14 (53 hour) quail embryo in a New culture. The laser pulse duration was 2 ms and the radiant exposure was 0.84 mJ/cm^2 per pulse. The frequency of the laser pulses were varied from 2 Hz to 3 Hz and back to 2 Hz to demonstrate the ability of the embryo heart to follow the pulse frequency. Laser stimulation (blue) and heart rate (red) traces were calculated from the video by plotting the pixel intensity of LED flashes triggered by the laser and intensity at the edge of the heart wall.

The radiant exposure threshold required to pace a day 2 embryonic quail heart in a New culture was determined by subjecting each embryo to a different radiant exposure level and noting whether pacing had occurred. Successful pacing was defined as one to one stimulation, laser pulse to heartbeat, over a twenty second interval. 25 embryos were tested and the results were fit to a normal cumulative distribution function as shown in Figure B-3. The threshold (50% probability point) was 0.81+/-0.01 J/cm^2 with a t-value of 79.9 and 95% confidence interval between 0.794 and 0.836 J/cm^2. The standard deviation of the distribution was 0.036+/-0.016 with a t-value of 2.32. In a shorter study we demonstrated that OP is feasible in embryos cultured on the yolk (see supplemental material). This method of embryo culture is compatible with longer viability of the embryos and would be useful for following long term effects of OP.

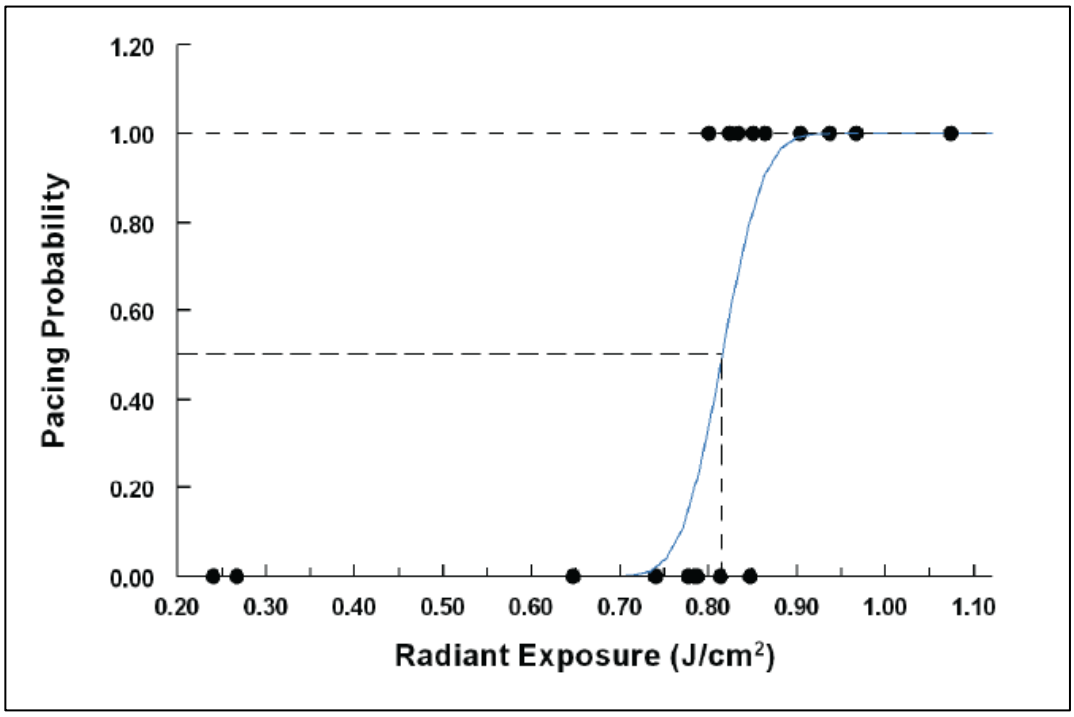

Figure B-3. Optical pacing threshold measurement. 25 embryos in New cultures were exposed to varying radiant exposures and the results were plotted in terms of pacing probability (successful pacing = 1, unsuccessful pacing = 0). The data were fit to a normal cumulative distribution function (blue line). The threshold (50% probability point) was 0.81+/-0.01 J/cm^2 with a t-value of 79.9 and 95% confidence interval between 0.794 and 0.836 J/cm^2. The standard deviation of the distribution was 0.036+/-0.016 with a t-value of 2.32.

Several approaches were used to determine if optical pacing damaged the embryo. Standard transmission electron microscopy (TEM) was employed to examine the ultrastructural detail of cardiomyocytes in the inflow region of the heart tube where the laser was aimed. Figure B-4a-c represent a control embryo (same experimental protocol, but no light exposure), an embryo paced slightly above threshold (0.88 J/cm^2) and an embryo paced well above threshold (4.33 J/cm^2). In hearts paced well above threshold, the mitochondria are vacuolated and the nuclear envelope and rough endoplasmic reticulum are slightly expanded, whereas the ultrastructure of the cardiomyocytes of embryos paced slightly above threshold looked similar to that of the controls. In all three examples several regions of the heart tube were examined in detail to look for anomalies and no clear indications of cellular damage were identified in the embryo paced slightly above threshold. Some subtle abnormalities in the mitochondrial cristae, small spaces within the cristae, are present in the control and threshold embryo and are likely the result of necessary embryo manipulations during harvest prior to fixation. Other damage assays showed no structural damage to embryo heart cardiomyocytes paced at threshold levels (supplemental material). At this point we did not detect evidence of damage resulting from optical pacing, but further study is warranted.

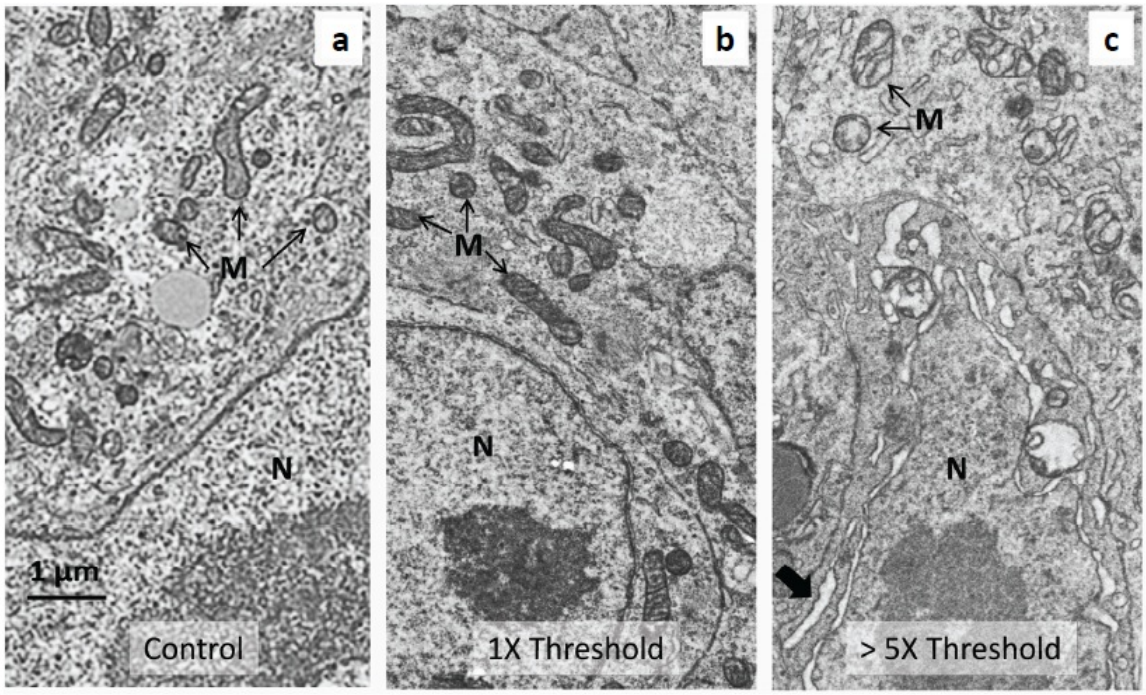

Figure B-4. Transmission electron microscopy after the optical pacing procedure. The transmission electron microscopy (TEM) images show a typical cardiomyocyte in the inflow (sinoatrial) region of the heart tube of three different quail embryos, where laser light was directed. Each embryo was between 52 to 58 hours of development. The torso of each embryo was excised and fixed immediately after OP. a, Control embryo. The embryo was exposed to the OP experimental procedure, except that the pacing laser was not turned on during the experiment. b, Embryo paced slightly above threshold. The embryo heart was paced for approximately 20 seconds with 2 ms pulses (2.64 mJ/pulse) at 2 Hz. c, Embryo paced well above threshold. The embryo heart was paced for approximately 20 seconds with 4 ms pulses (13 mJ/pulse) at 2 Hz. The micrograph image was taken from a border region separating severely damaged tissue (partially ablated) from apparently healthy tissue. The mitochondria are vacuolated and the nuclear envelope is swollen, as are elements of the rough ER (large arrow). The cells and mitochondria in 4a and b have a similar appearance and show no signs of damage from the pulsed laser light. Some subtle abnormalities in the cristae present in cells from both threshold paced and unpaced control hearts are due to the unavoidable delay in excising the embryonic torso. N - nucleus, M - mitochondria.

The mechanism of the observed phenomenon is at this point unclear. However, given the laser parameters used (wavelength, pulse duration and peak power), some inferences can be drawn. Gimeno et al used continuous visible light to increase the heart rate with maximum effect at 475 nm (photon energy = 2.61 eV) (Gimeno et al., 1967). Proposed mechanisms included acetylcholine sensitivity to light and inhibition of ATPase. In a different study, Smith et al showed that a focused near-infrared femtosecond laser caused contraction in cultured neonatal rat cardiomyocytes (Smith et al., 2008). A window for this effect was found to occur between 15 and 30 mW average power for an 80 fs, 82 MHz pulse train of 780 nm, using 8 ms exposures applied periodically at 1 to 2 Hz. Mechanistically this effect was attributed to the laser-induced release of intracellular calcium which has been shown in various cell types for these laser parameters. In contrast, our study used near infrared pulses (λ = 1,870 nm) and relatively long (ms) pulses of continuous laser light. Thus the photon energy (0.66 eV) is insufficient to directly drive photochemistry as was the case in Gimeno's work and the irradiance (W/cm^2) is too low for multiphoton effects as in Smith's work (irradiance from the fs pulses and diffraction limited spot size is roughly 8 orders of magnitude higher than we used). It is more likely that the mechanisms responsible for the effects seen in our study align with those described by Wells et al, who used identical laser parameters in the rat sciatic nerve and concluded that the laser-induced spatio-temporal temperature gradient was responsible for the induction of action potentials (APs) in excitable tissues (Wells et al., 2005a, Wells et al., 2007a). It has been shown that non-absorbing wavelengths with otherwise similar parameters do not result in APs in the peripheral nerve and pulse durations that violate the conditions of thermal confinement are similarly

unable to induce APs. We have shown here and in previous studies that optical stimulation with these laser parameters is feasible without inducing thermal damage (Wells et al., 2007b). The question of how the laser-induced thermal gradient ultimately results in the opening of ion channels remains unanswered although several hypotheses are currently under investigation.

Here, we have demonstrated a noninvasive method to pace embryonic hearts with pulsed infrared light. Compared to electrical pacing, OP does not require contact, has high spatial precision and avoids stimulation artifacts in electrode recordings. OP was consistently achieved with quail embryos ranging from stage 12 to stage 18 (looped heart stages prior to septation) in both New cultures and cultured on the yolk at radiant exposures well below levels at which damage was apparent. In the future we will make use of OP together with advanced imaging to study mechanotransduction (i.e. shear stress on the endocardium) by controlling the heart rate of the embryo, thereby manipulating mechanical stress (Jenkins et al., 2007, Jenkins et al., 2008, Gargesha et al., 2009, Jenkins et al., 2009). OP will not only enable a new class of experiments in developmental cardiology, but also may become a useful tool for investigating cardiac electrophysiology, single-cell (cardiomyocyte) dynamics, and cardiac tissue engineering. Furthermore, OP may potentially be capable of pacing the adult heart, which could lead to clinical applications.

B.3 Methods

B.3.1 Egg preparation

Fertilized quail (Coturnix conturnix) eggs were removed between 48-60 hours post-fertilization from a humidified, forced draft incubator (38 ^{o}F). Embryos were removed from the egg and either cultured on the yolk in a sterilized 3.5 cm diameter Petri dish or cultured using the New culture in which the embryo is inverted on an egg-agar substrate (New, 1955, Darnell and Schoenwolf, 2000). The New culture fully exposes the heart, which facilitates interventions, but decreases lifespan to a few days, whereas embryos cultured on the yolk can survive through gestation. Both techniques are routinely employed in the field. Figure B-1A shows a healthy 53-hour embryo in the New culture. For pacing experiments, embryos were placed upon a temperature-controlled heating plate (ATC 1000, WPI), which maintained the temperature at 37 ^{o}C.

B.3.2 Radiant exposure calculations

Radiant exposures (J/cm^2) were calculated by dividing the pulse energies by the laser spot size. Pulse energies were measured using a pyroelectric energy meter (PE50BB, Ophir) and spot size was computed using the numerical aperture, fiber diameter and fiber distance from the tissue. Laser light was delivered to the tissue via a 400+/-8 μm - diameter flat-polished multi-mode optical fiber (Ocean Optics) having a numerical aperture of 0.22 +/- 0.02. The fiber-to-heart distance was held constant at approximately 500 μm for each trial. The tissue was assumed to be perpendicular to the fiber. While the fiber was oriented at an angle to the membrane of approximately 37

degrees from perpendicular, the curvature of the membrane covering the heart was assumed to offset the angle of the fiber sufficiently to make these effects negligible.

B.3.3 Threshold measurements

25 embryos in New cultures were tested to determine the radiant exposure level needed to induce optical pacing. To quickly find to the precise location for optimal stimulation, the laser was turned to a level slightly above threshold and the position of the fiber was optimized, which normally took less than ten seconds. The optical fiber was positioned 500 μm from the embryo. Because the LDV fiber took a significant time to accurately place, for this experiment we relied on the LED flashes and heart motion in the microscope video to determine successful pacing. After a brief waiting period (~ 1 min) with the laser off, the radiant exposure was adjusted and the laser was turned on for 20-30 seconds. Embryos were then either fixed for further experiments or discarded. For each embryo we determined whether there was successful pacing (1) or failed pacing (0) and plotted the results in Figure B-3. Some embryos took two or three beats to synchronize to the laser pulses, but were counted as successful pacing if the heart rate was consistent after the first couple beats. Conversely, if the heart followed the laser pulses, but skipped more than one beat it was scored unsuccessful. The difference between successful pacing and unsuccessful pacing was easy to distinguish by closely observing the videos.

B.3.4 TEM preparation

The torso of the embryo was excised and immediately fixed by immersion in the triple aldehyde-DMSO mixture of Kalt and Tandler (Kalt and Tandler, 1971). After

rinsing, the tissues were postfixed in ferrocyanide-reduced osmium tetroxide(Karnovsky, 1971). After again rinsing, they were soaked overnight in acidified uranyl acetate (Tandler, 1990). Thin sections were sequentially stained with acidified uranyl acetate (Tandler, 1990) followed by Sato's triple lead stain as modified by Hanaichi et al. (Hanaichi et al., 1986) and examined in a JEOL 1200 electron microscope.

B.4 References

Allegre G, Avrillier S, Albe-Fessard D (1994) Stimulation in the rat of a nerve fiber bundle by a short UV pulse from an excimer laser. Neurosci Lett 180:261-264.

Balaban P, Esenaliev R, Karu T, Kutomkina E, Letokhov V, Oraevsky A, Ovcharenko N (1992) He-Ne laser irradiation of single identified neurons. Lasers Surg Med 12:329-337.

Bartman T, Hove J (2005) Mechanics and function in heart morphogenesis. Dev Dyn 233:373-381.

Darnell DK, Schoenwolf GC (2000) In: Methods in Molecular Biology, vol. 135 (Tuan, R. S. and Lo, C. W., eds), pp 31-38: Humana Press.

Fork RL (1971) Laser stimulation of nerve cells in Aplysia. Science 171:907-908.

Gargesha M, Jenkins MW, Wilson DL, Rollins AM (2009) High temporal resolution OCT using image-based retrospective gating. Opt Express 17:10786-10799.

Gimeno MA, Robets CM, Webb JL (1967) Acceleration of rate of the early chick embryo heart by visible light. Nature 214:1014-1016.

Hanaichi T, Sato T, Iwamoto T, Malavasi-Yamashiro J, Hoshino M, Mizuno N (1986) A stable lead by modification of Sato's method. J Electron Microsc 35:304-306.

Hirase H, Nikolenko V, Goldberg JH, Yuste R (2002) Multiphoton stimulation of neurons. J Neurobiol 51:237-247.

Jenkins MW, Adler DC, Gargesha M, Huber R, Rothenberg F, Belding J, Watanabe M, Wilson DL, Fujimoto JG, Rollins AM (2007) Ultrahigh-speed optical coherence tomography imaging and visualization of the embryonic avian heart using a buffered Fourier Domain Mode Locked laser. Opt Express 15:6251-6267.

Jenkins MW, Adler DC, Gargesha M, Huber R, Chughtai OQ, Pan Y, Peterson LM, Wilson DL, Watanabe M, Fujimoto JG, Rollins AM (2008) An environmental chamber based OCT system for high-throughput longitudinal imaging of the embryonic heart. In: Bios SPIE San Jose.

Jenkins MW, Gargesha M, Peterson LM, Gui S, Webb B, Linask KK, Watanabe M, Wilson DL, Rollins AM (2009) Shear stress in the developing heart tube. In: Bios, SPIE San Francisco.

Kalt MR, Tandler B (1971) A study of fixation of early amphibian embryos for electron microscopy. J Ultrastruct Res 36:633-645.

Karnovsky MJ (1971) Use of ferrocyanide-reduce osmium tetroxide in electron microscopy. In: 11th Annual Meeting of the American Society of Cell Biology, p 146 New Orleans, LA.

Nathan RD, Pooler JP, DeHaan RL (1976) Ultraviolet-induced alterations of beat rate and electrical properties of embryonic chick heart cell aggregates. J Gen Physiol 67:27-44.

New DAT (1955) A new technique for the cultivation of the chick embryo in vitro. J Embryol Exp Morphol 3:326-331.

North TE, Goessling W, Peeters M, Li P, Ceol C, Lord AM, Weber GJ, Harris J, Cutting CC, Huang P, Dzierzak E, Zon LI (2009) Hematopoietic stem cell development is dependent on blood flow. Cell 137:736-748.

Pardanaud L, Eichmann A (2009) Stem cells: The stress of forming blood cells. Nature 459:1068-1069.

Poelmann RE, Gittenberger-de Groot AC, Hierck BP (2008) The development of the heart and microcirculation: role of shear stress. Med Biol Eng Comput 46:479-484.

Smith NI, Kumamoto Y, Iwanaga S, Ando J, Fujita K, Kawata S (2008) A femtosecond laser pacemaker for heart muscle cells. Opt Express 16:8604-8616.

Tandler B (1990) Improved uranyl acetate staining for electron microscopy. J Electron Microsc Tech 16:81-82.

Wells J, Kao C, Jansen ED, Konrad P, Mahadevan-Jansen A (2005a) Application of infrared light for in vivo neural stimulation. J Biomed Opt 10:064003.

Wells J, Kao C, Mariappan K, Albea J, Jansen ED, Konrad P, Mahadevan-Jansen A (2005b) Optical stimulation of neural tissue in vivo. Opt Lett 30:504-506.

Wells J, Kao C, Konrad P, Milner T, Kim J, Mahadevan-Jansen A, Jansen ED (2007a) Biophysical mechanisms of transient optical stimulation of peripheral nerve. Biophys J 93:2567-2580.

Wells JD, Thomsen S, Whitaker P, Jansen ED, Kao CC, Konrad PE, Mahadevan-Jansen A (2007b) Optically mediated nerve stimulation: Identification of injury thresholds. Lasers Surg Med 39:513-526.